Laboratory studies of heterogeneous uptake relevant to the troposphere

Birgit Müller

Degree of Doctor of Philosophy

The University of Edinburgh

2000

Abstract

The reactions and fate of many natural and pollutant species in the atmosphere are influenced by the interaction between gas and liquid phase. Despite the acknowledged significance of these heterogeneous processes, some factors determining the uptake of gases have still to be elucidated.

Although the equilibrium water-air partitioning is characterised by the Henry's law coefficient, the kinetics of the uptake process are more complicated. The Resistance Model approach describes uptake as a combination of the individual transfer processes, i.e. gas diffusion, mass accommodation, liquid solubility and liquid reaction. The mass accommodation is defined as the probability of incorporation at the phase boundary on collision with the surface.

In this work, a new vertical wetted-wall flow reactor was constructed to study the accommodation of gas molecules by aqueous solutions. The trace gas was brought into contact with a liquid surface slowly flowing down the inside of the flow tube using a movable injector. Changes in gas phase concentration due to uptake by the liquid were monitored by wavelength-resolved UV absorption spectroscopy.

The apparatus was tested by measuring the reactive uptake of ozone on $Na_2S_2O_3$ solutions. The derived mass accommodation coefficient of $\alpha = 4.3 \times 10^{-2}$, with a lower limit of $> 2.7 \times 10^{-3}$, at 293 K agrees with previously published data. A rate coefficient of $k'' = 3.7 \times 10^{8}$ l mol^{-1} s^{-1} for the reaction of ozone with $Na_2S_2O_3$ in water at 293 K was calculated.

The main focus of this work was on phenols since some are phytotoxic and have been observed in the ambient atmosphere in the gas phase as well as in fog and rain water. The uptake was measured on water and bromine water to distinguish between solubility-limited and gas and interface controlled regimes. Mass accommodation coefficients of phenol, 2-nitrophenol and m-cresol were derived as a function of

temperature. At 293 K, measured values of α were 8.3×10^{-3}, 9.4×10^{-4} and 6.3×10^{-3}, respectively, for these compounds. These values imply that under tropospheric conditions mass accommodation could be the rate limiting process for transfer across the interface.

In the Resistance Model mass accommodation is depicted as a continuous process where only clusters of critical size are taken up by the liquid phase. From the temperature dependence of α it was possible to derive the enthalpy and entropy for the transition (mass accommodation) between gas and solvated state. The size of the critical cluster (defined by N*) was determined for each phenol.

A general lack of experimental data regarding the Henry's law coefficient of 2-nitrophenol necessitated independent measurement of this parameter in this work. A newly built bubble column was used to purge 2-nitrophenol from an aqueous solution. The Henry's law coefficient was derived from the observed loss in the liquid phase as measured by UV absorption spectroscopy. Highly consistent data as a function of temperature were obtained, ranging from 420 M atm^{-1} at 278 K to 60 M atm^{-1} at 303 K. The enthalpy and entropy of solubility were determined as -50.0 kJ mol^{-1} and -104.0 J mol^{-1} K^{-1}, respectively.

Declaration

I hereby declare that this thesis has been composed by myself and the work presented in it is my own unless otherwise stated.

March 2000

Acknowledgements

I would firstly like to express my gratitude and appreciation to my supervisor Dr. Mat Heal for his help, optimism and approachability. My thanks also go to Dr. Anita Jones for the encouragement in the early days. Special thanks to Dr. Ron Brown and Dr. Ian Harkness who were always willing to spare their time for my problems.

I would like to acknowledge the members of the technical staff for the assistance and good humour, in particular Stuart Mains and Stuart Johnstone. Thanks to Anne in the library for the ever friendly and efficient help.

Thanks also to the environmental group, especially to Nick and Keith.

I am grateful to the University of Edinburgh for the funding of my research.

Finally, I would like to thank my family for their encouragement and support throughout my time abroad, and the dear people I met in Edinburgh.

Courses and Conferences attended

Courses

Atmospheric chemistry

Atmospheric modelling

Environmental change

Environmental risk assessment

Meteorology

Tropospheric chemistry

Conferences

Gas kinetic group, Norwich, September 1997

EUROTRAC-2 Symposium, Garmisch-Partenkirchen, March 1998

15th International Symposium on Gas Kinetics, Bilbao, September 1998

Physical section meetings, Firbush Point Field Centre, June 1996 and 1997

Contents

List of Figures

List of Tables

List of symbols and units assigned to them in this work

A	absorbance
A_c	condensed surface to air volume ratio of clouds ($cm^2\ cm^{-3}$)
A_R	pre-exponential factor (first-order reaction: s^{-1}, second-order reaction: $l\ mol^{-1}\ s^{-1}$)
A_r	area (cm^2), also interfacial area in bubble column (cm^2)
a_i	activity of species i
b_1, b_2	empirical constants
c	velocity of gas flowing down the wetted-wall reactor ($cm\ s^{-1}$)
$c^{\ominus}$	standard concentration = $1\ mol\ l^{-1}$
D	diffusion coefficient ($cm^2\ s^{-1}$)
D_G^P	pressure-independent gas diffusion coefficient ($Torr\ cm^2\ s^{-1}$)
d	sphere diameter (cm)
E_a	activation energy ($J\ mol^{-1}$)
F	gas flow ($cm^3\ s^{-1}$)
F_z	mass flux as mass per cross-sectional area per time ($mol\ cm^{-2}\ s^{-1}$)
f_i	fugacity (atm)
g	gravitational acceleration (= 981 $cm\ s^{-2}$)
H	Henry's law coefficient ($M\ atm^{-1}$ = $mol\ l^{-1}\ atm^{-1}$)
H^*	effective Henry's law constant ($M\ atm^{-1}$)
H_{iD}	dimensionless Henry's law coefficient
H_S	Henry's law coefficient in salt water ($M\ atm^{-1}$)
h	Planck constant (= 6.62618×10^{-34} J s)
I	intensity of light (counts or $counts\ s^{-1}$)
I_S	ionic strength ($mol\ l^{-1}$)
J_{max}	maximum flux of gas into liquid ($molecules\ cm^{-2}\ s^{-1}$)
J_{net}	net flux of gas into liquid ($molecules\ cm^{-2}\ s^{-1}$)
K_A	equilibrium constant ($mol\ l^{-1}$ units)
K_H	equilibrium hydrolysis constant (e.g. $mol^2\ l^{-2}$)
K_{OL}	overall liquid phase mass transfer coefficient ($cm\ min^{-1}$)
k	Boltzmann constant (=$1.38066 \times 10^{-23}\ J\ K^{-1}$)
k''	rate coefficient of bimolecular reaction in water ($l\ mol^{-1}\ s^{-1}$)
k''_S	rate coefficient of bimolecular reaction in electrolyte ($l\ mol^{-1}\ s^{-1}$)
k_H	first-order rate coefficient of hydrolysis (s^{-1})
k_{RXN}	pseudo-first-order rate coefficient of gas in liquid (s^{-1})
k_S	Setchenow salt-out coefficient ($l\ mol^{-1}$)
k_S^+, k_S^-	Setchenow salt-out coefficient of single ions ($l\ mol^{-1}$)
k_S^{gas}	Setchenow salt-out coefficient of gas ($l\ mol^{-1}$)
K_s	deposition velocity ($cm\ s^{-1}$)
k_w	observed first-order loss rate of a substance from the gas phase (s^{-1})
k_w^{corr}	rate coefficient for first-order wall reaction (s^{-1})
k_z	constant (cm) relating bubble column length to bubble interfacial area
L	distance/length (cm)
L_c	condensed phase mixing ratio of clouds ($cm^3\ cm^{-3}$)
l	path length of light (cm)
M	molar mass ($g\ mol^{-1}$)
M_r	relative molecular mass or molecular weight, dimensionless
m	molecular mass (kg)
m	molality ($mol\ kg^{-1}$)
m_u	atomic mass unit, AMU (= 1.6606×10^{-27} kg)
N	molecular concentration ($molecule\ cm^{-3}$)
N^*	critical number of molecules (cluster model)

N_A Avogadro number (= 6.02205 x 10^{23} mol^{-1})

n number of moles (mol)

n_G gas concentration (molecules cm^{-3})

Pe Peclet number

p total gas pressure (atm or Torr)

p_i partial vapour pressure (atm or Torr)

p^*_i vapour pressure of the pure compound (atm or Torr)

R gas constant (= 8.314 J mol^{-1} K^{-1} = 8.205 x 10^{-2} dm^3 atm K^{-1} mol^{-1})

Re Reynolds number

RH relative humidity (%)

r inside radius of wetted-wall flow tube (cm)

S aqueous solubility (mol l^{-1})

S_r cross sectional area (cm^2)

T temperature (K)

T_c temperature (°C)

t liquid-gas contact time (s) in Resistance Model, or generally time (min or s)

t^{Adv} advection time (s)

t^{Diff} molecular diffusion time (s)

u velocity of the liquid film (cm s^{-1})

V volume (dm^3)

V_A molar volume of solute A at its normal boiling temperature (cm^3 mol^{-1}), method of Wilke and Chang

V_m molar volume (l mol^{-1}) of solvent

V_S molar volume (l mol^{-1}) of solution

v volumetric liquid flow rate (cm^3 s^{-1})

v fluid velocity (cm s^{-1})

x_i mole fraction in the liquid (mol (total mol)$^{-1}$)

y_i mole fraction in the gas (mol (total mol)$^{-1}$)

z injector position which is equivalent to length of contact in flow tube (cm); liquid height in bubble column (cm), also spatial axis (cm)

z_i charge number of ion

$\frac{d[i]}{dz}$ concentration gradient along axis z (mol l^{-1} cm^{-1})

[i] concentration of i in units of molarity (mol l^{-1} = M)

$\Delta a, \Delta b, g$ components of the free energy of activation of diffusing solute due to cation, anion and water in calculation of D_L^S (J mol^{-1})

$\Delta G°$ free energy of gas to liquid transfer in solution (Henry's law solubility) (J mol^{-1})

ΔG_{obs} free energy of transition between gas and solvated state (mass accommodation) (J mol^{-1})

ΔH_L enthalpy of liquid solubility including liquid diffusion ($H\sqrt{D_L}$) (J mol^{-1})

$\Delta H°$ standard enthalpy of gas to liquid transfer in solution (Henry's law solubility) (J mol^{-1})

ΔH_S^E excess enthalpy of solution (J mol^{-1})

ΔH_{fus} enthalpy of fusion (J mol^{-1})

ΔH_{obs} enthalpy of transition between gas phase and liquid phase solvation (mass accommodation) (J mol^{-1})

ΔH_S enthalpy of solution (J mol^{-1})

ΔH_{vap} enthalpy of vaporisation (J mol^{-1})

$\Delta S°$ standard entropy of gas to liquid transfer in solution (Henry's law solubility) (J mol^{-1} K^{-1})

ΔS_{obs} entropy of transition between gas phase and liquid phase solvation (mass accommodation) (J mol^{-1} K^{-1})

$\left(\sum v\right)_A$ atomic diffusion volume of compound A (method of Fuller), dimensionless

Δ finite difference in a property
Γ_G transfer rate for gas phase diffusion (Resistance Model)
Γ_{RXN} transfer rate for liquid reaction (Resistance Model)
Γ_{SOL} transfer rate for solubility (Resistance Model)
$\frac{1}{\Gamma_G}$ gas transport resistance (Resistance Model)
$\frac{1}{\Gamma_{RXN}}$ liquid reaction resistance (Resistance Model)
$\frac{1}{\Gamma_{SOL}}$ solubility resistance (Resistance Model)
$\frac{1}{\Gamma_{RXN}+\Gamma_{SOL}}$ liquid transfer resistance (Resistance Model)
$\frac{1}{\alpha}$ interfacial transfer resistance (Resistance Model)
$\frac{1}{\gamma}$ overall uptake resistance (Resistance Model)

α mass accommodation coefficient
γ uptake coefficient
γ_i activity coefficient
γ_i^{∞} infinite dilution activity coefficient
δ film thickness (cm)
ε molar absorption coefficient at a specific wavelength λ (l mol^{-1} cm^{-1})
λ wavelength (nm)
μ viscosity (centipoise cP = 10^{-2} g cm^{-1} s^{-1} = 1 mPa s = 10^3 μPa s)
ν frequency (s^{-1})
ρ density (g cm^{-3})
σ molecular absorption cross section (cm^2 $molecule^{-1}$)
τ gas-liquid contact time (s)
τ^L lifetime (s)
τ_{mix} mixing time for two gases (s)
ϕ association factor, dimensionless (Wilke and Chang method)
ϕ fugacity coeffcient
ω mean molecular velocity (cm s^{-1})

Subscripts

A air
avg average
coll collisional
con condensed phase
crit critical
exp experimental
f final

G/g	gas
H	referring to hydrolysis
i/0	initial
incorp	incorporated
L	liquid
min	minimum
mix	mixture or mixing
obs	observed
S	related to electrolyte solution or solution in general
s	surface
STP	standard temperature and pressure
W	water

Superscripts

aq	aqueous
corr	corrected
EXP	experimental
equi	at equilibrium
gas	gaseous
non-equi	not at equilibrium
S	on electrolyte solution
o	reference state

Statistics

P	probability (that R is zero)
R	correlation coefficient
SD	standard deviation

Abbreviations

eqn	equation
m.p.	melting point
PDA	photodiode array
RT	room temperature

1. INTRODUCTION

Heterogeneous processes have been acknowledged as highly significant in the chemistry of the atmosphere. The condensed phase is involved in major reaction mechanisms in both the troposphere and the stratosphere. Tropospheric chemistry studies have demonstrated that aqueous phase processes in droplets and fogs lead to the formation of sulphuric and nitric acids from SO_2 and NO_x. This not only causes acidic precipitation ("acid rain") but, after evaporation of water, tropospheric aerosols can be formed. These aerosols act as cloud condensation nuclei, promoting the formation of clouds, and scatter sunlight, thereby affecting the energy balance of the Earth directly and indirectly. The presence of cloud water affects the oxidative capacity of the troposphere [*Lelieveld and Crutzen*, 1990].

Heterogeneous processes are those that take place between species in more than one phase, i.e. gas, liquid, solid. The interaction between gas and liquid water is of special interest in tropospheric chemistry. The troposphere extends from the Earth's surface up to about 10 - 17 kilometres. Temperature decreases with altitude, reaching a minimum at the tropopause, the boundary between the troposphere and the next layer, the stratosphere. In the stratosphere, which extends up to ~ 50 km from the Earth's surface, the temperature rises again as a consequence of absorption of solar ultraviolet radiation by ozone. The low temperature at the tropopause (200 ~ 220 K) leads to condensation of water and other condensable materials. As a result, a wide variety of species, often from anthropogenic sources, as well as much of the liquid water of the atmosphere, is contained within the troposphere. The stratosphere, on the other hand, is relatively dry with typical water vapour mixing ratio of only about 3 ppmv [*Graedel and Crutzen*, 1993]. Whereas transport and mixing in the troposphere can be fast, although with spatial and temporal variations, mixing across the tropopause is inhibited, and is slow in the stratosphere. The abundance of liquid water and a myriad of trace species in the troposphere allow for highly complex heterogeneous interactions, which are closely linked with one another, and which can subsequently alter the chemistry of the atmosphere and the climate on Earth.

1.1 Laboratory studies of heterogeneous chemistry

Studies of gas-liquid interactions have been performed by bringing the gas and the liquid into contact, under controlled conditions, and measuring the loss of gas due to uptake by the liquid.

At long enough contact times an equilibrium between gas and liquid is established. No net uptake of gas is observed and the gas-liquid partitioning is determined by Henry's law. Henry's law coefficients are very useful in assessing the distribution of a species and indicating the direction of its transport. Atmospheric transport models use Henry's law coefficients to predict the fate of chemicals in the environment.

However, kinetic limitations often prevent the establishment of equilibrium, so in order to model heterogeneous chemistry it is necessary to quantify the uptake process.

The fundamental parameter that describes the rate of gas-liquid transfer across the interface is the mass accommodation coefficient, α. This is the fraction of molecules striking the surface that enter the condensed phase. The magnitude of α determines the maximum rate of mass transport from the gas to the liquid. However, the overall mass transfer is often limited by other processes. These include diffusion in the gas and liquid phases, Henry's law solvation and reaction in the liquid. The rates of these processes are governed by diffusion coefficients, solubility and rate of reaction. The measured net uptake is therefore often smaller than α. The experimental task is to separate the processes affecting the gas uptake and, in this way, determine the basic parameters of gas-liquid interaction.

In the last decade a wide number of experimental techniques have been developed for carrying out such uptake measurements, especially in the USA, France and Germany, e.g. *Worsnop et al.* [1989], *Utter et al.* [1992], *Ponche et al.* [1993], *Behnke et al.* [1997]. Data have been collected for different trace gases, such as SO_2, H_2O_2, N_2O_5, NO_2, $ClNO_2$.

1.2 Aromatics in the troposphere

Volatile organic compounds (VOC) are emitted in large quantities into the troposphere. The global output has been estimated to be about 60 - 140 Mt y^{-1} from anthropogenic sources and 30 - 1150 Mt y^{-1} from biogenic sources [*Atkinson*, 1998].

A particular subject of VOC research has been the aromatic compounds due to their abundance as constituents of petrol and automobile exhaust. Typical gasoline blends have an aromatic content of 20 - 30 % by volume [*Platz et al.*, 1998]. Urban ambient concentrations of benzene have been measured as ~ 10 to 200 ppbC [*Finlayson-Pitts and Pitts, Jr.*, 1986]. Some aromatics are identified as human carcinogens.

In various laboratory studies it has been demonstrated that the gas phase oxidation of aromatic compounds, such as benzene and toluene, by OH and NO_3 radicals leads to phenol and mono and dinitro substituted phenols.

1.2.1 Phenols and nitrated phenols in the troposphere

Phenols and nitrated phenols have become the focus of research following the recognition of their toxicity, even at trace levels. These compounds have been identified in air in the ng m^{-3} range and from levels of $\mu g\ l^{-1}$ up to the mg l^{-1} range in rain and fog [*Leuenberger et al.*, 1985] which makes them one of the most abundant organic compounds in rainwater [*Levsen et al.*, 1990; *Herterich and Herrmann*, 1990; *Richartz et al.*, 1990; *Grosjean*, 1991; *Tremp et al.*, 1993; *Lüttke et al.*, 1997]. This is of consequence for drinking water supplies and for the protection of aqueous organisms. Environmental concern has arisen from the phytotoxic properties of the nitrophenols. It has been suggested that they may be one factor for the observed forest decline in Europe and northern America [*Rippen et al.*, 1987]. Nitrophenols have been found in higher concentrations in leaves of damaged trees than healthy plants [*Natangelo et al.*, 1999]. Nitrophenols have been measured at higher concentrations in the more polluted areas, e.g. Mt. Brocken in Central Europe as

compared with Great Dun Fell in Northern England [*Lüttke et al.*, 1999]. The only exception was phenol itself which indicates that it degrades more quickly in polluted air masses, possibly forming nitrophenols.

The reactions between aromatic compounds and NO/NO_2 to form nitroaromatics remove active nitrogen constituents. The partitioning between organic and inorganic nitrogen affects the oxidative capacity of the troposphere since NO/NO_2 are coupled with ozone as well as OH chemistry.

1.2.1.1 Concentration of phenols

Although the toxicological potential of phenols has been identified, measurements of ambient concentrations are quite scattered. Table 1.1 shows a selection of data for phenol, 2-nitrophenol and m-cresol measured in different environmental compartments. *Richartz et al.* [1990] have attributed the generally highest aqueous concentrations in fog to smaller droplets and longer contact time with air compared with rain droplets. The same authors could not detect any 2-nitrophenol in their fog samples, possibly due to the relatively low Henry's law coefficient.

	concentration				
	gas phase	aqueous phase			
	/ng m^{-3}	cloud /mg l^{-1}	fog /mg l^{-1}	surface water /mg l^{-1}	rain /mg l^{-1}
Phenol	**14 - 70** [*Lüttke et al.*, 1997]	**2.8 - 8.9** [*Lüttke et al.*, 1997]	**0.94 - 92** [*Richartz et al.*, 1990]	**0.09 - 7.8** [*Schmidt-Bäumler et al.*, 1999]	**> 0.28** (mean) [*Leuenberger et al.*, 1985]
	320 (mean) [*Leuenberger et al.*, 1985]				**5.6** (mean) [*Levsen et al.*, 1990]
2-nitro-phenol	**0.8 - 6.4** [*Lüttke et al.*, 1997]	**0.02 - 0.60** [*Lüttke et al.*, 1997]		**0.03 - 0.34** [*Schmidt-Bäumler et al.*, 1999]	**0.059** (mean) [*Leuenberger et al.*, 1985]
	24 (mean) [*Leuenberger et al.*, 1985]				**0.18** (mean) [*Levsen et al.*, 1990]
					0.1 - 1.4 [*Rippen et al.*, 1987]
m-cresol	**130** (mean, m- and p-cresol) [*Leuenberger et al.*, 1985]		**1.1 - 11** (m- and p-cresol) [*Richartz et al.*, 1990]	**0.03 - 0.3** [*Schmidt-Bäumler et al.*, 1999]	**> 1.1** (mean, m- and p-cresol) [*Leuenberger et al.*, 1985]
					2.5 (mean, m- and p-cresol) [*Levsen et al.*, 1990]

Table 1.1 Reported concentrations of phenol, 2-nitrophenol and m-cresol in the environment.

1.3 Heterogeneous chemistry relevant to phenols

1.3.1 Sources of phenols

A number of sources have been identified for phenols and cresols. They are used as raw material in the chemical industry (in particular, for the manufacture of phenol-formaldehyde resins), pharmaceuticals, disinfectants, dyes and explosives, as well as pesticides and herbicides. They are found in industrial effluent and municipal waste.

Beside these direct sources, studies of atmospheric reaction mechanisms have revealed the importance of *in-situ* formation of phenols and nitrophenols from mono aromatic precursors, such as benzene and toluene. Phenol is formed during

combustion processes and emitted by motor vehicles. Cresols are a by-product of coal tar distillation [*Grosjean*, 1991]. The origins of nitrophenols are less clear. Phenol can react with OH or NO_3 radicals to produce nitrophenols in air. This has been shown in smog chamber experiments [*Nojima et al.*, 1975].

The possible pathways of gas-phase oxidation of benzene and alkylsubstituted benzenes have been extensively investigated and kinetic data collected (e.g. *Atkinson et al.* [1984], *Knispel et al.* [1990], *Atkinson et al.* [1992], *Kwok et al.* [1994], *Anderson and Hites* [1996], *Andino et al.* [1996], *Seuwen and Warneck* [1996], *Klotz et al.* [1998]). As illustrated in Figure 1.1 for benzene, reaction with OH radicals dominates the tropospheric removal process, the major pathway (> 90 %) being formation of the adduct. The adduct can further react with O_2 and NO_2 leading to phenol and ring-opened products. H atom abstraction in the OH-benzene reaction can produce phenol, nitro and dinitro phenol [*Grosjean*, 1991; *Atkinson et al.*, 1992; *Andino et al.*, 1996; *Seinfeld and Pandis*, 1998].

The fate of aromatics with respect to the aqueous phase, i.e. uptake of the gaseous species and subsequent reactions in the liquid phase, are less well understood.

Only recently, laboratory studies of aromatics with free radicals in the aqueous phase have been carried out [*Herrmann et al.*, 1995; *Herrmann et al.*, 1996; *vonSonntag*, 1996]. A comparison of the rate coefficients showed that aqueous phase reaction rates are much larger (e.g. ~ five orders of magnitude for reaction of benzene with NO_3) than in the gas phase. This could indicate an important sink for aromatics which competes with gas phase reactions. More water-soluble ring-retaining products of gas phase oxidation can be transferred into the aqueous phase and undergo further reactions [*Pun et al.*, 1999]. In addition to the importance for the fate of the aromatic compounds, these aqueous phase reactions between aromatic compounds and free radicals could also significantly influence the free radical budget in the aqueous phase and alter the oxidising strength of the aqueous medium.

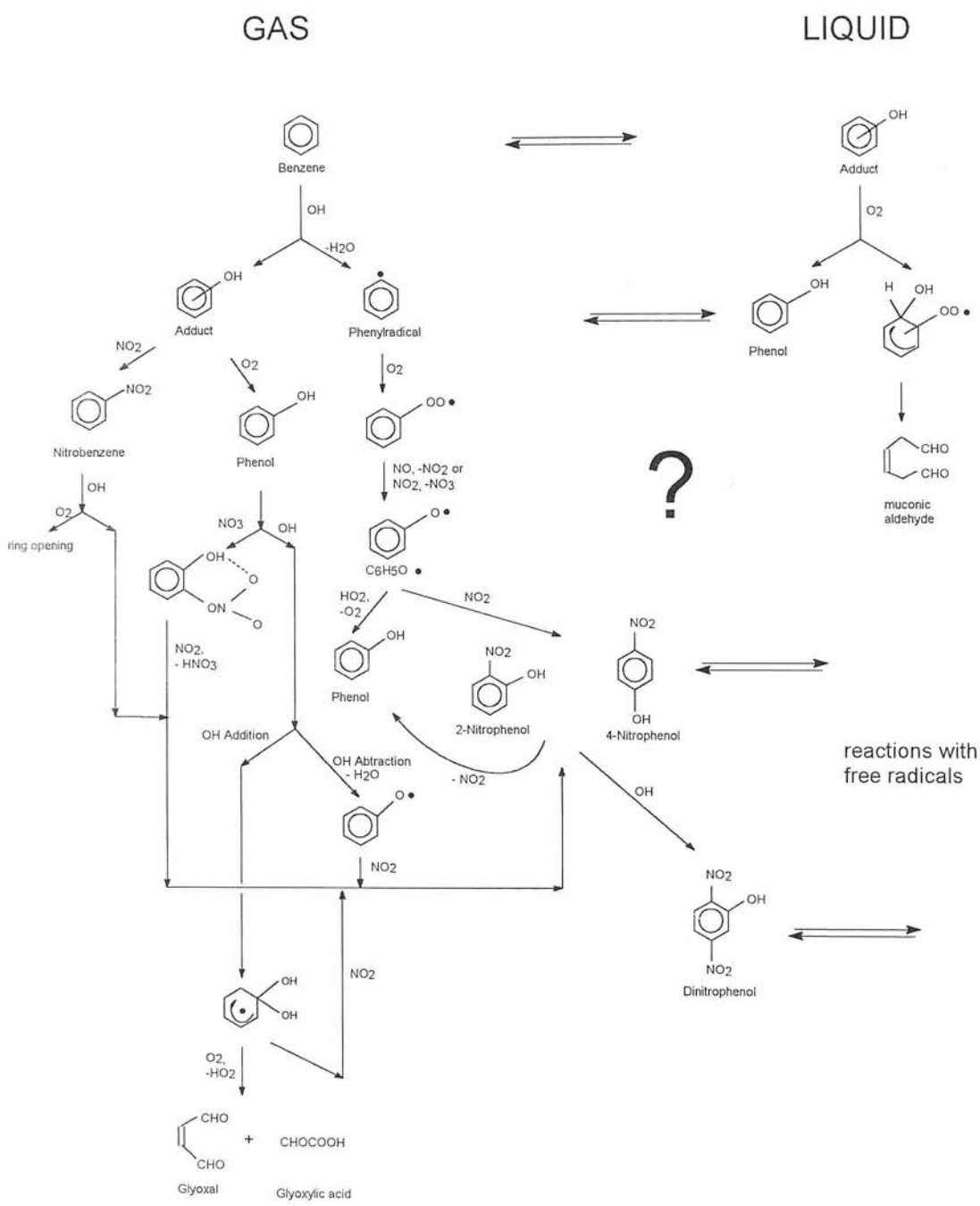

Figure 1.1 Oxidation scheme of benzene

1.4 Scope of the thesis

At present only very limited data are available with respect to the uptake of aromatics by the aqueous phase [*Heal et al.*, 1995; *Titcombe*, 1997]. This work focuses on the interaction of phenol, 2-nitrophenol and m-cresol with water. A wetted-wall flow reactor was built and tested, and used to investigate the uptake of these compounds at different temperatures.

The wetted-wall flow reactor was characterised by measuring the uptake of ozone. Ozone plays a central role in the chemistry of both the troposphere and the stratosphere. Tropospheric O_3 is an oxidant and acts as a greenhouse gas by absorbing UV and IR radiation and thus participating in climate forcing resulting in higher global temperatures. Increased ozone levels in the troposphere by anthropogenic emissions can cause respiratory effects in humans. In the stratosphere, ozone acts as shield against solar radiation and therefore protects living systems.

The uptake of ozone has been measured previously [*Tang and Lee*, 1987; *Utter et al.*, 1992; *Hu et al.*, 1995; *Magi et al.*, 1997]. Here it is used to characterise the wetted-wall flow reactor. In addition, the previous measured values vary considerably so that a further investigation will contribute to the existing data.

During the uptake measurements of 2-nitrophenol it became apparent that experimental data regarding its Henry's law coefficient are lacking. The Henry's law coefficient is necessary in the data analysis of the wetted-wall experiments. A bubble column was therefore built to obtain the Henry's law coefficient of 2-nitrophenol over an ambient temperature range.

This thesis is set out as follows. Chapter 2 gives the theoretical background to gas-liquid interactions. The equilibrium state between gas and liquid as well as the dynamics of gas uptake by a liquid are examined. An overview of the experimental techniques used in heterogeneous chemistry studies is presented. In Chapter 3 the

experimental methods applied in this work are described. The analysis of data is detailed in Chapter 4. Chapter 5 is concerned with the uptake of ozone. Uptake data are presented and compared with literature values. Experimental data for uptake measurements of phenol, 2-nitrophenol and m-cresol are presented in Chapters 6, 7 and 8, respectively. The following Chapter 9 summarises these results and relates them to the Resistance Model of gas uptake. Chapter 10 is concerned with the presentation and discussion of measurements of the Henry's law coefficient of 2-nitrophenol by means of a purge bubble column. The atmospheric significance of the findings with respect to the tropospheric lifetimes of the investigated phenols is discussed in the final Chapter 11.

2. THEORY

2.1 Introduction

The term heterogeneous chemistry applies to chemical reactions which involve the gas and the condensed phase. The latter can be represented either by solids like dust, soot, sea salt particles or by liquids e.g. cloud droplets.

The condensed phase functions in different ways. Many reactions do not occur or are very slow in the gas phase. However, in or on the condensed matter concentrations of species can often be enlarged and activation energies lowered, thereby presenting conditions sufficient to facilitate certain reactions. The aqueous phase can also provide alternative pathways to gas phase reactions, for example ionic. By taking up soluble species from the gas phase the liquid separates these from insoluble species and thus can change the chemical composition, and consequently the chemistry, of both phases, e.g. *Hanson and Ravishankara* [1991], *Hanson et al.* [1994], *Molina et al.* [1996a], *Ravishankara* [1997]. Thus, as well as the possible enhancement of reaction rates, the condensed phase can also act as a sink for reactive intermediates and lead to different reaction schemes.

Knowledge of gas-liquid partitioning not only predicts the concentration ratio at equilibrium but can also be used in deriving the direction and rate of transfer for systems evolving towards equilibrium. Such data are needed for modelling the environmental fate of pollutants as well as for the development of wastewater treatment strategies.

Henry's law coefficients as the property determining the gas-liquid partitioning are discussed in the next section. Methods of measuring and estimating Henry's law coefficients are described. The time to achieve equilibrium between gas and liquid phase, i.e. Henry's law, depends on the rate at which the gas can be transferred to the condensed phase. This gas uptake and the processes involved are dealt with in the

subsequent section. There are several model approaches in the literature which allow a quantitative treatment of the process. Of these, the focus here is on the so-called Resistance Model of gas uptake. Finally in this chapter, the experimental techniques used in heterogeneous chemistry are introduced.

2.2 Gas-liquid equilibria

2.2.1 Henry's law coefficient

The Henry's law coefficient H, also called Henry's law constant or water-air partitioning coefficient, is a fundamental physical property. It relates the concentration of a solute in a dilute aqueous solution, $[i]^{aq}$ (mol l^{-1}), to its concentration in the gas phase at equilibrium. Commonly the gas phase concentration is expressed as partial vapour pressure p_i (atm).

$$H_i = \frac{[i]^{aq}}{p_i} \qquad (2.1)$$

It is important to note that $[i]^{aq}$ and p_i in (2.1) refer to the same physical state of the pure compound. In the literature, different forms of Henry's law and a variety of units are used, often originating from historical conveniences in various research fields. For example, a dimensionless Henry's law coefficient

$$H_{iD} = \frac{[i]^{aq}}{[i]^{gas}} \qquad (2.2)$$

can be found in which the concentrations of i in water ($[i]^{aq}$) and air ($[i]^{gas}$) both use the same units, e.g. mol l^{-1}. In other references Henry's law coefficient may be expressed as an air-to-water (rather than water-to-air) ratio, again in a variety of units. Although all forms can be converted to each other, throughout this work the Henry's law coefficient is expressed as in (2.1) in units of M atm^{-1} in order to avoid confusion.

The equilibrium distribution between gas and liquid is determined by conditions such as temperature and concentration. Any change of these conditions which influences the equilibrium will change Henry's law coefficient. A few important factors which affect the partitioning and therefore Henry's law coefficient are given below.

Temperature

It is expected that H shows a strong temperature dependence. The partitioning equilibrium of a substance i between gas and aqueous solution of infinite dilution obeys the van't Hoff equation for equilibrium constants

$$\frac{d \ln H}{d\left(\frac{1}{T}\right)} = -\frac{\Delta H^{\circ}}{R} \qquad (2.3)$$

where H is Henry's law coefficient (M atm^{-1}), T is temperature (K), and R is the gas constant (J mol^{-1} K^{-1}). The enthalpy ΔH° corresponds to the hypothetical process of transferring the solute from the pure ideal gas state to a liquid state at infinite dilution in the solvent.

Over a relatively small temperature range ΔH° depends only weakly on T, and can be considered constant. Therefore integration yields

$$\ln\left(\frac{H_{T2}}{H_{T1}}\right) = -\frac{\Delta H^{\circ}}{R}\left(\frac{1}{T_2} - \frac{1}{T_1}\right). \qquad (2.4)$$

Rearrangement of (2.4) results in (2.5) which adequately predicts the Henry's law coefficient at one temperature if it is known at another

$$H_{T2} = H_{T1} \exp\left[-\frac{\Delta H^\circ}{R}\left(\frac{1}{T_2} - \frac{1}{T_1}\right)\right] .$$

(2.5)

From $\Delta G^\circ = -RT \ln H = \Delta H^\circ - T\Delta S^\circ$ it follows that

$$\ln H_T = -\frac{\Delta H^\circ}{RT} + \frac{\Delta S^\circ}{R}$$

(2.6)

where ΔG° is the free energy (J mol^{-1}) and ΔS° is the entropy (J mol^{-1} K^{-1}) for the Henry's law solubility [*Staudinger and Roberts*, 1996]. Plotting ln H_T *vs.* 1/T gives a straight line with a slope of $-\frac{\Delta H^\circ}{R}$ and an intercept of $\frac{\Delta S^\circ}{R}$.

The Henry's law coefficient generally increases in value as the temperature decreases, reflecting the greater aqueous solubility at lower temperatures [*Seinfeld and Pandis*, 1998]. The increase is typically of the order of a factor of two for a 10 K decrease in temperature around room temperature.

pH and hydrolysis

Many species undergo chemical transformations upon dissolution in water. The dissociation into ions, e.g.

$$HA + H_2O \rightleftharpoons H_3O^+ + A^-$$

(2.7)

is a reversible process that usually reaches equilibrium extremely fast. In sufficiently dilute solutions (a_{H_2O} = constant) the equilibrium constant, K_A, is given by

$$K_A = \frac{a_{H_3O^+}\, a_{A^-}}{a_{HA}}$$

(2.8)

where a_i is the activity of species i in aqueous solution. Equation (2.8) can be rewritten as

$$K_A = \frac{\gamma_{H_3O^+}[H_3O^+]\gamma_{A^-}[A^-]}{\gamma_{HA}[HA]c^{\ominus}} \qquad (2.9)$$

in which γ_i is the molar activity coefficient, [i] represents the concentration of species i in water (mol l^{-1}) and $c^{\ominus}$ is the standard concentration (= 1 mol l^{-1}). Equation (2.9) can often be further simplified to

$$K_A \approx \frac{[H^+][A^-]}{[HA]c^{\ominus}} \qquad (2.10)$$

where $[H_3O^+]$ is now represented by $[H^+]$ and γ_i values are taken as unity. Taking negative logarithms on both sides leads to

$$-\log K_A = -\log\frac{[H^+][A^-]}{[HA]c^{\ominus}} \quad \text{or} \quad pK_A = pH - \log\frac{[A^-]}{[HA]}. \qquad (2.11)$$

Since only undissociated species partition between air and water, an effective Henry's law coefficient, H^*, has been introduced

$$H^*_{HA} = \frac{[HA]^{aq}_{total}}{p_{HA}} \qquad (2.12)$$

in which $[HA]^{aq}_{total}$ is the total (i.e. dissociated and undissociated forms) concentration of HA in water. According to (2.7), (2.10) and (2.12)

$$H^*_{HA} = \frac{[HA]+[A^-]}{p_{HA}} = \frac{[HA]}{p_{HA}} + \frac{[HA]K_A c^{\ominus}}{p_{HA}[H^+]}. \qquad (2.13)$$

Substituting the Henry's coefficient of HA with $H_{HA} = \frac{[HA]}{p_{HA}}$ gives

$$H^*_{HA} = H_{HA}\left(1 + \frac{K_A c^{\ominus}}{[H^+]}\right) = H_{HA}\left(1 + 10^{pH-pK_A}\right). \qquad (2.14)$$

Equation (2.14) can be used to calculate the effective Henry's law coefficient for a substance with a known H and K_A. However, most natural waters exhibit a fairly narrow pH range of 5 to 8. Therefore, only species with a pK_A smaller than 6 to 9 will have a value of H^* significantly higher (> 10 %) than that of H [*Schwarzenbach et al.*, 1988; *Lyman et al.*, 1990; *Staudinger and Roberts*, 1996]

By analogy to the above discussion of changes to Henry's law coefficient arising from dissociation, an effective Henry's law coefficient also arises if hydrolysis takes place. Hydrolysis is a reaction in which a water molecule is substituted for a leaving group X in the original molecule

$$R\text{-}X + H_2O \longrightarrow R\text{-}OH + X^- + H^+ . \qquad (2.15)$$

In dilute solution the water concentration is essentially constant and the kinetics are pseudo-first-order at a fixed pH. The equilibrium hydrolysis constant, K_H, is given by

$$K_H = \frac{[ROH][H^+][X^-]}{[RX]} . \qquad (2.16)$$

Hydrolysis is considered to be irreversible, and has to be distinguished from other reactions of H_2O with organic chemicals which are either reversible (e.g. hydration of carbonyl to ketal) or do not take place at ambient temperature (e.g. addition of H_2O to alkenes to give alcohols) [*Lyman et al.*, 1990].

Since the more polar products of hydrolysis (ROH) have different properties from the parent compound an effective Henry's law coefficient is defined using (2.12), (2.15) and (2.16),

$$H^*_{RX} = \frac{[RX]^{aq}_{total}}{p_{RX}} = \frac{[RX]}{p_{RX}} + \frac{[RX]K_H}{p_{RX}[H^+][X^-]} . \qquad (2.17)$$

Substitution using $H_{RX} = \frac{[RX]}{p_{RX}}$ yields

$$H^*_{RX} = H_{HA}\left(1 + \frac{K_H}{[H^+][X^-]}\right)$$

(2.18)

[*Worsnop et al.*, 1989; *Lyman et al.*, 1990; *Schwarzenbach et al.*, 1993; *Staudinger and Roberts*, 1996].

Often K_H is approximated to

$$K_H = \frac{[ROH]}{[RX]},$$

(2.19)

which simplifies eqn (2.18) to

$$H^*_{RX} = H_{HA}\left(1 + K_H\right).$$

(2.20)

The higher polarity of the hydrolysis products will, in general, increase their solubility, so $H^* > H$. However, the overall rate of hydrolysis includes contribution from specific acid and base catalysed hydrolysis (i.e. reaction of neutral RX promoted by H^+ or OH^-) as well as neutral hydrolysis (i.e. pH independent neutral water reaction). The extent of hydrolysis is therefore a result of all these mechanisms at the relevant pH [*ECETOC*, 1998]. Typical classes of organic substances which undergo hydrolysis are esters, aliphatic halogens, amides, carbamates [*Howard et al.*, 1991].

Concentration

At equilibrium partitioning the fugacities of the aqueous and the gas phase, f_i^{aq} and f_i^{gas} (atm), are equal

$$f_i^{aq} = f_i^{gas}.$$

(2.21)

Fugacities are introduced as effective pressures to allow a real gas system to be considered by the same equations that apply to an ideal gas [*Academic Press dictionary of science and technology*, 1992]. By definition, (2.21) is equivalent to

$$x_i \gamma_i f_i^{aq\circ} = y_i \phi_i f_i^{gas\circ} \qquad (2.22)$$

where x_i and y_i are the mole fractions of i in the liquid and gas respectively, γ_i is the activity coefficient in the liquid phase, ϕ_i is the fugacity coefficient in the vapour phase and f_i° refers to the fugacity at a reference state (atm). [*Logan*, 1999]

For ideal solutions these fugacity expressions are simplified by assuming the following [*Mackay et al.*, 1979; *Suntio et al.*, 1988; *Logan*, 1999]:

a) $\phi_i = 1$ for relatively low pressures in typical environmental conditions ($\approx$ 1 atm)

b) $f_i^{gas\circ} = p$ with p being the total gas pressure (atm)

c) $f_i^{aq\circ} = p^*_i$ where p^*_i is the vapour pressure of the pure liquid solute i (atm)

d) $\gamma_i = 1$

e) The solute obeys Raoult's law which states that the vapour pressure of a gas over a solution is equal to the product of the vapour pressure of the pure compound and its mole fraction in the solution, i.e. $p_i = x_i p^*_i$.

On the basis of these assumptions (2.22) can be rewritten as

$$x_i p^*_i = y_i p = p_i \qquad (2.23)$$

and employed in the definition of Henry's law. Here, the liquid concentration is expressed using mole fraction (x_i) and molar volume of the solvent V_m (l mol^{-1}), the latter being the quotient of molar mass M (g mol^{-1}) and density ρ (for convenience here in g l^{-1}) of the solvent.

$$H_i = \frac{[i]^{aq}}{p_i} = \frac{\frac{x_i}{V_m}}{p_i} = \frac{\frac{x_i}{\left(\frac{M}{\rho}\right)}}{x_i\ p^*_i} = \frac{\rho}{M}\frac{1}{p^*_i}$$

(2.24)

Henry's law coefficient is defined for ideal dilute solutions. Although the vapour pressure of the solute is found to be proportional to its mole fraction at low concentration, the slope is no longer equal to the vapour pressure of the pure substance but to some other constant (that corresponds to Henry's law) [*Atkins*, 1986]. In this case, the solute-solvent interaction differs from the solvent-solvent interaction. This deviation from the ideal case is taken into account by introducing an activity coefficient γ_i. Therefore (2.24) changes to

$$H_i = \frac{\rho}{M}\frac{1}{\gamma_i\ p^*_i}.$$

(2.25)

Henry's law will be followed as long as γ_i stays constant. In general, for nonionizing compounds[1], $\gamma_i > 1$ for dilute solutions. It approaches a limiting value, γ_i^{∞}, as the solutions becomes increasingly dilute ("infinite dilution"). A general expression for the relation between the activity coefficient and the mole fraction has been given as [*Staudinger and Roberts*, 1996]

$$\gamma_i \cong \exp\left[\left(\ln \gamma_i^{\infty}\right)\left(1 - x_i\right)^2\right].$$

(2.26)

Thus for $x_i < 0.01$, γ_i will essentially be independent of x_i and furthermore $\gamma_i \cong \gamma_i^{\infty}$. This assumption is valid for aqueous solutions usually encountered in environmental surroundings. Equation (2.25) then becomes

---

[1] There are two common specifications under which $\gamma_i = 1$. Raoult's law is approached for a compound when its mole fraction approaches unity whereas Henry's law is approached when its mole fraction approaches zero. Based on these laws there are two conventions:

Convention I: $\gamma_i \rightarrow 1$ when $x_i \rightarrow 1$ (RAOULT) mostly for solutions of liquids

Convention II: $\gamma_i \rightarrow 1$ when $x_i \rightarrow 0$ (HENRY) mostly for solutions of solids and gases

$$H_i = \frac{\rho}{M} \frac{1}{\gamma_i^{\infty} \, p^*_i} .$$

(2.27)

According to eqn (2.27) the Henry's law coefficient can be determined if the infinite dilution activity coefficient γ_i^{∞} and the vapour pressure of a substance are known.

Organic compounds of atmospheric interest are often only slightly soluble in water so that at the saturation concentration the solute is still unhindered by other solute molecules. This has been verified in experimental studies which showed no significant increase in H when working with saturated solutions, e.g. *Mackay et al.* [1979], *Munz and Roberts* [1986], *Jayasinghe et al.* [1992]. *Prausnitz et al.* [1986] have suggested an upper limit of 3 mol % of solute concentration for a dilute solution. The fact that for slightly soluble compounds saturated solutions behave only marginally differently from dilute solutions has led to a widely used approximation for H

$$H_i = \frac{S}{p^*_i}$$

(2.28)

where S is the aqueous solubility or saturation concentration (mol l^{-1}) and p^*_i the vapour pressure of the pure compound (atm). Equation (2.28) implies that due to the small solubility of H_2O in the chemical its affects on the vapour pressure are negligible, and that γ_i does not vary appreciably with concentration [*Suntio et al.*, 1988]. These assumptions are only true if there exists little mutual miscibility between the chemical of interest and H_2O, i.e. solubility of the chemical in water and, *vice versa*, less than 5 % mol [*Suntio et al.*, 1988]. When using eqn (2.28) it is important to refer to the same physical state of i, i.e. liquid vapour pressure and solubility, or solid vapour pressure and solubility.

Salt

The presence of dissolved salt affects the fugacity of the compound in the aqueous phase only. The capacity of water to solvate gas phase species decreases with ionic

strength and is referred to as "salting out" [*De Bruyn et al.*, 1995]. Measurements on sea water confirm this trend [*Schwarzenbach et al.*, 1993]; *Mackay and Shiu* [1984] report a fall in solubility to 71 - 89 % of the distilled water value for a typical sea water salt concentration of about 0.5 mol l^{-1}.

Setchenow has derived an empirical relationship which adequately describes the change in Henry's law coefficient

$$\log_{10} \frac{H}{H_S} = k_S[\text{Salt}] \qquad (2.29)$$

where H and H_S are the Henry's law coefficient in pure water and in the salt solution respectively, [Salt] is the molarity of the ionic solution (mol l^{-1}) and k_S is the Setchenow salt-out coefficient (l mol^{-1}).

Other factors

It must be assumed that any other contaminant found in the water will affect Henry's law. This includes any solids and surfactants as well as co-solvent and co-solutes in multicomponent mixtures [*Munz and Roberts*, 1986; *Staudinger and Roberts*, 1996].

In summary, therefore, the Henry's law coefficient describes the partitioning between water and air. The equilibrium is controlled by a number of parameters of which temperature is most dominant. However, when using H for predicting environmental behaviour, or when measuring H in natural waters, deviations from standard laboratory values are likely due to the intricacy of the natural matrix and the possibly very complex interactions between all the parameters mentioned. Since the determination of Henry's law coefficient can be difficult and time consuming, values are often estimated.

2.2.2 Techniques for experimental determination of H

2.2.2.1 Measuring solubility and vapour pressure

Based on eqn (2.28), the Henry's law coefficient can be calculated from the aqueous solubility and vapour pressure of the pure compound, e.g. *Yaws et al.* [1991]. As summarised by *Suntio et al.* [1988] and already mentioned in the previous section, the key requirements for using this approach are a very small solubility of H_2O in the organic chemical (i.e. no affect on vapour pressure) and no change of the activity coefficient γ_i with concentration. This is not fulfilled if the solubility of H_2O in the chemical, and *vice versa*, exceeds 5 % mol, or for chemicals miscible with H_2O.

Vapour pressures above 10^{-3} atm can be easily measured and are available for many compounds in the literature [*CRC Handbook of chemistry and physics*, 1993]. However, many compounds of environmental concern have a very low vapour pressure (boiling points > 400 °C), and measurement of their vapour pressure is far more difficult and prone to errors. This is a major reason for the deficiency in environmental data that still exists for low volatility compounds [*Schwarzenbach et al.*, 1993]. Established methods for determining the vapour pressure include gas saturation, comparative ebulliometry and effusion methods, as referred to in *Mackay et al.* [1992]. More recently capillary gas chromatography has been used to estimate vapour pressures of nonpolar compounds [*Schwarzenbach et al.*, 1993].

The general method for determining aqueous solubility is to add an excess of the chemical under investigation to very pure water. After equilibration, which can take several days, the water is separated from any undissolved material and the solute concentration determined [*Lyman et al.*, 1990]. Difficulties arise with hydrophobic compounds which can form colloids or adsorb onto the glassware [*Staudinger and Roberts*, 1996]. If a substance ionises it is essential to report the pH [*Mackay et al.*, 1992].

Both aqueous solubility and vapour pressure are strong functions of temperature. Often there are no, or very scarce, data available with respect to the temperature dependence. Therefore an accurate temperature control has to be maintained when taking measurements. Other data are gained by extrapolation from higher temperature liquid phase data which can influence the accuracy [*Mackay et al.*, 1992].

2.2.2.2 Static partitioning

Henry's law coefficient can be measured directly by determining the partitioning concentrations after equilibrium has been reached in a closed system. Concentrations can be assessed either by measurement in both gas and liquid, or by mass balance in which the concentration is measured before and after equilibration in one phase only. Equilibrium can be established once or multiple times. In the latter approach the gas phase is removed after reaching equilibrium and replaced by solute free gas so that a concentration profile over a number of equilibrations is obtained. *Lincoff and Gossett* [1984] describe an Equilibrium Partitioning In Closed Systems (EPICS) technique whereby sealed bottles contain different liquid volumes and only relative concentrations are needed. The static approach has been widely used, e.g. *Munz and Roberts* [1986], *Betterton and Hoffmann* [1988], *Kames and Schurath* [1992].

2.2.2.3 Dynamic partitioning

Henry's law equilibrium has also been measured under flow conditions. It involves equilibration of solute between flowing liquid and/or gas phases and monitoring the change in concentration of the solute with time [*Jayasinghe et al.*, 1992]. The solute can either be stripped from the liquid with solute free gas or from solute loaded gas by pure liquid. Different devices have been employed in the realisation of the dynamic approach.

Mackay et al. [1979] have developed a stripping column where gas bubbles are continuously produced at the bottom and slowly rise to the top through the liquid. It is assumed that the liquid is well mixed and water-gas partitioning established before the bubble exits the liquid. The changes in concentration are constantly monitored. Many workers have applied this method, sometimes in slightly modified form, e.g. *Betterton and Hoffmann* [1988], *Dunnivant et al.* [1988], *Jayasinghe et al.* [1992], *Kames and Schurath* [1995], *Shiu and Mackay* [1997]. There are also a number of studies which have used both static and dynamic methods and compared the results [*Ashworth et al.*, 1988; *Hamelink et al.*, 1996].

Other groups have used microporous tubing which is immersed in the solution. Liquid is drawn to the inside wall by capillary action where it establishes equilibrium with the gas flowing slowly through the tube [*Dong and Dasgupta*, 1986; *Shepson et al.*, 1996]. *Fendinger and Glotfeldy* [1988; 1989] have made use of a wetted-wall column and a fog chamber (description in Section 2.4.2) to measure H for several pesticides and found excellent agreement between the results. *Swartz et al.* [1997] have used a horizontal bubble train for uptake measurements and extraction of Henry's law coefficients.

2.2.3 Estimation methods

The difficulties inherent in obtaining experimental data for Henry's law coefficient for organic compounds of environmental concern (i.e. low solubility, low vapour pressure) has led researchers to engage various estimation methods. Predictions of Henry's law coefficients are either made directly by models based on structure and property features, or calculated using estimated vapour pressures and solubilities.

Aqueous solubility can be assessed by fragment addition methods, e.g. method of Irrmann (1965) as found in *Lyman et al.* [1990] and *ECETOC* [1998], or by using one of several regression equations which need input parameters like the octanol-water partitioning coefficient and the melting point [*Lyman et al.*, 1990].

Estimation methods for vapour pressure are often modifications of the Clausius-Clapeyron equation

$$\frac{d \ln p_i^*}{dT} = \frac{\Delta H_{vap}}{RT^2} \qquad (2.30)$$

where ΔH_{vap} is the molar enthalpy of vaporisation (J mol^{-1}). Integration gives an equation of the form

$$\ln p_i^* = A - \frac{B}{T} \qquad (2.31)$$

with A and B being some constants. Equation (2.31) shows a simplified expression of established methods given by Antoine (1888) and Watson (1943) for estimation of the vapour pressure at a temperature T as described in *Lyman et al.* [1990] and *ECETOC* [1998].

An alternative is the so-called quantitative structure activity relationships (QSARs), recently extended to quantitative structure property relationships (QSPRs), which correlate the logarithms of H (log H) with compound structure terms [*Staudinger and Roberts*, 1996]. Each compound can be divided into subunits with specific structure features. The partitioning is considered to be the result of the combination of all these features and can be calculated by simply adding up the group contributions (see *Staudinger and Roberts* [1996] and *ECETOC* [1998]). UNIFAC is a specific model for calculating activity coefficients γ_i which in contrast to most other models allows temperature effects to be taken into account. It was introduced by Fredenslund in 1975 but has since been further developed (see *Schwarzenbach et al.* [1993], *Staudinger and Roberts* [1996], *ECETOC* [1998]).

It is difficult to give a general comment on the accuracy of the different models. Whereas for some classes of compounds the model is in very good agreement with measured values, for other more complex structures there are clearly limitations. For

example, certain isomers give the same descriptor but have different properties [*Mackay et al.*, 1992]. Another problem is the inconsistency of experimental input data which can vary considerably between groups.

Without doubt the structure models are valuable tools for atmospheric scientists, especially since they are often easy to apply. However, special attention should be given to significant errors which may arise in their application.

2.3 Gas uptake into liquid

2.3.1 Theory

Net exchange of a compound takes place between gas and condensed phases that are not at equilibrium. Mass transfer consists of different physical processes which will be described using the example of gas uptake into a liquid as illustrated in Figure 2.1.

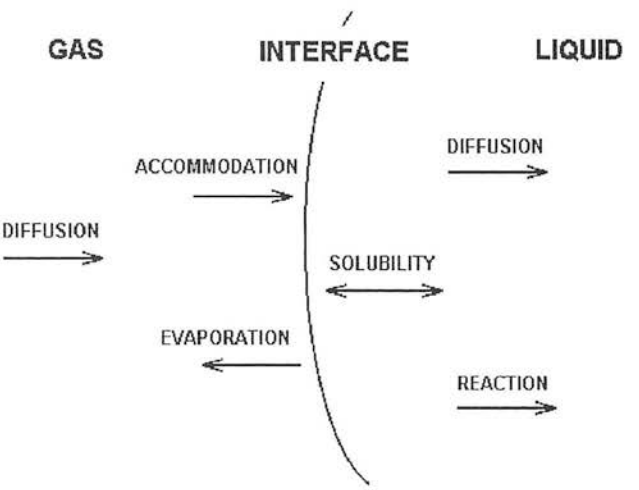

Figure 2.1 Schematic diagram of gas uptake into liquid

Gas phase molecules are transported to the liquid surface by diffusion. At the phase boundary, only a portion of the gas molecules will enter the surface, determined by

the sticking probability (mass accommodation) α, whereas other molecules will evaporate immediately back into the gas phase. Once inside the liquid phase the molecules move into the bulk according to liquid phase diffusion. There is also the possibility that chemical reaction with an aqueous reactant occurs. Possible products can either be transported back into the gas phase or diffuse within the liquid.

Researchers in the field have been engaged in visualising the uptake process in a simplified way. The problem of dividing the overall gas uptake into subprocesses has been formulated by *Schwartz* [1986]. He has given characteristic times for the different processes involved in order to assess the rate of the overall process and to identify the rate limiting (i.e. slowest) step under defined conditions. Through the development of models, analytical solutions describing the uptake process can be obtained.

2.3.2 Mass accommodation

2.3.2.1 Terminology

The mass accommodation coefficient α is a key parameter for the transport from the gas into the liquid phase. It is the probability that a molecule that strikes the liquid surface will enter into the bulk and is therefore also called the "sticking coefficient",

$$\alpha = \frac{\text{no. of molecules entering liquid phase}}{\text{no. of molecular collisions with surface}} \quad (2.32)$$

It can only have values between 0 and 1. Thus, α represents the transport in one direction (gas to liquid). Difficulties in the measurement of α arise because heterogeneous processes depend on the net transport across the interface. The net uptake from the gas phase is described by the uptake coefficient γ which is defined as

$$\gamma = \frac{\text{no. of molecules removed from the gas phase}}{\text{no. of molecular collisions with surface}} \quad (2.33)$$

If all other processes are fast compared with the transport across the interface, the measured uptake γ approaches α. Conversely, at equilibrium, γ tends to zero ($\gamma \rightarrow 0$). Therefore, α is always the upper limit for γ

$$\alpha \geq \gamma \quad .$$

(2.34)

α can be derived from uptake measurements if all the other correction factors are accurately known. In practice, this is often not the case. For that reason the easiest and most reliable method used is to make the interfacial transfer process the rate determining step. This can be achieved by using one, or a combination, of the following conditions:

- working at reduced pressures to enhance mass transport by diffusion in the gas phase
- addition of scavengers to the liquid phase
- applying short contact times between gas and liquid (i.e. far from equilibrium)
- measure gas absorption on very small droplets to reduce gas phase resistance

Several laboratory apparatus have been designed for this purpose (see Section 2.4.2).

2.3.2.2 Implications for the atmosphere

The mass accommodation coefficient α determines the maximum flux of transport of gas into the condensed phase, J_{max} (molecules cm^{-2} s^{-1}), which is given by

$$J_{max} = \alpha \frac{n_G \omega}{4}$$

(2.35)

where n_G $\omega/4$ is the molecular collision rate of gas (with an equilibrium Boltzmann velocity distribution), n_G is the gas concentration (molecules cm^{-3}), and ω is the mean molecular speed (cm s^{-1}). However, under particular conditions, gas phase diffusion and liquid saturation often limit the maximum flux so that the overall net gas uptake is described by

$$J_{net} = \gamma \frac{n_G \omega}{4} \qquad (2.36)$$

where γ is the uptake coefficient.

For identifying the rate limiting parameter in heterogeneous processes it is important to keep in mind that α describes the gas-liquid transport in one direction whereas the whole process depends on the net transport which is often much smaller. Under tropospheric conditions the mass transfer across the interface is only rate determining if $\alpha \leq 10^{-2}$ as *Schwartz* [1986] has shown. For larger values of α, the gas uptake is controlled by gas phase diffusion rather than by mass accommodation. The concentration of trace organics in the aqueous phase is in this case determined by their Henry's law solubility, and their aqueous chemistry by their liquid reaction rates. This is relevant in the assessment of the fate and the effect of organic compounds in the environment.

2.3.3 Uptake models

A number of models have been formulated to describe the mass transport between a gas and a liquid. One of the earliest is the "Two-film-theory" by Whitman (1923) where each of the well-mixed bulks is confined by a stagnant film. These layers, thought to be at equilibrium, show a linear concentration gradient and transfer takes place by molecular diffusion. *Liss and Slater* [1974] used this model to calculate the flux of various gases across the air-sea interface.

A different approach, based on the penetration theory by Higbie (1935), is the surface model. In this theory, the time of exposure of the liquid to the gas is used to determine the degree of saturation at various distances from the surface, leading to concentration-depth profiles for different exposure times. One can distinguish between "still surface" and "surface renewal". In the former, discontinuous convective disturbances of the stationary liquid are followed by diffusion until the next

disturbance. In the case of surface renewal, material from the bulk is brought to the surface where it is exposed to the second phase for a certain time before it is mixed with the bulk again. The exposure time can either be presumed to be the same for all the gas ("regular surface renewal") or follow a random distribution of ages as *Danckwerts* [1951] has suggested ("random surface renewal"). Combining elements of the two previous theories, the film-penetration theory interprets the interface as a laminar film but the transfer across as a non-steady state process. Another model assumes mass transfer as result of turbulence only (for review on theories for mass transfer see *Danckwerts* [1970] and *Coulson et al.* [1990]).

All these classical models focus on the mass transfer as a phenomenological process. The interface area is pictured in various simplified ways and different mathematical models have been evolved to calculate gas-liquid exchange processes. However, only a molecular interpretation can disclose the dependence of gas entry into liquids on its molecular structure and prevailing conditions such as temperature and chemical composition.

Until recently only very limited experimental data were available to help the development of molecular solubility mechanisms. The most commonly used model is the cavity model. The liquid forms a cavity of appropriate size to accommodate the solute. Once inside the cavity the molecule interacts with the surrounding solvent. Expressions for the molar Gibbs energy have been derived for both steps (i.e. cavity formation and interaction) and have been used in correlating gas solubilities. However, the model assumes the molecule to be rigid with no attractive forces and unchanged internal molecular degrees of freedom when dissolved, and this is only true for small molecules [*Prausnitz et al.*, 1986, *and references therein*; *Pollack*, 1991, *and references therein*].

The observation of discrepancies between experimental results and model predictions has led to the development of a new model. Developed by *Davidovits et al.* [1995] it proposes gas uptake *via* formation of clusters between an incoming gas molecule and

the solvent. When a defined number of molecules N* merge to form an aggregate of critical size, the cluster continues to grow and is subsequently embodied in the bulk liquid, whereas clusters smaller than the critical size re-evaporate into the gas phase. The critical number N* depends on the structure and properties of the molecule being taken up. The model has been tested on various reactive (e.g. SO_2 onto water, Cl_2 and Br_2 onto aqueous Br^- and I^- solutions) and non-reactive (e.g. a series of alkanols onto water) uptake data and the predictions have been found in good agreement with the experimental results [*Davidovits et al.*, 1995].

2.3.4 Transport processes

The exchange and uptake of material is associated with movement through phases and across boundaries. It is these transport processes that have to be understood in order to describe the uptake process mathematically. Transport in the environment is primarily performed by two kinds of physical processes. Mass can be passively carried by bulk movements of air or water, such as blowing winds and flowing rivers, which is called advection. The second type, diffusion, is due to random movements of single molecules (molecular diffusion) or random movements of the medium carrying the chemical (turbulent diffusion). The driving force behind diffusion is a concentration gradient along a spatial axis z. The mass flux in the z direction is proportional to this concentration gradient, as summarised in Fick's first law,

$$F_z = -D\frac{d[i]}{dz} \qquad (2.37)$$

where F_z is the mass flux in units of mass per cross-sectional area per time (mol cm^{-2} s^{-1}) and d[i]/dz is the concentration gradient (mol cm^{-4} = 10^3 mol l^{-1} cm^{-1}). D is known as the diffusion coefficient or diffusivity (cm^2 s^{-1}). It is a function of the moving substance as well as the surrounding medium and generally depends on temperature and pressure (for gases). Since a positive flux moves from the place of higher to lower concentration, a minus sign is required on the right hand side of the

eqn (2.37). The rate of diffusion increases with higher temperature, and decreases with bigger particle size and higher viscosity of the ambient medium.

To assess the relative importance of the diffusive processes for atmospheric transport one can compare characteristic transfer times. The Einstein-Smoluchowski equation gives the molecular diffusion time t^{Diff} (s) as

$$t^{Diff} = \frac{L^2}{2D} \qquad (2.38)$$

where L is the distance travelled (cm) and D is the diffusion coefficient ($cm^2\ s^{-1}$). The time for advection t^{Adv} (s) is

$$t^{Adv} = \frac{L}{v} \qquad (2.39)$$

with v being the constant current velocity of the medium ($cm\ s^{-1}$) [*Atkins*, 1986]. Table 2.1 (adopted from *Schwarzenbach et al.* [1993]) compares characteristic times for a substance to travel a distance L by molecular diffusion or by advection. Values for diffusivities (D_A and D_W) and velocities (v_A and v_W) typical for air and water have been used.

distance L /cm	**diffusion time /s**		**advection time /s**
	Water	Air	Water or Air
0.00001	5×10^{-6}	5×10^{-10}	1×10^{-6}
0.0001 (= 1 μm)	5×10^{-4}	5×10^{-8}	1×10^{-5}
0.001	0.05	5×10^{-6}	1×10^{-4}
0.01	5	5×10^{-4}	1×10^{-3}
0.1 (1 mm)	500 (≈ 8 min)	0.05	0.01
1	5×10^{4} (≈ 14 h)	5	0.1
10	5×10^{6} (≈ 58 days)	500 (≈ 8 min)	1

Table 2.1 Characteristic times for diffusion and advection in air and water. Typical values of $D_A = 0.1\ cm^2\ s^{-1}$, $D_W = 10^{-5}\ cm^2\ s^{-1}$, $v_A \approx v_W \approx 10\ cm\ s^{-1}$ were taken from *Schwarzenbach et al.* [1993] and *Finlayson-Pitts and Pitts, Jr.* [1986].

Diffusion in air is about four orders of magnitude faster than in water which is reflected in the respective molecular diffusion times shown in Table 2.1. It can also be seen that for small distances (up to about 0.01 cm) molecular diffusion in air is faster than advection in air. Over larger distances the reverse is true. In water, even distances as short as 0.1 μm will be travelled faster by advection than by molecular diffusion. Mathematically this can be described by setting (2.38) and (2.39) equal. Rearrangement allows the derivation of a critical distance L_{crit}

$$L_{crit} = \frac{2D}{v} . \qquad (2.40)$$

For distances larger than L_{crit} advection will govern the transport. This is the case for most environmental media where the dispersion of contaminants proceeds by turbulent mixing and advection, for example in rivers, lakes and oceans [*Lyman et al.*, 1990; *Kley*, 1997]. However, on the microscopic scale, e.g. in interstitial water of sediments, and across air-water interfaces, molecular diffusion underlies the transport [*Liss and Slater*, 1974; *Ghosh*, 1993; *Schwarzenbach et al.*, 1993]. Accurate determination of the molecular diffusion coefficients is the basis for investigation of the uptake process and its kinetics [*Lyman et al.*, 1990].

2.3.4.1 Availability of molecular diffusion coefficients

Experimental determination

Liquid diffusion coefficients can be determined by observing the rate at which a concentration boundary spreads, or the rate at which a more concentrated solution diffuses into a less concentrated one. Other methods draw conclusions from measuring particle size or viscosity. Common techniques used include capillary, diaphragm, centrifugal and chromatographic methods. Newer approaches are light scattering and field flow fractionation [*Atkins*, 1986; *Logan*, 1999].

Diffusion coefficients in the gas phase can be determined by following the rate of evaporation of a chemical into a gas stream. The conditions must ensure molecular diffusion only, i.e. there must be constant temperature and no turbulence [*Coulson et al.*, 1990; *Logan*, 1999]. Measured values of diffusivities are available in standard reference books, such as *CRC handbook of chemistry and physics* [1993].

Prediction of diffusion coefficients

In cases where no experimental data exist, molecular diffusion coefficients can be predicted by empirical or theoretical equations. Generally these equations give good estimates (within 5 - 10 % of experimental values) but discrepancies up to 20 % are possible [*Reid et al.*, 1987]. Restrictions with respect to the class of chemical compound, pressure, etc. must be checked before using any of the correlations. Two empirical methods are illustrated here (for original references and detailed discussion refer to *Reid et al.* [1987] and *Perry and Green* [1997]).

Gases: Fuller, Schettler and Giddings [*Fuller et al.*, 1969] provide an equation which is easy to apply and produces reliable estimates. It can be applied to binary mixtures of non-polar compounds at low pressures and temperature.

The diffusivity of A in B, in the gas phase, is given by

$$D_G{}^{P}{}_{AB} = \frac{10^{-3} T^{1.75} \left(\frac{1}{M_A} + \frac{1}{M_B} \right)^{1/2}}{p\left[\left(\sum v \right)_A^{1/3} + \left(\sum v \right)_B^{1/3} \right]^2} \qquad \textbf{(2.41)}$$

where $D_G{}^{P}{}_{(AB)}$ is the diffusion coefficient ($cm^2\ s^{-1}$) at 1 atm, T the temperature (K), p the pressure (atm) and M_A and M_B are the molar masses of compounds A and B respectively ($g\ mol^{-1}$). The atomic diffusion volumes of compounds A and B ($\left(\sum v\right)_A$ and $\left(\sum v\right)_B$) can be found by summation of the diffusion volumes for each element.

The dimensionless volume increments for atoms and simple molecules are listed in the reference [*Sinnott*, 1996; *Logan*, 1999].

Many other methods for estimating gas diffusivities have been proposed as collected in *Reid et al.* [1987], *Coulson et al.* [1990], *Perry and Green* [1997].

Liquids: Even though there are numerous correlations for diffusion coefficients in the liquid phase, careful consideration of their applicability is needed for reasonable estimates because of the complexity and greater extent of interaction in this phase.

A widely used equation has been developed by Wilke and Chang (1955)

$$D_{L(AB)} = \frac{7.4 \times 10^{-8} \left(\phi_B M_B\right)^{1/2} T}{\mu_B V_A^{0.6}} \qquad (2.42)$$

where $D_{L(AB)}$ is the liquid diffusion coefficient of A in B ($cm^2\ s^{-1}$), T the temperature (K) and M_B the molar mass of solvent B ($g\ mol^{-1}$). ϕ_B is a dimensionless association parameter for B and values are given for common solvents. μ_B is the viscosity of solvent B (centipoise $cP = 10^{-2}\ g\ cm^{-1}\ s^{-1}$). V_A is the molar volume of solute A at its normal boiling temperature ($cm^3\ mol^{-1}$), an estimate of V_A is provided by the additive methods of Schroeder (1949) and Le Bas (1915).

The Wilke and Chang equation predicts satisfactory liquid diffusivities for dilute binary mixtures. *Reid et al.* [1987] have compared estimated and experimental values of $D_{L(AB)}$, for a variety of solutes and different solvents, and found great variation in the % errors (over 60 % in some cases). Care must therefore be taken when choosing a correlation and using the data. Other methods for the estimation of liquid diffusion coefficients are available in *Reid et al.* [1987], *Lyman et al.* [1990] and *Perry and Green* [1997].

2.3.5 Mathematical description of uptake - The Resistance Model

Gas uptake is governed by four interacting processes: gas phase diffusion, mass accommodation, Henry's law solubility, and liquid phase reaction. Due to their interactions, gas-liquid uptake is described by coupled differential equations. Only for limited cases can exact solutions be found [*Danckwerts*, 1951]. The Resistance Model of gas uptake is based on the assumption that each of the processes determining the gas uptake can be considered independent of each other. By decoupling the transfer in such a way a simple approximation based on steady state solutions can be obtained.

By analogy to an electrical circuit, the Resistance Model considers the overall resistance to the gas uptake as the sum of the resistances to each individual step, as shown in Figure 2.2.

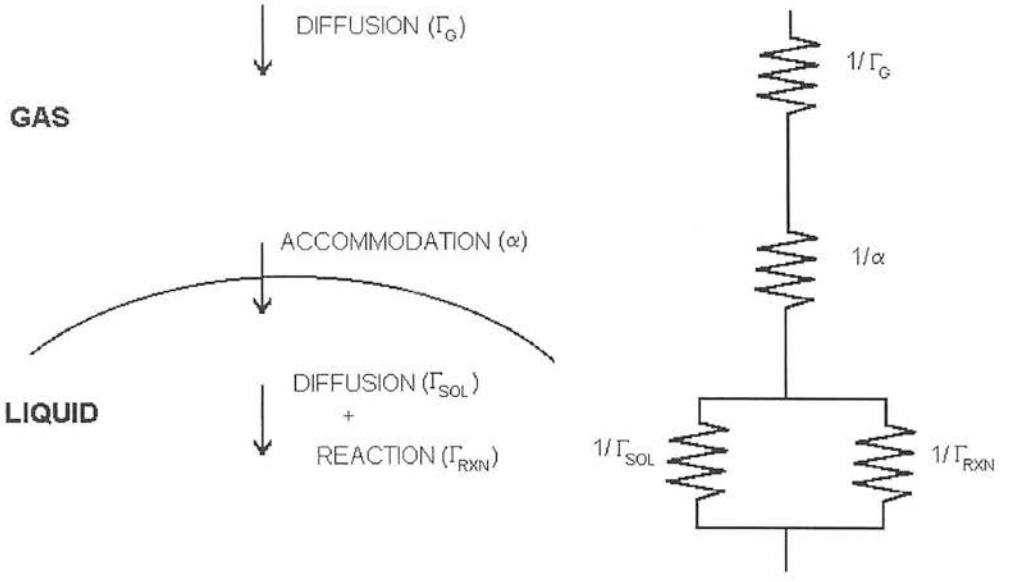

Figure 2.2 Resistance model as circuit

The Γ_G, Γ_{SOL} and Γ_{RXN} functions represent the dimensionless conductances (or mass transfer coefficients) for gas phase diffusion, Henry's law saturation and liquid phase reaction, respectively. These quantities are normalised transfer rates rather than probabilities (capitalised symbols), and can have values larger than unity. The resistances are expressed as uptake coefficients which are the inverse of the conductances. The overall uptake resistance is given by

$$\frac{1}{\gamma} = \frac{1}{\Gamma_G} + \frac{1}{\alpha} + \frac{1}{\Gamma_{SOL} + \Gamma_{RXN}} \quad \textbf{(2.43)}$$

overall	gas	interfacial	liquid transfer
uptake	transport	transfer	resistance (liquid
resistance	resistance	resistance	solubility and reaction)

The quantity γ is the net uptake coefficient for gas uptake into a liquid, and the overall resistance $1/\gamma$ incorporates the effect of all individual processes involved in the uptake. $1/\alpha$ describes the interfacial transfer resistance, wherein α is the mass accommodation coefficient. In the limit of large Γ_G and large Γ_{SOL} and/or Γ_{RXN}, the corresponding resistances become insignificant and γ approaches α. Since liquid phase transfer is, in general, the sum of both the solubility and reaction transfer coefficients, Γ_{SOL} and Γ_{RXN}, the total liquid phase resistance is represented by $1/(\Gamma_{SOL}+\Gamma_{RXN})$. The individual resistances can be expressed explicitly using gas kinetic theory [*Kolb et al.*, 1995; *Molina et al.*, 1996a].

Gas diffusion

The gas transport resistance $1/\Gamma_G$ to a spherical droplet is given by

$$\frac{1}{\Gamma_G} = \frac{\omega\, d}{8\, D_G} - \frac{1}{2} \quad \textbf{(2.44)}$$

with ω is the mean molecular velocity (cm s^{-1}), d the sphere diameter (cm) and D_G the gas diffusion coefficient (cm^2 s^{-1}). The equation is derived from the steady state solution for the gas phase diffusion of a species to the surface of a sphere. If there is net uptake the Boltzman collision rate which describes the gas kinetic flux to the surface is distorted. This is accounted for by the - ½ term in the expression as derived by *Motz and Wise* [1960]. The first term is attributed to gradients in gas concentration arising from gas transport by diffusion. According to (2.44) gas transport resistance is proportional to droplet diameter d and inversely proportional to D_G. The concentration gradient from bulk gas to surface becomes smaller with larger Γ_G.

Solubility

As mentioned above, liquid solubility and reaction combine within the liquid transfer resistance. In the absence of any liquid reaction solubility determines the transfer. The net uptake decreases with contact time between liquid and gas because the system approaches equilibrium and the fluxes due to accommodation and evaporation become equal. This is reflected in the following definition of the solubility resistance which is an approximation of the exact solution:

$$\frac{1}{\Gamma_{SOL}} = \frac{\pi^{1/2}\,\omega}{4\,H\,R\,T}\sqrt{\frac{t}{D_L}} \qquad (2.45)$$

H is the Henry's law coefficient (M atm^{-1}), R is the gas constant (l atm mol^{-1} K^{-1}), T is the temperature (K), t is the liquid-gas contact time (s), ω is the mean molecular velocity (cm s^{-1}) of the trace gas and D_L is the liquid diffusion coefficient (cm^2 s^{-1}). The quantity $1/\Gamma_{SOL}$ shows dependence on $\sqrt{t}$, as well as on $1/\sqrt{D_L}$. At equilibrium (i.e. as $t \rightarrow \infty$) the liquid is saturated and net uptake is zero ($\Gamma_{SOL} \rightarrow 0$). On the other hand, the shorter the contact time t the smaller the value of the $1/\Gamma_{SOL}$ resistance. Equation (2.45) can only be applied if the condensed phase is thicker than the value of $\sim (D_L t)^{1/2}$ [*Kolb et al.*, 1995].

Liquid reaction

When there is irreversible liquid reaction then liquid transfer is dominated by the reactive uptake coefficient Γ_{RXN}. In these circumstances the liquid transfer resistance is dominated by the liquid reaction resistance $1/\Gamma_{RXN}$:

$$\frac{1}{\Gamma_{RXN}} = \frac{\omega}{4\,H\,R\,T\left(D_L\,k_{RXN}\right)^{1/2}} \qquad (2.46)$$

where k_{RXN} is the pseudo-first-order reaction rate of the dissolved gas in the condensed phase (s^{-1}). In the case of a bimolecular reaction in solution, k_{RXN} is usually expressed as

$$k_{RXN} = k''\,[i] \qquad (2.47)$$

where k'' is the second-order rate coefficient (l mol^{-1} s^{-1}) and [i] is the concentration of reactant in solution (mol l^{-1}).

Equation (2.46) is valid for reactive uptake on a surface layer of $\sim (D_L/k_{RXN})^{1/2}$ thickness, i.e. the condensed phase must be thicker than $\sim (D_L/k_{RXN})^{1/2}$ [*Kolb et al.*, 1995].

2.4 Experimental techniques in heterogeneous chemistry

2.4.1 Experimental Approach

Gas uptake into a liquid consists of a sequence of steps: diffusion of the gas to the liquid surface, transport across the interface, diffusion and reaction within the liquid. The aim for atmospheric scientists is the quantification of heterogeneous processes and consequently their application to the atmosphere. For this purpose one could simulate the exact atmospheric conditions in the laboratory, such as temperature, pressure, particle size and composition. However, because of the enormous complexity the laboratory realisation of an atmospheric system is very difficult and

laborious. An alternative is to investigate each process and its dependence on relevant conditions separately. Subsequently the individual steps can be combined and the overall transfer rate determined. This second approach has a few advantages. By choosing appropriate conditions the step under investigation can be made rate limiting and examined as function of physical parameters (concentration, temperature, pressure, solubility, etc.). Once these data are established they can be applied to atmospheric interpretations and used in models to calculate the behaviour of a compound under varying conditions and in concurrence with other substances. In this way predictions can be made without direct measurements [*Hanson et al.*, 1994].

2.4.2 Experimental techniques used in heterogeneous chemistry

Measuring heterogeneous parameters for atmospheric chemistry consists, in principle, of exposing a condensed phase to the gas under investigation and following any loss processes. Difficulties emerge in adjusting the experimental set-up to ensure well-characterised conditions, in accordance with the underlying theory, in order subsequently to be able to unravel the overall process and extract physical parameters. Over the past decade a variety of techniques have been developed to study heterogeneous interactions. They differ mainly in length of contact time and shape of the heterogeneous boundary, as can be seen in Table 2.2, and will be described briefly.

Stop-flow technique

Early measurements of accommodation coefficients by *Tang and Lee* [1987; 1988] were performed using stop-flow techniques. A flow of gas is adjusted over a flowing liquid in a low pressure cell. As soon as stability is reached the gas flow is sealed off and the gas phase over the liquid becomes stagnant. Accommodation coefficients can be extracted from the decrease in gas phase concentration.

	Stop-flow technique [a b]	Knudsen cell [c d]	Aerosol chamber [e f g]	Aerosol flow tube [h i]	Wall-coated flow tube [d]	Droplet train [d e j]	Bubble column [d k]	Liquid jet [e l m]
typical working pressure /Torr	30 - 80	10^{-3}	760	630 - 780 [n]	10 - 80 [o]	10 -100	760	760 [p]
typical exposure time /s	10 - 1000	1000	> 100	10 - 100	~ 1	10^{-3}	10^{-1} - 1	10^{-3}
typical condensed surface area /cm^2	100	10	10^3	10^3	50 - 500	10^{-1}	10^3 - 10^4	10^{-2}
typical condensed surface to gas volume ratio /cm^2 cm^{-3}	10^{-1}	10^{-2}	10^{-5}	10^{-5}	2	10^{-4} - 10^{-3}	1 - 5	10
nature of surface	film	film	droplet	droplet	film	droplet	bubble	jet
detection limit of γ	10^{-4} - 10^{-2}	10^{-6} - 1.0	10^{-7} - 10^{-1}	10^{-4}	10^{-6} - 10^{-1} [q]	> 10^{-5}	10^{-7} - 10^{-4}	10^{-5} - 10^{-2}

Table 2.2 Typical experimental parameters for heterogeneous laboratory reactors.

[a] [*Tang and Lee*, 1987]
[b] [*Finlayson-Pitts and Pitts, Jr.*, 1986]
[c] [*Rossi*, 1996]
[d] [*Kolb et al.*, 1995]
[e] [*EUROTRAC*, 1996]
[f] [*Palm et al.*, 1997]
[g] [*Wahner et al.*, 1998]
[h] [*Lovejoy et al.*, 1995]
[i] [*Baker et al.*, 1999]
[j] [*Gardner et al.*, 1987]
[k] [*Shorter et al.*, 1995]
[l] [*Mertes and Wahner*, 1995]
[m] [*Kirchner et al.*, 1990]
[n] *Hanson and Lovejoy* [1996] also reported measurements at 180 Torr.
[o] *Behnke et al.* [1997] worked at atmospheric pressure.
[p] *Mertes and Wahner* [1995] worked at ~ 250 Torr.
[q] *Hanson and Lovejoy* [1996] have given an upper limit of $\gamma \sim 10^{-2}$ for uptake measurements on pure water at 273 K using the wetted-wall technique. Higher uptake can not be determined exactly due to the high partial vapour pressure of water which implements gas diffusion limitations.

Knudsen cell reactor

The Knudsen cell reactor is built of two chambers which are separated by a valve. The lower chamber contains either the liquid or the solid surface at a constant temperature. The gas enters the upper chamber and can exit through an aperture whose size can be varied. The pressure is low enough to ensure molecular flow. When the valve between the two chambers is opened gas phase is lost due to uptake by, reaction on, or diffusion into, the condensed phase. The gas concentration signal measured at the aperture decreases and is used to derive an uptake coefficient [*Golden et al.*, 1973; *Baldwin and Golden*, 1979; *Baldwin and Golden*, 1980]. The Knudsen cell is a straightforward technique. Recently *Rossi* [1996] reported on investigations of various heterogeneous reactions important in the atmosphere employing a Knudsen cell. However, the application is limited to surfaces with low vapour pressures to ensure constant pressure in the cell and slow processes due to long contact times of tens to hundreds of seconds.

Aerosol reactors

Aerosol reactors have long been used in uptake measurements (see *Finlayson-Pitts and Pitts* [1986] and *Kolb et al.* [1995] for references) but have recently been updated. An advantage of the aerosol technique is the significantly smaller gas diffusion resistance in comparison with bulk experiments. Since the correction for gas diffusion magnifies with the dimension of the surface, measurements on micron-sized aerosol particles need only small corrections. In addition, the uptake can be studied as a function of aerosol size [*Hanson and Lovejoy*, 1996].

The aerosol can be produced by commercial nebulisers [*Hu and Abbatt*, 1997] or obtained by atomising aqueous solutions and drying the droplets [*Molina et al.*, 1996b; *Behnke et al.*, 1997]. It is common to insert the aerosol into a flowing gas stream ("entrained aerosol flow tube"), e.g. *Lovejoy and Hanson* [1995], *Hanson and Lovejoy* [1996], *Hanson* [1997], *Baker et al.* [1999]. To prevent the particles from

settling the pressure is significantly higher than in other reactors, such as wetted-wall flow tube and Knudsen cell [*Lovejoy et al.*, 1995; *Molina et al.*, 1996b].

Aerosol uptake has also been investigated under static conditions whereby the aerosol is brought into a closed volume ("aerosol chamber"). *Behnke et al.* [1997] have used Teflon bags to investigate loss of N_2O_5 in smog chamber experiments.

Wall-coated flow tubes

Flow tubes have been used for many years to study gas-liquid interactions [*Danckwerts*, 1970]. With the growing awareness of the importance of heterogeneous chemistry flow tube techniques have been further innovated over the past decade. One can distinguish between two approaches which use either a static or a flowing surface lined along the inside of a cylindrical tube. The gas is introduced in the centre of the tube by a movable injector which allows variation in contact time. The wall loss of gas species to the liquid or solid surface is detected as a measure of gas uptake. In general, time scales studies are much faster when compared with techniques described above (see Table 2.2) allowing uptake measurements from 10^{-6} to 10^{-1}. The liquid surface area is known accurately and the mathematics of mass transport processes are well-defined in cylindrical tubes which is advantageous in data analysis [*Kolb et al.*, 1995]. However, gas diffusion can limit measurements of large uptake values.

Wetted-wall techniques have been widely used to study reactive uptake on liquids [*Hanson and Ravishankara*, 1991; *Utter et al.*, 1992; *Rudich et al.*, 1996a; *Behnke et al.*, 1997; *Imamura et al.*, 1997; *Scheer et al.*, 1997; *Frenzel et al.*, 1998; *Schweitzer et al.*, 1998]. The Aeronomy laboratory in Boulder, Colorado, have modified the flow tube for solubility measurements by mounting it horizontally thereby providing a static surface. The inside wall was coated either by applying the liquid with a rod at low temperatures (~ 200 K) [*Hanson and Ravishankara*, 1994; *Zhang and Leu*, 1997] or by rotating the flow reactor about the horizontal axis [*Lovejoy et al.*, 1995; *Hanson*, 1997]. In some experiments a trough-shaped container at the bottom of the flow tube

provided a planar liquid surface [*Hanson and Ravishankara*, 1993]. This arrangement has also been used for measurements on ice surfaces [*Hanson*, 1992]. In another modification of the technique, *Leu et al.* [1995] used a horizontal flow tube with a flat bottom to hold solid sodium chloride substrate in heterogeneous uptake studies of gaseous HNO_3 and N_2O_5.

Droplet train

Gas uptake can be measured by passing a fast moving train of droplets through a low pressure flow tube. The droplets are formed by forcing the liquid through a vibrating orifice. The gas of interest can enter at different inlets which, together with changes in droplet velocity, permit variation of contact times. By changing the droplet frequency it is possible to obtain different droplet surface areas. Careful pressure control is essential to ensure a constant surface temperature, and thus a constant droplet size, by preventing any growth or evaporation. Interaction times are typically between 1 - 20 ms which allows measurements of uptakes of $\gamma \geq 10^{-5}$ [*EUROTRAC*, 1996].

Gardner et al. [1987] and *Worsnop et al.* [1989] pioneered this technique but numerous droplet train studies have been reported since [*Van Doren et al.*, 1990; *Jayne et al.*, 1991; *Jayne et al.*, 1992; *Ponche et al.*, 1993; *George et al.*, 1994; *George et al.*, 1995; *Heal et al.*, 1995; *Hu et al.*, 1995; *Magi et al.*, 1997; *Scheer et al.*, 1997; *Schweitzer et al.*, 1998; *Shi et al.*, 1999a].

Bubble columns

To complement the droplet train *Shorter et al.* [1995] have employed a bubble column apparatus for heterogeneous experiments. This technique has interaction times between 0.1 - 1 s and is capable of measuring uptake in the range of 10^{-4} to 10^{-7}. The principle is that the gas enters a liquid filled column at the bottom where it forms bubbles. The bubbles rise through the liquid to the top. Deduction of quantitative

parameters requires knowledge of the size and shape of the bubbles [*De Bruyn et al.*, 1995].

To overcome limitations between mathematical description and experiment *Swartz et al.* [1997] have developed a horizontal bubble train where well-defined single bubbles travel horizontally in a liquid flow.

Liquid jet

Kirchner et al. [1990] describe a technique for ambient pressure whereby a thin jet of liquid comes into contact with the flowing gas surrounding the jet. The very short interaction times (0.03 - 1 ms) can be adjusted by changing the jet length. However, sophisticated data evaluation procedures are required for quantitative results. *Mertes and Wahner* [1995] have used the liquid jet technique in uptake measurements of gaseous NO_2 and HNO_2 on aqueous surfaces.

Other techniques

There exist other laboratory techniques which have also been used to study heterogeneous interactions. For example, *Takami et al.* [1998] have employed an impinging flow method, *Danckwerts* [1970] describes wetted-sphere and moving band absorbers which have been used in engineering science, whilst *Rubel and Gentry* [1984] have worked with so-called single particle levitation.

3. EXPERIMENTAL

3.1 Introduction

In this chapter the experimental apparatus employed in this work is described in detail. Uptake measurements were performed using a wetted-wall flow reactor. The equipment for the preparation of gaseous mixtures of ozone and for the control of the gas flows is discussed. Temperature dependent measurements of Henry's law coefficients were carried out in the thermostatically controlled bubble column. The analytical techniques applied are also specified.

3.2 Gas handling

A purpose-built vacuum line was constructed to handle the gaseous ozone and to prepare mixtures of ozone in helium. It was made of Pyrex glass incorporating Young's greaseless taps. Gas mixtures were admitted *via* isolable sidearms, storage taking place in two 6 l glass bulbs. For the ozone experiments the whole vacuum line was covered with black cloth to prevent decomposition of ozone. The line could be evacuated using a small oil diffusion pump backed by a rotary pump (Edwards, E2M5). Pressures were measured by a 0 - 1000 Torr range capacitance manometer (Edwards, Barocel 600AB). All gas lines were made of Teflon tubing, and stainless steel Ultratorr fittings were used as connectors. All gas flows were monitored with mass flow meters (Tylan, FC 280 SA, control box RO-28), with control ranges of 0 - 300 and 0 - 3000 standard cubic centimetres per minute (sccm).

3.3 Wetted-wall flow reactor for uptake measurements

3.3.1 Description of the wetted-wall flow reactor

The uptake of various gases on aqueous surfaces was investigated using a wetted-wall flow reactor designed and constructed entirely from scratch during this thesis work. A gas stream flows down a vertically mounted flow tube, the walls of which are covered by a thin liquid film continuously flowing down under the influence of gravity. The heterogeneous loss of compounds in the gas phase can be used to derive uptake parameters. The experimental set-up is similar to the one described by *Utter et al.* [1992]. The wetted-wall reactor is pictured in Figure 3.1; a schematic diagram is shown in Figure 3.2.

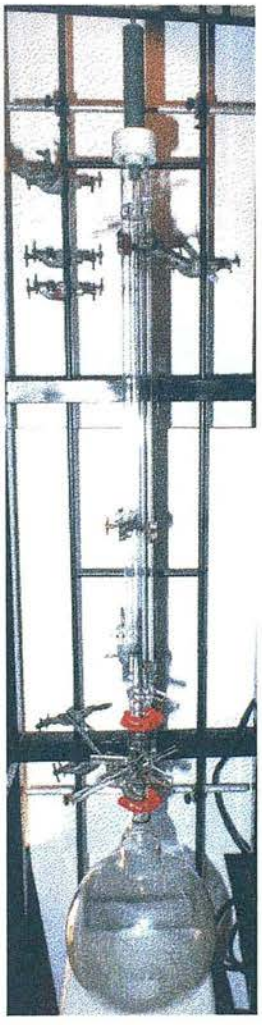

Figure 3.1 The wetted-wall flow reactor

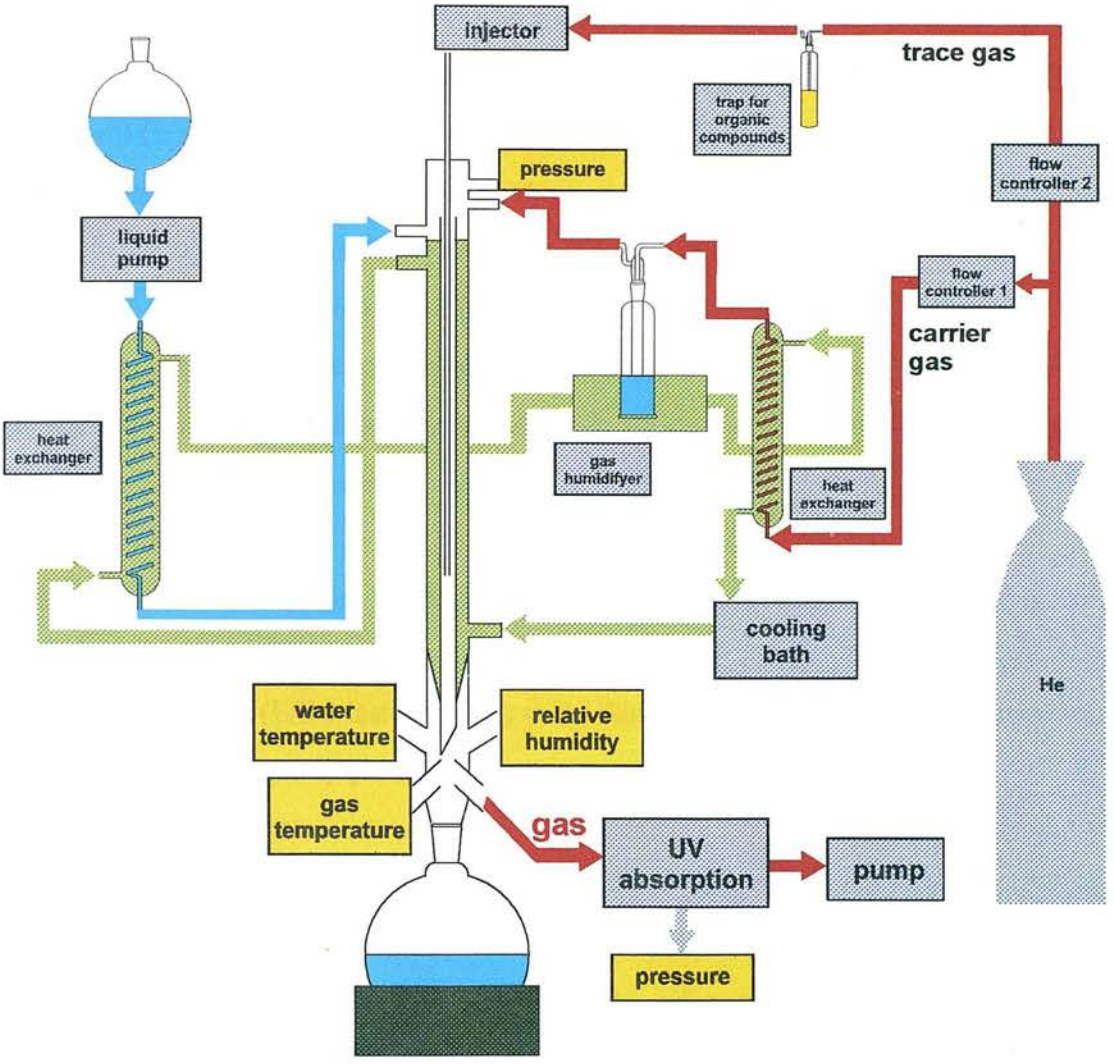

Figure 3.2 Schematic diagram of the entire wetted-wall flow reactor system

The reactor, constructed of Pyrex glass, was about 90 cm long with an internal diameter of 1.6 cm. To maintain a constant experimental temperature the flow tube was surrounded by a glass jacket containing a 1:1 mixture of ethylene glycol with water as coolant fluid. A recirculating chiller (Cole-Parmer, Polystat) was used to pump coolant through the system and also to pre-cool the aqueous solution and the carrier gas, prior to their entering the reactor. For this purpose two glass coil heat exchangers (28 and 50 cm long) were built.

The water, used pure or to make aqueous solutions, was deionised to a resistivity of 10 MΩ cm (Whatman, Analyst 25) and stored in a 6 l tank above the flow tube. For some experiments the water was degassed by either bubbling helium gas through the tank for different lengths of time (30 min to up to 24 h) or by using an ultrasonic bath (Grant, XB14). After passing through a heat exchanger the water reached a collecting space in the upper reactor. By spilling over the attached lip, the water formed a thin film of downwards flowing liquid, wetting the entire inner surface uniformly. The water was gathered at the bottom of the reactor using a 6 l flask, which was cooled by an ice-salt mixture to a temperature of about -15 °C to prevent back streaming of water vapour into the flow tube.

Initially water was supplied to the flow reactor by gravity feed and measured using a Teflon flow meter (Cole Parmer). In later experiments the liquid was pumped by a digital liquid pump (L/S Masterflex). A pulse dampener (Cole Parmer) was fitted into the line to eliminate pump pulsing.

During the construction of the wetted-wall flow reactor other methods of supplying the water film at a constant rate down the reactor walls were considered. In a variation on a spray tower, the water from the pressurised reservoir was splashed directly onto the inner walls of the reactor. However, it proved difficult to construct the glass-made sprayer with symmetrical holes. Another idea of dripping the water onto a rotating magnet plate which would spread the water onto the inside of the reactor was not realised since it would require very sophisticated mechanical constructions located in the upper part of the flow reactor. Therefore, the overflow method was utilised to supply water as a liquid film in the wetted-wall flow reactor.

It was necessary to clean the inner surface of the flow tube regularly to ensure uniform wetting. This was done by washing the wall with detergent, followed by rinsing with deionised water. When the reactor was not used for longer periods it was filled with cleaning solution. Various detergents were tried: chromic acid, NaOH solution and Decon 90 (Prolabo); eventually, it was decided to use Decon 90

exclusively. It was explored whether the uniform wetting of the flow tube could be helped by modifying the overflow tip. A Teflon insert was built which fitted exactly into the top of the inner tube of the flow reactor leaving only a very narrow space between insert and flow tube. The water was forced through this gap in order to distribute it more evenly around the inside walls of the flow reactor. However, difficulties were experienced in holding the insert in a fixed place and since the wetting seemed to be only marginally ameliorated use of the insert was discontinued.

The water lines consisted of ¼ " Nylon tubing (Cole Parmer) which were jacketed by foamed rubber tubing (Cole Parmer) for temperature insulation. The reactor was additionally covered with bubble wrap for experiments at low temperatures (~ 278 K).

The trace gas of interest entered the reactor through the movable injector with an inner diameter of 3 mm. Different exposure times could be achieved by varying the injector position. A specially designed injector holder ensured the central alignment of the injector, even when the injector was at its most fully extended (lower) position. The gas exited the reactor *via* a side arm below the wetted film.

The helium carrier gas entered the reactor at a side arm. It was humidified before entering the reactor to avoid evaporative cooling of the liquid film and to maintain a well-defined temperature in the reactor. Humidification was achieved by passing the gas through a thermostatically controlled water bubbler containing deionised water. The relative humidity was measured using a humidity meter (Vaisala, HMP 234).

The gas flow rates were regulated by calibrated electronic mass flow meters (Tylan, FC 280 SA; control box RO-28), with control ranges of 0 - 300 and 0 - 3000 standard cubic centimetres per minute (sccm). The total gas flow was varied in the range of 0.3 - 3 l min^{-1} (STP) which corresponds to a linear gas velocity (c) of 50 - 2000 cm s^{-1} under the experimental conditions used.

Even though the reactor has a total length of 90 cm with a maximum contact length of 80 cm, the usable reaction zone is only ~ 68 cm long. The first 12 cm region was allowed for the laminar gas flow to establish and for the water vapour to saturate the helium stream. The remaining reaction zone leads typically to contact times between gas and liquid in the range of 0.03 - 0.3 s.

Although the uptake measurements in this work are based on the analysis of the gas phase only, future work could include the investigation of the aqueous phase. For this purpose a Pyrex glass adapter with greaseless Young's taps was built for the bottom end of the flow tube. It allows the attachment of up to three flasks which can be switched over during a flow experiment and are isolable. In this way, sequential samples of the aqueous phase can be taken without having to stop the experiment, which is the case when only a single receiver flask is connected to the reactor.

Liquid flow rates were calibrated using a specially built flask. It had the form of a large test tube (inside diameter of 46 mm, 35 cm length) and was connected to the bottom of the flow reactor. A measuring scale (0 - 50 cm; 1 mm divisions) was calibrated for liquid volumes.

The experiments were performed in a temperature range of 278 - 303 K. The temperature of the flowing liquid and the gas were checked by immersing thermocouples (RS, air and general purpose probe, type K) at the bottom of the reactor. The gas temperature was double-checked by comparing it with the temperature reading at the humidity meter.

The wetted-wall flow reactor was operated at low pressures, typically 10 - 100 Torr. The pressure for a specified flow rate was adjusted by a precision needle valve (RS). The low pressure flow was provided by an Edwards E2M12 rotary pump. The pressures were monitored using capacitance manometers (Edwards, Barocel 600AB) with either 0 - 100 or 0 - 1000 Torr scales. Pressures within the system were measured at the top as well as at the UV cell.

Uptake coefficients for gases onto liquid water surfaces in the region of 10^{-6} to ~ 10^{-1} can be measured with the described wetted-wall technique. The method has the advantages that the liquid surface is constantly renewed, and therefore the composition of the liquid film remains essentially constant. The well-established mass transport theory for cylindrical flow tube reactors can be applied to the data analysis (see Chapter 4) [*Kolb et al.*, 1995].

3.3.2 UV absorption detection

Changes in trace gas concentrations were measured using long path wavelength-resolved UV absorption spectroscopy in the range 200 - 350 nm.

After contact with the liquid surface the gas exited the wetted-wall flow reactor through a sidearm at the bottom of the reactor. It flowed through a 90 cm long cylindrical gas cell which was made of Pyrex glass. Two quartz windows (U.Q.G., Spectrosil B), with a diameter of 60 mm and a thickness of 3 mm, were attached at both ends of the cell using Halocarbon wax.

The light source was a 150 W Xe lamp (Osram, XBO). The light beam passed through an iris, the gas cell and a 10 cm focusing lens (Ealing) onto the spectrograph. A shutter (Oriel) controlled by the software was fitted to the lamp housing. Different neutral density filters (Lambda Photometrix), with an optical density ($= \log(I_{\text{before filter}}/I_{\text{after filter}})$) of 0.1 (79 % transmission) and 0.3 (50 % transmission), were used during the course of the work to attenuate the intensity of the light beam in order to prevent saturation of the detector. Wavelength calibration of the Xe lamp was achieved by comparison of known line positions from a low pressure mercury lamp [*CRC Handbook of chemistry and physics*, 1993]. The gas cell as well as any lenses and filters were mounted onto an optical bench to achieve optimum co-linear alignment. At least 30 min were allowed for the lamp warm-up.

The UV was dispersed using a f/4 grating spectrometer (Instrument SA, 270M Rapid Scanning Imaging Spectrograph) with a focal length of 270 mm. Two different gratings were available as dispersion elements: a 300 groove mm^{-1} grating with a 250 nm blaze, and a 600 groove mm^{-1} grating with a 500 nm blaze, which covered wavelength ranges of 316 nm and 158 nm, respectively. A total spectral range from about 170 to 500 nm for the 300 groove mm^{-1} grating and from about 330 to 1000 nm for the 600 groove mm^{-1} grating could be scanned. The gratings gave a dispersion of approximately 12.4 nm mm^{-1} (0.310 nm $pixel^{-1}$) and 6.2 nm mm^{-1} (0.155 nm $pixel^{-1}$), respectively, onto the photodiode array detector (PDA). The maximum resolution on the PDA was approximately 3 pixels width (for a 10 μm entrance slit) which corresponds to about 0.9 nm for the 300 groove mm^{-1} grating and 0.5 nm for the 600 groove mm^{-1} grating.

The dispersed light was detected with a 1024 element photodiode array (Instrument SA, QuikScan). As a multichannel detector, the PDA had the advantageous feature of allowing the simultaneous measurement of a complete spectrum with a scanning rate of 12.8 μs $diode^{-1}$ which could measure a spectrum in 13.3 ms. The size of a PDA element was 25 μm x 2.5 mm, resulting in a light sensitive area of 25.6 mm x 2.5 mm.

The output of the Xe lamp rose steeply between 240 and 270 nm. The absorption maxima for the compounds investigated were in the wavelength range of about 260 - 280 nm. A part of the PDA was therefore masked out to permit detection of high intensity of light at the wavelength range of interest without saturating the detector.

The integrated software package (Instrument SA, SpectraMax) was used for the control of the spectrograph as well as for data acquisition and analysis. The software allowed data manipulation in real time and was also used to trigger the safety shutter. Raw spectral information from the PDA was linearized into wavelength units (nm). Various acquisition methods were created and could be stored for further use; these featured multiple repetitions and delay sequences.

Measurements were performed by, firstly, measuring a spectrum of the background signal. This background spectrum was stored and subtracted automatically from all following spectra by the SpectraMax software. This compensated for the electronic amplifier offset and the dark current of the PDA. Then, a spectrum of the evacuated gas cell was taken as the initial light intensity I_0 (see Chapter 4). This spectrum was also stored. Finally, the absorption spectra of the gaseous species were measured.

Typically, 10 single measurements ("accumulations") were summed up and averaged to give one spectrum. For each injector position at least 5 spectra were recorded. Often, an experiment consisted of measuring at all six injector positions, moving the injector out (from position 0 to 5) and then in (position 5 to 0) recording 5 spectra at each position. The data analysis were therefore based on a total of 100 integrations for each position. Spectra could be repeated ("cycles") without any delay or at intervals of parts of seconds to up to several minutes ("cycle time"). As a result, a row of spectra representing different injector positions was obtained. When loaded into a 3-D display (x-axis: wavelength, y-axis: absorbance, z-axis: spectrum number), as shown in Figure 3.3, it was possible to obtain a cut through all spectra at the absorption maximum which resulted in a plot of absorbance *vs.* spectrum number at the wavelength of maximum absorbance (Figure 3.4). This was used in the data analysis (see Chapter 4).

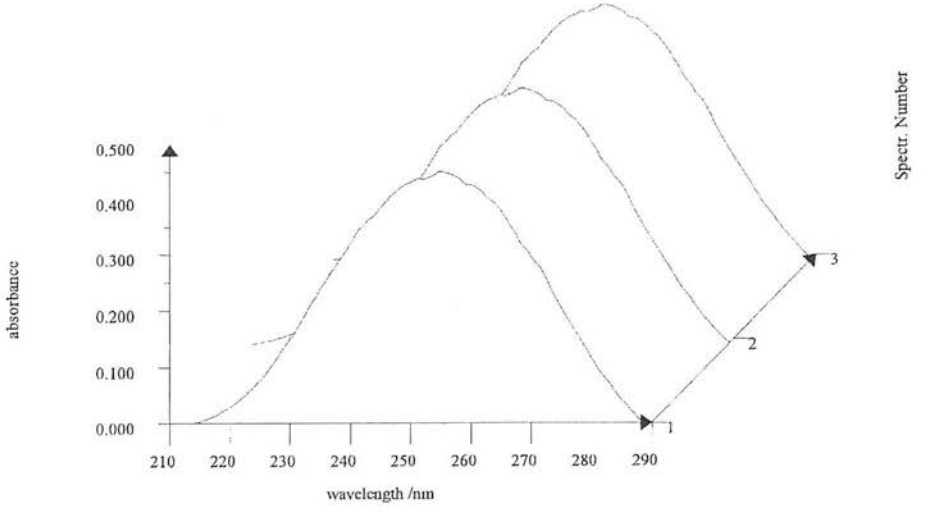

Figure 3.3 3-D display of absorption spectra of ozone.

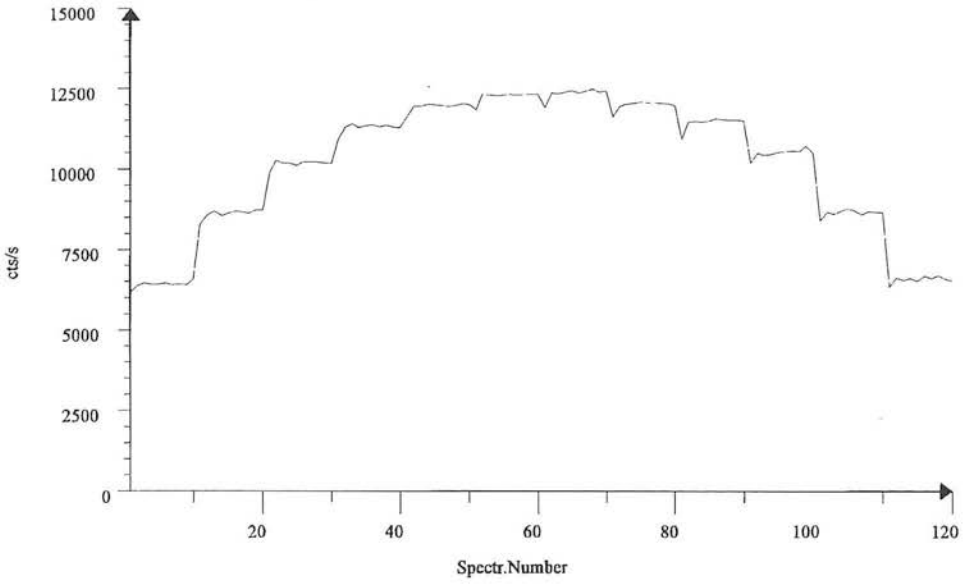

Figure 3.4 Change of detector signal with change of injector position obtained by cutting through the absorption maximum of 3-D display, as shown in Figure 3.3 and described in the text. 10 spectra were taken at each injector position (spectrum 1 to 60: moving the injector out; spectrum 61 to 120: moving injector in).

3.3.3 Chemicals

3.3.3.1 Ozone

Generation

Ozone was produced by an electrical discharge generator (Argentox, GL 10). A flow of oxygen (BOC) was passed through the generator and the ozone trapped on a dry ice - ethanol trap (~ 195 K). The trap was filled with silica gel (Fisons, 1 - 3 mm, 6 -16 mesh). Discharge conditions were varied between 150 - 220 V and 0.34 - 0.64 A with oxygen flow rates of 0.8 - 1.5 l min^{-1}. Enough ozone was usually produced after 20 - 60 min, visible from the deep purple colour of the silica gel. It was possible to store the ozone in the cold trap for several months.

Mixtures of ozone

Mixtures of ozone in helium were prepared on the vacuum line. After evacuation of the line, the silica trap with the adsorbed ozone was opened and the trap slowly warmed to room temperature by removing the dewar containing the ethanol - dry ice mixture from around the trap. The desorption of the ozone was followed by the pressure rise in the vacuum line, and by the decolourization of the silica gel. Helium (BOC) as the carrier gas was admitted *via* a sidearm. It was possible to keep the mixture for a few days in the darkened bulbs of the line; the ozone content would slowly go down over several hours and days.

Determination of ozone concentration

The ozone concentration of the gaseous mixtures of ozone in helium was determined by UV absorption spectroscopy with the system described above (see Section 3.3.2). The Beer-Lambert law states that the absorbance, A, of a substance i is proportional to its concentration, [i] (mol l^{-1}),

$$A = \varepsilon l [i] \qquad (3.1)$$

where l is the path length (cm) and ε is the molar absorption coefficient (l mol^{-1} cm^{-1}), also called molar absorption cross section, for i at a given wavelength. The concentration can be calculated if the absorption coefficient is known.

3.3.3.2 Aromatic compounds for uptake measurements

The aromatic compounds investigated are all in a condensed physical state at the temperatures at which the experiments were performed. A small trap of about 10 cm length was used to hold the substance. Two Young's taps allowed easy filling. Crystalline phenol (BDH, > 99 %) and 2-nitrophenol (BDH, > 99 %) were ground in a mortar before transferring them into the trap. The liquid m-cresol (BHD, > 98 %) was placed directly in the trap. The helium for the trace gas flow, controlled by a mass

flow meter (Tylan, FC 280 SA; control box RO-28), was passed through the trap. The tube from which the gas emerged ended in a sintered disk to support an intensive contact between the gas and the aromatic compound. In this way a continuous flow of trace gas could be provided. However, this method of entrainment is only applicable for compounds with a high enough vapour pressure at ambient temperature.

3.3.3.3 Other test substances

When the UV spectrometer unit was initially set up, other substances were used to compare the spectra obtained with spectra of another UV spectrometer available in the department (Unicam, UV2). Acetone (Fisher, > 99 %) and sodium dichromate (Fisons, > 99 %) were chosen as test substances since they were available in the laboratory and they absorb in the UV region of the electromagnetic spectrum. The high vapour pressure of acetone allows the easy preparation of gaseous mixtures in helium which were prepared in a similar manner to that described for ozone (see Section 3.3.3.1). Sodium dichromate, $Na_2Cr_2O_7 \cdot 2H_2O$, was prepared as solution in water in concentration ranges of 10^{-5} - 10^{-4} mol l^{-1}. The absorbance of the solution was measured in disposable UV cuvettes made of optical methacrylate (Merck, 10 mm path length) using a standard cuvette sample holder.

A second cylindrical gas cell of 9.9 cm length was made for the measurements on the Unicam spectrometer. The body consisted of Pyrex glass and two Young's taps allowed gas flow through the cell for flushing and filling. The quartz windows (U.Q.G., Spectrosil B), with a diameter of 25 mm and a thickness of 2 mm, were attached by means of Halocarbon wax.

3.3.3.4 Scavenger solutions

Ozone is not very soluble in pure water, with a Henry's law coefficient of 1.15 x 10^{-2} M atm^{-1} at 298 K [*Magi et al.*, 1997]. The uptake can be limited by surface saturation.

The addition of a scavenger to the liquid phase, which reacts with ozone, removes the ozone from the surface and enhances the uptake rate of ozone.

Sodium thiosulfate, $Na_2S_2O_3$, (Acros, > 99 %) was chosen as scavenger in our experiments. Solutions with concentrations between 0.02 and 0.20 mol l^{-1} were prepared by weighing out (Mettler balance, AJ150) the appropriate amount of $Na_2S_2O_3$ and dissolving it in deionised water using an ultrasonic bath (Grant, XB14). The solution was then transferred to the reservoir tank above the flow reactor.

A similar approach of using a scavenger was tried for the aromatics. It is known that phenol reacts readily with bromine water [*Beyer et al.*, 1997] which is visible from the decolourisation of the yellow-brownish bromine water. The bromine water was prepared by transferring 1-2 ml bromine (Fisher, > 99 %) into a water volume of about 2.5 l of deionised water. The mixture was stirred overnight with a magnetic stirrer. Uptake measurements were performed on bromine water for phenol, 2-nitrophenol and m-cresol. However, it was noticed that the aggressive bromine fumes damaged the humidity probe, and so the experiments involving bromine were discontinued.

3.4 The bubble column for Henry's law coefficient measurements

3.4.1 Description of the bubble column

A bubble column apparatus was built to measure Henry's law coefficients. Gas is bubbled through the aqueous solution containing the solute of interest which is stripped from the solution. By measuring the decrease in aqueous concentration the Henry's law coefficient can be deduced. The bubble column is shown in Figure 3.5; Figure 3.6 shows a schematic diagram of the apparatus.

Figure 3.5 Bubble column for measuring Henry's law coefficients

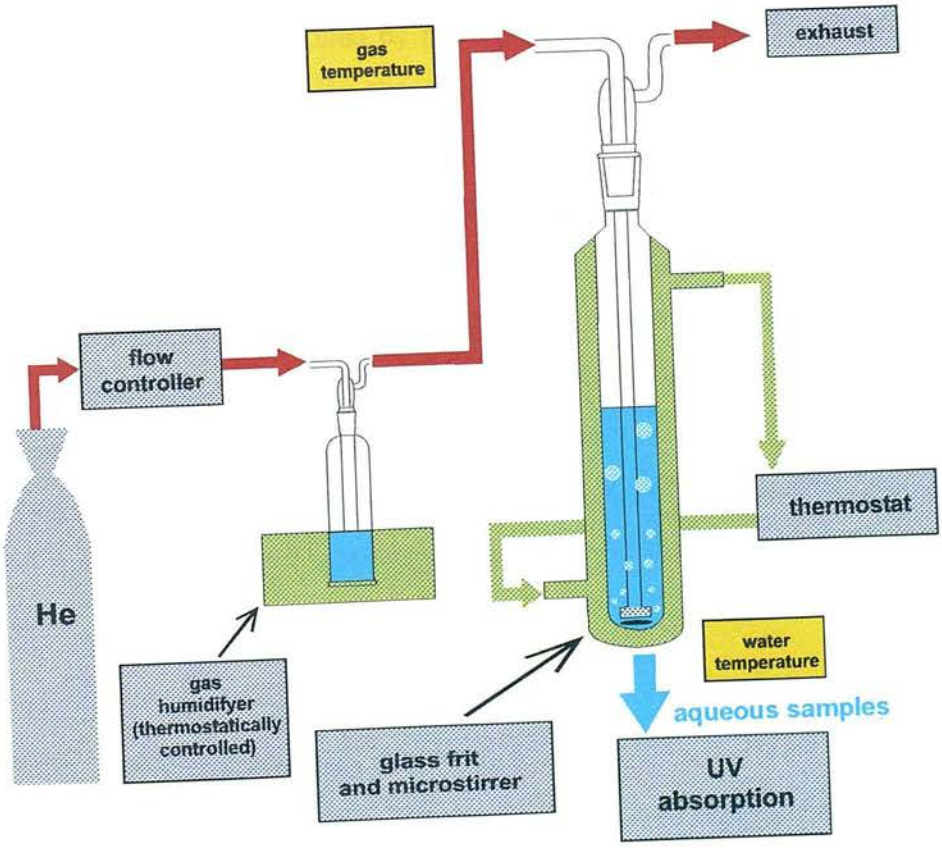

Figure 3.6 Schematic diagram of the entire bubble column apparatus

The Pyrex glass bubble column was 51 cm high with an internal diameter of 2.4 cm. The gas was introduced through a sintered glass disk (Pyrex 2, 40 - 100 μm) into the bottom of the column. Care had to be taken to ensure the free rise of the gas bubble through the liquid. In initial trials the bubbles got caught underneath the frit, merged together and rose unsteadily to the surface. Therefore, the pores of the disk were opened to the sides which subsequently allowed unhindered ascent. A linear scale (1 mm unit) was fixed to the column and calibrated for liquid volumes.

The liquid temperature was controlled by a coolant (1:1 mixture of ethylene glycol and water; Cole Parmer) flowing through the jacket surrounding the bubble column (Cole Parmer, recirculation bath). A powerful magnetic micro stirrer (Cole Parmer) ensured vigorous mixing of the liquid in the bubble column; random tests confirmed a uniform liquid concentration over the whole column height. The measurements were taken at 5 K intervals between 278 and 303 K.

The gas flow was controlled by mass flow meters (Tylan, FC 280 SA; control box RO-28) and were between 100 - 1000 cm^3 min^{-1} (STP). The gas, typically helium (BOC), was humidified prior to entering the bubble column to prevent water evaporation from the stripping column. For this purpose the gas was passed through a vessel containing deionised water (10 MΩ cm, Whatman, Analyst 25). The vessel was immersed into a water bath set to the same temperature as the bubble column. The temperature was checked with a liquid temperature probe (RS, general purpose probe, type K). No change of liquid volume was noticed, even after stripping for several hours. The measurements were taken at low and atmospheric pressures; the pressure was measured by a capacitance manometer (Edwards, Barocel 600AB).

3.4.2 Analytical methods

The process of solute elution was monitored alternatively by measuring the concentration of the purged solute in the gas phase or by determining the decrease of solute concentration in the liquid phase.

3.4.2.1 Gas phase

Gas phase concentrations were measured using UV absorption spectroscopy. The system description can be found in Section 3.3.2. The UV cell was connected to the gas outlet of the bubble column. The gas exiting the bubble column passed through the UV cell. A rotary pump (Edwards, E2M12) was used for experiments at low pressure.

3.4.2.2 Liquid phase

For the bulk of the stripping experiments the change of the liquid phase concentration was analysed. The process of solute elution was monitored between 30 min to up to 2 h. During that time liquid samples were taken in intervals of 5 - 25 min depending on gas flow rate and liquid volume. After purging for several minutes the gas flow was stopped and a sample of about 3 cm^3 of the liquid solution taken. The UV absorbance was measured in a double beam spectrometer (Shimadzu, UV 160A) against pure water using a matching pair of UV quartz cuvettes (Hellma, path length of 10 mm). The measured sample was then placed back into the bubble column taking care to ensure a transfer free of losses. No diminution of volume was detected. For different liquid heights in the bubble column (about 8 for one temperature and one gas flow rate) at least four single absorption measurements were taken. Therefore, one H value for one temperature and one gas flow rate consisted of at least 32 single absorption measurements.

3.4.3 Chemicals

Henry's law is only valid for dilute solutions (see Chapter 2). Aqueous solutions (10^{-5} - 10^{-4} mol l^{-1}) of 2-nitrophenol were prepared by weighing out the appropriate amount of chemical and dissolving it in deionised water (10 MΩ cm, Whatman, Analyst 25) with the aid of an ultrasonic bath (Grant, XB14).

4. DATA ANALYSIS

4.1 Introduction

This chapter describes the procedures employed in the analysis of the acquired data. To obtain uptake coefficients it is essential to know the exact experimental conditions in the wetted-wall apparatus. The features which determine these conditions are outlined for the gas phase as well as for the liquid phase. Following the description for the calculation of the uptake coefficients is a section which examines the dependence on time for these processes. The extraction of Henry's law coefficients is given for the bubble column in the last section of this chapter. Important factors which influence Henry's law equilibrium are investigated.

4.2 Wetted-wall flow reactor

The uptake coefficients of a trace gas into a liquid phase were calculated from the measured loss of this trace component from the gas phase following exposure to the liquid surface. In the following section it is shown how the data were treated and the procedures for extracting uptake coefficients from the raw data are described. Table 4.1 shows a typical spreadsheet which was compiled for data collection.

4.2.1 General features

4.2.1.1 Injector position and contact length

The wetted-wall flow reactor had six injector positions (0, 1, 2, 3, 4 and 5) marked on the outside, with a distance of 10 cm between each other and sub-units of 0.5 cm. Position "0" was 18 cm above the gas exit. The maximum contact length between gas and water was 68 cm. The injector was moved manually to change injector positions.

Gas

	Inj. pos.	distance from pos. "0"	length of contact between gas and liquid	File	cycle N°	Date	water temp.	gas temp.	F_{STP}	p_{total}	RH	p^*_{H2O}	p_{H2O}
		/cm	/cm				/K	/K	/cm^3 s^{-1}	/Torr	%	/Torr	/Torr
1	0	0.0	18.0	oz3	1	9.3.98	293.0	293.0	5.83	12.0	50	17.5	8.76
2	1	10.0	28.0	oz3	2	9.3.98	293.0	293.0	5.83	12.0	50	17.5	8.76
3	2	20.0	38.0	oz3	3	9.3.98	293.0	293.0	5.83	12.0	50	17.5	8.76
4	3	30.0	48.0	oz3	4	9.3.98	293.0	293.0	5.83	12.0	50	17.5	8.76
5	4	40.0	58.0	oz3	5	9.3.98	293.0	293.0	5.83	12.0	50	17.5	8.76
6	5	50.0	68.0	oz3	6	9.3.98	293.0	293.0	5.83	12.0	50	17.5	8.76

	p_{He+O_3}	F_{exp}	ω	τ	c	D_G	$D_G^P{}_{(O_3-H_2O)}$	$D_G^P{}_{(O_3-He)}$	I_0	I	A	ln A	Re_G
	/Torr	/cm^3 s^{-1}	/cm s^{-1}	/s	/cm s^{-1}	/cm^2 s^{-1}	/Torr cm^2 s^{-1}	/Torr cm^2 s^{-1}	/Cts	/Cts			
1	3.24	1470	3.58×10^4	0.025	731	17.7	175	507	36790	34840	0.024	-3.744	98
2	3.24	1470	3.58×10^4	0.038	731	17.7	175	507	36790	35230	0.019	-3.973	98
3	3.24	1470	3.58×10^4	0.052	731	17.7	175	507	36790	35520	0.015	-4.183	98
4	3.24	1470	3.58×10^4	0.066	731	17.7	175	507	36790	35730	0.013	-4.366	98
5	3.24	1470	3.58×10^4	0.079	731	17.7	175	507	36790	35960	0.010	-4.614	98
6	3.24	1470	3.58×10^4	0.093	731	17.7	175	507	36790	36230	0.007	-5.011	98

Water

	v	v	μ	ρ	δ	u_{avg}	u_s	t	Re_w
	/cm^3 min^{-1}	/cm^3 s^{-1}	/g cm^{-1} s^{-1}	/g cm^{-3}	/cm	/cm s^{-1}	/cm s^{-1}	/s	
1	100	1.67	1.009×10^{-2}	0.998	2.17×10^{-2}	15.3	22.9	0.79	33
2	100	1.67	1.009×10^{-2}	0.998	2.17×10^{-2}	15.3	22.9	1.22	33
3	100	1.67	1.009×10^{-2}	0.998	2.17×10^{-2}	15.3	22.9	1.66	33
4	100	1.67	1.009×10^{-2}	0.998	2.17×10^{-2}	15.3	22.9	2.09	33
5	100	1.67	1.009×10^{-2}	0.998	2.17×10^{-2}	15.3	22.9	2.53	33
6	100	1.67	1.009×10^{-2}	0.998	2.17×10^{-2}	15.3	22.9	2.97	33

Table 4.1 Typical spreadsheet for uptake measurements of ozone.

4.2.1.2 File name, cycle number and date

The date and file name were recorded. One experimental run often consisted of a number of measurements (cycles) within which only the injector position was altered, all other conditions were kept constant. The injector was moved in and out of the flow tube and the positions were changed either systematically or in a random order. The position of the injector for a particular experiment can be derived from the cycle number.

4.2.1.3 Temperature

The temperature set on the thermostat was noted. The thermostat was used to control the temperature of the reactor as well as thermally equilibrate the carrier gas and the liquid prior to their entering the flow reactor. The temperature of the gas and of the liquid were measured at the bottom of the reactor using two temperature probes. The gas temperature was also monitored at the humidity probe. The experiments were performed at temperatures between 278 K and 303 K.

4.2.1.4 Contact area

The area of contact between gas and liquid, A_r (cm^2), is the area of the cylindrical inside-wall of the wetted-wall flow reactor between the injector end (gas entrance) and the end of the flow tube (gas exit). It is calculated from

$$A_r = 2 \pi r z \qquad (4.1)$$

where r is the inside radius of the flow tube (= 0.8 cm) and z is the contact length (cm). The change of contact area by movement of the injector is the difference of the two contact areas, i.e.

$$\Delta A_r = A_{r2} - A_{r1} = 2\,\pi\,r\,(z_2 - z_1).$$

(4.2)

The minimum contact area in the flow reactor was 90 cm^2, and the maximum 342 cm^2.

4.2.2 Characteristics of the gas phase

4.2.2.1 Pressures and relative humidity

The total pressure was continuously monitored in the reactor. The relative humidity and the gas temperature were read at the humidity meter. The vapour pressure of water at the experimental temperature had to be known to be able to work out the partial pressures of water and of the helium gas mixture in the flow reactor. For this purpose known values of the vapour pressure of water [*CRC Handbook of chemistry and physics*, 1993] were plotted against temperature, as shown in Figure 4.1.

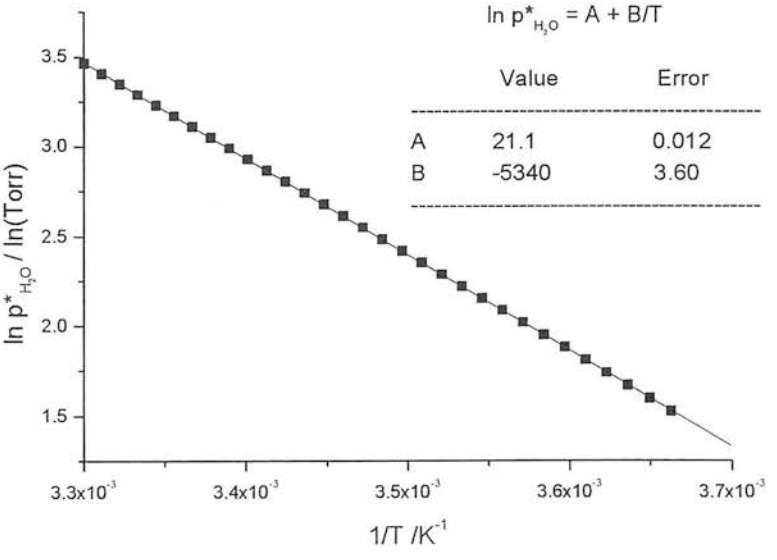

Figure 4.1 Temperature dependence of vapour pressure of water. Values were taken from *CRC Handbook of chemistry and physics* [1993].

The fitted curve (see Section 2.2.3) was used for the calculation of the water vapour pressure, $p^*_{H_2O}$ (Torr), at the experimental temperature, T (K), i.e.

$$p^*_{H_2O} = \exp\left(21.1 - \frac{5340}{T}\right) \tag{4.3}$$

Since the relative humidity, RH (%), is the ratio of the partial pressure of water vapour, p_{H_2O} (Torr), to its vapour pressure at that temperature, $p^*_{H_2O}$ (Torr),

$$RH = 100\frac{p_{H_2O}}{p^*_{H_2O}} \tag{4.4}$$

the partial pressure of water in the flow reactor can be calculated from the measured relative humidity, i.e.

$$p_{H_2O} = \frac{RH\ p^*_{H_2O}}{100}. \tag{4.5}$$

The partial pressure of the gas (i.e. sum of trace and carrier gas), p_g (Torr), is the difference between total pressure, p (Torr), and partial pressure of water, p_{H_2O} (Torr),

$$p_g = p - p_{H_2O}. \tag{4.6}$$

No humidity measurements existed for the first uptake measurements. In this case the humidity was estimated from later measurements at the same temperature, injector position and liquid flow rate.

4.2.2.2 Gas flows

All gas flows were controlled by calibrated mass flow controllers. Their sum is the total gas flow, F ($cm^3\ s^{-1}$), under standard temperature and pressure (STP[1]). The gas flow at the experimental conditions can be calculated from the ideal gas law

$$\frac{p_1 V_1}{T_1} = \frac{p_2 V_2}{T_2} \tag{4.7}$$

where p is the pressure, V is the volume and T is the temperature at two different conditions ($_1$ and $_2$). Using volumetric flows instead of volumes and rearranging eqn (4.7) gives an expression for the experimental gas flow, F_{exp}

$$F_{exp} = \frac{p_{STP} F_{STP}}{T_{STP}} \frac{T_{exp}}{p_g}. \tag{4.8}$$

For example, the following experimental gas flow F_{exp} would be calculated using a standard gas flow F_{STP} of 25 $cm^3\ s^{-1}$, an experimental temperature T_{exp} of 293 K and an experimental pressure p_g of 35 Torr

$$F_{exp} = \frac{760\ \text{Torr} \times 25\ cm^3\ s^{-1}}{273\ K} \frac{293\ K}{35\ \text{Torr}} = \underline{\underline{583\ cm^3\ s^{-1}}}. \tag{4.9}$$

The experimental flow rates were in the range of 100 to 4000 $cm^3\ s^{-1}$.

4.2.2.3 Mean molecular gas velocity

The mean molecular gas velocity, ω, is defined as

$$\omega = \sqrt{\frac{8\ k\ T}{\pi\ m}} \tag{4.10}$$

[1] Note: Standard temperature and pressure, STP, correspond to 0 °C and 1 atm.

where k is the Boltzmann constant (= 1.38066 x 10^{-23} J K^{-1}) and T is the temperature. The molecular mass m can be calculated by multiplying the relative molecular mass M_r by the atomic mass unit m_u (= 1.6606 x 10^{-27} kg).

The molecular velocity for phenol at 293 K is

$$\omega = \sqrt{\frac{8 \times 1.38 \times 10^{-23}\ \text{J K}^{-1} \times 293\ \text{K}}{\pi \left(94.1 \times 1.67 \times 10^{-27}\ \text{kg}\right)}} = 256.0\ \text{m s}^{-1} = \underline{\underline{2.56 \times 10^{4}\ \text{cm s}^{-1}}}\ .$$

(4.11)

4.2.2.4 Gas velocity down the flow reactor

The velocity of the gas, c (cm s^{-1}), flowing down the wetted-wall reactor is calculated by dividing the experimental gas flow, F_{exp}, by the cross sectional area of the flow tube, i.e.

$$c = \frac{F_{exp}}{\pi r^2}$$

(4.12)

where r is the inside radius of the flow tube. For the experimental flow of F_{exp} = 583 cm^3 s^{-1} (from eqn (4.9)), it follows that

$$c = \frac{583\ \text{cm}^3\ \text{s}^{-1}}{\pi\ (0.8\ \text{cm})^2} = \underline{\underline{290\ \text{cm s}^{-1}}}$$

(4.13)

Gas velocities varied between 50 and 2000 cm s^{-1}.

4.2.2.5 Gas mixing time

The calculation of the gas velocity is based on the assumption that the gas and water vapour are completely mixed over the gas-liquid interaction length. The mixing time,

τ_{mix} (s), for two gases in a cylinder is approximately [*Keyser*, 1984; *Hanson et al.*, 1992]

$$\tau_{mix} = \frac{r^2}{5\,D_G} \qquad (4.14)$$

where r is the radius of the cylinder (cm) and D_G is the gas diffusion coefficient ($cm^2\ s^{-1}$). The mixing time is about 28 ms for a typical pressure of 40 Torr at 293 K assuming a D_G of 4.6 $cm^2\ s^{-1}$ estimated by the Fuller method (see Section 4.2.4.3). This mixing time corresponds to a 8 cm length of flow tube for a typical gas velocity of 290 cm s^{-1}. Since the first 12 cm region was not used in the data analysis, it can be assumed that the calculated gas flow rates are valid. For higher gas velocities only the lower injector positions were used in the evaluation of the data.

4.2.2.6 Contact time gas-liquid

The contact time of the gas with the liquid, τ (s), is given by

$$\tau = \frac{z}{c} \qquad (4.15)$$

where z is the contact length (cm) and c is the gas velocity (cm s^{-1}) down the flow tube. Gas contact times were typically between 0.03 and 0.3 s but could have values of 9×10^{-3} to 1.4 s.

4.2.2.7 Reynolds number of the gas flow

The dimensionless Reynolds number is a criterion by which the type of flow can be characterised. In a laminar flow, the fluid travels along well defined streamlines whereas in a turbulent flow, local velocities and pressures fluctuate irregularly and randomly. Below a critical value of the Reynolds number (< 2100) the flow is laminar,

while above this value (2100 - 5000) a transition to turbulent flow (> 5000) occurs. The Reynolds number of the gas flow, Re_G, is given by [*Perry and Green*, 1997]

$$Re_G = \frac{2rc\rho}{\mu} \qquad (4.16)$$

where r is the radius of the flow tube (= 0.8 cm), c is the gas velocity (cm s^{-1}), ρ is the density of the gas mixture (g cm^{-3}) and μ is the viscosity of the mixture (g cm^{-1} s^{-1}). The Reynolds number of a mixture of 35 Torr He and 5 Torr H_2O (p = 40 Torr = 0.0526 atm) at 293 K can be calculated by applying eqn (4.16) after first estimating ρ and μ of the mixture.

The molar weight of the mixture, M_{mix}, was estimated to be 5.75 g mol^{-1}, which can then be used to calculate the density as follows

$$\rho_{mix} = \frac{p\, M_{mix}}{RT} = \frac{0.0526 \text{ atm} \times 5.75 \text{ g mol}^{-1}}{0.08205 \text{ atm dm}^3 \text{ mol}^{-1} \text{ K}^{-1} \times 293 \text{ K}}$$

$$= 0.0126 \text{ g dm}^{-3} = \underline{\underline{1.26 \times 10^{-5} \text{ g cm}^{-3}}} .$$

(4.17)

The viscosity of a binary gas mixture, μ_{mix} (g cm^{-1} s^{-1}) can be estimated as described in *Reid et al.* [1987] according to

$$\mu_{mix} = \frac{y_{He}\, \mu_{He}}{y_{He} + y_{H_2O}\left(\frac{M_{H_2O}}{M_{He}}\right)^{1/2}} + \frac{y_{H_2O}\, \mu_{H_2O}}{y_{H_2O} + y_{He}\left(\frac{M_{He}}{M_{H_2O}}\right)^{1/2}} \qquad (4.18)$$

where y denotes the mole fraction of He and H_2O, respectively. Using μ_{He}^{293K} = 19.7 μPa s and $\mu_{H_2O}^{293K}$ = 9.7 μPa s [*CRC Handbook of chemistry and physics*, 1993], eqn (4.18) leads to a viscosity of μ_{mix} = 17.4 μPa s = 1.74×10^{-4} g cm^{-1} s^{-1}. The Reynolds number of the mixture is then, according to eqn (4.16) and using a c of 290 cm s^{-1},

$$Re_G = \frac{2 \text{ x } 0.8 \text{ cm x } 290 \text{ cm s}^{-1} \text{ x } 1.26 \text{ x } 10^{-5} \text{ g cm}^{-3}}{1.74 \text{ x } 10^{-4} \text{ g cm}^{-1} \text{ s}^{-1}} = \underline{\underline{34}}$$

(4.19)

Highest values of Re_G of about 150 were observed for the maximum gas velocity of about 2000 cm s^{-1}. The gas flow was therefore laminar.

4.2.3 Characteristics of the liquid film

4.2.3.1 Water volume flow rate

The water volume flow rate, v (cm^3 s^{-1}), was adjusted on a Teflon flow meter, or on a digital liquid pump in later experiments. Water volume flow rates were varied in the range of 30 - 200 ml min^{-1} which corresponds to 0.5 - 3.3 cm^3 s^{-1}.

4.2.3.2 Thickness of the liquid film

Danckwerts [1970] has given the following equation which can be applied to calculate the thickness of the liquid film, δ (cm), flowing down the cylindrical flow reactor

$$\delta = \left(\frac{3\mu v}{2\pi g r \rho} \right)^{1/3} .$$

(4.20)

Here, μ is the viscosity of the liquid (g cm^{-1} s^{-1}), v is the volumetric liquid flow rate (cm^3 s^{-1}), g is the gravitational acceleration (= 981 cm s^{-2}), r is the radius of the flow tube (cm) and ρ is the density of the liquid (g cm^{-3}). Known values of the viscosity of water [*Kaye and Laby*, 1995] and the density of water [*CRC Handbook of chemistry and physics*, 1993] were plotted against temperature as shown in Figure 4.2 and Figure 4.3.

The viscosity of a liquid decreases with temperature according to an equation of the form [*Reid et al.*, 1987; *Kaye and Laby*, 1995]

$$\ln \mu = A + \frac{B}{T} \tag{4.21}$$

where A and B are characteristic constants.

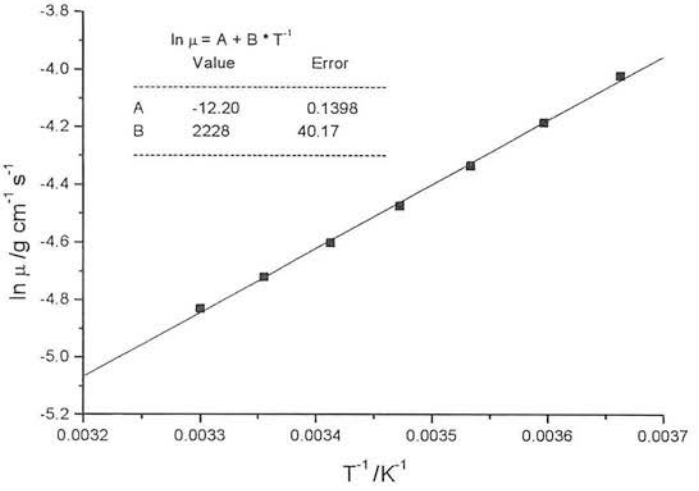

Figure 4.2 Plot of ln μ of water *vs.* 1/T. Values were taken from *Kaye and Laby* [1995].

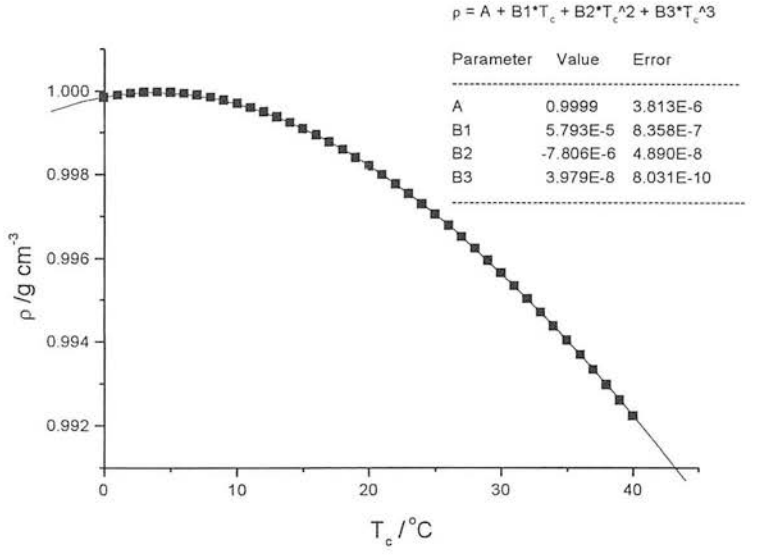

Figure 4.3 Plot of density of water *vs.* temperature. Values were taken from *CRC Handbook of chemistry and physics* [1993].

The fitted equations provided a quick way of obtaining the values of viscosity and density of water at a particular experimental temperature. Generally, the thickness of the water film was between 0.013 and 0.031 cm. It should be noted that these values were also used in the cases where scavenger solutions were applied. The effect of the solute on viscosity and density was neglected since the solutions were all dilute.

4.2.3.3 Water velocity

The average velocity of the liquid film, u_{avg} (cm s^{-1}), can be obtained from (e.g. [*Logan*, 1999])

$$u_{avg} = \frac{\rho g \delta^2}{3\mu} \quad . \tag{4.22}$$

The average linear velocity of the water was about 6 - 26 cm s^{-1} in these experiments.

4.2.3.4 Contact time liquid-gas

The time of contact of the liquid with the gas, t (s), is given by

$$t = \frac{z}{u_s} \tag{4.23}$$

where z is the length of contact (cm) and u_s is the velocity at the surface of the liquid film (cm s^{-1}). u_s is given by [*Danckwerts*, 1970]

$$u_s = \frac{3}{2}\left(\frac{v}{2\pi r}\right)^{2/3}\left(\frac{\rho g}{3\mu}\right)^{1/3} \tag{4.24}$$

Surface velocities of the liquid film were calculated to be between 9 and 39 cm s^{-1}. This resulted in liquid-gas contact times of 0.5 to 8.0 s.

4.2.3.5 Reynolds number of the liquid film

The Reynolds number of the liquid film, Re_W, was calculated according to [*Danckwerts*, 1970; *Logan*, 1999]

$$Re_W = \frac{u_{avg}\delta\rho}{\mu} = \frac{g\delta^3\rho^2}{3\mu^2} \qquad (4.25)$$

This Reynolds number is sometimes presented as a quantity four times larger than Re_W given here, e.g. [*Utter et al.*, 1992; *Perry and Green*, 1997], which has mainly historical reasons, as pointed out by *Logan* [1999]. Using eqn (4.25), Reynolds numbers of 5 to 80 were calculated. The transition between laminar and turbulent fluid occurs at Re_W of 250 to 400 [*Logan*, 1999] which indicates a laminar flow regime at the conditions used in this work. However, wavy flow can occur at Re_W as low as 10 [*Logan*, 1999]. Some rippling was observed at the higher water flow rates used.

4.2.4 Uptake coefficients

4.2.4.1 Approach

The data analysis was based on an overall first-order loss process for the trace gas. The uptake coefficients of a substance i into the liquid were calculated from the variation of signal in the gas phase, [i], with injector position according to

$$\frac{d[i]}{dt} = -k_W[i]. \qquad (4.26)$$

Since $\Delta\tau = \Delta z/c$ (eqn (4.15)), it follows after integration that

$$[i]_{z_2} = [i]_{z_1} \exp\left(-k_W \frac{\Delta z}{c}\right), \qquad (4.27)$$

where $[i]_{z_1}$ and $[i]_{z_2}$ are the concentrations of i at the detector (with the injector at the injector positions z_1 and z_2 (cm) and $\Delta z = z_2 - z_1$) and c is the gas flow velocity in the reactor (cm s^{-1}). k_w (s^{-1}) is the first-order rate coefficient for loss of i from the gas phase. A plot of ln [i] *vs.* injector position yields a straight line with the slope of $-k_w/c$ as shown in Figure 4.4.

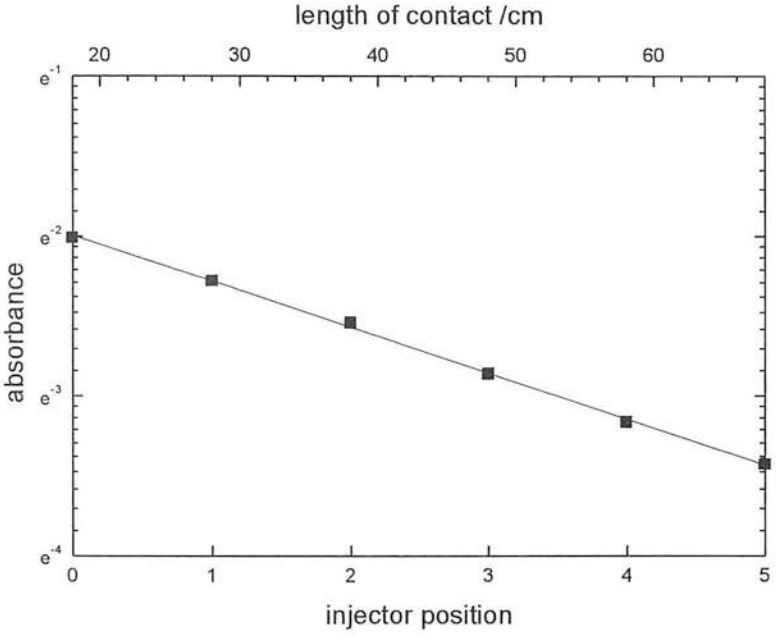

Figure 4.4 Plot of ozone concentration *vs.* injector position (exposure distance). $[Na_2S_2O_3]$ was 0.0309 mol l^{-1}, pressure in the reactor was 18 Torr at 20 °C and c = 293 cm s^{-1}.

The efficient uptake of i into the liquid can cause a radial concentration gradient in i in the gas phase. The experimental k_w was therefore corrected to k_w^{corr} using the method developed by *Brown* [1978]. Finally, the uptake coefficient γ can be extracted using the relation for a cylindrical reactor [*Howard*, 1979]

$$\gamma = \frac{2\, r\, k_w^{corr}}{\omega} \qquad (4.28)$$

where r is the radius of the flow tube (cm), k_w^{corr} is the corrected first-order rate coefficient (s^{-1}) and ω is the average molecular velocity of trace gas i (cm s^{-1}).

Eqn (4.28) is the equivalent to an expression derived from gas kinetic theory, given as eqn (4.29), which is commonly used in uptake experiments. Since the uptake, γ, is the ratio of the number of molecules removed from the gas phase to the number of molecular collisions with the surface (see Chapter 2), γ can be defined as

$$\gamma = \frac{F\,\Delta n_G}{\frac{1}{4}\,\omega\,A_r\,n_G} \qquad \textbf{(4.29)}$$

where F is the gas volumetric flow rate ($cm^3\ s^{-1}$), A_r is the liquid surface area (cm^2), n_G is the trace gas concentration (molecules cm^{-3}) before interaction and ω is the average thermal velocity of the trace gas ($cm\ s^{-1}$). Δn_G ($= n_i - n_f$) denotes the change in trace gas concentration after interaction with the surface has taken place.

The numerator in eqn (4.29) gives the number of molecules removed from the gas phase per unit time (molecules s^{-1}) whilst the denominator describes the total number of molecular collisions per unit time (molecules s^{-1}), which is obtained from multiplying the number of molecular collisions per unit time per unit area (molecules $cm^{-2}\ s^{-1}$) by the total condensed area (cm^2) [*Atkins*, 1986; *Gardner et al.*, 1987; *Worsnop et al.*, 1989].

Rearrangement of (4.29) gives

$$\frac{\Delta n_G}{n_G} = \frac{\omega\,\gamma\,A_r}{4\,F}. \qquad \textbf{(4.30)}$$

However, if significant amounts of gas are taken up by the liquid, the concentration of trace gas along the length of the reactor, L (cm), decreases and a concentration gradient along the flow tube distance, x, is established

$$\frac{\Delta n_G}{L} = \frac{dn_G}{dx} = -\frac{n_G\left(\frac{\omega\,\gamma\,A_r}{4\,F}\right)}{L}. \qquad \textbf{(4.31)}$$

Rearrangement and integration over the whole interaction length leads to

$$\int_{n_{G_i}}^{n_{G_f}} \frac{dn_G}{n_G} = -\frac{\omega \gamma A_r}{4 L F} \int_0^L dx$$

(4.32)

$$\ln n_G \Big|_{n_{G_i}}^{n_{G_f}} = -\frac{\omega \gamma A_r}{4 L F} x \Big|_0^L$$

(4.33)

$$\ln\left(\frac{n_{G_i}}{n_{G_f}}\right) = \frac{\omega \gamma A_r}{4 F}$$

(4.34)

Finally, the expression for the uptake is

$$\gamma = \frac{4 F}{\omega A_r} \ln\left(\frac{n_{G_i}}{n_{G_f}}\right).$$

(4.35)

If the expressions for the volume gas flow rate (F) and area (A_r) are now replaced by the appropriate formulae for cylindrical tubes, eqn (4.35) changes to

$$\gamma = \frac{4\left(\frac{\pi r^2 z}{\tau}\right)}{\omega (2 \pi r z)} \ln\left(\frac{n_{G_i}}{n_{G_f}}\right) = \frac{2 r}{\omega} \frac{\ln\left(\frac{n_{G_i}}{n_{G_f}}\right)}{\tau}.$$

(4.36)

From eqn (4.15) and (4.27) it follows that (see also Figure 4.4)

$$\frac{\ln\left(\frac{n_{G_i}}{n_{G_f}}\right)}{\tau} = k_w$$

(4.37)

where τ is the gas-liquid contact time (s) and k_w is the first-order rate coefficient for loss of molecules from the gas phase (s^{-1}). When inserted in (4.36) it results in the following expression for γ

$$\gamma = \frac{2\,r\,k_w}{\omega}$$

(4.38)

which is exactly the same expression as eqn (4.28) above, if k_w is replaced by the corrected first-order rate coefficient k_w^{corr}. This means all the following expressions are equivalent:

$$\gamma = \frac{2\,r\,k_w}{\omega} = \frac{4\,F}{\omega\,A_r}\ln\left(\frac{n_{G_i}}{n_{G_f}}\right) = \frac{2\,r}{\omega}\,\frac{\ln\left(\frac{n_{G_i}}{n_{G_f}}\right)}{\tau}.$$

(4.39)

4.2.4.2 Correction for radial gas phase diffusion in the reactor

To obtain γ, a value for k_w^{corr} is required (see eqn (4.28)). The observed first-order loss rate coefficient, k_w, has to be corrected since the expression for the observed change in concentration in the wetted-wall reactor (eqn (4.27)) is only approximate. The reason is that a laminar gas flow has a parabolic velocity profile across the tube which gives rise to a radial concentration gradient if gas phase loss occurs. A radial concentration gradient also arises if there is loss (or uptake) of gas at the wall surface. However, the concentration profile remains exponential along the tube [*Brown*, 1978].

In the situation of no gas phase loss and first-order loss at the wall (which is the case here), the equation describing the time dependence of the radial concentration as a function of the distance from the tube centre, $[i]_{(a)}$, is

$$[i]_{(a)} = [i]^0_{(a)}\exp\left(-k_w\frac{z}{c}\right).$$

(4.40)

$[i]^0$ is the concentration of i when the distance z along the tube is zero. c is the gas flow velocity in the reactor and a is the distance from the tube centre. k_w is the

observed first-order rate coefficient for loss of i from the gas phase. k_w is a function of the true first-order rate coefficient for wall reaction, k_w^{corr}, the gas diffusion coefficient, $D_{G(i)}$ and the gas velocity. Once the value of k_w has been determined by experiment it must therefore be related back to k_w^{corr} which can be used in the expression (4.28). To obtain k_w^{corr} from k_w requires solving the partial differential equation describing first-order wall loss in a laminar gas flow in cylindrical symmetry

$$2c\left(1-\frac{a^2}{r^2}\right)\frac{\partial[i]}{\partial z} = D_G\left(\frac{\partial^2[i]}{\partial a^2}+\frac{1}{a}\frac{\partial[i]}{\partial a}+\frac{\partial^2[i]}{\partial z^2}\right) \qquad \textbf{(4.41)}$$

with the boundary condition at the wall of

$$D_G\left(\frac{\partial[i]}{\partial a}\right)_{a=r} = -k_w^{corr}[i]_{a=r} \qquad \textbf{(4.42)}$$

Note that, in converse to common notation, here r is the radius of the tube and a the distance from the centre of the tube. Following the method given by *Brown* [1978], a short computer program was written in FORTRAN 90, which derived the value of k_w^{corr} for given input values of k_w, $D_{G(i)}$ and c (see Appendix).

4.2.4.3 Gas phase diffusion coefficients

Brown [1978] has presented a method to obtain corrected first-order rate coefficients from observed decay parameters in cylindrical gas flows (see Section 4.2.4.2). An input parameter needed is the gas diffusion coefficient of substance i, $D_{G(i)}$ ($cm^2\ s^{-1}$) in the mixture of helium and water present in the flow reactor. It can be calculated from the following equation [*Hanson et al.*, 1992]

$$\frac{1}{D_{G(i)}} = \frac{p_{H_2O}}{D_G^{P}{}_{(i-H_2O)}} + \frac{p_{He}}{D_G^{P}{}_{(i-He)}} \qquad \textbf{(4.43)}$$

where p_{H_2O} and p_{He} are the partial pressures of water and helium (Torr), respectively. $D_G^{P}{}_{(i-H_2O)}$ and $D_G^{P}{}_{(i-He)}$ are the pressure-independent binary diffusion coefficients

(Torr cm^2 s^{-1}) of i in H_2O and helium[2]. They were estimated using the method of Fuller, Schettler and Giddings [*Fuller et al.*, 1969] (see Section 2.3.4.1).

For example, the gas diffusivity of phenol in H_2O is given by

$$D_G{}^{P}{}_{(C_6H_5OH-H_2O)} = \frac{10^{-3}T^{1.75}\left(\frac{1}{M_{C_6H_5OH}}+\frac{1}{M_{H_2O}}\right)^{1/2}}{p\left[\left(\sum v\right)_{C_6H_5OH}{}^{1/3}+\left(\sum v\right)_{H_2O}{}^{1/3}\right]^2} \qquad (4.44)$$

where $D_G{}^{P}{}_{(C_6H_5OH\text{-}H_2O)}$ is the diffusion coefficient (cm^2 s^{-1}) at 1 atm, T is the temperature (K), p is the pressure (atm) and $M_{C_6H_5OH}$ and M_{H_2O} are the molar masses of phenol and water, respectively (g mol^{-1}). The molecular diffusion volumes $\left(\sum v\right)$ can be found by summation of the atomic diffusion volumes [*Reid et al.*, 1987]. Here, the optimised values of the atomic diffusion volumes are used, which were given by *Fuller at al.* [1969] .

			$\left(\sum v\right)_{C_6H_5OH}$	$\left(\sum v\right)_{H_2O}$
			C_6H_5OH	**H_2O**
element	atomic diffusion volume	number		
C	15.9	6	95.4	
H	2.31	6	13.86	
O	6.11	1	6.11	
aromatic ring	-18.3	1	-18.3	
			97.1	**13.1**

Table 4.2 Molecular diffusion volume after *Fuller et al.* [1969]. The volume for H_2O was given in the reference.

Therefore, the gas diffusivity of phenol in water at 293 K is

[2] By multiplying D_G with the pressure p one obtains $D_G{}^{P}$, the pressure-independent binary diffusion coefficient.

$$D_G{}^{P}{}_{(C_6H_5OH-H_2O)} = \frac{10^{-3} \times 293^{1.75}\left(\frac{1}{94.1}+\frac{1}{18.0}\right)^{1/2}}{1\left[(97.1)^{1/3}+(13.1)^{1/3}\right]^2} = 0.1104 \text{ atm cm}^2\text{s}^{-1} = 83.9 \text{ Torr cm}^2 \text{ s}^{-1}.$$

(4.45)

Similarly, the diffusivity of phenol in helium can be calculated as $D_G{}^{P}{}_{(C_6H_5OH\text{-}He)} = 0.296$ atm cm^2 s^{-1} $\cong$ 225 Torr cm^2 s^{-1}, using a diffusion volume of 2.67 for helium [*Fuller et al.*, 1969; *Reid et al.*, 1987]. Hence, the gas diffusion coefficient for phenol in a mixture with partial pressures of 35 Torr Helium and 5 Torr H_2O at 293 K, using eqn (4.43), is estimated as

$$\frac{1}{D_{G(C_6H_5OH)}} = \frac{5 \text{ Torr}}{83.9 \text{ Torr cm}^2 \text{ s}^{-1}} + \frac{35 \text{ Torr}}{225 \text{ Torr cm}^2 \text{ s}^{-1}} = 0.2152 \text{ cm}^{-2} \text{ s}$$

$$\underline{\underline{D_{G(C_6H_5OH)} = 4.65 \text{ cm}^2 \text{ s}^{-1}}}.$$

(4.46)

4.2.4.4 Liquid diffusion coefficients

Liquid diffusion coefficients are important if the uptake is limited by solubility and/or liquid reaction (see Chapter 2). Since experimental data are scarce, liquid diffusivities have frequently to be estimated using the Wilke and Chang correlation as described in *Reid et al.* [1987] (see Section 2.3.4.1).

For phenol in water this is

$$D_{L(C_6H_5OH-H_2O)} = \frac{7.4 \times 10^{-8}\left(\phi_{H_2O} M_{H_2O}\right)^{1/2} T}{\mu_{H_2O} V_{C_6H_5OH}^{0.6}}$$

(4.47)

where $D_{L(C_6H_5OH\text{-}H_2O)}$ is the liquid diffusion coefficient of phenol in H_2O (cm^2 s^{-1}), T the temperature (K) and M_{H_2O} the molar mass of H_2O (g mol^{-1}). ϕ_{H_2O} is a dimensionless

association parameter which is recommended as 2.6 for H_2O. μ_{H_2O} is the viscosity of H_2O in units of centipoise. $V_{C_6H_5OH}$ is the molar volume of phenol at its normal boiling temperature ($cm^3\ mol^{-1}$). It was estimated from the Le Bas method by adding volume increments of each element [*Reid et al.*, 1987].

element	volume increments	number	$V_{C_6H_5OH}$ / $cm^3\ mol^{-1}$ **C_6H_5OH**
C	14.8	6	88.8
H	3.7	6	22.2
O	7.4	1	7.4
aromatic ring	-15.0	1	-15.0
			103.4

Table 4.3 Calculation of molar volume of phenol by Le Bas method [*Reid et al.*, 1987].

Using a viscosity of μ_{H_2O}=1.002 cp [*CRC Handbook of chemistry and physics*, 1993], the estimated diffusivity of phenol in water at 293 K is then

$$D_{L(C_6H_5OH-H_2O)} = \frac{7.4 \times 10^{-8}\ (2.6 \times 18.0)^{1/2}\ 293}{1.002 \times 103.4^{0.6}} = \underline{\underline{9.15 \times 10^{-6}\ cm^2\ s^{-1}}} \qquad \textbf{(4.48)}$$

For some compounds *Yaws* [1995] has given an expression to calculate the liquid diffusion coefficient in water based on both experimental and estimated data.

4.2.4.5 Derivation of k_w from changes in absorption

The concentration of trace gas at the exit of the wetted-wall flow reactor was determined by UV absorption spectroscopy. The absorbance A is defined as

$$A = \log\frac{I_0}{I} \qquad \textbf{(4.49)}$$

where I_0 is the initial intensity of light incident on the sample and I the intensity of the light transmitted through the sample. The system used in this work gives the option of measuring either the light intensities, e.g. in unit of counts (cts), which requires subsequent calculation of the absorbance, or the direct absorption measurement. Both possibilities were used in the uptake measurements.

Since the absorbance is proportional to the concentration (see Chapter 3), the uptake coefficient was calculated by comparing the absorbances of two different injector positions, A_1 and A_2.

$$\gamma = \frac{2\,r}{\omega}\left(\frac{\ln\left(\frac{A_1}{A_2}\right)}{\Delta\tau}\right)^{corr} \qquad \textbf{(4.50)}$$

where $\Delta\tau$ is the difference in gas-liquid contact times between position 1 and 2, i.e. $\Delta\tau = \tau_1 - \tau_2$. The term $[\ln (A_1/A_2)]/\Delta\tau]$ was corrected for radial concentration gradients using the method of *Brown* [1978] as described in Section 4.2.4.2. Both absorbances, A_1 and A_2, were recorded with the same I_0, i.e.

$$\gamma = \frac{2\,r}{\omega}\left(\frac{\ln\left(\frac{\log\frac{I_0}{I_1}}{\log\frac{I_0}{I_2}}\right)}{\Delta\tau}\right)^{corr} \qquad \textbf{(4.51)}$$

4.2.4.6 Pressure correction

Care had to be taken to ensure a constant pressure over the duration of one experiment. This is important for guaranteeing a constant gas flow under the

experimental conditions. Another reason is that a change in pressure means a change in gas phase concentration which could change the absorbance regardless of any gas uptake.

Small variations in pressure (between 0.1 and 0.5 Torr) were corrected for by standardising all measurements to the same pressure, which was arbitrarily chosen using the procedure described below.

The partial pressure of the gas, i.e. sum of trace and carrier gas, was computed according to eqn (4.6) and the absorbance signal measured at that experimental pressure. Since the signal was zero at zero pressure, it was possible to correlate the signal for a particular pressure by linear regression. This procedure was applied in both the case where the light intensities were measured (and the absorption calculated afterwards), as well as the case where the absorption was determined directly.

By measurement of the light intensities

The signal of the light intensity at experimental pressure p_1, $I_{(p1)}$, was correlated to the origin of a signal *vs.* pressure diagram. The slope of the linear regression line was used to calculate the signal at any other required pressure p_2, i.e.

$$I_{(p2)} = \frac{I_{(p1)}}{p_1} p_2 \quad . \tag{4.52}$$

All measured signals could therefore be corrected to a uniform pressure, i.e. p_2.

By measurement of absorbances

The principle of the procedure was exactly the same as the one described above but using the definition for the absorbance (eqn (4.49)). The absorbance $A_{(p2)}$ at a chosen pressure (p_2) was calculated from the measured absorbance $A_{(p1)}$ at pressure p_1

$$A_{(p2)} = \log \frac{I_0}{I_{(p2)}} = \frac{A_{(p1)}}{p_1} p_2$$

(4.53)

which gives the expression for the signal $I_{(p2)}$ as

$$I_{(p2)} = \frac{I_0}{10^{\left(\frac{A_{(p1)}}{p_1} p_2\right)}}.$$

(4.54)

4.2.5 Time dependence of uptake

It was shown in Chapter 2 that the overall uptake can be calculated by summing the individual resistances of each process using the Resistance Model of gas uptake, i.e.

$$\frac{1}{\gamma} = \frac{1}{\Gamma_G} + \frac{1}{\alpha} + \frac{1}{\Gamma_{SOL} + \Gamma_{RXN}}.$$

(2.43)

In the case of gas diffusion limitation, i.e. $\gamma \approx \Gamma_G$, the diffusion limited loss rate coefficient k_G (s^{-1}) for a cylindrical reactor of radius r is given by [*Hanson et al.*, 1992]

$$k_G = \frac{3.66\, D_G}{r^2}$$

(4.55)

where D_G is the gas phase diffusion coefficient ($cm^2\ s^{-1}$). It follows that (see also eqn (4.38))

$$\Gamma_G = \frac{2\, r\, k_G}{\omega} = \frac{2\,(3.66\, D_G)}{\omega\, r}.$$

(4.56)

Eqn (4.55) and (4.56) are valid if the gas flow velocity is much greater than the axial diffusion velocity which can be checked be calculating the Peclet number, Pe [*Fickert et al.*, 1998]

$$Pe = \frac{2\,r\,c}{D_G} \,.$$

(4.57)

A value of Pe > 10 indicates that the axial diffusion velocity can be neglected. Even at the smallest gas velocity used (≈ 50 cm s^{-1}) this was true (Pe ≈ 17) for a typical mixture of 5 Torr H_2O and 35 Torr Helium at 293 K using a D_G of 4.6 cm^2 s^{-1}.

Similar expressions to eqn (4.56) can be defined for solubility or reaction limited uptake processes, as already shown in Chapter 2,

$$\Gamma_{SOL} = \frac{4\,H\,R\,T}{\pi^{1/2}\,\omega}\sqrt{\frac{D_L}{t}}$$

(4.58)

$$\Gamma_{RXN} = \frac{4\,H\,R\,T\,\sqrt{D_L\,k_{RXN}}}{\omega} \,.$$

(4.59)

In these equations, H is the Henry's law coefficient (M atm^{-1}), R is the gas constant (l atm mol^{-1} K^{-1}), T is the temperature (K), t is the liquid-gas contact time (s), ω is the mean molecular velocity (cm s^{-1}) of the trace compound and D_L is the liquid diffusion coefficient (cm^2 s^{-1}). k_{RXN} is the pseudo-first-order reaction rate coefficient of the gas with the condensed phase (s^{-1}).

It can be seen that the solubility resistance $1/\Gamma_{SOL}$ is the only time dependent term whereas the liquid reaction resistance is determined by the reaction rate k_{RXN}. This is important in the derivation of the uptake term since it is common to use only the limiting term for simplicity.

4.2.5.1 Time dependent uptake

The physical uptake of a species of low solubility and without significant reactive loss leads to a time dependent uptake [*Hanson and Ravishankara*, 1993; *Kolb et al.*, 1995]

$$\frac{1}{\gamma} = \frac{1}{\Gamma_G} + \frac{1}{\alpha} + \frac{\pi^{1/2}\,\omega}{4\,H\,R\,T\sqrt{D_L}}\sqrt{t} \quad . \tag{4.60}$$

In this case, a plot of $1/\gamma$ *vs.* $\sqrt{t}$ gives a straight line with a slope proportional to $1/(H\sqrt{D_L})$. The intercept gives information about Γ_G, which is often negligible, and α.

It is expected that the uptake of phenol and 2-nitrophenol onto water shows time dependence. *Heal et al.* [1995] have found the dependence to be in the lower ms range using a droplet train apparatus. Clearly, here the wetted-wall flow reactor is limited since the minimum liquid-gas contact time is about 500 ms but more often is of the order of seconds.

The described method (see Section 4.2.4.1) of plotting the signal against different injector positions to obtain k_w could not be used for time-dependent uptake. The reason is that a change in injector position changes the contact time and thereby γ. Therefore, the approach to measure γ in this case was slightly varied. If the contact area (i.e. injector position) is changed by small steps only, it can be assumed that γ does not change significantly. Then γ can be derived by plotting the detection signal against injector position as long as the change in absorption due to uptake is big enough to detect. In a second method the pressure, and therefore F, was changed for a given contact distance (i.e. the same injector position). Different $\ln(A_1/A_2)$ were plotted against $\omega A_r/(4F)$ for different F (see eqn (4.39)). The straight line through the origin yielded γ.

4.2.5.2 Time independent uptake

The uptake of a species of low solubility and a fast irreversible reaction in the liquid results in time independent, reaction limited uptake where Γ_{SOL} approaches zero [*Kolb et al.*, 1995]

$$\frac{1}{\gamma} = \frac{1}{\Gamma_G} + \frac{1}{\alpha} + \frac{\omega}{4\,H\,R\,T\,(D_L\,k_{RXN})^{1/2}} \cdot$$

(4.61)

The pseudo-first-order rate coefficient is $k_{RXN} = k''\,[i]$ for a bimolecular reaction of i in the liquid where k'' is the second-order rate coefficient (l mol^{-1} s^{-1}). Therefore a plot of $1/\gamma$ *vs.* $[i]^{-1/2}$ leading to a straight line would indicate a reaction limited uptake. From the slope of such a line the quantity $(H\sqrt{k''})$ can be calculated. This was found to be the case for the uptake of ozone onto $Na_2S_2O_3$ solutions and for uptake of phenol onto bromine water. The method described above, where the detection signal was plotted against different injector positions to derive k_w (see Section 4.2.4.1, eqn (4.27) and eqn (4.28)), was used.

Interestingly, it has been found experimentally that the loss rate (and therefore the uptake) increases with concentration of [i] only in the lower concentration ranges. Further increase of [i] does not result in larger uptake. Rather, the uptake becomes diffusion controlled where the diffusion of the gas to the surface is the slowest step in the uptake process which is in accordance with the Resistance Model [*Rudich et al.*, 1996b].

Equation (4.61) reduces to

$$\frac{1}{\gamma} = \frac{1}{\alpha} + \frac{\omega}{4\,H\,R\,T\,(D_L\,k''\,[i])^{1/2}}$$

(4.62)

in concentration ranges where the reactive loss in the liquid is the rate limiting step. The intercept of the $1/\gamma$ *vs.* $[i]^{-1/2}$ plot can be used to deduce the mass accommodation coefficient α. It should be noted however, that the derived value of α is very sensitive to the fitting of the straight line. *Schweitzer et al.* [1998] have even found a negative

intercept for the reactive uptake of nitryl chloride, $ClNO_2$, onto NaI solutions which is physically not possible. It has been attributed to a second reaction path at the liquid surface. Similar surface-enhanced reactions have been observed for Cl_2, Br_2 and $ClONO_2$ [*Hanson and Ravishankara*, 1994; *Hu et al.*, 1995]. They are facilitated by the lack of any limitations from liquid diffusivity and expected higher concentrations in the interface. Such surface reactions are not included in the Resistance Model since the reactive uptake term is defined for bulk reactions (see Chapter 2). Because of the uncertainties in the intercept, values of α derived in this way can only be considered an estimate.

In cases where the uptake is not limited by mass accommodation, i.e. $\omega/(4HRT\sqrt{D_L k''[i]}) \gg 1/\alpha$, eqn (4.62) reduces further to

$$\frac{1}{\gamma} = \frac{\omega}{4\,H\,R\,T\,(D_L\ k''\ [i])^{1/2}}\ . \qquad \textbf{(4.63)}$$

Rearranging and taking the logarithm of (4.63) results in

$$\log\gamma = \log\frac{4\,H\,R\,T\sqrt{D_L\ k''}}{\omega} + \frac{1}{2}\log\left(a_i c^{\ominus}\right)\ . \qquad \textbf{(4.64)}$$

In (4.64), the concentration of i, [i], was replaced by the term $(a_i c^{\ominus})$, which is explained in more detail in the following section. A straight line with a slope of 0.5 of a plot of log γ *vs.* log $(a_i c^{\ominus})$ would indicate that the above simplifications (i.e. $\omega/(4HRT\sqrt{D_L k''[i]}) \gg 1/\alpha$) are valid. The intercept (extrapolated to $(a_i c^{\ominus}) = 1$ mol l^{-1}) gives information about the second-order rate coefficient k" (l mol^{-1} s^{-1}).

Activity of solute i

In the previous section the pseudo-first-order rate coefficient was defined as $k_{RXN} = k''\,[i]$ where [i] is the concentration of i in the liquid. However, especially at higher concentration of i, activity rather than concentration should be used as a measure of reactivity. The activity can be thought of as corrected concentration that

takes the non-ideal behaviour into account (also see Chapter 2). In an electrolyte solution the electrostatic (Coulomb) interactions are primarily responsible for the departure from ideality [*Atkins*, 1986].

The activity a_i is related to the concentration of i, [i] (mol l^{-1}), by

$$a_i = \frac{\gamma_i [i]}{c^{\ominus}} \tag{4.65}$$

where γ_i is the dimensionless activity coefficient and $c^{\ominus}$ is the standard concentration of 1 mol l^{-1}. The activity coefficient is very close to unity (i.e. $a_i c^{\ominus} \approx [i]$) only at ionic strength of less than about 0.001 [*Hemond and Fechner*, 1994]. The ionic strength I_S (mol l^{-1}) is defined as

$$I_S = \frac{1}{2} \sum (z_i)^2 [i]^{aq} \tag{4.66}$$

where z_i is the charge number of each ion in solution and $[i]^{aq}$ represents the concentration (mol l^{-1}). The summation is over all ions in solution.

For example, the ionic strength of 0.14 M $Na_2S_2O_3$ solution, assuming complete dissociation, is

$$I_S = \frac{1}{2} \left[(+1)^2[Na^+] + (-2)^2[S_2O_3^{2-}] + (+1)^2[H^+] + (-1)^2[OH^-]\right] \tag{4.67}$$

The contribution of the water to the ionic strength can be neglected since the concentration of the ions formed is far less than the concentration of the electrolyte, i.e.

$$I_S = \frac{1}{2} \left[(+1)^2[0.28] + (-2)^2[0.14]\right] = \underline{\underline{0.42}} \tag{4.68}$$

This is far above the given limit of 0.001 where the activity coefficient can be assumed to be one. Therefore, in the results chapters the reactive uptake was plotted against activity (i.e. $a_i c^{\ominus}$ rather than [i]) when applying the above described procedure.

Activity coefficients (also called mean activity coefficients) of $Na_2S_2O_3$ at 25 °C [*Robinson and Stokes*, 1959] were plotted against concentration, as shown in Figure 4.5. The fitted equation was used to deduce the activity coefficient for any particular concentration.

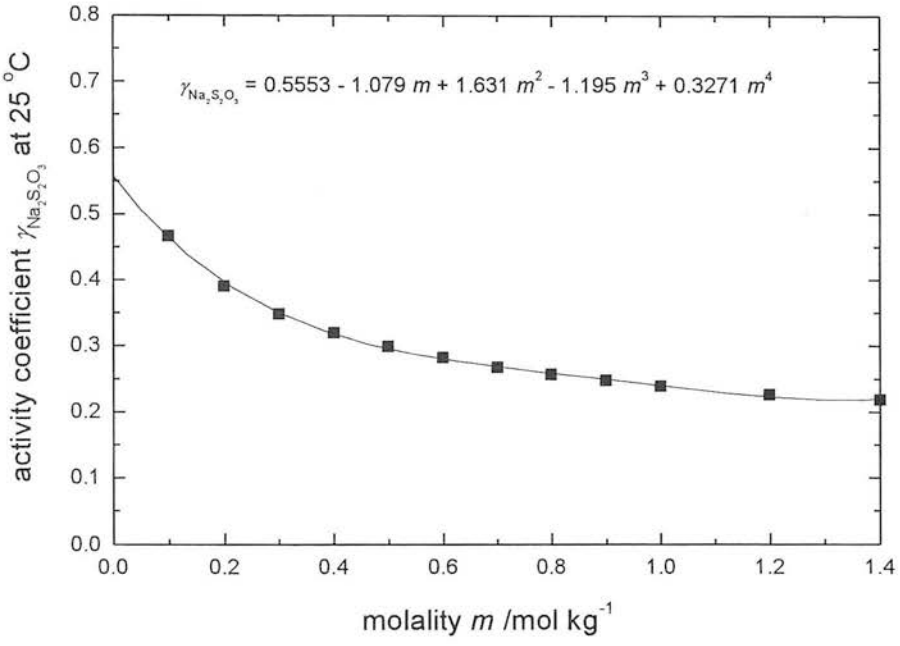

Figure 4.5 Plot of activity coefficient *vs.* concentration at 25 °C. Values were taken from *Robinson and Stokes* [1959]. Although the concentration is expressed as temperature-independent molality, concentration ≈ molality for dilute solutions in water at room temperature.

Prausnitz et al. [1986] have given an empirical correlation for the temperature dependence of the activity coefficient

$$\ln \gamma_i = b_1 + b_2 T^{-1} \qquad (4.69)$$

where b_1 and b_2 are empirical constants that depend on composition. To simplify, either one of two approximations are made, in which it is assumed either that γ_i does

not change with temperature (athermal, i.e. $b_2 = 0$), or that ln γ_i at constant composition is proportional to the reciprocal of temperature ($b_1 = 0$). However, the change of γ_i with temperature is often not significant in vapour-liquid equilibria since the vapour pressure is a much stronger function of temperature and the system appears insensitive to variations in γ_i with T. Therefore, the temperature effect on γ_i was neglected in this work.

4.3 The bubble column

Henry's law coefficients were calculated from purge-rate data on the basis of the method developed by *Mackay et al.* [1979]. The number of moles lost from the liquid phase per unit time equals the number of moles per unit time gained in the gas phase. The mass balance for the stripping process can therefore be derived from

$$-\frac{dn^{aq}}{dt} = +\frac{dn^{gas}}{dt}. \tag{4.70}$$

Since $n^{aq} = V^{aq}\,[i]^{aq}$ and $n^{gas} = F\,[i]^{gas}\,t$, it follows that

$$-V^{aq}\frac{d[i]^{aq}}{dt} = \frac{d(F\,[i]^{gas}\,t)}{dt} = F\,[i]^{gas} = F\,\frac{n^{gas}}{V^{gas}} = F\,\frac{p_i}{R\,T}. \tag{4.71}$$

Substituting for p_i ($H = [i]^{aq}/p_i$) leads to

$$-V^{aq}\frac{d[i]^{aq}}{dt} = F\,\frac{[i]^{aq}}{H\,R\,T}. \tag{4.72}$$

Rearrangement and integration yields

$$\int_{[i]_0^{aq}}^{[i]_t^{aq}} \frac{d[i]^{aq}}{[i]^{aq}} = -\frac{F}{H\,R\,T\,V^{aq}}\int_0^t dt \tag{4.73}$$

$$\ln\left(\frac{[i]_t^{aq}}{[i]_0^{aq}}\right) = -\frac{F}{H\,R\,T\,V^{aq}}t\,. \qquad (4.74)$$

In the above equations, p_i is the partial vapour pressure, V is the volume, n is the number of moles, R is the gas constant, T is the temperature, $[i]_0^{aq}$ and $[i]_t^{aq}$ are the aqueous concentrations at time 0 and t respectively, F is the gas flow rate and H is the Henry's law coefficient.

A plot of ln concentration *vs.* time was linear with the gradient [1] of -(F/HRTV^{aq}). In practice, the absorption signal was plotted *in lieu* of concentration. In this way, an H value for a constant F and constant V^{aq} could be obtained. A typical plot is shown in Figure 4.6.

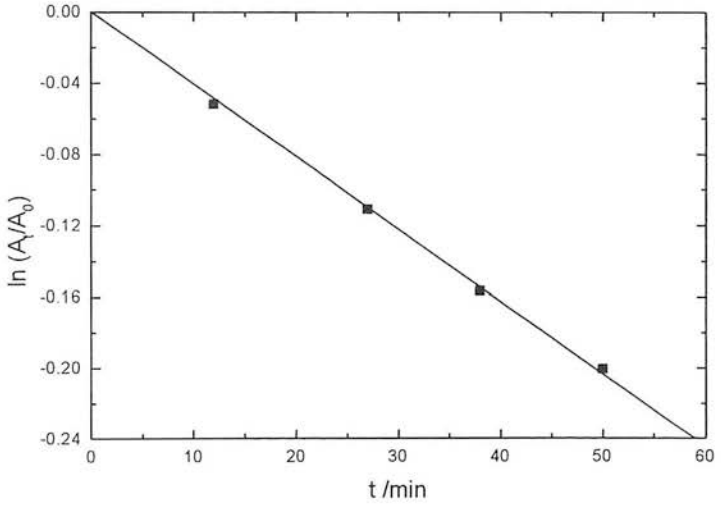

Figure 4.6 Plot of ln (A_t/A_0) *vs.* time for 2-nitrophenol. Conditions were T = 298 K, F = 300 ml min^{-1} (STP), V^{aq} = 46 cm^3. Gradient [1] = -(F/HRTV^{aq}) = -4.02 x 10^{-3} min^{-1}.

Liquid heights were changed, i.e. different liquid volumes used, keeping the gas flow rate constant. Plotting F/(HRTV^{aq}) (= - gradient [1]) *vs.* F/V^{aq} gave a gradient [2] of 1/(HRT). For each temperature and one flow rate typically 8 different liquid volumes, i.e. 8 different F/V^{aq} ratios, each consisting of at least 4 measurements, were carried out. Figure 4.7 shows a typical plot of F/(HRTV^{aq}) *vs.* F/V^{aq}.

The H obtained from gradient [2] was therefore an average of at least 32 measurements giving an H for one temperature and one gas flow rate. Typical flow rates were 100, 300, 500 and 1000 $cm^3\ min^{-1}$ (STP), though 300 $cm^3\ min^{-1}$ was employed for the bulk of the measurements. This procedure was applied to all temperatures investigated.

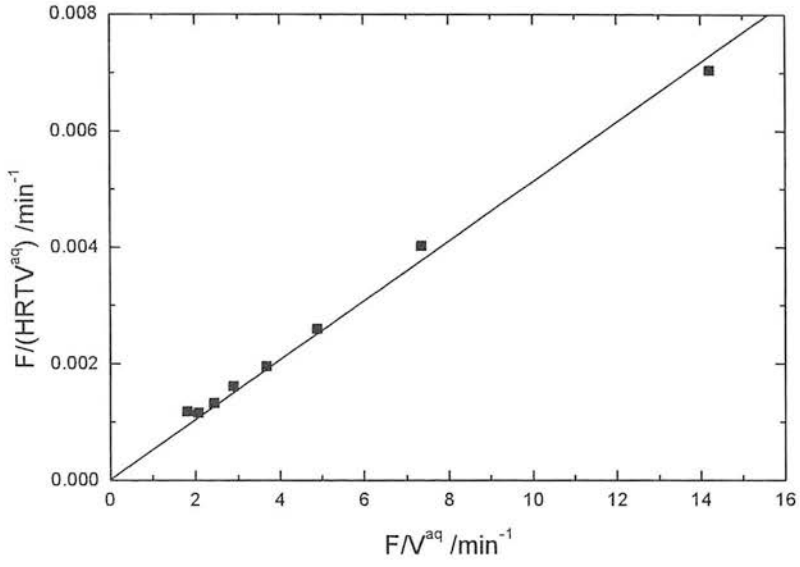

Figure 4.7 Plotting $F/(HRTV^{aq})$ *vs.* F/V^{aq} for 2-nitrophenol. Conditions were T = 298 K and F = 300 ml min^{-1} (STP). Gradient [2] = 1/HRT = 5.12×10^{-4}.

The Henry's law coefficient can be related to the free energy change of the process $i^{gas} \rightarrow i^{aq}$ by [*Kames and Schurath*, 1992]

$$H = \exp\left(-\frac{\Delta G^\circ}{RT}\right) = \exp\left(-\frac{\Delta H^\circ}{RT} + \frac{\Delta S^\circ}{R}\right) \qquad (4.75)$$

as shown in Chapter 2. Here, ΔG° is the free energy of gas to liquid transfer in solution (J mol^{-1}), ΔH° is the enthalpy of this transfer (J mol^{-1}), ΔS° is the entropy of this transfer (J $mol^{-1}\ K^{-1}$) and R is the gas constant (J $mol^{-1}\ K^{-1}$). The enthalpies and entropies were determined by plotting ln H *vs.* 1/T.

4.3.1 Approach to equilibrium

4.3.1.1 Extraction of the equilibrium Henry's law coefficient

The accuracy of the method depends primarily on the degree of equilibrium reached between gas and liquid phase. In the mathematical description given above it was assumed that the solution is homogeneous in concentration and that the solute in the exit vapour is in equilibrium with the liquid. *Mackay et al.* [1979] have derived an expression for the mass transfer rate for circumstances when the partial pressure in the gas at the exit is not in equilibrium with the liquid in the reactor. In this derivation, it is assumed that the solution is well mixed (i.e. $[i]^{aq}$ is vertically constant) and that the solute partial pressure in the gas rises by dp_i (atm) during exposure to an interfacial area increment of dA_r (cm^2). From the definition of Henry's law coefficient (see Chapter 2) it follows that

$$[i]^{aq} = H\, p_i \ . \tag{2.1}$$

Away from equilibrium an equilibrium potential Δ^{equi} can be imagined, i.e.

$$\Delta^{equi} = [i]^{aq} - H\, p_i \ . \tag{4.76}$$

Δ^{equi} (in units of concentration, i.e. mol l^{-1}) is a measure of the rate at which equilibrium is approached: far from equilibrium Δ^{equi} is large and the system approaches equilibrium fast, whereas at equilibrium Δ^{equi} equals zero. Therefore, the pressure rise in the gas with interfacial area increment is proportional to Δ^{equi} and inversely proportional to F, i.e.

$$\frac{dp_i}{dA_r} \propto \frac{\Delta^{equi}}{F} \ . \tag{4.77}$$

Introducing a factor K_{OL} and rearrangement gives

$$F \frac{dp_i}{R\,T} = K_{OL}\, dA_r\, ([i]^{aq} - H\, p_i) \tag{4.78}$$

where, K_{OL} is the overall liquid phase mass transfer coefficient in units of length per unit time (e.g. cm min^{-1} or m h^{-1}). Eqn (4.78) is further rearranged before integration.

$$\frac{dp_i}{[i]^{aq} - H\,p_i} = \frac{K_{OL}\,R\,T}{F} dA_r \tag{4.79}$$

$$\int_0^{p_i} \frac{dp_i}{\frac{[i]^{aq}}{H} - p_i} = \frac{K_{OL}\,H\,R\,T}{F} \int_0^{A_r} dA_r \tag{4.80}$$

$$-\ln\left(\frac{[i]^{aq}}{H} - p_i\right)\Bigg|_0^{p_i} = \frac{K_{OL}\,H\,R\,T}{F} A_r\Big|_0^{A_r} \tag{4.81}$$

$$\ln\left(\frac{\left(\frac{[i]^{aq}}{H} - p_i\right)}{\frac{[i]^{aq}}{H}}\right) = -\frac{K_{OL}\,H\,R\,T\,A_r}{F} \tag{4.82}$$

$$\left(\frac{[i]^{aq}}{H} - p_i\right) = \frac{[i]^{aq}}{H} \exp\left(-\frac{K_{OL}\,H\,R\,T\,A_r}{F}\right). \tag{4.83}$$

Rearranging gives the expression for the non-equilibrium partial pressure

$$p_i^{\,non-equi} = \frac{[i]^{aq}}{H^{equi}}\left(1 - \exp\left(-\frac{K_{OL}\,H^{equi}\,R\,T\,A_r}{F}\right)\right) \tag{4.84}$$

where A_r is the interfacial area of the column (cm^2). But the non-equilibrium partial pressure can be written in terms of the measured non-equilibrium Henry's law coefficient through

$$p_i^{\,non-equi} = \frac{[i]^{aq}}{H^{non-equi}}. \tag{4.85}$$

Therefore, from eqn (4.84) and eqn (4.85) it follows that the measured Henry's law coefficient is given by

$$H^{non-equi} = \frac{H^{equi}}{\left(1 - \exp\left(-\frac{K_{OL}\, H^{equi}\, R\, T\, A_r}{F}\right)\right)}. \qquad (4.86)$$

4.3.1.2 Approach to equilibrium as function of liquid depth

Equation (4.86) gives a relation between $H^{non-equi}$, i.e. the measured H, and the true equilibrium H, H^{equi}. It is important to check if the partial vapour pressure equilibrates to sufficient extent within the length of the bubble column. To do that eqn (4.86) has to be written as a function of liquid height, z (cm). The interfacial area is proportional to z, so

$$A_r = k_z\, z \qquad (4.87)$$

where k_z is a constant with unit of length (cm). Inserting (4.87) into (4.86) gives the final expression which links $H^{non-equi}$, H^{equi} and z

$$H^{non-equi} = \frac{H^{equi}}{\left(1 - \exp\left(-\frac{K_{OL}\, k_z\, R\, T\, H^{equi}\, z}{F}\right)\right)}. \qquad (4.88)$$

Equation (4.88) correctly describes the expected behaviour, since in the limit of $z \to 0$, $H^{non-equi} \to H^{equi}/(1-1) \to \infty$; whereas when $z \to \infty$, $H^{non-equi} \to H^{equi}/(1-0) \to H^{equi}$.

The liquid height is the length of the liquid column above the sintered glass disk, measured when no gas was flowing through the liquid. About half a centimetre of liquid was below the sintered disk as dead volume due to construction constraints.

In practice, it was found that plots of $H^{non\text{-}equi}$ *vs.* z according to eqn (4.88) were not showing clear trends, especially if a high extent of equilibrium was reached at height z, i.e. $H^{non\text{-}equi} \approx H^{equi}$. Small variation in experimental conditions were giving ambiguous results. Equation (4.88) was modified by substituting the expression -gradient [1] = $(F/H^{non\text{-}equi}RTV^{aq})$ (see Section 4.3) and $V^{aq} = (S_r\, z)$ where S_r is the cross-sectional area of the bubble column. Thus

$$H^{non-equi} = \frac{F}{(-\text{gradient}\,[1])\;R\,T\,S_r\,z} = \frac{H^{equi}}{\left(1-\exp\left(-\frac{K_{OL}\,k_z\,R\,T\,H^{equi}\,z}{F}\right)\right)} \tag{4.89}$$

$$(-\text{gradient}\,[1]) = \frac{F}{R\,T\,S_r\,H^{equi}}\;\frac{\left(1-\exp\left(-\frac{K_{OL}\,k_z\,R\,T\,H^{equi}\,z}{F}\right)\right)}{z}. \tag{4.90}$$

Equation (4.90) can be simplified to

$$(-\text{gradient}\,[1]) = \frac{B}{H^{equi}}\;\frac{\left(1-\exp\left(-A\,H^{equi}\,z\right)\right)}{z} \tag{4.91}$$

where $B = F/(RTS_r)$ and $A = K_{OL}k_zRT/F$. Thus, when (-gradient [1]) (see Figure 4.6) is plotted against liquid height, z, the equilibrium value of Henry's law, H^{equi}, can be obtained by fitting eqn (4.91) to the data using H^{equi} and A as adjustable parameters in the fitting program. All values of B are known.

Equation (4.88) can be used to determine the column depth that corresponds to a given extent of equilibration. For example, a 99 % approach to equilibrium is expressed as

$$H^{non-equi} = \frac{H^{equi}}{0.99} = \frac{H^{equi}}{\left(1-\exp\left(-\frac{k_z\,R\,T\,K_{OL}\,H^{equi}\,z_{(99\%)}}{F}\right)\right)} \tag{4.92}$$

$$1-\exp\left(-\frac{k_z R T K_{OL} H^{equi} z_{(99\%)}}{F}\right)=0.99$$

(4.93)

$$z_{(99\%)}=-\frac{F \ln(0.01)}{k_z R T K_{OL} H^{equi}}.$$

(4.94)

Similarly, the heights for other degrees of saturation can be obtained. Note that in order to apply eqn (4.88), the measured values of $H^{non\text{-}equi}$ must be obtained from experiments in which the gas flow F is kept constant.

4.3.2 pH dependence of equilibrium partitioning of 2-nitrophenol

4.3.2.1 Effect of pH on Henry's law coefficient

Phenols are acidic and have a tendency to dissociate in aqueous solution, i.e. for 2-nitrophenol

$$C_6H_4(NO_2)OH + H_2O \rightleftharpoons H_3O^+ + C_6H_4(NO_2)O^-$$

(4.95)

with an equilibrium constant $K_{A(2NP)}$ of

$$K_{A(2NP)}=\frac{\left[H_3O^+\right]\left[C_6H_4(NO_2)O^-\right]}{\left[C_6H_4(NO_2)OH\right]}.$$

(4.96)

Since only the undissociated species undergo gas exchange, an effective Henry's law coefficient H^* is introduced, as shown in Chapter 2. For 2-nitrophenol this is

$$H^*_{(2NP)}=H_{(2NP)}\left(1+10^{pH-pK_{A(2NP)}}\right).$$

(4.97)

The $pK_{A(2NP)}$ has been given as 7.23 at room temperature [*Schwarzenbach et al.*, 1988]. The pH of a solution of a weak acid is [*Atkins*, 1986]

$$pH = \frac{1}{2} pK_{A(2NP)} - \frac{1}{2} \log [2NP].$$

(4.98)

Equation (4.98) predicts a pH range from about 6.1 to 5.6 for the concentration ranges applicable in this study (i.e. 10^{-5} to 10^{-4} mol l^{-1}). Using a Henry's law coefficient of 74.1 M atm^{-1} at 20 °C [*Schwarzenbach et al.*, 1988] and eqn (4.97), the effective Henry's law coefficients of $H^*_{(10^{-5}\,M)} = 79.6$ and $H^*_{(10^{-4}\,M)} = 75.8$ M atm^{-1} can be calculated. As expected for the conditions used (see Chapter 2), the effective H^* are therefore less than 10 % higher than H and the influence of the pH on the partitioning was neglected.

4.3.2.2 Influence of pH on the absorbance of 2-nitrophenol

The undissociated ($C_6H_4(NO_2)OH$) and dissociated ($C_6H_4(NO_2)O^-$) forms of 2-nitrophenol have different absorption maxima in water [*Schwarzenbach et al.*, 1988].

	λ_{max} /nm	ε_{max} /M^{-1} cm^{-1}
$C_6H_4(NO_2)OH$	278	6250
$C_6H_4(NO_2)O^-$	282	4000

During purging, the concentration of 2-nitrophenol in the aqueous solution changes which leads to changes in pH and hence the degree of dissociation changes. Such changes could cause errors if the absorption coefficients ε of the undissociated and dissociated species are different at a given wavelength, i.e. in addition to changes in absorption due to the purging progress (decrease in aqueous concentration), the absorption could be influenced by a changing degree in dissociation. This was checked in an example calculation.

According to (4.95), the fraction dissociated is described by

$$x_{[C_6H_4(NO_2)O^-]} = \frac{[C_6H_4(NO_2)O^-]}{[C_6H_4(NO_2)OH] + [C_6H_4(NO_2)O^-]} \quad \textbf{(4.99)}$$

Using eqn (4.96) gives

$$\frac{1}{x_{[C_6H_4(NO_2)O^-]}} = \frac{[C_6H_4(NO_2)OH]}{[C_6H_4(NO_2)O^-]} + 1 = \frac{[H_3O^+]}{K_{A(2NP)}} + 1 \quad \textbf{(4.100)}$$

$$x_{[C_6H_4(NO_2)O^-]} = \frac{K_{A(2NP)}}{K_{A(2NP)} + [H_3O^+]} \quad \textbf{(4.101)}$$

The concentrations of the aqueous solutions of 2-nitrophenol used were in the range of 10^{-5} - 10^{-4} mol l^{-1}. The concentrations of dissociated species for these solutions were calculated as detailed in Table 4.4.

The ratio of the concentration of $C_6H_4(NO_2)OH$ at 10^{-4} and 10^{-5} mol l^{-1} total concentration is

$$\frac{[C_6H_4(NO_2)OH]_{10^{-4}}}{[C_6H_4(NO_2)OH]_{10^{-5}}} = \frac{9.771 \times 10^{-5}}{9.310 \times 10^{-6}} = \underline{\underline{10.495}} \quad \textbf{(4.102)}$$

$[2NP]_{total}$ /mol l^{-1}	10^{-5}	10^{-4}
pH (see eqn (4.98))	6.1	5.6
$[H_3O^+]$ /mol l^{-1}	7.94×10^{-7}	2.51×10^{-6}
$x_{[C_6H_4(NO_2)O^-]}$ (see eqn (4.101))	0.0690	0.0229
$[C_6H_4(NO_2)O^-]$ /mol l^{-1} $(=[2NP]_{total}\ x_{[C_6H_4(NO_2)O^-]})$	6.901×10^{-7}	2.291×10^{-6}
$x_{[C_6H_4(NO_2)OH]}$ $(=1- x_{[C_6H_4(NO_2)O^-]})$	0.9310	0.9771
$[C_6H_4(NO_2)OH]$ /mol l^{-1} $(=[2NP]_{total}\ x_{[C_6H_4(NO_2)OH]})$	9.310×10^{-6}	9.771×10^{-5}

Table 4.4 pH, fraction dissociated and concentrations for a given total 2-nitrophenol concentration.

The total absorption is calculated by

$$A = \varepsilon\, l\, [i] = \left(\varepsilon_{(C_6H_4(NO_2)OH)}\, l\, [C_6H_4(NO_2)OH]\right) + \left(\varepsilon_{(C_6H_4(NO_2)O^-)}\, l\, [C_6H_4(NO_2)O^-]\right). \quad \textbf{(4.103)}$$

Suppose $\varepsilon_{[C_6H_4(NO_2)O^-]} = 0.5\ \varepsilon_{[C_6H_4(NO_2)OH]}$ at a specific λ and $l = 1$ cm then the absorbance at a total 2-nitrophenol concentration of 10^{-4} mol l^{-1} can be calculated as

$$A_{10^{-4}} = \left[\left(1000\ \text{mol}^{-1}\ l\ \text{cm}^{-1} \times 9.771 \times 10^{-5}\ \text{mol}\ l^{-1}\right) + \left(500\ \text{mol}^{-1}\ l\ \text{cm}^{-1} \times 2.291 \times 10^{-6}\ \text{mol}\ l^{-1}\right)\right] 1\ \text{cm} \quad \textbf{(4.104)}$$

$$A_{10^{-4}} = 9.886 \times 10^{-2}$$

(4.105)

using an arbitrary value of $\varepsilon_{[C_6H_4(NO_2)OH]} = 1000$ mol^{-1} l cm^{-1} and the values of Table 4.4. Similarly, a value $A_{10^{-5}} = 9.655 \times 10^{-3}$ can be calculated for a total concentration of 10^{-5} mol l^{-1}. The ratio of absorptions at the two concentrations is then

$$\frac{A_{10^{-4}}}{A_{10^{-5}}} = \frac{9.886 \times 10^{-2}}{9.655 \times 10^{-3}} = \underline{\underline{10.239}}$$

(4.106)

The discrepancy between the results of eqn (4.106) and of eqn (4.102) is less than 3 %. The ratio of $[10^{-4}]/[10^{-5}]$ covers the overall concentration range of interest. However, the maximum change in absorption was 0.05 for any one experiment to extract a Henry's law coefficient (i.e. constant liquid volume and flow rate). This change in absorbance (= 0.05) corresponds to a change in concentration of about 8.0×10^{-6} mol l^{-1}. This is less than a tenth of the example calculated (change in concentration there is 9×10^{-5} mol l^{-1}). Subsequently, the change in absorption due to a different grade of dissociation will be smaller. Additionally, the approximation of $\varepsilon_{[C_6H_4(NO_2)O^-]} = 1/2\ \varepsilon_{[C_6H_4(NO_2)OH]}$ is probably an overestimation. Consequently, the effect on measured absorption of a shift of the dissociation equilibrium during purging was neglected.

4.3.3 Hydrolysis

Hydrolysis refers to the irreversible reaction with water (see Chapter 2). If hydrolysis of the species being purged takes place, the overall mass balance is

$$-\frac{dn^{aq}}{dt} = +\frac{dn^{gas}}{dt} - \frac{dn_H{}^{aq}}{dt}$$

(4.107)

where $n_H{}^{aq}$ refers to the molecules in the aqueous phase which undergo hydrolysis. The rate of hydrolysis is

$$-\frac{d[i]^{aq}}{dt} = k_H[i]^{aq}$$

(4.108)

where k_H is the first-order rate coefficient (s^{-1}). Therefore, if hydrolysis occurs, by analogy to the derivation in Section 4.3, the first-order decay in aqueous phase concentration is modified to

$$\ln\left(\frac{[i]_t^{aq}}{[i]_0^{aq}}\right) = -\left(\frac{F}{H\,R\,T\,V^{aq}} + k_H\right)t\,.$$

(4.109)

However, phenols have no hydrolysable functional groups and therefore the measured Henry's law coefficients are unaffected by hydrolysis. This was also stated in the extensive review by *Mabey et al.* [1982] where the hydrolysis rate coefficient is given a value of zero for 2-nitrophenol.

5. UPTAKE OF OZONE

The experimental results for the uptake measurements of ozone are presented in this chapter. The set-up of the spectrometer is described. All calculations for the uptake measurements are based on the data analysis techniques described comprehensively in Chapter 4. The results are compared with data of other groups found in the literature. Possible sources of errors and uncertainties are discussed.

5.1 Set-up of the spectrometer

As described in the experimental chapter, initially the performance of the spectrometer system was tested against another UV spectrometer available in the department. The chemicals used for these comparisons were acetone vapour and a solution of sodium dichromate. The spectra for both compounds, measured on the Instrument SA spectrometer, are shown in Figure 5.1 and Figure 5.2.

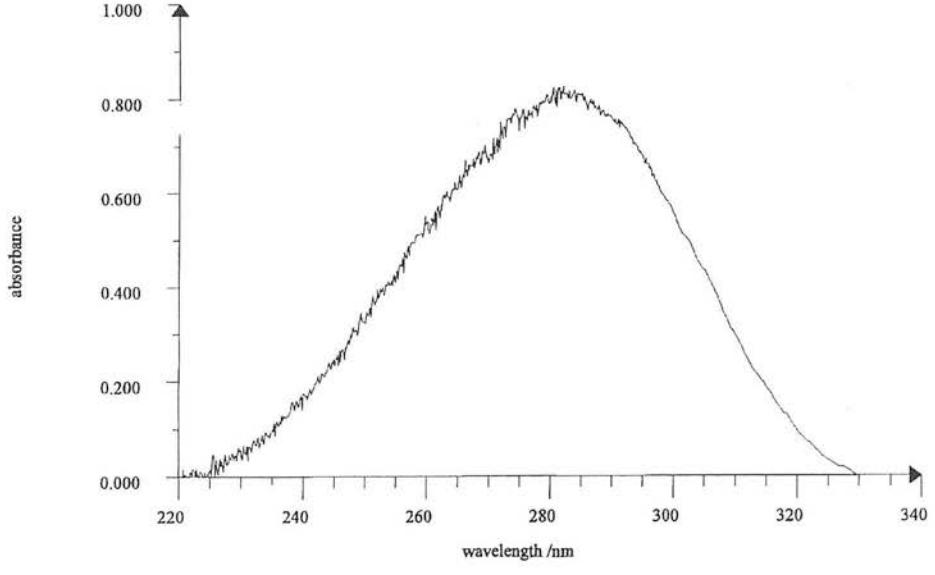

Figure 5.1 UV absorption spectrum of gas phase acetone

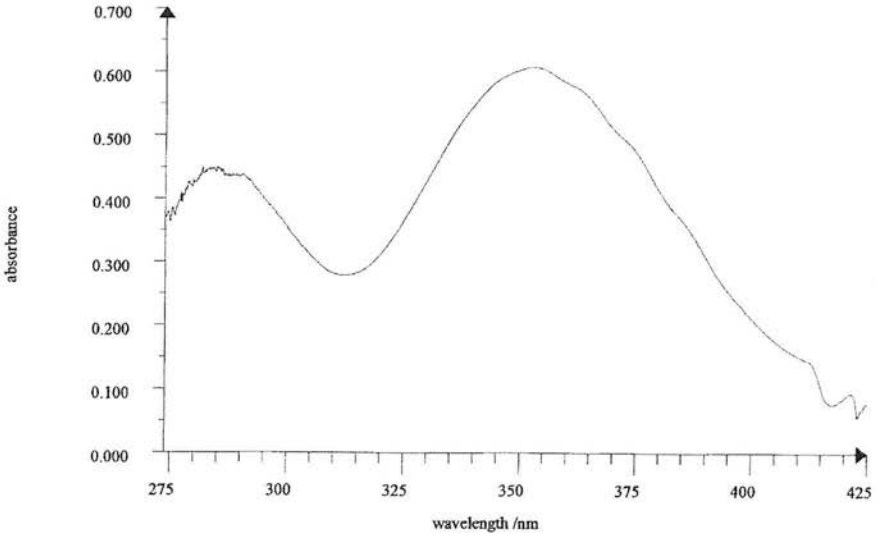

Figure 5.2 UV absorption spectrum of a solution of $Na_2Cr_2O_7 \cdot 2H_2O$

The measured absorbances for different concentrations of sodium dichromate at 350 nm are plotted in Figure 5.3 for both the Instrument SA and the Unicam spectrometer.

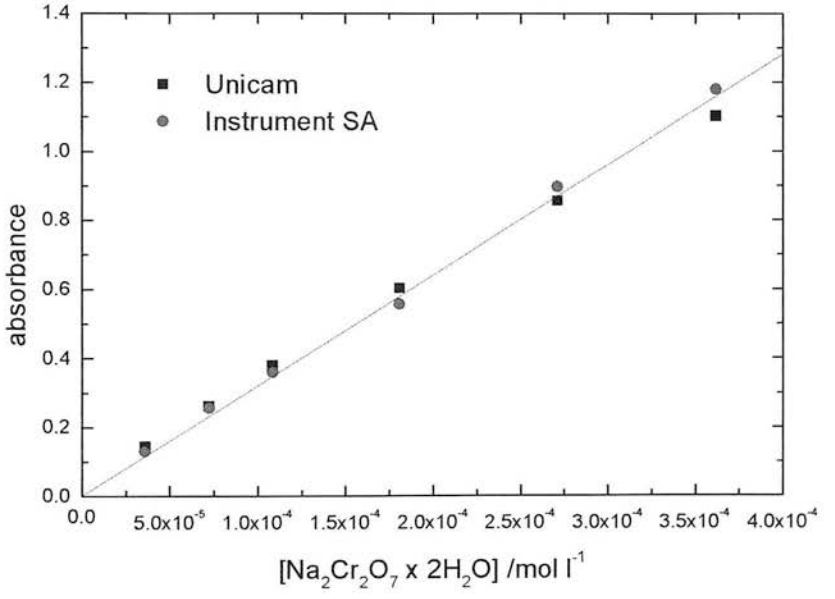

Figure 5.3 Plot of absorbance at 350 nm *vs.* concentration of $Na_2Cr_2O_7 \cdot 2H_2O$ solution for the Instrument SA and Unicam spectrometers.

The straight line is the linear best-fit to the average of both absorption measurements. Figure 5.3 shows that the absorbances of both instruments are linearly dependent on the dichromate concentration and in reasonable agreement.

Similarly, the absorbances for a mixture of acetone in helium showed agreement between the Unicam and the Instrument SA spectrometer.

5.2 Absorbance of ozone and determination of its concentration

Figure 5.4 shows an absorption spectrum of ozone over the wavelength range 210 to 290 nm measured using the Instrument SA spectrometer.

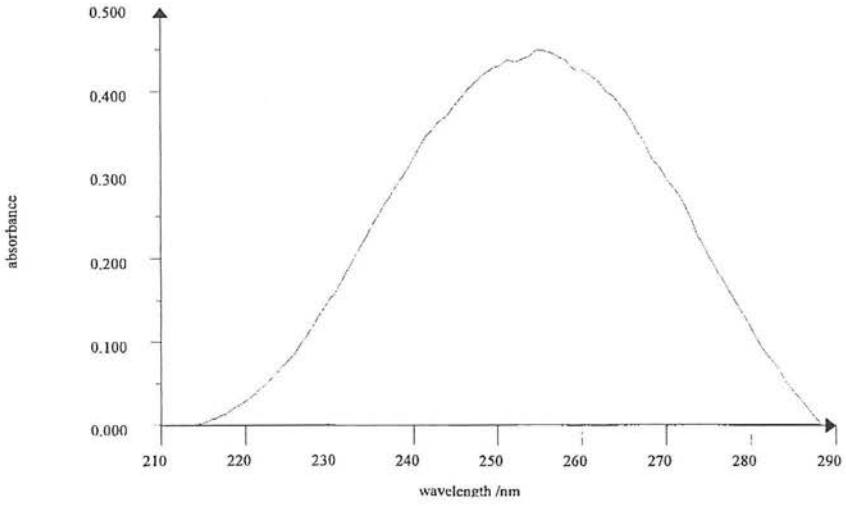

Figure 5.4 UV absorption spectrum of ozone

Various mixtures of ozone in helium were prepared in order to confirm linearity of absorption with partial pressure of ozone in the cell. Example data are plotted in Figure 5.5.

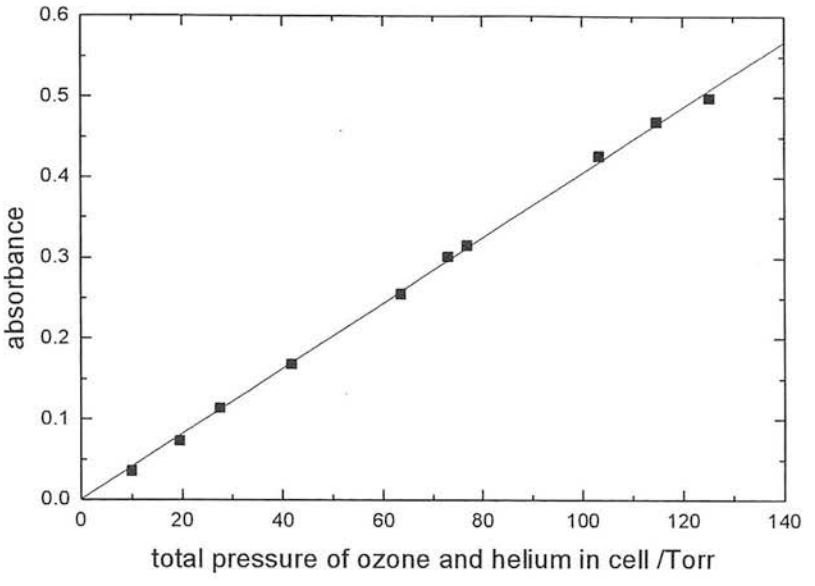

Figure 5.5 Plot of absorbance *vs.* pressure of ozone-helium mixture.

In molecular units for the Beer-Lambert law,

$$\ln \frac{I_0}{I} = \sigma \, l \, N \qquad (5.1)$$

where σ is the absorption cross section (cm^2 $molecule^{-1}$), l is the path length (cm) and N is the molecular concentration (molecule cm^{-3}). The highest absorption of about 0.5[1] in Figure 5.5 corresponds therefore to a concentration of about 10^{15} molecule cm^{-3}, using σ = 1.11 x 10^{-17} cm^2 $molecule^{-1}$ [*Finlayson-Pitts and Pitts, Jr.*, 1986] at λ = 258 nm and 298 K. The path length was 90 cm. Typical concentrations for the uptake measurements of ozone were in the range 10^{15} to 10^{17} molecules cm^{-3}.

5.3 Uptake measurements of ozone

The uptake of ozone onto pure water is determined by its physical solubility since no reaction is expected. The order of magnitude of the uptake can be estimated using

[1] Note that the absorbance in Figure 5.5 corresponds to $\log \frac{I_0}{I}$.

equations for the wetted-wall flow reactor, as given in Chapter 4, and estimated bulk properties, i.e.

$$\frac{1}{\gamma} = \frac{1}{\Gamma_G} + \frac{1}{\alpha} + \frac{1}{\Gamma_{SOL}}$$

$$= \frac{\omega\, r}{2\,(3.66)\,D_G} + \frac{1}{\alpha} + \frac{\sqrt{\pi}\,\omega\,\sqrt{t}}{4\,H\,R\,T\,\sqrt{D_L}} \,. \qquad (5.2)$$

The parameters for a typical experimental run are listed in Table 5.1.

Parameter	Numerical value	Source/comments
ω	3.58×10^4 cm s^{-1}	calculated at T = 293 K, p = 16 Torr, F = 400 cm^3 min^{-1} (STP), RH = 50 %
r	0.8 cm	radius of wetted-wall reactor
D_G	15.5 cm^2 s^{-1}	calculated at experimental conditions given above in this table (calculation shown in more detail below in this section)
α	> 0.002 at 276 K	*Utter et al.* [1992]
t	1 s	typical liquid-gas contact time
H	1.30×10^{-2} M atm^{-1}	*Herrmann et al.* [1999]
T	293 K	
D_L	2.30×10^{-5} cm^2 s^{-1}	calculated using Wilke-Chang correlation (shown in more detail below)

Table 5.1 Bulk properties for estimating the uptake of ozone onto pure water at the experimental conditions.

The estimated value of uptake coefficient $\gamma \approx 10^{-7}$, calculated using the listed parameters, was below the detection limit of the wetted-wall flow reactor. Therefore, the scavenger $Na_2S_2O_3$ was added to the water, as already described in Chapter 3, so that observed uptake was reaction controlled rather than solubility limited. All ozone measurements were performed at 293 K.

The natural logarithm of the absorbance was plotted against the injector position to extract the first-order rate coefficient for loss of ozone from the gas phase, k_w (s^{-1}).

After correction for the radial concentration gradient, k_w^{corr} (s^{-1}) was used to obtain γ (see Chapter 4 for detailed description). The effect of the correction can be seen in Figure 5.6 where the observed and the corrected absorption values for an example run are plotted together.

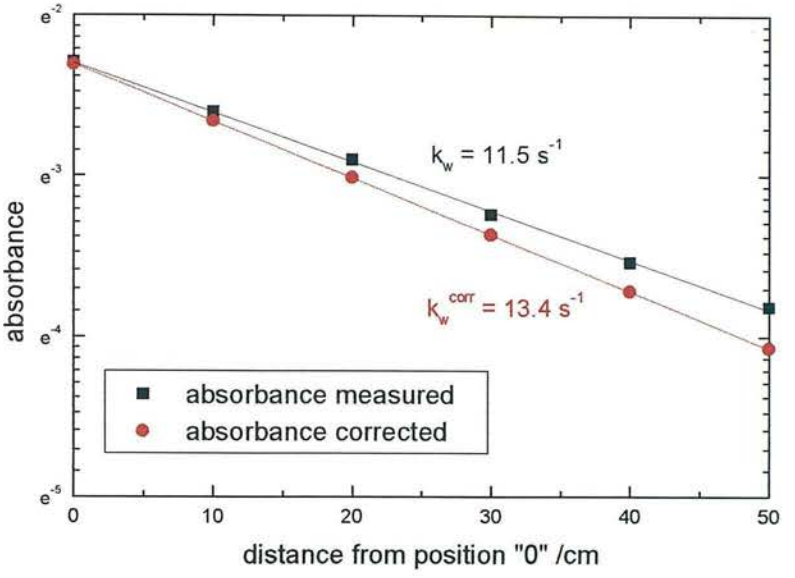

Figure 5.6 Plot of absorbance *vs.* distance from injector position "0" before (black line) and after (red line) correction for radial concentration gradient. Slopes are $-k_w/c$ and $-k_w^{corr}/c$, respectively, with c = 379 cm s^{-1}.

The experiment was repeated for different concentrations of $Na_2S_2O_3$ and the relevant data are shown in Table 5.2.

total pressure p /Torr	concentration $[Na_2S_2O_3]$ /mol l^{-1}	activity coefficient γ_i	$(c^{\ominus} a_{Na_2S_2O_3})$ /mol l^{-1}	k_w /s^{-1}	k_w^{corr} /s^{-1}	γ
12.0	0.19898	0.393	0.07820	17.6	21.8	9.73×10^{-4}
17.1	0.09912	0.464	0.04595	12.8	15.3	6.84×10^{-4}
19.0	0.07634	0.485	0.03699	10.2	11.8	5.28×10^{-4}
15.0	0.05984	0.504	0.03016	11.5	13.4	5.98×10^{-4}
17.1	0.04100	0.539	0.02209	8.9	10.0	4.48×10^{-4}
19.6	0.03587	0.553	0.01984	8.8	10.0	4.48×10^{-4}
18.0	0.03090	0.571	0.01763	8.5	9.5	4.25×10^{-4}
18.0	0.03090	0.571	0.01763	8.4	9.5	4.22×10^{-4}
14.0	0.02026	0.627	0.01270	7.5	8.2	3.66×10^{-4}

Table 5.2 Experimental parameters and results for uptake measurements of ozone onto $Na_2S_2O_3$ solutions at 293 K.

As described in Chapter 4 [*Kolb et al.*, 1995], a reaction controlled uptake according to the following equation

$$\frac{1}{\gamma} = \frac{1}{\Gamma_G} + \frac{1}{\alpha} + \frac{\omega}{4\,H\,R\,T\sqrt{D_L\,k''}}\,\frac{1}{\sqrt{c^{\ominus}\,a_{Na_2S_2O_3}}}, \qquad \textbf{(5.3)}$$

leads to a straight line for a plot of $1/\gamma$ *vs.* $1/\sqrt{c^{\ominus}\,a_{Na_2S_2O_3}}$. Since the extracted uptake coefficients γ in Table 5.2 have already been corrected for gas diffusion, (5.3) reduces to

$$\frac{1}{\gamma} = \frac{1}{\alpha} + \frac{\omega}{4\,H\,R\,T\sqrt{D_L\,k''}}\,\frac{1}{\sqrt{c^{\ominus}\,a_{Na_2S_2O_3}}}. \qquad \textbf{(5.4)}$$

The plot of $1/\gamma$ *vs.* $1/\sqrt{c^{\ominus}\,a_{Na_2S_2O_3}}$ is shown in Figure 5.7.

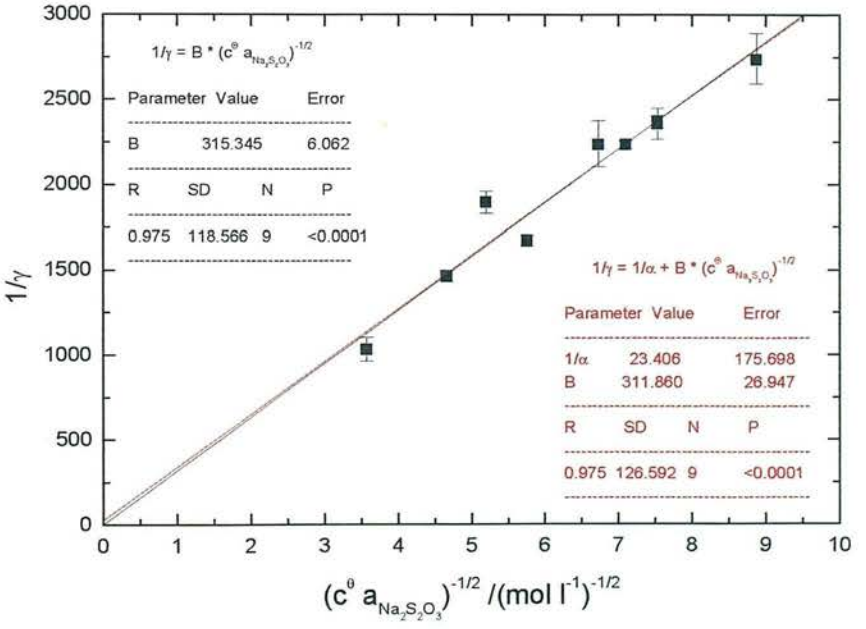

Figure 5.7 Plot of $1/\gamma$ *vs.* $1/\sqrt{c^{\ominus}\,a_{Na_2S_2O_3}}$ for uptake of ozone at 293 K. The red line is a linear fit to the data. The slope corresponds to $\omega/(4HRT\sqrt{D_L k''})$. The black line is a linear fit through the origin for the case that α equals or is close to unity and the intercept becomes negligible (see text). The errors of the individual points are the statistical errors obtained by plotting ln absorbance *vs.* distance to derive k_w (see Figure 5.6).

The slope ($\omega/(4HRT\sqrt{D_L k''})$) of the fitted straight line (= 311.9 $(mol\ l^{-1})^{1/2}$) yields k", provided H and D_L are known (see eqn (5.4)). Using the values in Table 5.1, a rate coefficient of $k'' = \left(3.67\ ^{+0.73}_{-0.56}\right) \times 10^8\ l\ mol^{-1}\ s^{-1}$ for the reaction of ozone with $Na_2S_2O_3$ in water was calculated, where the quoted errors refer to errors in the fitted line.

According to eqn (5.4) the intercept of the $1/\gamma$ *vs.* $1/\sqrt{c^{\ominus}\, a_{Na_2S_2O_3}}$ plot equals α^{-1}. Figure 5.7 indicates that mass accommodation is unimportant under these conditions. The intercept of 23.4 in Figure 5.7 yields an α of 4.3×10^{-2}. The statistical error gives a lower limit of $\alpha > 2.7 \times 10^{-3}$. Unfortunately the error is very large because extrapolation of the data to the intercept is extremely sensitive to the quality of the linear fit. The upper error limit gives a negative intercept which is not physically possible; though an intercept of one falls into this error range which allows α to be one or very close to one. Overall therefore, it can be concluded that the mass accommodation coefficient for ozone at 293 K is 4.3×10^{-2}, with a lower limit of $> 2.7 \times 10^{-3}$ but is possibly very close to unity.

The data can be analysed in an alternative manner. If it is assumed that α is very close to unity, i.e. the resistance to mass accommodation, $1/\alpha$, is very small compared with the resistance due to reactive uptake, the intercept $\rightarrow 1$ and is considered negligible. The measured uptake is then determined by γ_{RXN} (solid black line in Figure 5.7) and the equation

$$\log \gamma = \log \frac{4\,H\,R\,T\sqrt{D_L\ k''}}{\omega} + \frac{1}{2}\log\left(a_i c^{\ominus}\right) \qquad \textbf{(4.64)}$$

can be derived, as shown in Chapter 4. According to eqn (4.64), the plot of $\log \gamma$ *vs.* $\log\left(c^{\ominus} a_{Na_2S_2O_3}\right)$ should give a straight line of gradient 0.5 which would validate the assumption $1/\gamma_{RXN} \gg 1/\alpha$. Such a plot for the above data (Table 5.2) is presented in Figure 5.8.

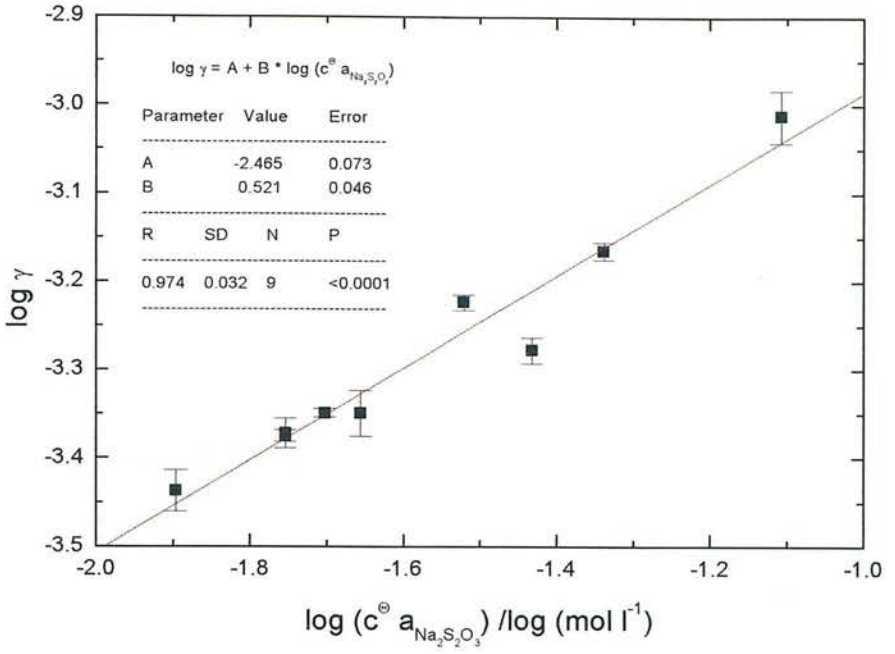

Figure 5.8 Plot of log γ *vs.* log ($c^{\ominus} a_{Na_2S_2O_3}$) for uptake of ozone at 293 K. The intercept equals $\log \frac{4 H R T \sqrt{D_L k''}}{\omega}$, and the slope B should be 0.5 if $1/\gamma_{RXN} \gg 1/\alpha$. The errors are the statistical errors obtained in the derivation of k_w (see Figure 5.6).

The slope in Figure 5.8 is 0.52 ± 0.05 (where the error range is for the statistical fit to the data) and verifies a reaction controlled uptake. The intercept equals $\log \frac{4 H R T \sqrt{D_L k''}}{\omega}$ (see eqn (4.64)). The value of the rate coefficient k" was calculated as $\left(4.19 \, {}^{+1.67}_{-1.20}\right)$ x 10^8 l mol^{-1} s^{-1} using the values in Table 5.1. The calculated rate coefficients from both approaches are listed in Table 5.3.

	k" from Figure 5.7 /l mol^{-1} s^{-1}	k" from Figure 5.8 /l mol^{-1} s^{-1}
k''_{max}	4.39 x 10^8	5.86 x 10^8
k"	**3.67 x 10^8**	**4.19 x 10^8**
k''_{min}	3.11 x 10^8	2.99 x 10^8

Table 5.3 Comparison of two approaches to extract k". k" was calculated using bulk properties listed in Table 5.1.

The extrapolation to the intercept of Figure 5.8 is more sensitive to experimental uncertainties in the data than derivation of the slope in Figure 5.7 so preference was given to the $1/\gamma$ *vs.* $1/\sqrt{c^{\ominus} a_{Na_2S_2O_3}}$ plot for extracting k". The $\log \gamma$ *vs.* $\log (c^{\ominus} a_{Na_2S_2O_3})$ plot (Figure 5.8) confirms reaction limited loss of ozone for the given experimental conditions, i.e. $1/\alpha << \omega/(4HRT\sqrt{D_L k_{RXN}})$.

5.3.1 Calculation of the gas diffusion coefficients

The pressure-independent binary diffusion coefficients (Torr cm^2 s^{-1}) of ozone in H_2O and helium, $D_G^P{}_{(O_3\text{-}H_2O)}$ and $D_G^P{}_{(O_3\text{-}He)}$, were calculated according to the Fuller-Schettler-Giddings [*Fuller et al.*, 1969] estimation method, as described in Chapter 4. Table 5.4 details the parameters used.

Parameter/ unit	Symbol	Value	Source/comments
temperature /K	T	293	
molar mass of ozone /g mol^{-1}	M_{O_3}	48.0	
molar mass of water /g mol^{-1}	M_{H_2O}	18.0	
molar mass of helium /g mol^{-1}	M_{He}	4.0	
atomic diffusion volume of ozone	$(\sum v)_{O_3}$	18.33	calculated from values given in *Fuller et al.* [1969]
atomic diffusion volume of water	$(\sum v)_{H_2O}$	13.1	given in *Fuller et al.* [1969]
atomic diffusion volume of helium	$(\sum v)_{He}$	2.67	given in *Fuller et al.* [1969]
gas diffusion coefficient O_3-H_2O /Torr cm^2 s^{-1}	$D_G^P{}_{(O_3\text{-}H_2O)}$	174.8	
gas diffusion coefficient O_3-He /Torr cm^2 s^{-1}	$D_G^P{}_{(O_3\text{-}He)}$	506.8	

Table 5.4 Parameters used to calculate pressure-independent binary gas diffusion coefficients of O_3 in H_2O and He following the method of Fuller-Schettler-Giddings [*Fuller et al.*, 1969].

5.3.2 Calculation of the liquid diffusion coefficient

The liquid diffusion coefficient for ozone in water was estimated by the Wilke-Chang method, as described in Chapter 4. The parameters used are listed in Table 5.5.

Parameter/ unit	Symbol	Value	Source/comments
association factor of solvent	ϕ_{H_2O}	2.6	*Reid et al.* [1987]
molar mass of water /g mol^{-1}	M_{H_2O}	18	
temperature /K	T	293	
viscosity of water /cP	μ_{H_2O}	1.002	*Kaye and Laby* [1995]
molar volume of ozone at boiling temperature /cm^3 mol^{-1}	V_{O_3}	22.2	Le Bas method as found in *Reid et al.* [1987]
liquid diffusion coefficient for ozone in water /cm^2 s^{-1}	$D_{L(O_3\text{-}H_2O)}$	2.30×10^{-5}	

Table 5.5 Parameters used to calculate the liquid diffusion coefficient of O_3 in H_2O following the method of Wilke and Chang as described in *Reid et al.* [1987].

5.4 Discussion

5.4.1 Comparison with other results

Several workers (e.g. *Utter et al.* [1992], *Magi et al.* [1997]) have studied the ozone uptake so that data for comparison are available. Mass accommodation values, α, of ozone uptake measurements reported in previous studies are listed in Table 5.6.

α	T /K	comment	liquid scavenger species	k" for reaction of O_3 with scavenger /l mol^{-1} s^{-1}	reference
2×10^{-3} to 1	276		SO_3^{2-} $S_2O_3^{2-}$ Sn^{2+}	3.9×10^8 2.2×10^8 8.5×10^8	*Utter et al.* [1992]
0.1	277	considered an estimate	I^-	4×10^9	*Hu et al.* [1995]
0.1	281	as lower limit	I^-	3.2×10^8 (at 275 K) to 2.4×10^9 (at 293 K)	*Magi et al.* [1997]
5.3×10^{-4}	283		SO_3^{2-}		*Tang and Lee* [1987]
1×10^{-2}	291	assumed for a model			*Chameides* [1984]
5×10^{-3}	RT	possibly underestimated (low k")	I^-	1×10^6	Wunderlich as cited in *Magi et al.* [1997]
4.3×10^{-2}	293		$S_2O_3^{2-}$	3.7×10^8	this work
5×10^{-2}	298	assumed for a model	SO_3^{2-}	1.5×10^9	*Herrmann et al.* [1999]

Table 5.6 Comparison of ozone mass accommodation values and liquid scavenger rate coefficients.

The mass accommodation coefficient derived in this work of 4.3×10^{-2} has a lower limit $\alpha > 2.7 \times 10^{-3}$ based on the intercept in Figure 5.7. This value falls in the range of values reported by other groups. The early measurements of *Tang and Lee* [1987] as well as the value given by Wunderlich (as cited in *Magi et al.* [1997]) seem to be the lower limit of α. *Chameides* [1984] chose a single value of α for different species in his box model investigation due to lack of experimental data and for simplicity.

Most reaction rates increase with temperature, as described by the Arrhenius equation, i.e.

$$\ln k'' = \ln A_R - \frac{E_a}{RT} \quad \text{or} \quad k'' = A_R \exp\left(-\frac{E_a}{RT}\right) \tag{5.5}$$

where E_a is the activation energy (e.g. in J mol^{-1}) and A_R (e.g. in l mol^{-1} s^{-1}) is called the pre-exponential factor. If it is assumed that eqn (5.5) is applicable to the

scavenging reaction between O_3 and $Na_2S_2O_3$ then the following Arrhenius parameters for k" can be derived using measurements at 293 K from this work and at 276 K by *Utter et al.* [1992]:

$$E_a = 20.2 \text{ kJ mol}^{-1}$$
$$A_R = 1.49 \times 10^{12} \text{ l mol}^{-1} \text{ s}^{-1}.$$

This calculation is of limited confidence, of course, since only two measurements are available.

5.4.2 **Possible sources of error in γ**

5.4.2.1 Uncertainties in the experiment

There are a number of factors in the wetted-wall flow experiment which can cause possible errors in the measured uptake coefficient. A major source of error is the uncertainty in the relative humidity which is dealt with in the following section. Other errors include fluctuations in temperature and pressure along the flow tube (≤ 1 %) and the manual adjustment of the injector position ($\sim$ 0.6 %). The reading of the absorption signal and fluctuations in the UV lamp output are estimated to introduce an error of 5 to 10 %.

The uniform wetting of the whole inside wall of the reactor is essential for the data analysis. Experiments were performed only when the wall was completely wetted. However, this was only checked visually. Ripples were noticed at high water flow rates ($>$ 150 ml min^{-1}). This is a problem since rippling enhances absorption rates [*Danckwerts*, 1970] and mass transport in the liquid by factors of 2-3 [*Hanson et al.*, 1992]. High water flow rates were therefore avoided.

Relative humidity

As described in Chapter 4, no measurements of the relative humidity exist for the first uptake measurements. The above results are based on a value of 50 % relative humidity which was measured in replicate conditions of the uptake measurements.

Variations in the relative humidity during one experiment can lead to significant changes in the uptake data, since the calculation of the gas flow velocity and the gas diffusion coefficient under experimental conditions, and therefore k_w, rely on the exact knowledge of the humidity in the flow reactor. The effect of a higher relative humidity (60 % RH) on the first-order rate coefficients can be seen in Figure 5.9.

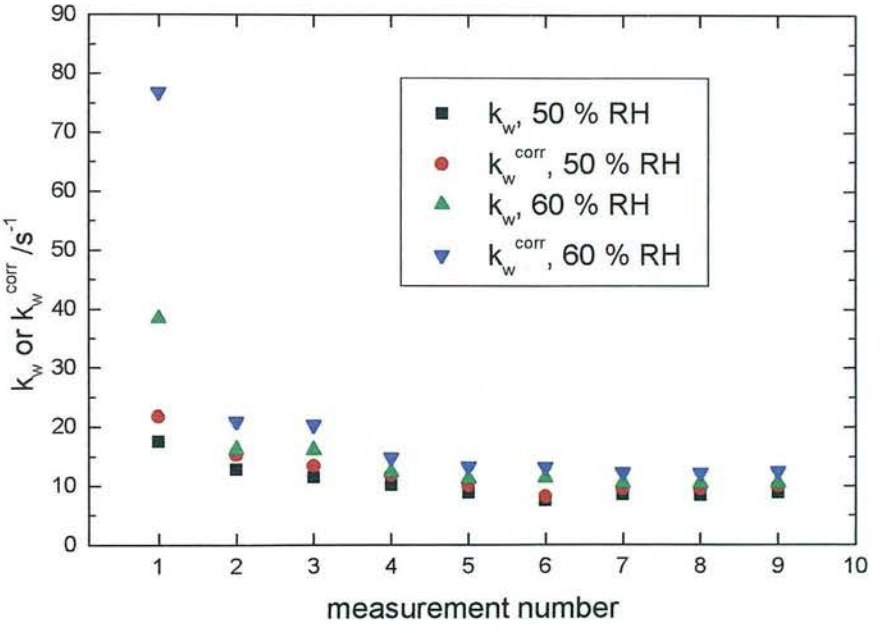

Figure 5.9 Comparison between the measured first-order loss rates (k_w) and after correction for radial diffusion (k_w^{corr}) with either 50 % or 60 % RH.

The uncorrected and corrected k_w are plotted in Figure 5.9. Two effects are visible. Firstly, k_w is higher at a higher RH but the impact is not large at k_w values below 20 s^{-1}. However, above that value the $k_w^{60\%RH}$ becomes notably higher than the $k_w^{50\%RH}$. Secondly, at about the same limit the correction for gas diffusion of $k_w^{60\%RH}$ (≈ 80 s^{-1}) is double the measured k_w (≈ 40 s^{-1}). This introduces errors due to uncertainties in the diffusion coefficients of ozone in the gas mixture under the

experimental conditions. On the other hand, the correction for the smaller $k_w^{50\%RH}$ are much smaller, and therefore less prone to errors.

The relative humidity is also a strong function of temperature. A change of 1 K at 50 % RH at 293 K corresponds to a change in relative humidity of ± 3.2 % RH [*A guide to the measurement of humidity*, 1996].

It can be concluded that the exact knowledge of RH is essential in the data analysis. Although the humidity was measured in replicate conditions, errors can not be ruled out. The overall error in γ due to uncertainties in the relative humidity is probably ± 20 %.

5.4.2.2 Other uncertainties

Effect of ionic strength on Henry's law coefficient

The presence of $Na_2S_2O_3$ in the solution on the Henry's law coefficient for ozone has so far been ignored in the analysis. *Kosak-Channing and Helz* [1983] have reported the change in Henry's law coefficient of ozone with ionic strength. Their values are shown in Table 5.7 for 293 K. The experiments were performed using sodium sulfate solutions rather than sodium thiosulfate solutions.

ionic strength $I_S^{Na_2SO_4}$ /mol l^{-1}	0.00	0.15	0.30	0.60
H /M atm^{-1}	1.28×10^{-2}	1.22×10^{-2}	1.17×10^{-2}	1.06×10^{-2}

Table 5.7 Change of H of ozone with ionic strength. Values are at 293 K, measured on Na_2SO_4 solutions [*Kosak-Channing and Helz*, 1983].

The scavenger concentrations used in this study ranged from 0.02 to 0.2 mol l^{-1} which correspond to ionic strengths of 0.06 to 0.6 mol l^{-1} (see Chapter 4 for calculation). Unfortunately, only limited data are available on salting-out coefficients of other salt

solutions (e.g. *Pawlikowski and Prausnitz* [1983; 1984]). It was therefore assumed for this discussion that the behaviour of ozone in $Na_2S_2O_3$ solutions was similar to solutions of Na_2SO_4, rather than trying to estimate the salting-out constant since, as far as can be ascertained, no salting-out parameters have been reported for either $Na_2S_2O_3$ or for the individual $S_2O_3^{2-}$ ion.

The Henry's law coefficient of ozone in $Na_2S_2O_3$, $H_S^{O_3}$, for the concentrations used here can be calculated by employing the Setchenow expression, as described in Chapter 2, and using data for Na_2SO_4 as a surrogate for $Na_2S_2O_3$, i.e.

$$\log \frac{H^{O_3}}{H_S^{O_3}} = k_S \left[Na_2SO_4\right] \tag{5.6}$$

where H^{O_3} and $H_S^{O_3}$ are the Henry's law coefficient of ozone in pure water and in the salt solution, respectively, $[Na_2SO_4]$ is the molarity of the Na_2SO_4 solution (mol l^{-1}) and k_S is the Setchenow salting-out coefficient (l mol^{-1}). The quantity k_S can be described as the sum of contributions of the negative and positive species in solution and of the gas [*Danckwerts*, 1970], i.e.

$$k_S = k_S^{Na^+} + k_S^{SO_4^{2-}} + k_S^{O_3} . \tag{5.7}$$

$k_S^{Na^+}$ and $k_S^{SO_4^{2-}}$ were taken from *Danckwerts* [1970] and are independent of temperature. *Magi et al.* [1997] have given a value of $k_S^{O_3}$ at 293 K, based on the results of *Kosak-Channing and Helz* [1983] on Na_2SO_4 solutions. This leads to

$$k_S = 0.091 + 0.022 + 0.0211 = \underline{0.1341 \text{ l mol}^{-1}}. \tag{5.8}$$

$H_S^{O_3}$ for the different experimental salt concentrations of $Na_2S_2O_3$ were calculated (Table 5.8). Agreement of both approaches, i.e. calculation *via* salting-out coefficients of single ions, and the experimental values determined for four ionic strengths by

Kosak-Channing and Helz [1983], was confirmed by plotting $H_S^{O_3}$ *vs.* ionic strength (Figure 5.10).

$[Na_2S_2O_3]$	I_s	$H_S^{O_3}$	k''_S
/mol l^{-1}	/mol l^{-1}	/M atm^{-1}	/l mol^{-1} s^{-1}
0.19898	0.597	1.081×10^{-2}	5.31×10^{8}
0.09912	0.297	1.186×10^{-2}	4.41×10^{8}
0.07634	0.229	1.211×10^{-2}	4.23×10^{8}
0.05984	0.180	1.230×10^{-2}	4.10×10^{8}
0.04100	0.123	1.252×10^{-2}	3.96×10^{8}
0.03587	0.108	1.258×10^{-2}	3.92×10^{8}
0.03090	0.093	1.263×10^{-2}	3.89×10^{8}
0.02026	0.061	1.276×10^{-2}	3.81×10^{8}

Table 5.8 Estimated Henry's law coefficient of ozone as a function of ionic strength for O_3 in $Na_2S_2O_3$ at 293 K. H_S was calculated using the Setchenow equation, with a value of H on pure water of 1.30×10^{-2} M atm^{-1} [*Herrmann et al.*, 1999]. k''_S is the second-order rate constant calculated using H_S, the parameters from Table 5.1 and the slope of Figure 5.7.

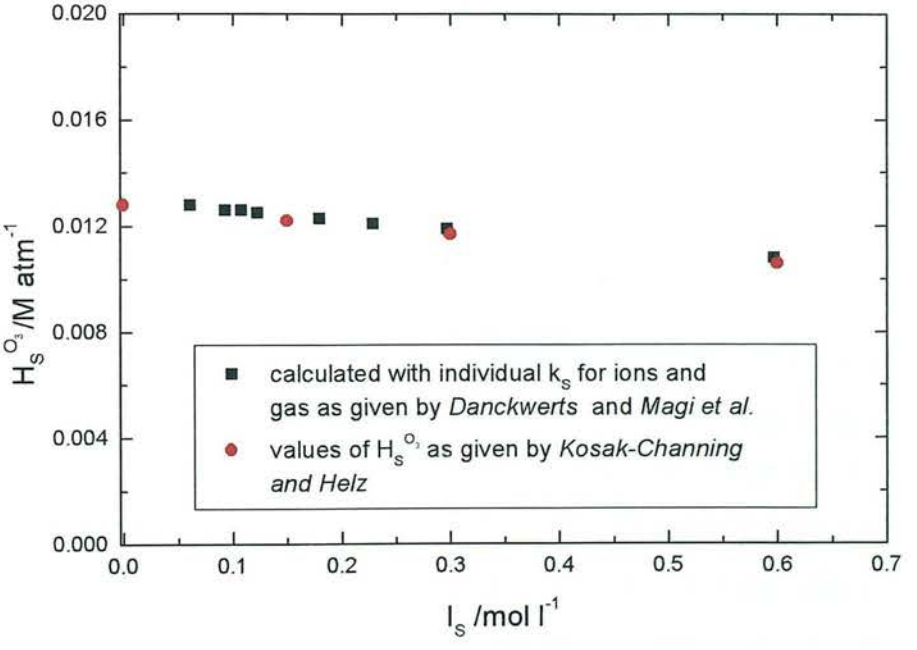

Figure 5.10 The Henry's law coefficient of ozone as a function of ionic strength at 293 K. Shown are the values from Table 5.8, calculated from *Danckwerts* [1970] and *Magi et al.* [1997], as well as the Henry's law coefficients given by *Kosak-Channing and Helz* [1983] for ozone on Na_2SO_4 solutions at 293 K.

Since the slope of Figure 5.7 is linear the product $H\sqrt{k''}$ is constant. From $H\sqrt{k''} = H_s^{O_3}\sqrt{k''_s}$, the second-order rate constant k''_s in the electrolyte can be calculated which takes into account the ionic strength. These values for k''_s are also listed in Table 5.8.

Since $I_s \propto [i]$ (see eqn (4.66)), it follows from eqn (5.6) and (5.4) that

$$\frac{1}{H_s} \propto 10^{I_s} \quad \text{and} \quad \sqrt{k''_s} \propto \frac{1}{H_s} \tag{5.9}$$

and therefore

$$\sqrt{k''_s} \propto 10^{I_s}, \tag{5.10}$$

i.e. k''_s increases with ionic strength (see Table 5.8). However, all k''_s are within the error limit of k", apart from the highest ionic strength. Therefore, the effect of ionic strength on Henry's law coefficient was neglected. It should be kept in mind that, due to lack of $Na_2S_2O_3$ data, all calculations were done using parameters for Na_2SO_4 instead.

Salt activity

For the treatment of data in this work, activities rather than concentrations of $Na_2S_2O_3$ at 25 °C were applied, as described in Chapter 4. Some researchers neglect the activity in the data treatment for reactive uptake and use concentrations instead, e.g. *Fickert et al.* [1998] used [Br^-] up to 0.1 M when investigating uptake of $ClNO_2$. Figure 5.11 is the analogous plot to Figure 5.7 and illustrates the effect of using concentrations rather than activities. The dotted line in Figure 5.11 is fitted to the activity values for easy comparison.

The intercept of 385 yields a value for α of 2.6×10^{-3}. The slope yields a value of $k'' = \left(2.95\ ^{+0.63}_{-0.48}\right) \times 10^8$ l mol^{-1} s^{-1}, using the parameters of Table 5.1 with H^{O_3} on pure

water. Table 5.9 shows these results in comparison with the results obtained using activities (see Figure 5.7).

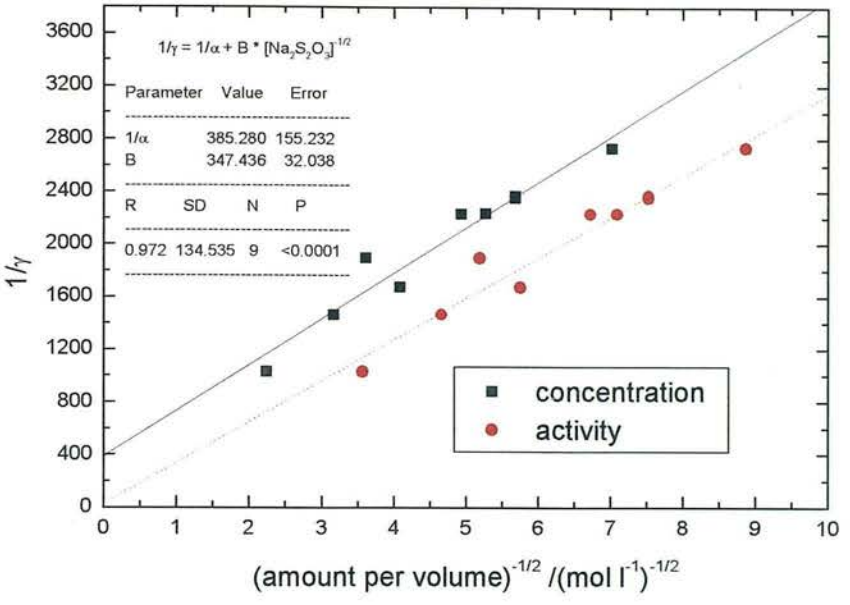

Figure 5.11 Plot of $1/\gamma$ *vs.* $1/\sqrt{[Na_2S_2O_3]}$ (black squares) and *vs.* $1/\sqrt{c^{\ominus}\, a_{Na_2S_2O_3}}$ (red dots), respectively, for reactive uptake of O_3 on $Na_2S_2O_3$ solution at 293 K. The black solid line is a linear fit to the concentration data; values for intercept (= $1/\alpha$) and slope (= $\omega/(4HRT\sqrt{D_L k''})$) are given in the plot. The dotted red line is a fit to the activity values as previously shown in Figure 5.7.

analysis using	α	lower limit of α	k" for reaction of O_3 with $Na_2S_2O_3$ / l mol^{-1} s^{-1}
activities	4.3×10^{-2}	$> 2.7 \times 10^{-3}$	$\left(3.67\ ^{+0.73}_{-0.56}\right) \times 10^{8}$
concentration	2.6×10^{-3}	$> 1.4 \times 10^{-3}$	$\left(2.95\ ^{+0.63}_{-0.48}\right) \times 10^{8}$

Table 5.9 Comparison of mass accommodation of ozone and rate coefficient for reaction of O_3 with $Na_2S_2O_3$ at 293 K using either activities or concentration in the data analysis.

The difference in α between these two approaches is quite significant (by a factor of about 16). The lower limit obtained by the concentration approach is smaller only by a factor of 1.9 due to the large error in the intercept. However, the intercept for the lower limit of $1/\alpha = 696$ appears to be rather large, especially since analysis confirmed

a reaction controlled mechanism (see Figure 5.8). Although errors might be introduced from uncertainties in the activity coefficients, these seem to be minor compared with the difference in the results. It can be concluded that the α value obtained using activities is more reliable. The slopes of concentration and activity plot are comparable which is the reason that the rate coefficients derived from them are in the same range.

Effect of ionic strength on the liquid diffusion coefficient

Akita [1981] has presented a method to predict diffusivities of gases in aqueous electrolyte solutions, if gas diffusivities in pure water and the densities of the solutions are available.

$$D_L^{\,S} = \left(\frac{k}{h}\right)\left(\frac{V_S}{N_A}\right)^{2/3} T \exp\left(-\frac{\Delta a\, x_{Na^+} + \Delta b\, x_{S_2O_3^{2-}} + g}{RT}\right) \qquad \textbf{(5.11)}$$

where $D_L^{\,S}$ is the diffusion coefficient in the electrolyte ($cm^2\ s^{-1}$), k is Boltzmann's constant (=1.38066 x 10^{-23} J K^{-1}), h is the Planck constant (= 6.62618 x 10^{-34} J s), V_S is the molar volume ($cm^3\ mol^{-1}$) of the solution, N_A is Avogadro number (= 6.02205 x 10^{23} mol^{-1}), T is the temperature (K) and R is the gas constant (= 8.314 J mol^{-1} K^{-1}). x_{Na^+} and $x_{S_2O_3^{2-}}$ are the mole fractions of anion and cation, respectively. Δa, Δb and g are components of the free energy of activation of diffusing solute due to cation, anion and water, respectively (J mol^{-1}). No Δb for $S_2O_3^{2-}$ was given, therefore Δb for SO_4^{2-} was used instead.

The following calculation to assess the effect of ionic strength on D_L was done for the highest concentration used, i.e. 0.2 M. The molar volume of the solution is given by

$$V_S = \frac{1}{[Na^+] + [SO_4^{\,2-}] + [H_2O]} \qquad \textbf{(5.12)}$$

where the concentration of water is defined as [*Akita*, 1981]

$$[H_2O] = \frac{\rho_S - M_{Na^+}[Na^+] - M_{SO_4^{2-}}[SO_4^{2-}]}{M_{H_2O}}$$

(5.13)

in which ρ_S is the density of the solution (g l^{-1}) and M_{Na^+}, $M_{SO_4^{2-}}$ and M_{H_2O} are the molar masses (g mol^{-1}) of Na^+, SO_4^{2-} and water, respectively. Using an estimated ρ_S of 1.026×10^3 g l^{-1} for a 0.2 M solution [*Landolt-Börnstein Physikalisch-Chemische Tabellen*, 1931] the water concentration was $[H_2O] = 55.38$ mol l^{-1}, which results in a molar solution volume $V_S = 17.86 \times 10^{-3}$ l $mol^{-1} = 17.86$ cm^3 mol^{-1}.

Akita [1981] also gives an expression for evaluating *g* which is

$$D_L = \left(\frac{k}{h}\right)\left(\frac{V_{H_2O}}{N_A}\right)^{2/3} T \exp\left(-\frac{g}{RT}\right).$$

(5.14)

Here, V_{H_2O} is the molar volume of water. It can be calculated as 18.05 cm^3 mol^{-1}. The parameter *g* was than obtained for 293 K, using a D_L of 2.30×10^{-5} cm^2 s^{-1},

$$g = (-RT)\ \ln\left(\frac{D_L}{\left(\frac{k}{h}\right)\left(\frac{V_{H_2O}}{N_A}\right)^{2/3} T}\right) = \underline{\underline{13510 \text{ J mol}^{-1}}}.$$

(5.15)

The mole fraction x_i is

$$x_i = V_S\,[i]$$

(5.16)

with $\sum x_i = 1$. According to eqn (5.11) and with the given values of Δa_{Na^+} (10.0×10^3 J mol^{-1}) and $\Delta b_{SO_4^{2-}}$ (12.7×10^3 J mol^{-1}) [*Akita*, 1981], D_L^S was calculated.

$$D_L^{\,S} = \left(\frac{1.38 \times 10^{-23}\ \text{J K}^{-1}}{6.626 \times 10^{-34}\ \text{J s}}\right)\left(\frac{17.86\ \text{cm}^3\ \text{mol}^{-1}}{6.022 \times 10^{23}\ \text{mol}^{-1}}\right)^{2/3} 293\ \text{K} \times$$

$$\exp\left(-\frac{\left[\left(10.0 \times 10^3 \times 7.144 \times 10^{-3}\right)+\left(12.7 \times 10^3 \times 3.572 \times 10^{-3}\right)+\left(13.51 \times 10^3\right)\right]\text{J mol}^{-1}}{8.314\ \text{J mol}^{-1}\ \text{K}^{-1} \times 293\ \text{K}}\right)$$

(5.17)

$$\underline{\underline{D_L^{\,S} = 2.18 \times 10^{-5}\ \text{cm}^2\ \text{s}^{-1}}}$$

(5.18)

Since this is only marginally different from the diffusion coefficient in pure water, the effect of the ionic strength on the liquid diffusivity can be ignored.

5.5 Conclusion

The uptake of ozone onto $Na_2S_2O_3$ solutions at 293 K has been investigated in order to gain experience in the operation of the newly set-up wetted-wall flow reactor.

The highest uptake was found to be $\sim 10^{-3}$ at a $Na_2S_2O_3$ concentration of about 0.2 mol l^{-1}. The uptake increases with increasing $Na_2S_2O_3$ activity which indicates a reaction controlled mechanism. The second-order rate coefficient k" was calculated as $\left(3.67\ ^{+0.73}_{-0.56}\right) \times 10^8$ l mol^{-1} s^{-1} for the reaction of ozone with $Na_2S_2O_3$ in water. A mass accommodation coefficient of 4.3×10^{-2} was derived, with a lower limit of $> 2.7 \times 10^{-3}$. The agreement with existing data in the literature is good. The biggest source of error in the uptake measurements comes from uncertainties in the relative humidity.

6. UPTAKE OF PHENOL

The results of the uptake measurements of phenol are presented in this chapter. As discussed previously, time dependent uptake requires a different measurement procedure from uptake independent of time. Both techniques were applied. Time dependent uptake was investigated on pure water. In the second approach the uptake was measured on bromine water. The fast reaction between phenol and bromine allows measurement of the uptake independent of time. Results of both methods are compared and discussed.

6.1 UV absorption spectrum of phenol

A gas phase absorption spectrum of phenol over the wavelength range 200 to 300 nm, measured using the Instrument SA spectrometer, is shown in Figure 6.1.

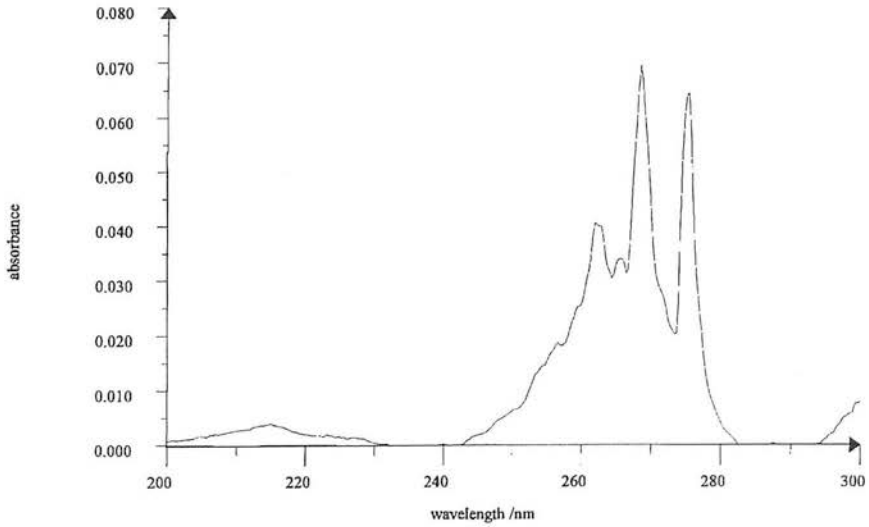

Figure 6.1 UV absorption spectrum of phenol

The linearity of the detector signal of phenol as a function of phenol concentration was checked by measuring the absorption signal for different total pressures of a typical phenol-helium mixture. Example data are plotted in Figure 6.2.

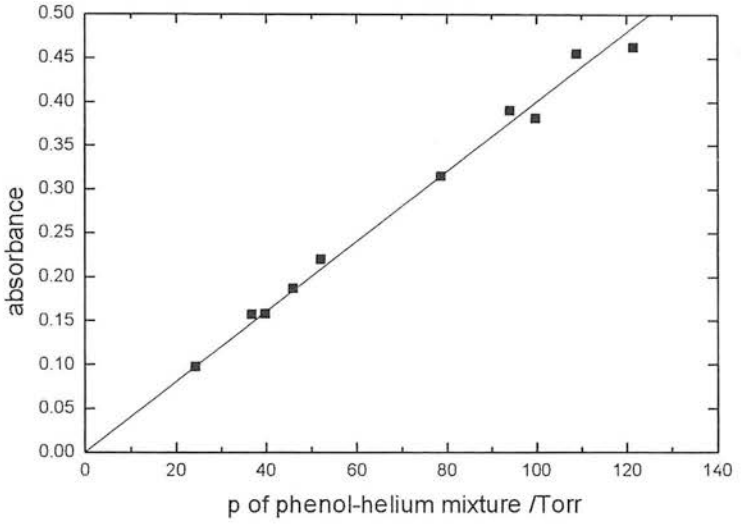

Figure 6.2 Plot of absorbance *vs.* total pressure of typical phenol-helium mixture at room temperature.

Trost et al. [1997] have given an absorption cross section of gas phase phenol of $\sigma = 25 \times 10^{-18}$ cm^2 molecule^{-1} at $\lambda = 269$ nm at 293 K. Therefore the calculated maximum initial phenol concentration for uptake measurements in this work was around 5×10^{14} molecules cm^{-3} but was typically about 5×10^{13} molecules cm^{-3}.

6.2 Uptake measurements of phenol

6.2.1 Influence of pH

The uptake of phenol on water is controlled by gas diffusion and liquid solubility since no reaction is expected (no hydrolysable groups). However, as a weak acid phenol dissociates in water. In principle, the effect of dissociation on the Henry's law coefficient can be checked by calculating the effective Henry's law coefficient H^* as a

function of pH, as shown in Chapters 2 and 4. The effective Henry's law coefficient for phenol is

$$H^*_{(Phenol)} = H_{(Phenol)}\left(1+10^{pH-pK_{A(Phenol)}}\right). \quad (4.97)$$

The value of $pK_{A(Phenol)}$ is 9.89 at 293 K [*CRC Handbook of chemistry and physics*, 1993]. However, there is considerable divergence in the literature regarding Henry's law coefficient for phenol, as shown in Table 6.1 for four temperatures.

T /K	H /M atm^{-1}	reference
278	9207 (exp) 3858 (cal)	*Lüttke and Levsen* [1997]
283	356	Janini and Quaddora (1986) as cited in *Titcombe* [1997]
	430	*Heal et al.* [1995]; *Titcombe* [1997]
	770	Werner et al. (1987) as cited in *Heal et al.* [1995]
	4949	Dohnal and Fenclova (1995) as cited in *Titcombe* [1997]
	6860	USEPA (1982) as cited in *Titcombe* [1997]
293	1558	*Tremp et al.* [1993]
	2188	*Sawyer et al.* [1994]
298	> 422	*Altschuh et al.* [1999]
	769	*Reible* [1999]
	1317	*Yaws* [1999]
	1948	*Leuenberger et al.* [1985]
	2203	*Mabey et al.* [1982]
	2455	*Schwarzenbach et al.* [1993]
	2528	*Verschueren* [1996]
	3003	*Howard and Meylan* [1997]
	3007	*Staudinger and Roberts* [1996]
	5447	*Thibodeaux* [1996]

Table 6.1 Comparison of Henry's law coefficients of phenol at four temperatures.

The effective Henry's law coefficient calculated using the value H^{293K} = 1558 M atm^{-1} [*Tremp et al.*, 1993] is plotted as a function of pH in Figure 6.3.

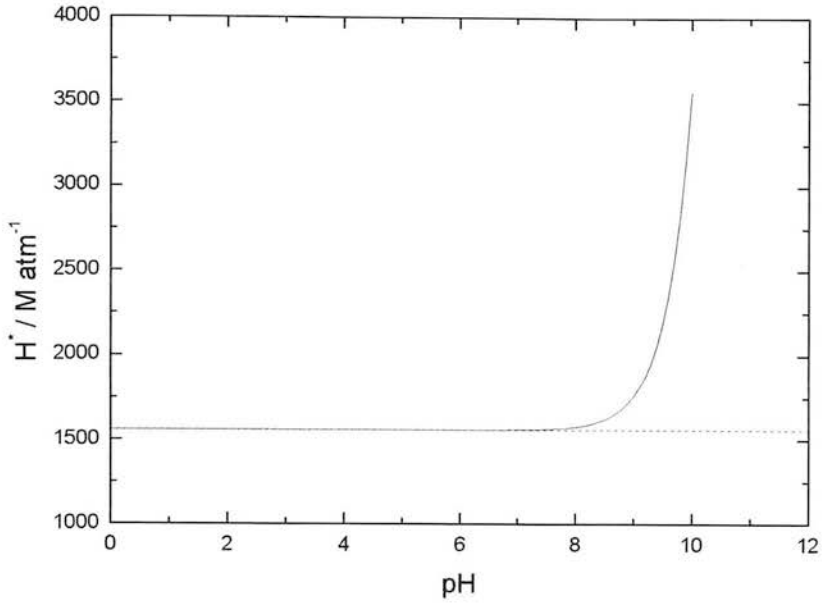

Figure 6.3 Effective Henry's law coefficient H^* as a function of pH as predicted by eqn (4.97) (black solid line). The red dashed line is $H = 1558$ M atm^{-1}.

Figure 6.3 shows that below pH = 8, the Henry's law coefficient is independent of pH. The change of pH caused by phenol uptake to water can be calculated. The initial concentration of phenol was about 5×10^{14} molecules cm^{-3} (see Section 6.1) which corresponds to 8.3×10^{-10} mol cm^{-3}. If it is assumed that all gas phase phenol is taken up (highest change in pH), the predicted phenol concentration in water is 1.60×10^{-4} mol l^{-1}, using a liquid flow rate of 140 ml min^{-1} and a gas flow of 450 ml s^{-1} (experimental conditions given in Table 6.2). Utilising eqn (4.98) the pH of this resulting solution is

$$\mathrm{pH} = \frac{9.89}{2} - \frac{1}{2}\log(1.60 \times 10^{-4}) = \underline{\underline{6.84}} \qquad \textbf{(6.1)}$$

as expected for a weak acid. The actual change in pH will be far smaller than this since only a fraction of gas phase phenol is taken up. The change in pH due to uptake was therefore neglected.

6.2.2 Approach to uptake measurements

In the absence of a reaction on the surface, the experimentally measured uptake is described by

$$\frac{1}{\gamma} = \frac{1}{\Gamma_G} + \frac{1}{\alpha} + \frac{1}{\Gamma_{SOL}}, \tag{5.2}$$

which simplifies when observed uptake is corrected for gas diffusion to

$$\frac{1}{\gamma} = \frac{1}{\alpha} + \frac{\sqrt{\pi}\,\omega\,\sqrt{t}}{4\,H\,R\,T\,\sqrt{D_L}}. \tag{6.2}$$

The solubility uptake coefficient is therefore described by

$$\Gamma_{SOL} = \frac{4\,H\,R\,T}{\pi^{1/2}\,\omega}\sqrt{\frac{D_L}{t}}, \tag{4.58}$$

as shown previously in Chapter 4. Using the bulk properties listed in Table 6.2, the solubility controlled uptake coefficient at a particular time can be estimated. Figure 6.4 plots a fit of Γ_{SOL} as function of liquid-gas contact time as described by eqn (4.58) using these estimates.

Parameter	Numerical value	Source/comments
ω	2.56×10^4 cm s^{-1}	calculated at T = 293 K, p = 40 Torr, F = 500 cm^3 min^{-1} (STP), RH = 64 %
r	0.8 cm	radius of wetted-wall reactor
D_G	2.5 cm^2 s^{-1}	calculated at experimental conditions given above in this table
α	1.2×10^{-2} at 293 K	extrapolated from *Titcombe* [1997][1]
t	1 s	typical liquid-gas contact time
H	1558 M atm^{-1}	*Tremp et al.* [1993]
T	293 K	
D_L	9.2×10^{-6} cm^2 s^{-1}	calculated using Wilke-Chang correlation (see Chapter 4)

Table 6.2 Bulk properties for estimating the uptake of phenol onto pure water at the experimental conditions.

[1] The expression for the temperature dependence of α for phenol was given for the temperature range of 263 to 283 K.

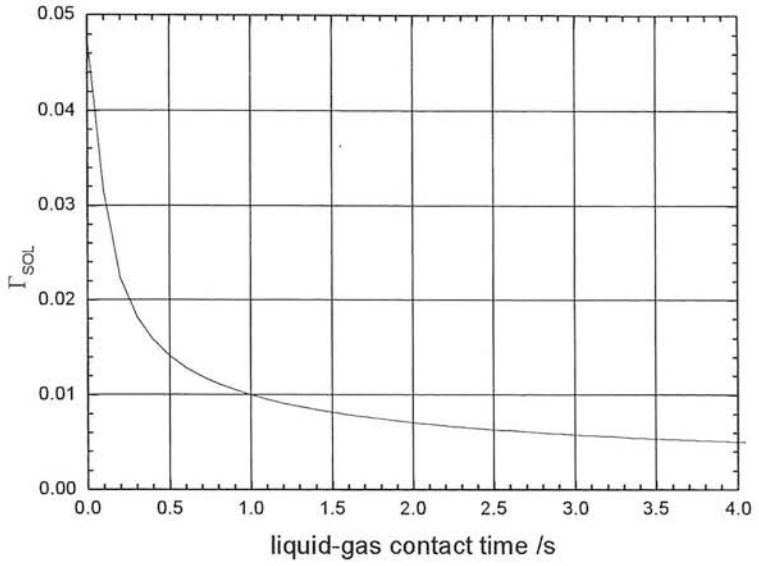

Figure 6.4 Variation of Γ_{SOL} with liquid-gas contact time for phenol at 293 K using eqn (4.58) and estimates of bulk properties in Table 6.2.

The time dependent solubility-limited uptake term has highest values in the millisecond range whereas the wetted-wall flow reactor typically has a liquid-gas contact time up to a few seconds. This comparatively long contact time in the wetted-wall method can be a problem in the determination of time dependent uptakes. However, Γ_{SOL} of phenol at 293 K still changes notably in the second time range (e.g. change of 30 % between 1 and 2 s) before approaching zero at infinite time. In contrast to the droplet train technique, the wetted-wall flow reactor does not permit change of contact area for one contact time. Two approaches were used to overcome this problem and measure the uptake of phenol using the wetted-wall flow reactor.

In the first approach (see Section 6.2.3), the position of the injector was changed by very small steps only. The maximum movement of the injector during one experiment was 2 cm which is equivalent to an area of 10 cm^2 and a change in liquid-gas contact time of 0.12 s (for a typical liquid velocity of 17 cm s^{-1}). It is assumed that the uptake (although time dependent) is constant within this small change in contact time. The shallow curve in Figure 6.4 confirms the validity of this assumption for contact times $> \sim 1$ s. With this assumption, the uptake coefficient can be derived from the change

in absorption signal due to the small change in area using (see also eqn (3.1) and (4.39))

$$\gamma = \frac{4\,F}{\omega\,\Delta A_r} \ln\left(\frac{A_1}{A_2}\right). \qquad (6.3)$$

The second approach (see Section 6.2.5) was to measure uptake in the limit of liquid reaction control. In this limit, solubility and liquid reaction give a combined resistance that is small compared to the gas diffusion resistance.

6.2.3 Uptake measured from changes in contact area

The uptake of phenol was investigated at four different temperatures. The gradient of a plot of ln (A_1/A_2) as function of $\omega\Delta A_r/(4F)$ is the uptake coefficient γ_{obs}. An example is shown in Figure 6.5. The good fit gives confidence that the uptake is constant for small changes in ΔA_r.

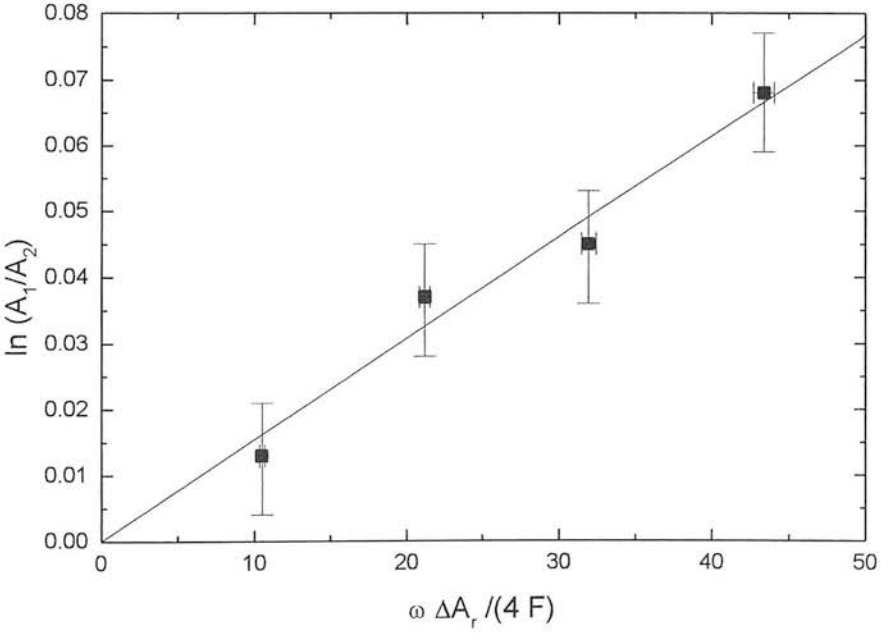

Figure 6.5 A typical plot of ln (A_1/A_2) *vs.* $\omega\ \Delta A_r/(4F)$ for the uptake of phenol onto water at 278 K. The gradient is the uptake coefficient γ_{obs}. The error bars represent a 10 % error in RH.

However, the γ_{obs} must be corrected for radial gas diffusion limitations. Therefore, the observed first-order loss rate of phenol from the gas phase, $k_w = \frac{\ln\left(\frac{A_1}{A_2}\right)}{\Delta\tau}$ (see Chapter 4), was corrected for radial gas phase diffusion using the method of *Brown* [1978], and the corrected first-order loss rate coefficient k_w^{corr} used to derive a corrected value for $\left(\ln\frac{A_1}{A_2}\right)^{corr}$. This was used to derive the uptake coefficients corrected for gas diffusion limitations in plots similar to Figure 6.5. Results are given in Table 6.3. Figure 6.6 shows the uncorrected (γ_{obs}) and corrected (γ) uptake values as a function of the averaged liquid-gas contact time, at 298 K as an example.

T /K	contact time liquid-gas /s	D_G /cm^2 s^{-1}	γ_{obs}	γ
278	1.042	5.81	1.53×10^{-3}	1.94×10^{-2}
	1.415	5.77	1.44×10^{-3}	1.03×10^{-2}
	1.787	5.80	1.39×10^{-3}	7.94×10^{-3}
288	0.981	4.90	1.22×10^{-3}	2.37×10^{-2}
	1.332	4.78	1.12×10^{-3}	8.76×10^{-3}
	1.682	4.86	1.07×10^{-3}	4.81×10^{-3}
	2.032	4.79	1.03×10^{-3}	4.47×10^{-3}
293	1.157	4.40	7.94×10^{-4}	1.70×10^{-3}
	1.497	4.28	6.48×10^{-4}	1.23×10^{-3}
	1.838	4.21	5.67×10^{-4}	9.78×10^{-4}
	2.178	4.18	5.20×10^{-4}	8.56×10^{-4}
	2.518	4.20	3.36×10^{-4}	4.52×10^{-4}
298	0.929	4.30	9.04×10^{-4}	4.28×10^{-3}
	1.261	4.05	8.36×10^{-4}	3.05×10^{-3}
	1.593	4.01	6.67×10^{-4}	1.63×10^{-3}
	1.925	3.84	6.24×10^{-4}	1.35×10^{-3}

Table 6.3 The observed (γ_{obs}) and gas diffusion-corrected (γ) uptake coefficients of phenol onto water at different temperatures.

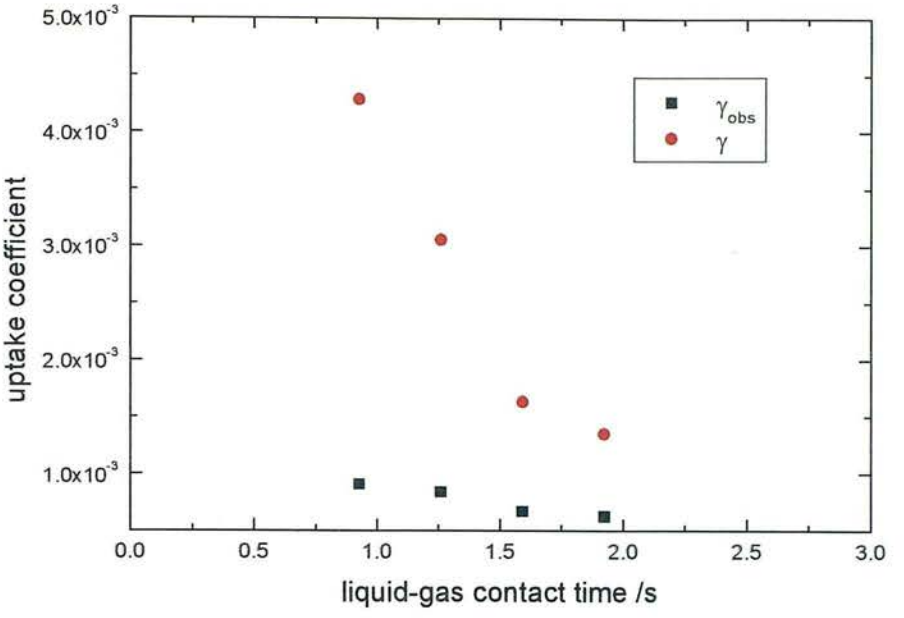

Figure 6.6 The uptake coefficient before (γ_{obs}, black squares) and after (γ, red dots) correction for gas diffusion as a function of liquid-gas contact time for uptake of phenol at 298 K.

The corrected uptake coefficient of phenol under these conditions as a function of liquid-gas contact time at four different temperatures is shown in Figure 6.7.

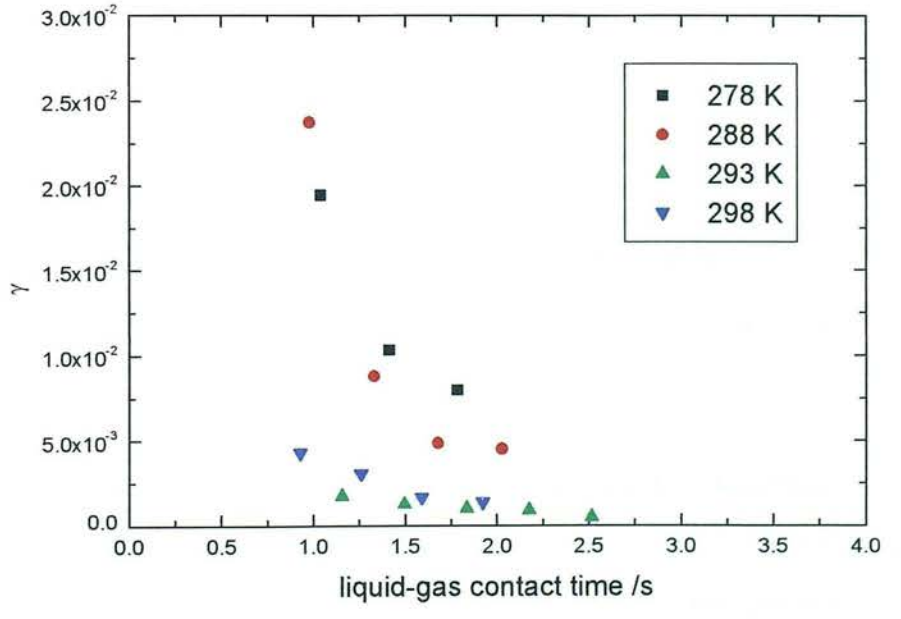

Figure 6.7 The corrected uptake of phenol as a function of liquid-gas contact time at four temperatures.

Figure 6.7 shows that the uptake decreases as a function of liquid-gas contact time, as expected. Also apparent is that the uptake has a negative temperature dependence.

According to eqn (6.2) a plot of $1/\gamma$ *vs.* $\sqrt{t}$ should yield a straight line with a gradient of $\frac{\sqrt{\pi}\,\omega}{4\,H\,R\,T\sqrt{D_L}}$ and an intercept of $1/\alpha$. Figure 6.8 shows such plots for the four temperatures; the lines are linear fits to the data (apart from the point at $\sqrt{t}$ =1.59 $s^{1/2}$ at 293 K which was excluded from the fitting).

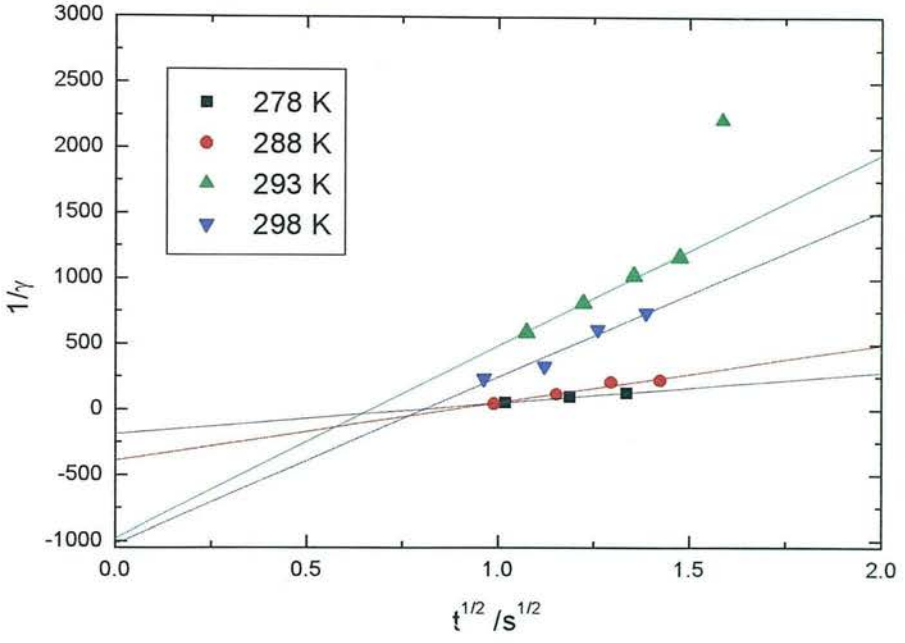

Figure 6.8 Plot of $1/\gamma$ *vs.* $\sqrt{t}$ for phenol at four temperatures. The gradient corresponds to $\frac{\sqrt{\pi}\,\omega}{4\,H\,R\,T\sqrt{D_L}}$ and the intercept equals $1/\alpha$. Note that the straight line for 293 K was fitted without the highest value at $\sqrt{t}$ = 1.59 $s^{1/2}$.

Figure 6.8 shows a linear dependence of $1/\gamma$ on $\sqrt{t}$ for all temperatures, which is consistent with a time dependent uptake as described by eqn (6.2). However, all fitted straight lines display negative intercepts (= $1/\alpha$) which is not physically possible ($1/\alpha \geq 1$). This makes it unrealisable to derive a value of α. Likewise the gradients

seem to be rather large (e.g. 1466 $s^{-1/2}$ at 293 K) when compared with an estimation of ~ 100 $s^{-1/2}$ using the values of Table 6.2.

6.2.3.1 Gas diffusion coefficients

The pressure-independent binary diffusion coefficients (Torr cm^2 s^{-1}) of phenol in H_2O and helium, $D_G^P{}_{(C_6H_5OH\text{-}H_2O)}$ and $D_G^P{}_{(C_6H_5OH\text{-}He)}$, were calculated according to the Fuller-Schettler-Giddings [*Fuller et al.*, 1969] estimation method, as described in Chapter 4. Table 6.4 details the parameters used.

Parameter/ unit	Symbol	Value	Source/comments
molar mass of phenol /g mol^{-1}	$M_{C_6H_5OH}$	94.1	
molar mass of water /g mol^{-1}	M_{H_2O}	18.0	
molar mass of helium /g mol^{-1}	M_{He}	4.0	
atomic diffusion volume of phenol	$(\sum v)_{C_6H_5OH}$	97.1	calculated from values given in *Fuller et al.* [1969]
atomic diffusion volume of water	$(\sum v)_{H_2O}$	13.1	given in *Fuller et al.* [1969]
atomic diffusion volume of helium	$(\sum v)_{He}$	2.67	given in *Fuller et al.* [1969]

Table 6.4 Parameters used to calculate pressure-independent binary gas diffusion coefficients of phenol in H_2O and He following the method of *Fuller et al.* [1969].

The calculated gas diffusion coefficients at the different temperatures are listed in Table 6.5.

T /K	$D_G^P{}_{(C_6H_6O\text{-}H_2O)}$ /Torr cm^2 s^{-1}	$D_G^P{}_{(C_6H_6O\text{-}He)}$ /Torr cm^2 s^{-1}
278	76.5	205.1
288	81.4	218.2
293	83.9	224.9
298	86.4	231.6

Table 6.5 Pressure-independent gas diffusion coefficients for phenol in H_2O and in helium at the experimental temperatures following the method of *Fuller et al.* [1969].

6.2.3.2 Liquid diffusion coefficients

The liquid diffusion coefficients for phenol in water at the experimental temperatures were calculated by the Wilke-Chang method, as described in Chapter 4, using a molar volume of phenol at boiling temperature $V_{C_6H_5OH} = 103.4\ cm^3\ mol^{-1}$. The values are listed in Table 6.6.

T /K	$D_{L(C_6H_5OH\text{-}H_2O)}$ used in this work (Wilke-Chang) /$cm^2\ s^{-1}$	$D_{L(C_6H_5OH\text{-}H_2O)}$ as given in *Yaws* [1995] /$cm^2\ s^{-1}$
278	5.7×10^{-6}	5.6×10^{-6}
288	7.9×10^{-6}	7.3×10^{-6}
293	9.2×10^{-6}	8.4×10^{-6}
298	1.0×10^{-5}	9.6×10^{-6}

Table 6.6 Liquid diffusion coefficients for phenol in water at different temperatures. The values in this work were calculated using the Wilke and Chang method [*Reid et al.*, 1987]. The viscosity values of water for this calculation of $D_{L(C_6H_5OH\text{-}H_2O)}$ were taken from *Kaye and Laby* [1995]. For comparison, the liquid diffusion coefficients as given by *Yaws* [1995] are also shown.

Table 6.6 compares the liquid diffusion coefficients with values calculated from an expression given by *Yaws* [1995] for the temperature dependence of the phenol liquid diffusion coefficient in water. There is good agreement between both data.

6.2.4 Uptake of phenol as a function of pressure

The uptake coefficients plotted in Figure 6.8 were corrected for radial gas diffusion as described previously. However, some experimentally observed uptakes could not be included in the final results since correction required unreliably large extrapolations, e.g. values of k_w^{corr} two orders of magnitude greater than k_w.

As an alternative method, one experiment was performed by changing the pressure of the helium carrier gas in the wetted-wall flow reactor, and thereby the gas flow rate,

at a fixed injector position. The data treatment was adopted from *Pöschl et al.* [1998]. Their analysis used additivity of kinetic resistances without prior correction of observed first-order loss for radial gas diffusion, i.e. the resistance to the observed first-order wall loss of phenol from the gas phase is the sum of the diffusive resistance ($1/\Gamma_G$) and the surface uptake resistance ($1/\Gamma_s$). Since the uptake is proportional to the rate coefficients of these processes (see Chapter 4), the following equation can be written

$$\frac{1}{k_w} = \frac{1}{k_G} + \frac{1}{k_s} \quad . \tag{6.4}$$

The diffusion limited loss rate k_G for a cylindrical reactor of radius r is given by [*Hanson et al.*, 1992]

$$k_G = \frac{3.66\, D_G}{r^2} \tag{4.55}$$

where D_G is the diffusion coefficient at the experimental pressure. Rewriting in terms of the pressure-independent diffusion coefficient of phenol D_G^P gives

$$k_G = \frac{3.66\, D_G^P}{r^2\, p} \quad . \tag{6.5}$$

The surface uptake rate is obtained by multiplying the wall loss velocity K_s (equivalent to a deposition velocity in units of cm s^{-1}) with the surface-to-volume ratio of the reactor

$$k_s = \frac{2\, K_s}{r} \quad . \tag{6.6}$$

Combining eqn (6.4), (6.5) and (6.6) results in

$$\frac{1}{k_w} = \left(\frac{r^2}{3.66\, D_G^P} \right) p + \frac{r}{2\, K_s} \quad . \tag{6.7}$$

Since

$$\frac{1}{D_{G(i)}} = \frac{p_{H_2O}}{D_G{}^{P}{}_{(i-H_2O)}} + \frac{p_{He}}{D_G{}^{P}{}_{(i-He)}},$$

(4.43)

eqn (6.7) can also be written as

$$\frac{1}{k_w} = \frac{r^2}{3.66\, D_G{}^{P}{}_{(C_6H_5OH-H_2O)}} p_{H_2O} + \frac{r^2}{3.66\, D_G{}^{P}{}_{(C_6H_5OH-He)}} p_{He} + \frac{r}{2\, K_s}$$

(6.8)

by combining eqn (6.4), (4.55) and (4.43).

According to eqn (6.7) a plot of $1/k_w$ *vs.* the total pressure in the apparatus should give a straight line with a gradient proportional to $1/D_G{}^{P}$. The intercept yields a value for K_s. With the known K_s it is then possible to derive a value of $D_G{}^{P}{}_{(C_6H_5OH\text{-}H_2O)}$ from the intercept of a plot of $1/k_w$ *vs.* p_{He} according to eqn (6.8). The gradient of the second plot yields $D_G{}^{P}{}_{(C_6H_5OH\text{-}He)}$. The observed first-order loss rates as function of pressure are given in Table 6.7 and the associated plots are shown in Figure 6.9.

p /Torr	p_{H_2O} /Torr	p_{He} /Torr	k_w /s^{-1}
35.2	1.5	33.7	11.72
35.8	1.4	34.4	9.31
37.1	1.5	35.6	9.31
37.5	1.4	36.1	8.16
39.5	1.5	38.0	8.57
41.2	1.5	39.7	7.69
45.2	1.5	43.7	7.85
52.6	1.5	51.1	6.74
66.8	1.6	65.2	6.02

Table 6.7 Total and partial pressure of water and helium and observed first-order wall loss rate of phenol at 278 K and a gas flow of 2000 cm^3 min^{-1} (STP).

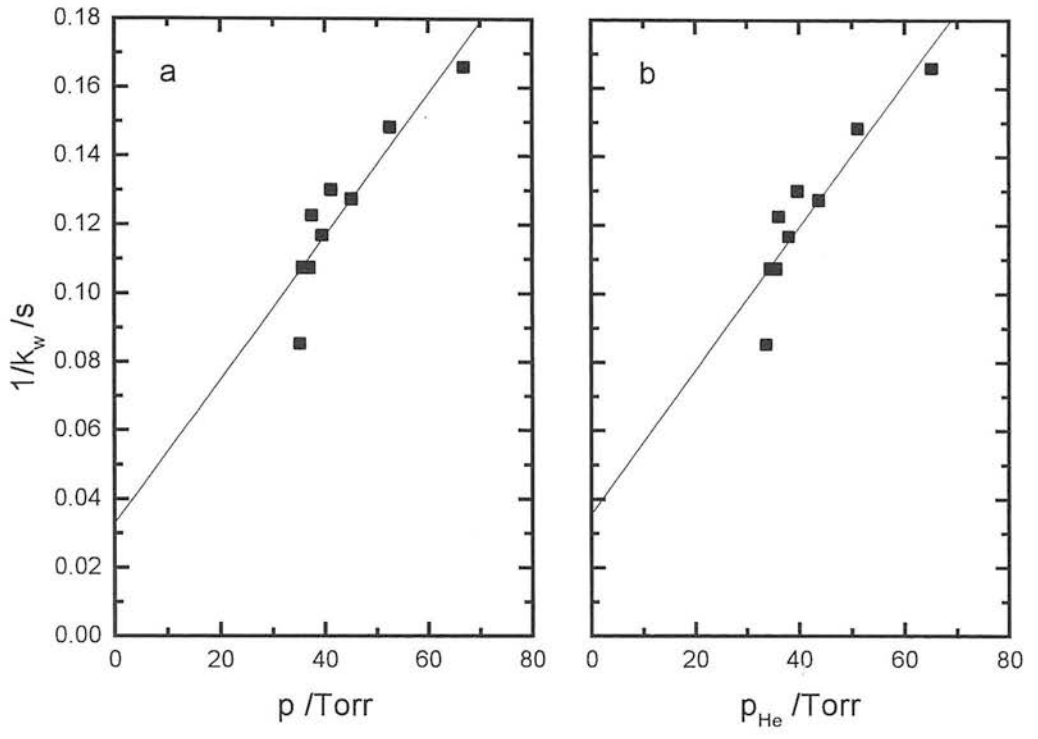

Figure 6.9 Plot of $1/k_w$ as function of total pressure (a) and as function of helium partial pressure (b). k_w is the observed first-order loss rate of phenol at 278 K at a gas flow of 2000 cm^3 min^{-1} (STP).

The gradient of Figure 6.9 (a) gives a value of D_G^P = 83.67 Torr cm^2 s^{-1}. The intercept of Figure 6.9 (a) yields a value of K_s = 12.21 cm s^{-1}. This was used to calculate a value of $D_G^P{}_{(C_6H_5OH\text{-}H_2O)}$ = 98.69 Torr cm^2 s^{-1} from the intercept of Figure 6.9 (b) using an average p_{H_2O} of 1.49 Torr. A value of $D_G^P{}_{(C_6H_5OH\text{-}He)}$ = 83.23 Torr cm^2 s^{-1} was calculated from the gradient of Figure 6.9 (b).

The mass accommodation α is the ratio of the net flux of molecules incorporated into the liquid to the net collisional flux to the wall which, in the notation of the wall loss velocity, is given by [*Pöschl et al.*, 1998]

$$\alpha = \frac{J_{incorp}}{J_{coll}} = \frac{K_s\,[C_6H_5OH]}{[C_6H_5OH]\,\frac{\omega}{4}} = \frac{4\,K_s}{\omega} \quad . \tag{6.9}$$

Equation (6.9) yields an α of 1.96×10^{-3} with the observed K_s of 12.2 cm s^{-1} and an ω of 2.49×10^4 cm s^{-1}.

6.2.5 Reactive uptake of phenol

The bromination of phenol in aqueous solution takes place readily yielding 2:4:6 tribromophenol [*Hickinbottom*, 1962]. *Bell and Rawlinson* [1961] have measured the rate coefficient of this reaction as 1.8×10^5 l mol^{-1} s^{-1} at 25 °C although they state a low accuracy for this value since the reaction between phenol and bromine in aqueous solution is very fast. A newer value, also at 25 °C, has been given by *Tee et al.* [1989] which was used to calculate k" as 1.98×10^6 l mol^{-1} s^{-1} for a pH of 7[2]. An estimation of the uptake regime under these condition leads to the following calculations for the gas diffusion, liquid solubility and liquid transport coefficients (see eqn 4.56, 4.58, 4.59 and Table 6.2).

$$\Gamma_G = \frac{2\,(3.66\,D_G)}{\omega\,r} = \frac{2\,(3.66 \times 2.5\ \text{cm}^2\ \text{s}^{-1})}{2.56 \times 10^4\ \text{cm s}^{-1} \times 0.8\ \text{cm}} = \underline{8.936 \times 10^{-4}} \qquad \textbf{(6.10)}$$

$$\Gamma_{SOL} = \frac{4\,H\,R\,T}{\pi^{1/2}\,\omega}\sqrt{\frac{D_L}{t}} = \frac{4 \times 1558\ \text{M atm}^{-1} \times 0.08205\ \text{l atm mol}^{-1}\ \text{K}^{-1} \times 293\ \text{K}}{\pi^{1/2} \times 2.56 \times 10^4\ \text{cm s}^{-1}} \times \sqrt{\frac{9.2 \times 10^{-6}\ \text{cm}^2\ \text{s}^{-1}}{1\ \text{s}}} = \underline{1.001 \times 10^{-2}} \qquad \textbf{(6.11)}$$

[2] The reaction between phenol and bromine follows a second-order rate law: first-order in phenol and bromine. The rate coefficient is calculated depending on the pH using $k'' = k_1 + k_2 K_A/[H^+]$ where k_1 is the rate coefficient for the reaction of the undissociated phenol and k_2 is that for the phenoxide ion ($C_6H_5O^-$) with bromine. They have been given as $k_1 = 4.3 \times 10^5$ M^{-1} s^{-1} and $k_2 = \sim 1.2 \times 10^9$ M^{-1} s^{-1} [*Tee et al.*, 1989]. Although both rate coefficients are at 25 °C, they were used in this estimation for 293 K. The pK_A of phenol was given earlier as 9.89 at 25 °C [*CRC Handbook of chemistry and physics*, 1993].

The concentration of bromine in the water was estimated to be about 0.02 mol l^{-1} using a ρ_{Br_2} of 3.119 g cm^3 at 293 K (see Section 3.3.3.4) [*CRC Handbook of chemistry and physics*, 1993]. This leads to

$k_{RXN} = k''\ [Br_2] = 1.98 \times 10^6$ l mol^{-1} s^{-1} x 0.02 mol $l^{-1} = 39600\ s^{-1}$ and

$$\Gamma_{RXN} = \frac{4\,H\,R\,T\,\sqrt{D_L\,k_{RXN}}}{\omega} = \frac{4 \times 1558\ M\ atm^{-1} \times 0.08205\ l\ atm\ mol^{-1}\ K^{-1} \times 293\ K}{2.56 \times 10^4\ cm\ s^{-1}} \times$$

$$\sqrt{9.2 \times 10^{-6}\ cm^2\ s^{-1} \times 39600\ s^{-1}} = \underline{3.532}$$

(6.12)

The overall estimated resistance obtained by combination of the individual transfers, for these conditions, is therefore (see eqn (2.43))

$$\frac{1}{\gamma} = \frac{1}{\Gamma_G} + \frac{1}{\alpha} + \frac{1}{\Gamma_{SOL} + \Gamma_{RXN}} = \frac{1}{8.936 \times 10^{-4}} + \frac{1}{\alpha} + \frac{1}{0.010 + 3.532} = 1119 + \frac{1}{\alpha} + 0.282$$

(6.13)

Since the resistance due to gas diffusion is the dominant term in eqn (6.13), the overall uptake under these conditions will be limited by gas diffusion. Liquid uptake resistance from solubility and reaction is much smaller than the gas diffusion resistance. Mass accommodation will also be significant, in addition to gas diffusion, if $\alpha < \sim 0.01$.

The uptake of phenol on bromine water was measured at four temperatures. The data analysis had to be altered slightly since the exact concentration of the bromine in the water could not be determined for two reasons. Firstly, in the method of preparation, the liquid bromine is vigorously mixed for several hours, but the exact amount dissolved after that time is not known. Secondly, when using the solution, bromine fumes constantly evaporate from the solution which modifies the concentration. The estimate of the concentration above is based on the amount of bromine used. However, the concentration of bromine is not required as long as it is sufficient to ensure that reactive uptake is not rate limiting.

Rudich et al. [1996b] have measured the uptake of NO_3 on KI solutions in a similar regime where the measured uptake is limited by gas diffusion and α, not by the liquid uptake resistance. They presented the following equation

$$\frac{3.66}{r^2\ k_w} = \left(\frac{1}{D_G}\right) + \frac{7.32}{\omega\ r}\left(\frac{\alpha+\gamma}{\alpha\gamma}\right) = \left(\frac{p_{H_2O}}{D_G^{\ P}{}_{(C_6H_5OH-H_2O)}} + \frac{p_{He}}{D_G^{\ P}{}_{(C_6H_5OH-He)}}\right) + \frac{7.32}{\omega\ r}\left(\frac{\alpha+\gamma}{\alpha\gamma}\right)$$

(6.14)

The experiments in this work were not performed over a wide enough pressure range to enable a plot of $3.66/(r^2\ k_w)$ *vs.* p_{He}. However, eqn (6.14) was rearranged to yield the expression

$$\frac{1}{\alpha} = \frac{\omega}{2\ r\ k_w} - \frac{\omega\ r}{7.32\ D_G} - \frac{1}{\gamma}.$$

(6.15)

As before, k_w was obtained from plots of ln A *vs.* injector position. An example first-order uptake is shown in Figure 6.10. The uptake was calculated from $\gamma = 2rk_w/\omega$, as used previously.

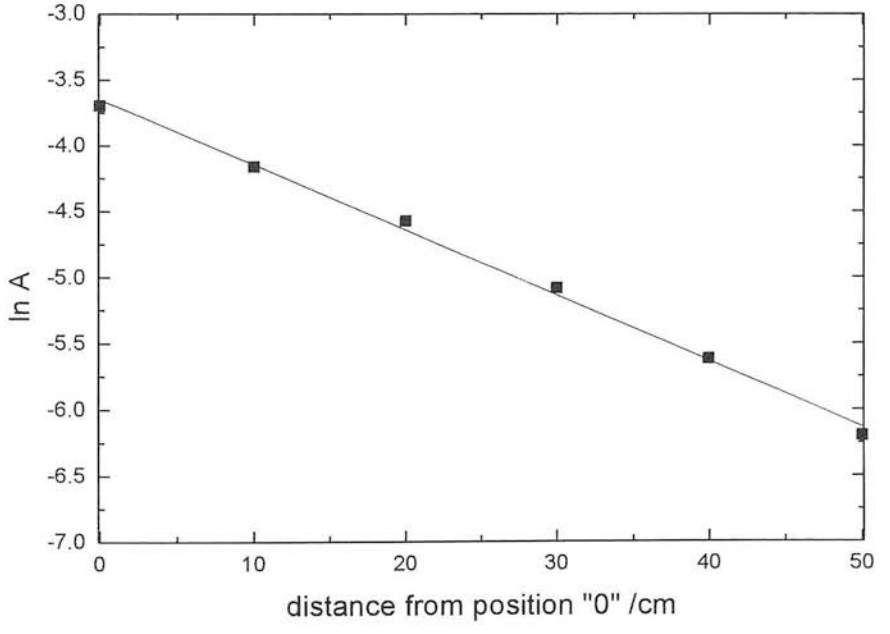

Figure 6.10 Plot of ln absorbance *vs.* distance for phenol onto bromine water to obtain k_w. Experiment at 293 K and with a gas velocity of c = 251 cm s^{-1}.

Table 6.8 shows the mass accommodation coefficients which were obtained using eqn (6.15). Each α value is an average of at least five experimental runs with different observed first-order loss coefficients, k_w.

T /K	α
278	3.75×10^{-2}
288	1.18×10^{-2}
293	8.29×10^{-3}
298	6.60×10^{-3}

Table 6.8 Mass accommodation coefficients of phenol at different temperatures calculated using eqn (6.15).

Figure 6.11 shows the dependence of the calculated mass accommodation of phenol on temperature.

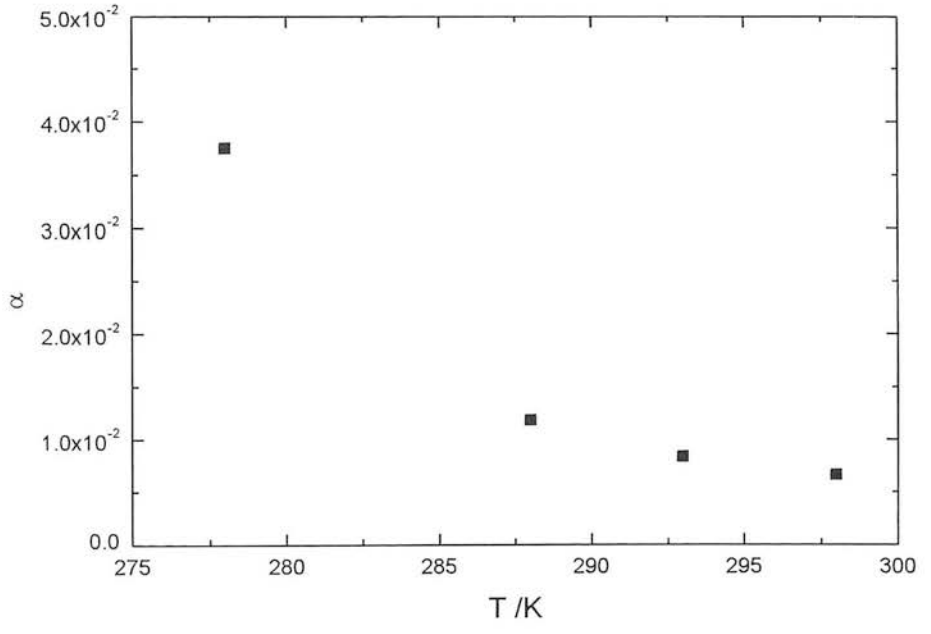

Figure 6.11 Mass accommodation of phenol as function of temperature.

6.3 Discussion

6.3.1 Uptake of phenol derived by changing A_r

The uptake of phenol on water was measured at four temperatures using this method. The highest observed uptake was 1.5×10^{-3} at 278 K and 9.0×10^{-4} at 298 K and at about 1 s liquid-gas contact time. After correction for radial gas diffusion in the reactor these uptakes are 1.9×10^{-2} at 278 K and 4.3×10^{-3} at 298 K.

A negative temperature dependence of the uptake was observed. The uptake values at 298 K are slightly above the values at 293 K which is likely to arise from small temperature inconsistencies of the water (± 1 K).

The uptake of phenol in these experiments is time dependent. The measured uptakes decrease with liquid-gas contact time for all temperatures which indicates a solubility limited uptake mechanism. If the uptake is solubility limited, a plot of $1/\gamma$ *vs.* $\sqrt{t}$ should yield a straight line with a gradient of $\frac{\sqrt{\pi}\,\omega}{4\,H\,R\,T\sqrt{D_L}}$ and an intercept of $1/\alpha$ according to eqn (6.2). The results of the fitted lines in Figure 6.8 are shown in Table 6.9.

T /K	gradient [= $\pi^{1/2}\omega/(4HRTD_L^{1/2})$] /$s^{-1/2}$	error gradient /$s^{-1/2}$	intercept [= $1/\alpha$]	error intercept
278	236.3	21.31	-187.8	25.34
288	443.9	66.84	-393.2	82.05
293[3]	1466	53.60	-982.0	69.21
298	1274	198.3	-1030	236.9

Table 6.9 Results of the linear fits of $1/\gamma$ *vs.* $\sqrt{t}$ for phenol at four temperatures (Figure 6.8).

The straight lines fit the data points well which confirms the solubility limitation of the uptake. However, it can be seen that all intercepts are negative. Since α can only have

[3] without the highest value at $\sqrt{t} = 1.59\ s^{1/2}$

values between 0 and 1, this probably points to a systematic error in the measurement. *Shi et al.* [1999b] reported a negative intercept (= α^{-1}) in a similar plot to Figure 6.8 for ammonia at pH = 13. The authors attribute this to a possible surface complex formation of ammonia (NH_4^+-OH^-) which is not accounted for in the Resistance Model. However, it is unclear if phenol interacts with the surface in a particular way. It is therefore not possible to derive a value of α from these experiments.

Although the intercepts (= $1/\alpha$) in Figure 6.8 were negative, the correlation coefficients to the fitted straight lines were all > 0.97. The gradients $\left(= \frac{\sqrt{\pi}\,\omega}{4\,H\,R\,T\sqrt{D_L}} \right)$ were therefore used to derive the parameter $H\sqrt{D_L}$. The Henry's law coefficients were calculated using the liquid diffusion coefficients above (see Table 6.6). The results are shown in Table 6.10.

T /K	ω /cm s^{-1}	$HD_L^{1/2}$ /M atm^{-1} $(cm^2\ s^{-1})^{1/2}$	D_L /$cm^2\ s^{-1}$	H /M atm^{-1}
278	2.49×10^4	2.047	5.7×10^{-6}	855
288	2.54×10^4	1.073	7.9×10^{-6}	381
293	2.56×10^4	0.322	9.2×10^{-6}	106
298	2.58×10^4	0.367	1.0×10^{-5}	113

Table 6.10 $H\sqrt{D_L}$ derived from the gradients of Figure 6.8 for different temperatures. The Henry's law coefficients were calculated using the liquid diffusion coefficients from Table 6.6.

The quantity $H\sqrt{D_L}$ is a temperature dependent parameter which increases with decreasing temperature. In general, physical solubility increases with decreasing temperature. The liquid diffusion coefficient on the other hand decreases with decreasing temperature (see Table 6.6). So, the overall negative temperature dependence of $H\sqrt{D_L}$ leads to the conclusion that H is a stronger function of temperature than $\sqrt{D_L}$.

The only other known values of $H\sqrt{D_L}$ of phenol have been given between 263 and 283 K [*Titcombe*, 1997]. The temperature dependence of $H\sqrt{D_L}$ can be written as [*Jayne et al.*, 1991]

$$\left[H\sqrt{D_L}\right]_{T2} = \left[H\sqrt{D_L}\right]_{T1} \exp\left[\frac{-\Delta H_L}{R}\left(\frac{1}{T_2} - \frac{1}{T_1}\right)\right] \qquad \textbf{(6.16)}$$

where ΔH_L is the enthalpy of the liquid solubility (including liquid diffusion). A plot of $\ln[H\sqrt{D_L}]$ *vs.* 1/T should therefore yield a straight line. Such a plot is shown in Figure 6.12.

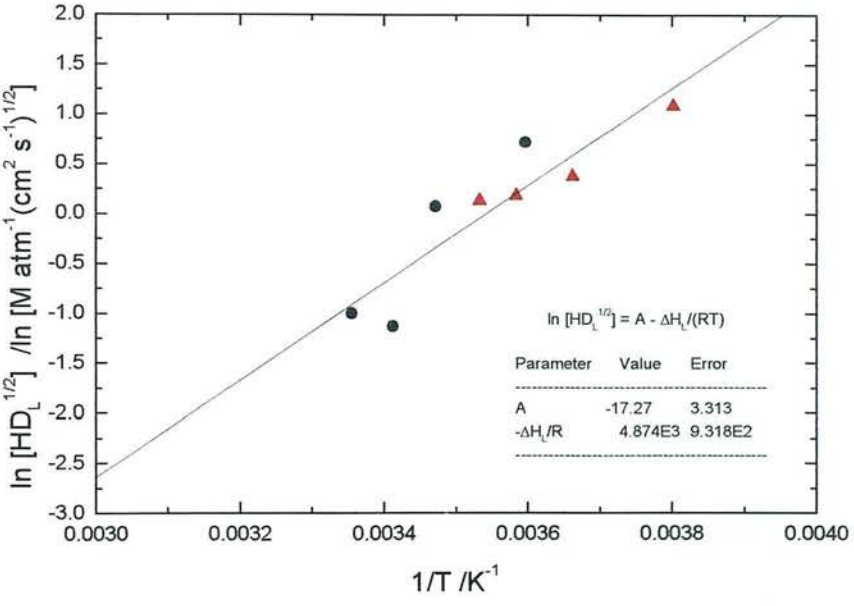

Figure 6.12 Plot of $\ln[H\sqrt{D_L}]$ *vs.* the reciprocal temperature for phenol. Shown are the values from this work (black dots) and the data taken from *Titcombe* [1997] (red triangles). The straight line was fitted to all data.

The data of this work show reasonable agreement with the results of *Titcombe* [1997]. All points were included in the fit. The gradient yields a value for ΔH_L of -40.5 ± 7.7 kJ mol^{-1}. This is comparable with the value of $\Delta H_L = -46.1$ kJ mol^{-1} for ethanol [*Jayne et al.*, 1991]. Ethanol and phenol have similar Henry's law coefficients and liquid diffusion coefficients (Table 6.11). NB. The value of $\Delta H_L = -46.1$ kJ mol^{-1}

for ethanol has been predicted from literature values but the experimentally determined value is far lower at ΔH_L^{EXP} = -18.0 kJ mol^{-1}) [*Jayne et al.*, 1991].

	$H^{273\ K}$	$D_L^{273\ K}$
ethanol	**1470 M atm^{-1}** [*Jayne et al.*, 1991]	**0.67 x 10^{-5} cm^2 s^{-1}** [*Jayne et al.*, 1991]
phenol	**821 M atm^{-1}** (estimation from Figure 6.12)	**0.48 x 10^{-5} cm^2 s^{-1}** (estimation after Wilke and Chang)

Table 6.11 Comparison of Henry's law coefficient and liquid diffusion coefficient of phenol and ethanol.

The Henry's law coefficients derived in these uptake measurements (Table 6.10) are generally low compared with literature H values for phenol summarised previously in Table 6.1. The H values of phenol in Table 6.10 show the usual negative temperature dependence. In their extensive review *Staudinger and Roberts* [1996] give two expressions for the estimated temperature dependence of the Henry's law coefficient of phenol. In comparison (see Table 6.12) the values from this work lie within the range of the estimated values, though the two estimation equations differ by about an order of magnitude in their value of H.

The temperature dependence of H was used to derive the enthalpy and entropy for the gas-liquid transfer[4]. A plot of ln H *vs.* 1/T

[4] The relation between the enthalpy of gas-liquid transfer $\Delta H°$ and the enthalpy of the liquid solubility ΔH_L (including liquid diffusion) defined earlier is based on their definitions, i.e.

$$\left[H\sqrt{D_L}\right]_{T2} = \left[H\sqrt{D_L}\right]_{T1} \exp\left[\frac{-\Delta H_L}{R}\left(\frac{1}{T_2}-\frac{1}{T_1}\right)\right]$$

and

$$H_{T2} = H_{T1} \exp\left[-\frac{\Delta H°}{R}\left(\frac{1}{T_2}-\frac{1}{T_1}\right)\right].$$

Rearrangement gives

$$\Delta H_L - \Delta H° = \frac{1}{2} R \left(\frac{1}{T_2}-\frac{1}{T_1}\right)^{-1} \ln\left(\frac{D_{L(T1)}}{D_{L(T2)}}\right).$$

$\left(\text{gradient of } -\frac{\Delta H^\circ}{R} \text{ and intercept of } \frac{\Delta S^\circ}{R}\right)$ is shown in Figure 6.13.

	this work	*Staudinger and Roberts* [1996] Estimation from measured infinite dilution activity coefficient	*Staudinger and Roberts* [1996] Estimation from vapour pressure and aqueous solubility
T /K	H /M atm^{-1}	H /M atm^{-1}	H /M atm^{-1}
278	855	446	10898
288	381	286	4388
293	106	231	2849
298	113	188	1876

Table 6.12 Comparison of Henry's law coefficients of phenol at different temperatures.

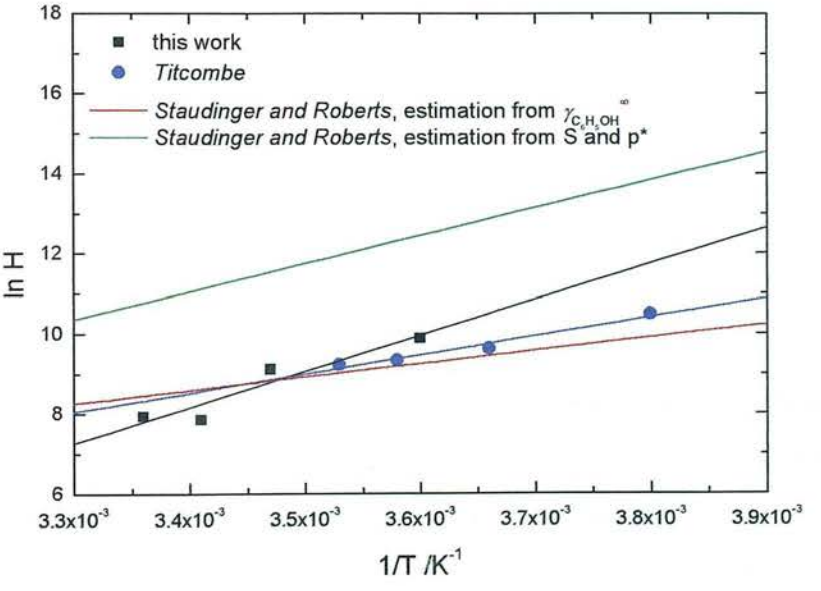

Figure 6.13 Plot of ln H *vs.* 1/T. Plotted are the experimental data from this work and *Titcombe* [1997] and estimated values [*Staudinger and Roberts*, 1996]. Note that the H in this plot is the dimensionless liquid/gas Henry's law coefficient.

The values for ΔH° and ΔS° for the gas-to-liquid-transfer derived from the data in Figure 6.13 are listed in Table 6.13.

	ΔH° /kJ mol^{-1}	ΔS° /J mol^{-1} K^{-1}
this work	-74.6	-185.7
Titcombe [1997]	-39.4	-63.2
this work and *Titcombe* [1997]	-49.6	-99.8
Staudinger and Roberts (est. from γ^{∞})	-27.5	-22.1
Staudinger and Roberts (est. from p* and S)	-58.0	-105.6

Table 6.13 Values of ΔH° and ΔS° for the gas to liquid solubility derived from Figure 6.13.

Table 6.13 shows that there is disagreement between these five estimates and more work is needed to derive values for ΔH° and ΔS° with more confidence. The closest agreement is between the combined values from this work and *Titcombe* [1997] and the estimate using the vapour pressure and solubility of phenol [*Staudinger and Roberts*, 1996].

6.3.2 Uptake of phenol by changing p

The pressure in the flow tube was changed by changing the helium carrier gas pressure. The water vapour pressure and the injector position were kept constant. It was shown that the observed first-order loss rates depend on the pressure, which indicates that gas diffusion influences the uptake at the experimental conditions chosen.

The data analysis procedure [*Pöschl et al.*, 1998] is straightforward and simple to use. The experimentally derived $D_G{}^P{}_{(C_6H_5OH\text{-}H_2O)}$ of 98.69 Torr cm^2 s^{-1} agrees reasonably with the one calculated after Fuller-Schettler-Giddings [*Fuller et al.*, 1969] which is $D_G{}^P{}_{(C_6H_5OH\text{-}H_2O)} = 76.37$ Torr cm^2 s^{-1}. This is not the case for $D_G{}^P{}_{(C_6H_5OH\text{-}He)}$, for which there is a major discrepancy between the two values (see Table 6.14). The same is

noted for D_G^P, which is not surprising since D_G^P must be close in value to $D_G^{P}{}_{(C_6H_5OH\text{-}He)}$ due to the small water vapour pressure present in the flow reactor under the experimental conditions (see Table 6.7).

	$D_G^{P}{}_{(C_6H_5OH\text{-}H_2O)}$ / Torr cm^2 s^{-1}	$D_G^{P}{}_{(C_6H_5OH\text{-}He)}$ / Torr cm^2 s^{-1}	D_G^P / Torr cm^2 s^{-1}
experiment (see Figure 6.9)	98.7	83.2	83.7
Fuller estimation	76.4	205	194

Table 6.14 Comparison between experimental and estimated diffusion coefficients of phenol.

The experimentally derived $D_G^{P}{}_{(C_6H_5OH\text{-}He)}$ seems very small. A general assumption is that the diffusion coefficient in water is about a factor 2.5 to 3 lower than in helium [*Fickert et al.*, 1999]. This is true for the $D_G^{P}{}_{(C_6H_5OH\text{-}He)}$(FULLER) which reinforces the doubts about $D_G^{P}{}_{(C_6H_5OH\text{-}He)}$(EXP). Figure 6.14 is a replot of Figure 6.9 which includes the fittings obtained by using the diffusion coefficients calculated after *Fuller et al.* [1969].

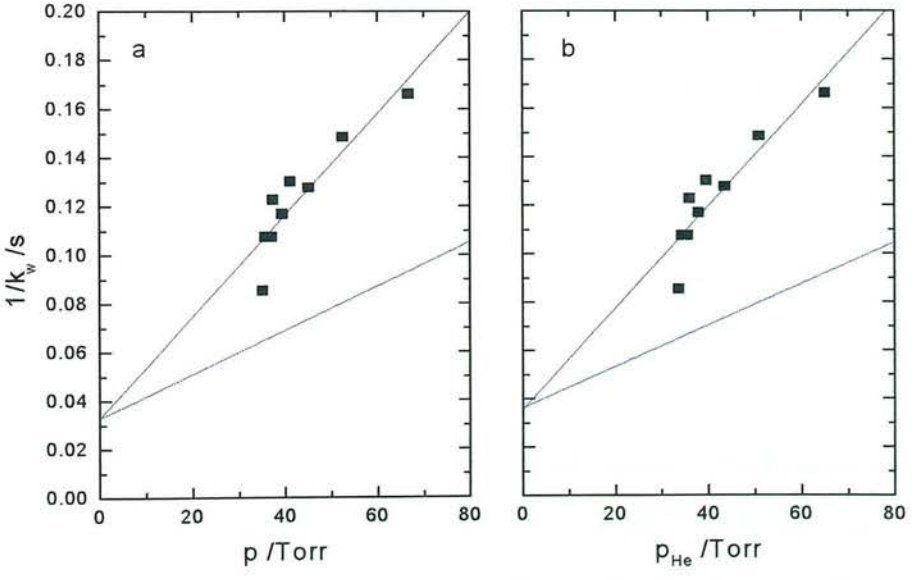

Figure 6.14 Plot of $1/k_w$ as function of total pressure (a) and as function of helium partial pressure (b). k_w is the observed first-order loss rate of phenol at 278 K using a gas flow of 2000 cm^3 min^{-1} (STP). The black solid lines are a replot of Figure 6.9. The blue lines are fitted using diffusion coefficients from Table 6.14, p_{H_2O} as listed in Table 6.7 and a value of K_s of 12.21 cm s^{-1} as derived from Figure 6.9.

Clearly, there is a major difference in the experimental and calculated plots. A problem in applying this pressure variation approach with the system used in this work is that the measurement of the gas absorbance as a detection method is directly and strongly dependent on the pressure in the absorption cell. Therefore a change in pressure changes the absorbance independently of the change in gas flow and the change in uptake. All absorption values were corrected for pressure as described in Section 4.2.4.6 which could introduce a systematic error. The pressure ranges used were 35 to 67 Torr. This is comparatively high but was necessary in order to inject enough gas phase phenol for detection. The intercept is then very sensitive to small changes in the fit. The intercept in Figure 6.9 (a) yields a value of $1/K_s = (8.19 \pm 4.02)$ x 10^{-2} cm^{-1} s, i.e. the statistical error is 49 %. The resulting K_s is $12.21^{+11.77}_{-4.02}$ cm s^{-1}. These errors of 96 and 33 %, respectively, are reflected in $\alpha = \left(1.96^{+1.89}_{-0.65}\right) \times 10^{-3}$. To justify the application of the *Pöschl et al.* [1998] approach more data at lower pressures are necessary.

The above analysis assumes no change in D_G^P over the pressure range used. Based on calculated diffusion coefficients [*Fuller et al.*, 1969], the D_G^P at the lowest (D_G^P = 191.4 Torr cm^2 s^{-1} at p = 35.2 Torr) and the highest total pressure (D_G^P = 196.6 Torr cm^2 s^{-1} at p = 66.8 Torr) were estimated. The variation in the D_G^P can be neglected and, therefore, the assumption of a constant D_G^P is reasonable.

6.3.3 Reactive uptake of phenol

Reactive uptake of phenol on bromine water was measured at four temperatures. It was possible to derive a value for the mass accommodation coefficient at each temperature. The values range from 3.75 x 10^{-2} at 278 K to 6.60 x 10^{-3} at 298 K. A negative temperature dependence was noted. Figure 6.15 displays the change of the mass accommodation with temperature of phenol measured by different researchers. For comparison, the mass accommodation of ethanol is also shown.

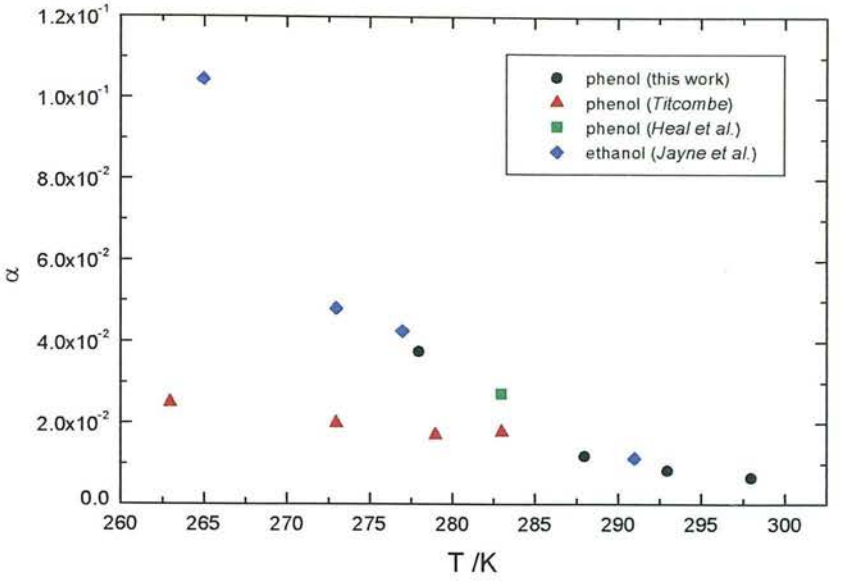

Figure 6.15 Temperature dependence of mass accommodation. Data points presented here were taken from this work (black dots), *Titcombe* [1997] (red triangles) and *Heal et al.* [1995] (green square) for phenol. For comparison, there were also values for ethanol (blue diamonds) included [*Jayne et al.*, 1991].

The mass accommodation coefficients of phenol measured in this work are consistent with the one given by *Heal et al.* [1995]. However, there is a discrepancy between these results and the study by *Titcombe* [1997]. Only the mass accommodation coefficient at 283 K fits with the results from this work if it is assumed that the lower temperature values follow the trend found between 278 and 298 K. The mass accommodation measured in this work shows a much stronger dependence on temperature than was observed by *Titcombe* [1997], using their droplet train apparatus.

The mass accommodation coefficient of ethanol exhibits a strong temperature dependence [*Jayne et al.*, 1991], very similar to the mass accommodation data for phenol observed in this work.

As described in Chapter 2, *Davidovits et al.* [1991; 1995] have developed a model to explain the uptake of gases by liquids. In this model the mass accommodation coefficient is expressed as

$$\ln\left(\frac{\alpha}{1-\alpha}\right) = -\frac{\Delta G_{obs}}{RT} = -\frac{\left(\Delta H_{obs} - T\Delta S_{obs}\right)}{RT} \qquad (6.17)$$

where ΔG_{obs} can be regarded as the Gibbs free energy barrier of the transition state between gas and solvated state. The enthalpy ΔH_{obs} and entropy ΔS_{obs} can be derived from a plot of $\ln(\alpha/(1-\alpha))$ *vs.* 1/T. Such a plot is shown in Figure 6.16 for the data obtained in this work.

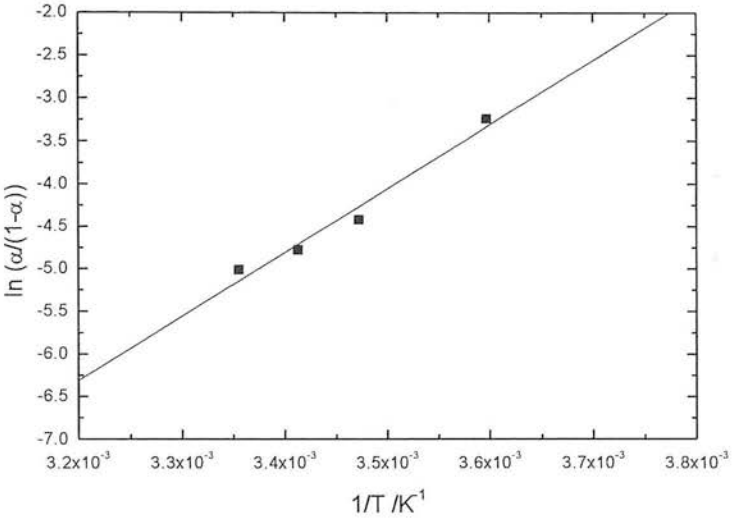

Figure 6.16 Plot of $\ln(\alpha/(1-\alpha))$ *vs.* 1/T for phenol.

The values obtained for ΔH_{obs} and ΔS_{obs} from Figure 6.16 are -62.3 ± 7.7 kJ mol^{-1} and -251.9 ± 26.5 J mol^{-1} K^{-1}. Again, these values are more consistent with ethanol (ΔH_{obs} = -46.1 kJ mol^{-1} and ΔS_{obs} = -193.6 J mol^{-1} K^{-1}) [*Jayne et al.*, 1991] than with phenol (ΔH_{obs} = -10.9 kJ mol^{-1} and ΔS_{obs} = -73.5 J mol^{-1} K^{-1}) given by *Titcombe* [1997].

In the depiction of the mass accommodation as a continuous process ΔH_{obs} and ΔS_{obs} exhibit a direct relationship which is governed by N*. Applying this model and performing calculations based on formulas for ΔH_{obs} and ΔS_{obs} given by *Nathanson et al.* [1996] , the measured values of ΔH_{obs} and ΔS_{obs} lead to a value of N* ≈ 3.2 for the critical size of cluster for phenol in the mass accommodation process (see Chapter 9 for a fuller discussion).

6.4 Conclusion

The uptake of phenol has been investigated at different temperatures. Two approaches were applied. The solubility limited uptake of phenol is time dependent. In this regime the highest uptakes were 1.94×10^{-2} at 278 K and 4.28×10^{-3} at 298 K measured at about 1s liquid-gas contact time. No mass accommodation could be derived. However, changing the regime to liquid-reaction controlled uptake, it was possible to derive mass accommodation coefficients for phenol. They range from 3.75×10^{-2} at 278 K to 6.60×10^{-3} at 298 K and show a negative temperature dependence. The results yield values of ΔH_{obs} and ΔS_{obs} -62.3 ± 7.7 kJ mol^{-1} and -251.9 ± 26.5 J mol^{-1} K^{-1} which corresponds to a critical cluster size of $N^* \approx 3.2$.

7. UPTAKE OF 2-NITROPHENOL

This chapter describes the uptake measurements of 2-nitrophenol. In the first section of the chapter the absorption spectrum is shown. The measurements were performed in a similar manner to the uptake experiments of phenol. The uptake of 2-nitrophenol was measured on water and on bromine water to be able to distinguish between solubility and liquid reaction controlled uptake. Results are compared and discussed in the final part of the chapter.

7.1 UV absorption spectrum of 2-nitrophenol

A gas-phase absorption spectrum of 2-nitrophenol over the wavelength range 200 to 400 nm, measured using the Instrument SA spectrometer, is shown in Figure 7.1.

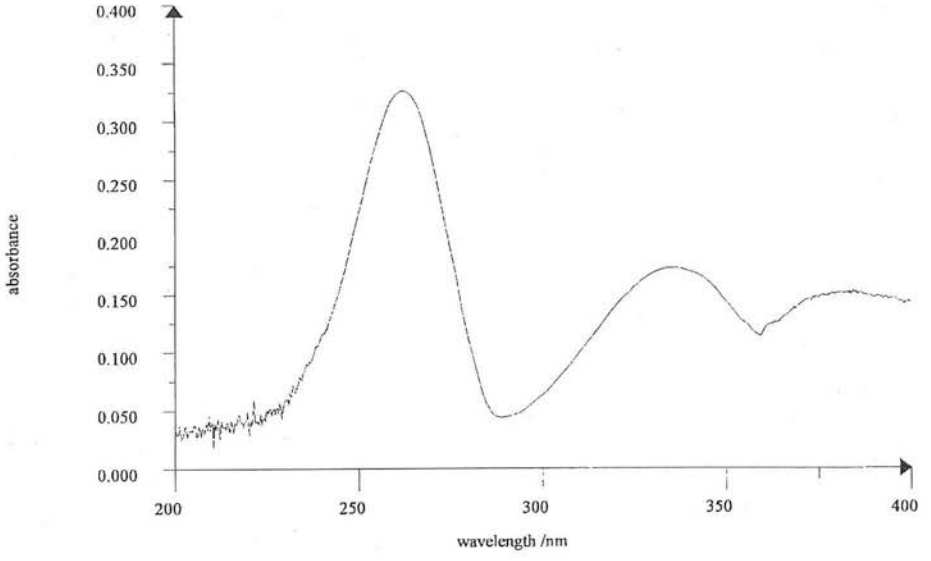

Figure 7.1 UV absorption spectrum of 2-nitrophenol

The wavelength of 258 nm, at maximum absorbance, was used for detection. The linearity of the detector signal as a function of concentration was confirmed by measuring the absorption signal for different total pressures of a typical mixture of 2-nitrophenol in helium on the Instrument SA spectrometer. Example data are plotted in Figure 7.2.

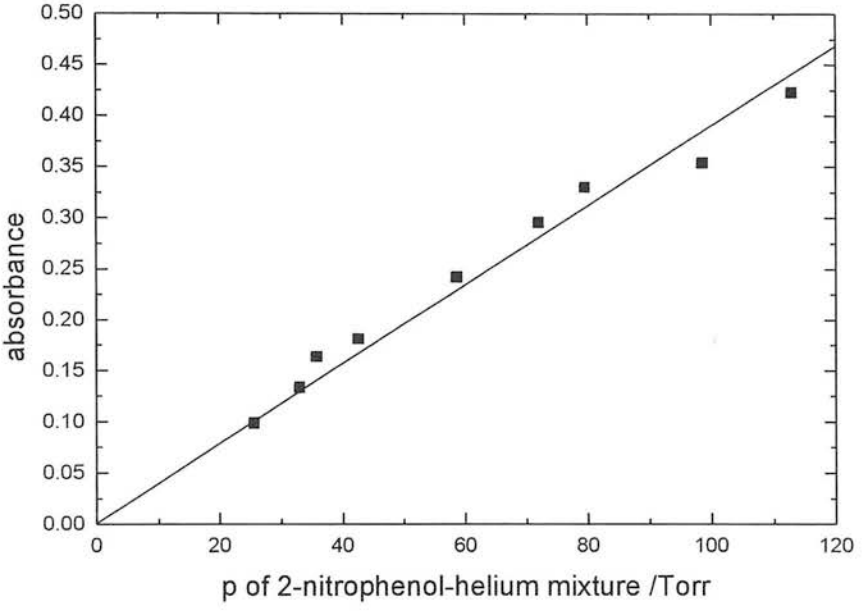

Figure 7.2 Plot of absorbance at 258 nm *vs.* total pressure in absorption cell of a typical mixture of 2-nitrophenol in helium.

No absorption cross section for 2-nitrophenol in the gas phase could be found to determine its initial concentration. However, phenol and 2-nitrophenol have similar melting points ($m.p._{(phenol)}$: 40.6 °C and $m.p._{(2\text{-nitrophenol})}$: 49.3 °C) and the vapour pressures are comparable (Figure 7.3), especially at room temperature. It was therefore assumed that the initial concentration of 2-nitrophenol was similar to that of phenol (~ 10^{14} molecules cm^{-3}).

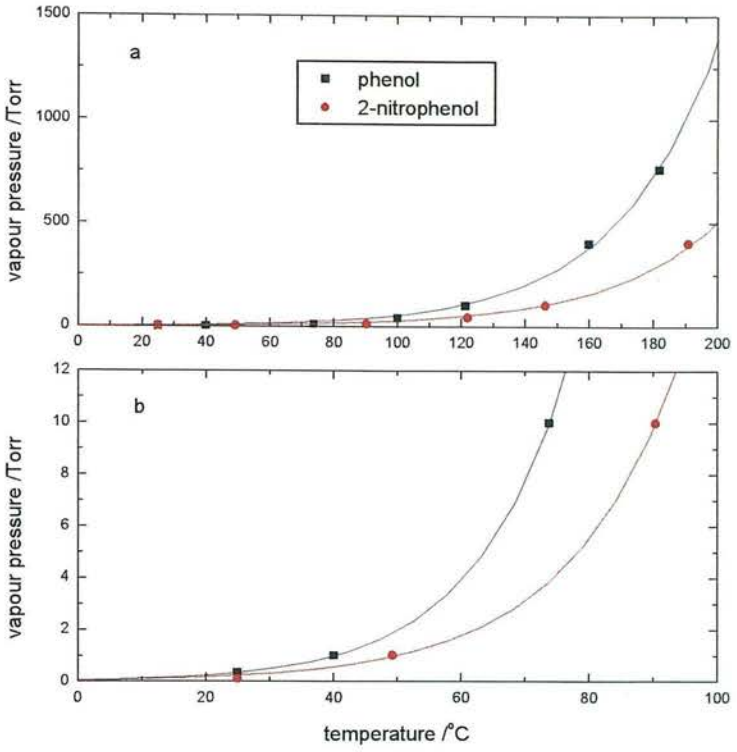

Figure 7.3 Plot of the vapour pressure as a function of temperature for phenol and 2-nitrophenol. b is an expanded portion of a. Data were taken from *CRC Handbook of chemistry and physics* [1993] and *Howard and Meylan* [1997].

7.2 Uptake measurements of 2-nitrophenol

7.2.1 Approach

The uptake regimes of 2-nitrophenol were estimated in a similar manner as described already for phenol. Firstly, the effect of pH was assessed. Using an initial concentration of 2-nitrophenol of about 10^{14} molecules cm^{-3} (1.66×10^{-10} mol cm^{-3}), the maximum pH change in the water (assuming complete loss from the gas phase) was (see eqn (4.98))

$$\mathrm{pH} = \frac{7.17}{2} - \frac{1}{2}\log(7.97 \times 10^{-5}) = \underline{\underline{5.63}}. \qquad (7.1)$$

The 2-nitrophenol concentration in water of 7.97×10^{-5} mol l^{-1} was calculated using a liquid flow rate of 50 ml min^{-1} and an experimental gas flow of 400 ml s^{-1} as the typical conditions at which the uptake experiments of 2-nitrophenol were performed. The pK_A of 7.17 at 298 K was taken from the *CRC Handbook of chemistry and Physics* [1993].

The literature values for the Henry's law coefficients of 2-nitrophenol are given Table 7.1.

T /K	value of H /M atm^{-1}	reference
278	1359 (exp) 197 (cal)	*Lüttke and Levsen* [1997]
281	288	solubility estimated, *Leuenberger et al.* [1985]
293	74	*Schwarzenbach et al.* [1988]
	80	*Tremp et al.* [1993]
	91	estimated, *Staudinger and Roberts* [1996]
	132	calculated from vapour pressure and solubility, *Mabey et al.* [1982]
	139	*Rippen et al.* [1987]
298	64[1]	*Leuenberger et al.* [1985]
	70	estimated, *Staudinger and Roberts* [1996]
	80	*Rippen et al.* [1987]
	106	estimated from vapour pressure and solubility, *Howard and Meylan* [1997]
	124	calculated from infinite dilution activity coefficient[2] given by *Benes and Dohnal* [1999]
303	40	*Tremp et al.* [1993]

Table 7.1 Henry's law coefficients of 2-nitrophenol found in the literature.

[1] Calculated with solubility at 20 °C.

[2] Henry's law coefficient can be described by eqn (2.27) $H_i = \frac{\rho}{M \gamma_i^{\infty} p_i^*}$. *Benes and Dohnal* [1999] have given the infinite dilution activity coefficient of 2-nitrophenol at four temperatures (283, 293, 303 and 313). Since γ_i^{∞} has a van't Hoff temperature dependence [*Benes and Dohnal*, 1999] a value of 3016 for $\gamma_{C_6H_4(NO_2)OH}^{\infty}$ at 25 °C could be derived. The vapour pressure of 2-nitrophenol was taken as 1.13×10^{-1} Torr [*Howard and Meylan*, 1997] at 25 °C.

The effect of the pH on the Henry's law coefficient is shown in Figure 7.4 using H^{298K} = 80 M atm^{-1} [*Rippen et al.*, 1987]. Below pH = 6 the effective Henry's law constant is only marginally different (85 M atm^{-1} at pH 6) from the Henry's law coefficient which includes the above calculated pH. However, realistically the pH change caused by the uptake of 2-nitrophenol is likely to be much less than in the calculation with the assumption of a complete uptake. For example, a pH of 6.6 would be caused by an uptake of 1 % of gas phase 2-nitrophenol into the water. The effective Henry's law coefficient of 102 M atm^{-1} at that pH exceeds the Henry's law coefficient by almost 30 %. Therefore, one has to be aware that the Henry's law coefficients derived in this experiment might exceed the Henry's law coefficient in neutral solution.

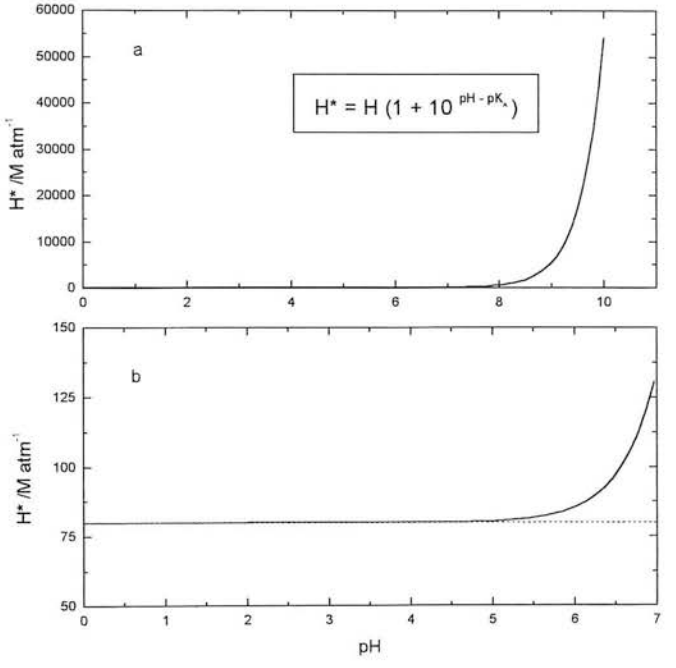

Figure 7.4 The effective Henry's law coefficient H^* of 2-nitrophenol as a function of pH at 298 K. b is a replot of a showing only the pH range 0 to 7. The red dotted line in b represents H = 80 M atm^{-1} [*Rippen et al.*, 1987]. $pK_{A(2NP)}$ = 7.17 at 298 K [*CRC Handbook of chemistry and physics*, 1993].

Table 7.2 lists the properties that were used to estimate the individual transport coefficients (given in Table 7.3) applicable to the uptake of 2-nitrophenol onto water and bromine water at 293 K for the experimental conditions in this work.

Parameter	Numerical value	Source/comments
ω	2.11×10^4 cm s^{-1}	calculated at T = 293 K, p = 55 Torr, F = 1350 cm^3 min^{-1} (STP), RH = 70 %
r	0.8 cm	radius of wetted-wall reactor
D_G	2.6 cm^2 s^{-1}	calculated at experimental conditions given above in this table
t	1 s	typical liquid-gas contact time
H^*	102 M atm^{-1}	calculated above for pH 6.6 (temperature difference of 5 K was neglected for this calculation)
pH	6.6	assumed for this estimation
T	293 K	
k" [3]	4.6×10^8 l mol^{-1} s^{-1}	
$[Br_2]$	0.02 mol l^{-1}	estimated (see Chapter 6, Section 6.2.5)
D_L	7.91×10^{-6} cm^2 s^{-1}	calculated using Wilke-Chang correlation (see Chapter 4)

Table 7.2 Properties used to estimate uptake of 2-nitrophenol onto water and bromine water at 293 K.

uptake coefficient	symbol	formula	value	resistance	value
gas diffusion	Γ_G	$\frac{2\,(3.66\,D_G)}{\omega\,r}$	1.127×10^{-3}	GAS: $\frac{1}{\Gamma_G}$	887
liquid solubility	Γ_{SOL}	$\frac{4\,H^*\,R\,T}{\pi^{1/2}\,\omega}\sqrt{\frac{D_L}{t}}$	7.376×10^{-4}	LIQUID: (pure water) $\frac{1}{\Gamma_{SOL}}$	1356
liquid reaction	Γ_{RXN}	$\frac{4\,H^*R\,T\,\sqrt{D_L k"\,[Br_2]}}{\omega}$	3.966	LIQUID: (bromine water) $\frac{1}{\Gamma_{SOL}+\Gamma_{RXN}}$	0.252

Table 7.3 Estimated resistances for the uptake of 2-nitrophenol onto water and bromine water at 293 K using the properties listed in Table 7.2.

[3] As for phenol (see earlier footnote), $k"= k_1 + k_2K_A/[H^+]$. The rate coefficients are $k_1 < 100$ M^{-1} s^{-1} and $k_2 = 1.7 \times 10^9$ M^{-1} s^{-1} [*Tee et al.*, 1989] and the pK_A of 2-nitrophenol is 7.17 [*CRC Handbook of chemistry and physics*, 1993]. All values are at 25 °C (temperature difference of 5 K was neglected for this estimation calculation). The k" was calculated for a pH of 6.6.

The results in Table 7.3 show that the uptake of 2-nitrophenol onto bromine water will be gas diffusion controlled. For uptake onto pure water, the resistances of gas diffusion and solubility are of the same order of magnitude. In either case, mass accommodation becomes limiting if $\alpha < 10^{-3}$. The solubility controlled uptake as a function of liquid-gas contact time is shown in Figure 7.5 where the data are based on Table 7.3.

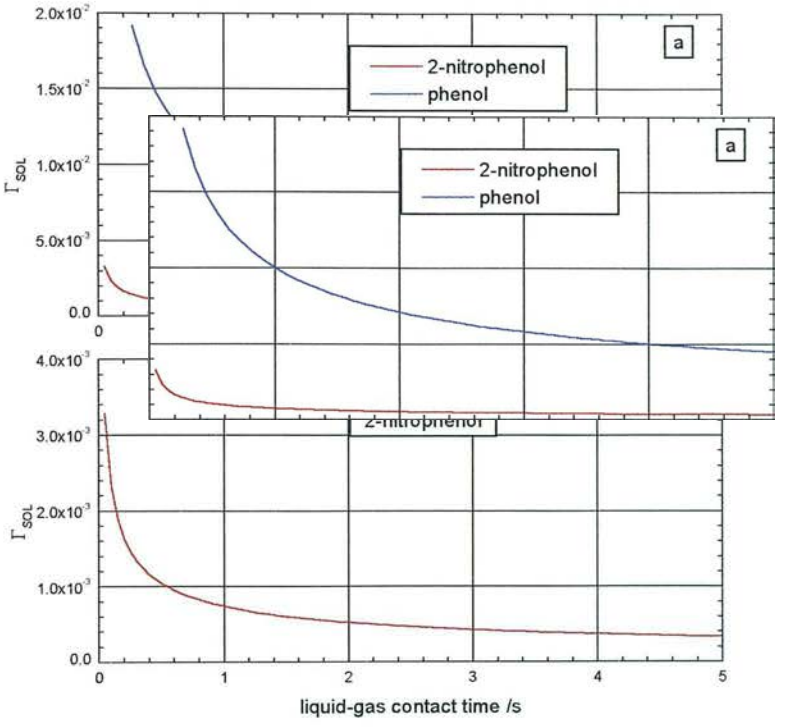

Figure 7.5 Calculated change of Γ_{SOL} with liquid-gas contact time at 293 K, where $\Gamma_{SOL} = \frac{4\,H^{*}\,R\,T}{\pi^{1/2}\,\omega}\sqrt{\frac{D_L}{t}}$.

Figure 7.5 a shows Γ_{SOL} of phenol (calculated as described in Chapter 6) and 2-nitrophenol, calculated according to Table 7.3. Figure 7.5 b is an expanded view of a, showing only the change of Γ_{SOL} of 2-nitrophenol.

There is clearly a difference between the solubility controlled uptake of phenol and 2-nitrophenol. The Γ_{SOL} of 2-nitrophenol is expected to be smaller compared with the Γ_{SOL} of phenol due to the smaller effective Henry's law coefficient. When the Henry's law coefficient of 2-nitrophenol (74 M atm^{-1}) is used instead of H^{*}, the regime is still the same with $\frac{1}{\Gamma_{SOL}} = 1869$ and $\frac{1}{\Gamma_{SOL} + \Gamma_{RXN}} = 0.348$.

The uptake of 2-nitrophenol onto water was investigated in two ways: Firstly, the contact area between liquid and gas was changed in small steps, with the assumption that the solubility-controlled uptake, although time dependent, does not change significantly over small changes in contact time. Figure 7.5 shows that this is the case with a change in Γ_{SOL} of ~ 2.2×10^{-4} from 1 to 2 s liquid-gas contact time which decreases to ~ 0.4×10^{-4} from 4 to 5 s and ~ 0.07×10^{-4} from 14 to 15 s (calculated). The bulk of the measurements were performed in the range of 5 to 15 s contact time. Secondly, bromine water was employed to investigate the uptake in a reaction controlled uptake regime. The procedures for the data analysis were the same as described for phenol.

7.2.2 Uptake measured from changes in contact area

The uptake of 2-nitrophenol was investigated at four different temperatures. The first-order loss rate of 2-nitrophenol from the gas phase was obtained from $k_w = \frac{\ln\left(\frac{A_1}{A_2}\right)}{\Delta\tau}$ and corrected for radial gas phase diffusion [*Brown*, 1978]. The corrected first-order loss rate coefficient k_w^{corr} (s^{-1}) was used to obtain $\left(\ln\frac{A_1}{A_2}\right)^{corr}$. Values of γ were derived from the gradient of a plot of $\left(\ln\frac{A_1}{A_2}\right)^{corr}$ *vs.* $\omega\,\Delta A_r/(4F)$. Table 7.4 shows the results of these measurements which are displayed as a function of liquid-gas contact time in Figure 7.6.

T /K	liquid-gas contact time /s	γ
281	2.151	1.31×10^{-3}
	4.578	1.21×10^{-3}
	8.092	8.76×10^{-4}
288	4.618	1.01×10^{-4}
	5.622	1.05×10^{-4}
	9.638	7.10×10^{-5}
	13.706	6.65×10^{-5}
291	5.500	4.89×10^{-5}
	6.482	4.26×10^{-5}
	7.172	4.15×10^{-5}
	8.731	4.51×10^{-5}
	11.849	3.20×10^{-5}
303	8.068	2.92×10^{-5}
	10.949	2.61×10^{-5}
	13.830	2.56×10^{-5}
	16.712	2.18×10^{-5}
	19.593	2.01×10^{-5}

Table 7.4 The time-dependent uptake coefficients of 2-nitrophenol onto water at different temperatures.

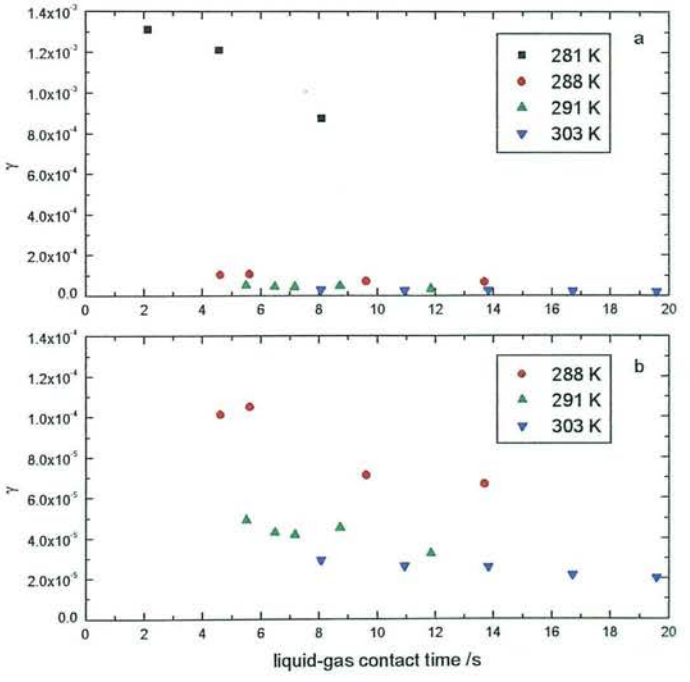

Figure 7.6 Uptake of 2-nitrophenol onto water as a function of liquid-gas contact time at different temperatures. Graph b shows an expanded portion of a.

Figure 7.6 confirms the time dependence of the uptake at all temperatures and shows that the time dependence of γ is stronger at lower temperatures. Furthermore, the absolute values of uptake decrease with temperature, although values of γ at 281 K appear high compared with the values at the other temperatures.

According to eqn (6.2) a plot of $1/\gamma$ *vs.* $\sqrt{t}$ should yield a straight line with a gradient of $\frac{\sqrt{\pi}\,\omega}{4\,H\,R\,T\sqrt{D_L}}$ and an intercept of $1/\alpha$. These plots are displayed in Figure 7.7.

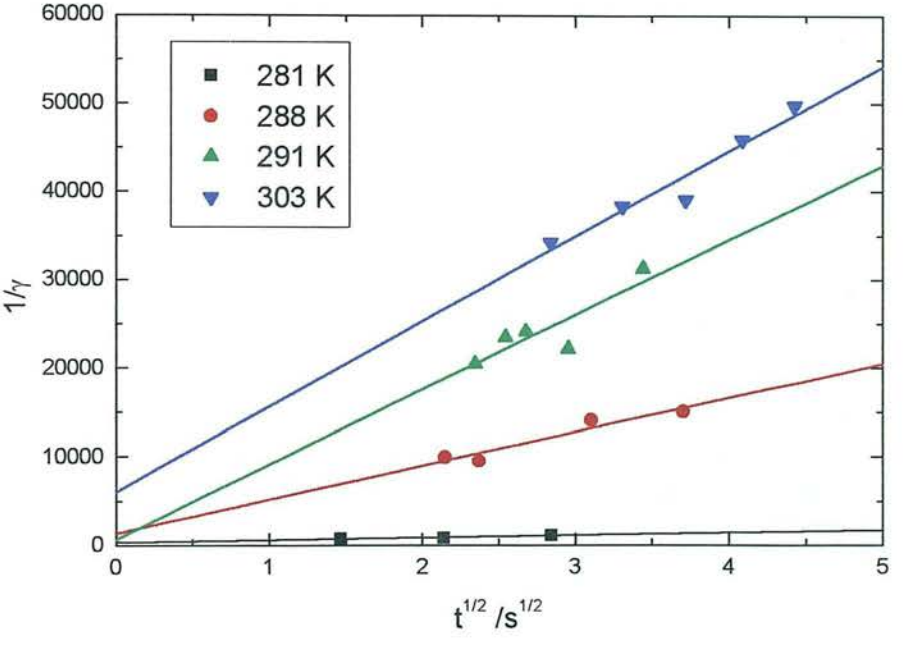

Figure 7.7 Plot of $1/\gamma$ *vs.* $\sqrt{t}$ for 2-nitrophenol at four temperatures. The gradient is $\frac{\sqrt{\pi}\,\omega}{4\,H\,R\,T\sqrt{D_L}}$ and the intercept is $1/\alpha$.

The values for $H\sqrt{D_L}$ and α derived from Figure 7.7 are given in Table 7.5 and Table 7.6, respectively. Values of D_L in Table 7.5 were estimated using the Wilke-Chang method.

T /K	gradient ($=\pi^{1/2}\omega/(4HRTD_L^{1/2})$ /$s^{-1/2}$	ω /cm s^{-1}	$HD_L^{1/2}$ /M atm^{-1} $(cm^2\ s^{-1})^{1/2}$	D_L estimated /$cm^2\ s^{-1}$	H /M atm^{-1}
281	276	2.06×10^4	1.44	5.46×10^{-6}	615^{+360}_{-166}
288	3830	2.09×10^4	0.102	6.79×10^{-6}	39^{+10}_{-6}
291	8470	2.10×10^4	0.046	7.43×10^{-6}	17^{+8}_{-4}
303	9640	2.14×10^4	0.040	1.05×10^{-5}	12^{+2}_{-1}

Table 7.5 Values of $H\sqrt{D_L}$ of 2-nitrophenol derived from the gradient in Figure 7.7. The liquid diffusion coefficients were estimated after Wilke-Chang [*Reid et al.*, 1987]. The errors in H refer only to statistical error in the linear fit.

T /K	intercept (=1/α)	α	lower limit of α
281	317	3.15×10^{-3}	1.84×10^{-3}
288	1290	7.76×10^{-4}	2.80×10^{-4}
291	629	1.59×10^{-3}	1.19×10^{-3}
303	5990	1.67×10^{-4}	8.75×10^{-5}

Table 7.6 Values of α of 2-nitrophenol derived from the intercept in Figure 7.7. The lower limits are calculated from the standard error of the intercept.

7.2.2.1 Gas diffusion coefficients

The pressure-independent binary diffusion coefficients (Torr $cm^2\ s^{-1}$) of 2-nitrophenol in H_2O and helium, $D_G^P{}_{(C_6H_4(NO_2)OH\text{-}H_2O)}$ and $D_G^P{}_{(C_6H_4(NO_2)OH\text{-}He)}$, were calculated according to the Fuller-Schettler-Giddings estimation method [*Fuller et al.*, 1969], as described in Chapter 4, using the parameters listed in Table 7.7.

Parameter/ unit	Symbol	Value	Source/comments
molar mass of 2-nitrophenol /g mol^{-1}	$M_{C_6H_4(NO_2)OH}$	139.1	
molar mass of water /g mol^{-1}	M_{H_2O}	18.0	
molar mass of helium /g mol^{-1}	M_{He}	4.0	
atomic diffusion volume of 2-nitrophenol	$(\sum v)_{C_6H_4(NO_2)OH}$	111.5	calculated from values given in *Fuller et al.* [1969]
atomic diffusion volume of water	$(\sum v)_{H_2O}$	13.1	given in *Fuller et al.* [1969]
atomic diffusion volume of helium	$(\sum v)_{He}$	2.67	given in *Fuller et al.* [1969]

Table 7.7 Parameters used to calculate pressure-independent binary gas diffusion coefficients of 2-nitrophenol in H_2O and He following the method of *Fuller et al.* [1969].

The calculated gas diffusion coefficients at the different temperatures are listed in Table 7.8.

T /K	D_G^P $_{(C_6H_4(NO_2)OH\text{-}H_2O)}$ /Torr cm^2 s^{-1}	D_G^P $_{(C_6H_4(NO_2)OH\text{-}He)}$ /Torr cm^2 s^{-1}
281	71.3	192.9
288	74.4	201.4
291	75.8	205.1
303	81.3	220.1

Table 7.8 Pressure-independent gas diffusion coefficients for 2-nitrophenol in H_2O and in helium at the experimental temperatures following the method of *Fuller et al.* [1969].

7.2.2.2 Liquid diffusion coefficients

The liquid diffusion coefficients for 2-nitrophenol in water at the experimental temperatures were calculated by the Wilke-Chang method, as described in Chapter 4, using a molar volume of 2-nitrophenol at boiling temperature $V_{C_6H_4(NO_2)OH}$ = 131.0 cm^3 mol^{-1}. The diffusion coefficients are listed in Table 7.5.

7.2.3 Reactive uptake of 2-nitrophenol

Reactive uptake of 2-nitrophenol was investigated using bromine water. Since there is reaction in the liquid phase, the liquid phase solubility is not rate limiting. Therefore, γ is no longer time dependent and it is valid to use first-order uptake from changes in gas contact time along the whole length of the flow tube. The same approach as described in Section 6.2.5 for phenol was employed to obtain mass accommodation coefficients of 2-nitrophenol as a function of temperature, using the expression given by *Rudich et al.* [1996b]

$$\frac{1}{\alpha} = \frac{\omega}{2\,r\,k_w} - \frac{\omega\,r}{7.32\,D_G} - \frac{1}{\gamma} \qquad \textbf{(6.15)}$$

k_w was determined from plots of ln absorbance *vs.* injector distance from position "0". An example plot is shown in Figure 7.8.

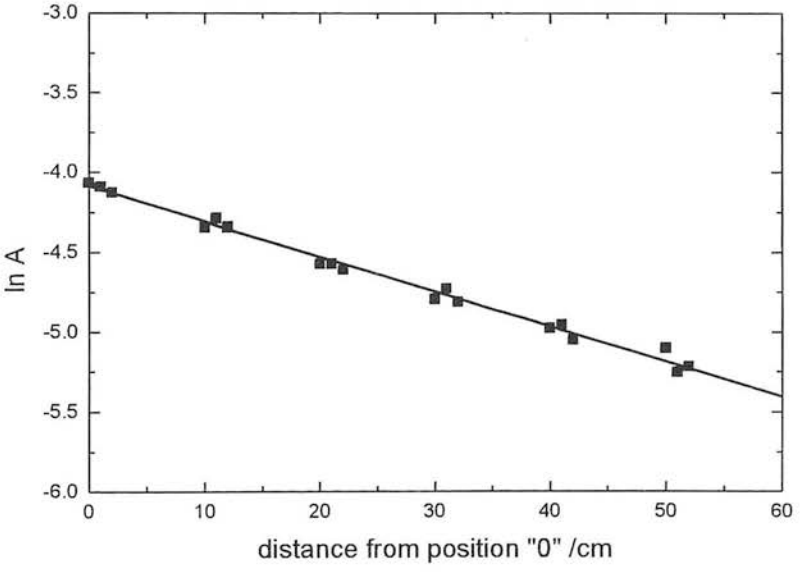

Figure 7.8 Typical plot of ln A *vs.* distance from injector position "0". Experiment at 288 K with gas velocity c = 197 cm s^{-1}.

The mass accommodation coefficients derived using eqn (6.15) are listed in Table 7.9 together with the corresponding experimental parameters.

T /K	ω /cm s^{-1}	D_G /cm^2 s^{-1}	k_w /s^{-1}	γ	α
278	2.05×10^4	3.323	7.946	1.17×10^{-3}	1.21×10^{-2}
283	2.07×10^4	3.160	3.682	3.74×10^{-4}	8.21×10^{-3}
288	2.09×10^4	2.748	3.342	3.44×10^{-4}	5.90×10^{-3}
293	2.11×10^4	2.670	3.091	4.19×10^{-4}	9.92×10^{-4}

Table 7.9 Experimental parameters and mass accommodation coefficients of 2-nitrophenol at different temperatures measured on bromine water.

7.3 Discussion

7.3.1 Solubility limited uptake

The solubility limited uptake of 2-nitrophenol was measured at four different temperatures. The time dependent uptake coefficients were measured at various liquid-gas contact times and decreased with increasing contact time (see Table 7.4). The measured uptakes showed a negative dependence on temperature.

A plot of $1/\gamma$ *vs.* $\sqrt{t}$ (see Figure 7.7) showed linearity at all temperatures, from which value for $H\sqrt{D_L}$ and H were derived (see Table 7.5). The Henry's law coefficients derived appear low compared with previously reported values of H (see Table 7.1), especially if the pH might be slightly below 7 due to uptake of 2-nitrophenol (see Section 7.2.1).

The enthalpy and entropy for the gas-liquid solubility are obtained from a plot of ln H (where H is the dimensionless Henry's constant) *vs.* 1/T. Figure 7.9 shows such a plot. The gradient corresponds to $-\frac{\Delta H^\circ}{R}$ and the intercept to $\frac{\Delta S^\circ}{R}$. In addition to values from this work, various literature data are also included.

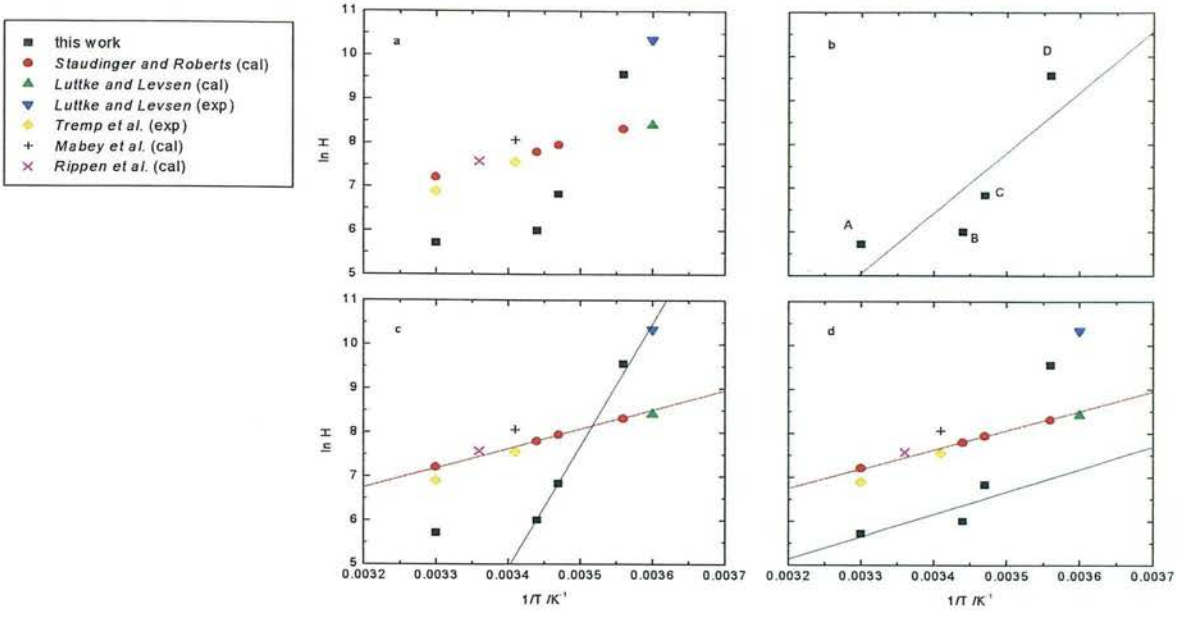

Figure 7.9 Plots of ln H (dimensionless liquid-to-gas ratio) *vs.* 1/T. In addition to H measured in this work, various values taken from other references are plotted [*Staudinger and Roberts*, 1996; *Lüttke and Levsen*, 1997; *Tremp et al.*, 1993; *Mabey et al.*, 1982; *Rippen et al.*, 1987] (a). A straight line was fitted to the measured values of this work (b). A black solid line was fitted to values from this work and *Lüttke and Levsen* (exp) [1997] (except for point A) (c) and to values from this work (except for point D) (d), respectively, and compared to a fit (red solid line) through values from *Staudinger and Roberts* [1996], *Lüttke and Levsen* (cal) [1997], *Tremp et al.* [1993], *Mabey et al.* [1982] and *Rippen et al.* [1987]. Experimental values of H are labelled (exp) in the legend whereas (cal) represents calculated values.

There is considerable diversity amongst existing values of H. It should be noted that the experimental value of H given by *Lüttke and Levsen* [1997] agrees very well with the values found in this work. A line was therefore also fitted through these points ignoring point A (Figure 7.9 c, black line). These values are different from the values of H derived mainly by calculation and represented by the red line in Figure 7.9 c and d. Only *Tremp et al.* [1993] determined H experimentally, all other literature values are calculated. Alternatively, ignoring point D in the fitting of data obtained in this work leads to a line (Figure 7.9 d, black solid line) with a similar gradient to the one obtained from calculated values of H. For comparison, Table 7.10 lists the different values of $\Delta H°$ and $\Delta S°$ derived from Figure 7.9 b-d, as described above.

values taken from	corresponding to	ΔH° /kJ mol^{-1}	ΔS° /J mol^{-1} K^{-1}
Staudinger and Roberts [1996], *Lüttke and Levsen* (cal) [1997], *Tremp et al.* [1993], *Mabey et al.* [1982] and *Rippen et al.* [1987]	red line, Figure 7.9 c and d	-36.8 ± 5.6	-61.6 ± 19.1
this work except point D	black line, Figure 7.9 d	-42.7 ± 31.5	-93.9 ± 107
this work	black line, Figure 7.9 b	-115 ± 51	-337 ± 174
this work, except point A, plus *Lüttke and Levsen* (exp) [1997]	black line, Figure 7.9 c	-232 ± 11	-747 ± 38

Table 7.10 ΔH° and ΔS° derived from Figure 7.9 b-d. The errors given for ΔH° and ΔS° refer to the errors in the fitted lines.

The difference between all obtained ΔH° and ΔS° approaches an order of magnitude, although some values have very large errors. Since only four temperatures were used to derive ΔH° and ΔS° in this work the uncertainties are high and ignoring one datum point in the fitting results in very different values. It is not possible to conclude if the difference between the experimentally determined H values and the calculated H values arises from a genuine discrepancy or from errors in the practical determination. *Lüttke and Levsen* [1997] have suggested that organic compounds can be enriched in small droplets in excess of that predicted by Henry's law due to additional adsorption at the air-water interface. However, different models used to describe this adsorption behaviour and based mainly on the octanol-water partitioning coefficient and/or the solubility fail to provide a satisfactory explanation in the case of 2-nitrophenol. More data regarding the physical properties of 2-nitrophenol are needed to interpret these findings more satisfactorily.

Comparison between these data and similar compounds, such as phenol and ethanol, leads to the conclusion that the ΔH° and ΔS° values from fits to all points of this work (Figure 7.9 b) and to all except A (Figure 7.9 c, black line) are quite possibly too high. The values obtained when point D is ignored (Figure 7.9 d, black line) are in best agreement with the other references. These ΔH° and ΔS° values of -42.7 kJ mol^{-1} and -93.9 J mol^{-1} K^{-1}, respectively, also coincide best with the phenol data which were

found to be $\Delta H° = -74.6$ kJ mol^{-1} and $\Delta S° = -185$ J mol^{-1} K^{-1}. The values of $\Delta H° = -42.7$ kJ mol^{-1} and $\Delta S° = -93.9$ J mol^{-1} K^{-1} are therefore the best estimates for 2-nitrophenol derived from this work.

By plotting $1/\gamma$ *vs.* $t^{1/2}$ (see Figure 7.7) it was possible to extract mass accommodation coefficients for 2-nitrophenol (see Table 7.6). They range from 3.15×10^{-3} at 281 K to 1.67×10^{-4} at 303 K. The mass accommodation coefficients show a negative temperature dependence, although the value at 291 K is higher than that at 288 K. The large standard error associated with the intercepts only allowed the estimation of a lower limit of α (upper limit yielded negative values for 288 and 291 K).

7.3.2 Reaction controlled uptake of 2-nitrophenol

The reaction controlled uptake of 2-nitrophenol on bromine water was measured at four temperatures. Values of uptakes were measured in the range from 1.17×10^{-3} at 278 K to 4.19×10^{-4} at 293 K. The derived mass accommodation coefficients ranged from 1.21×10^{-2} at 278 K to 9.92×10^{-4} at 293 K. A negative temperature dependence in α was noted.

7.3.3 Mass accommodation coefficient of 2-nitrophenol and comparison to that of phenol

Figure 7.10 shows the mass accommodation coefficient of 2-nitrophenol as a function of temperature, derived from measurements on both water and bromine water.

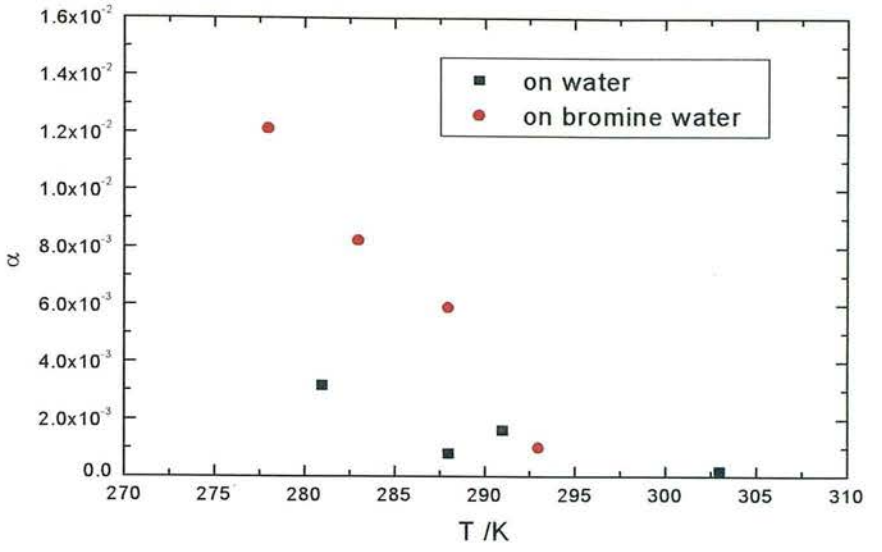

Figure 7.10 Mass accommodation coefficients of 2-nitrophenol as function of temperature.

The mass accommodation coefficients agree well at the higher temperatures (> 290 K), but at temperatures below 290 K mass accommodation coefficients measured on water are significantly smaller than measured on bromine water. Since α should be independent of the composition of the aqueous solution this indicates a possible systematic error between the measurements.

The mass accommodation measured on water is derived from the intercept $1/\gamma$ *vs.* $t^{1/2}$. The errors in the extrapolation to an intercept (Figure 7.7) are very large and allow only a lower error estimation of α. Therefore there are genuine reasons for supposing that the black squares, i.e. uptake values on water, in Figure 7.10 are too low.

On the other hand, the approach adopted from *Rudich et al.* [1996b] for the reaction controlled uptake might also include sources of errors, e.g. uncertainties in p_{H_2O} and D_G. The authors themselves were unable to derive a value of α from their uptake measurements of NO_3 on KI solutions and give only a lower limit of α.

Despite these discrepancies the mass accommodation of 2-nitrophenol is smaller than that of phenol as shown in Figure 7.11.

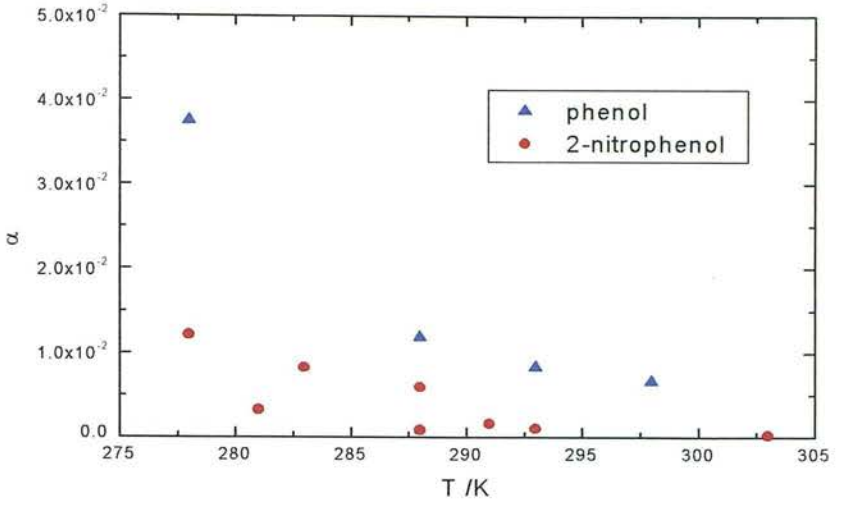

Figure 7.11 Mass accommodation of phenol and 2-nitrophenol as function of temperature.

In accordance with the cluster model (see Chapters 2 and 6), a plot of $\ln(\alpha/(1-\alpha))$ *vs.* 1/T enables derivation of ΔH_{obs} and ΔS_{obs} for mass accommodation, as well as the critical number of molecules N* necessary to form a cluster. Such a plot for 2-nitrophenol is shown in Figure 7.12. The fitted line yields $\Delta H_{obs} = -113 \pm 24$ kJ mol^{-1} and $\Delta S_{obs} = -442 \pm 83$ J mol^{-1} K^{-1} where errors represent only those in the statistical fit. These results are discussed in Chapter 9 in terms of the critical cluster model.

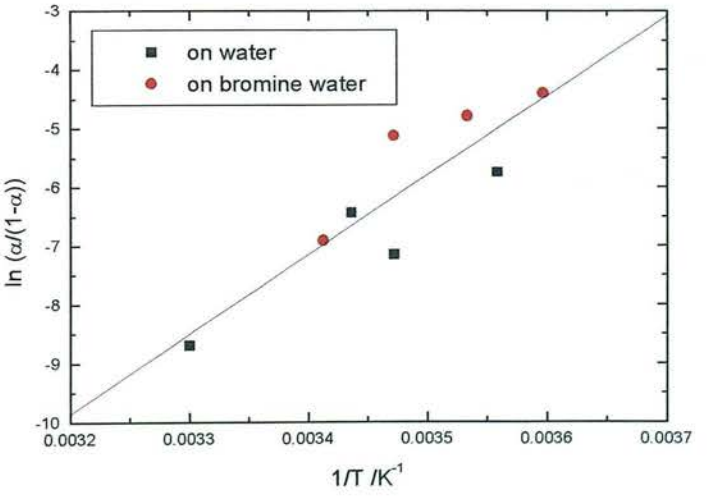

Figure 7.12 Plot of ln $(\alpha/(1-\alpha))$ *vs.* 1/T for 2-nitrophenol. Displayed are the results from measurements on water and on bromine water. The line was fitted to all points.

The fit in Figure 7.12 was used to derive values of the mass accommodation coefficient of 2-nitrophenol from the combination of all measurements. These data are listed in Table 7.11.

T /K	α calculated from fit in Figure 7.12
278	1.12×10^{-2}
281	6.70×10^{-3}
283	4.77×10^{-3}
288	2.08×10^{-3}
291	1.28×10^{-3}
293	9.35×10^{-4}
303	2.03×10^{-4}

Table 7.11 Values of mass accommodation coefficient of 2-nitrophenol at different temperatures using the fit in Figure 7.12.

7.4 Conclusion

The uptake of 2-nitrophenol was investigated. Two approaches, i.e. time dependent and time independent uptake, were used to derive α. Although both approaches gave different results, these were combined to yield values of the mass accommodation coefficient of 2-nitrophenol. These range from 1.12×10^{-2} at 278 K to 2.03×10^{-4} at 303 K.

Values of ΔH_{obs} of -113 ± 24 kJ mol^{-1} and $\Delta S_{obs} = -442 \pm 83$ J mol^{-1} K^{-1} for the mass accommodation coefficient of 2-nitrophenol were extracted using the critical cluster model. This corresponds to a critical number of molecules of $N^* \sim 5$ which is larger than those obtained for phenol and aliphatic alcohols.

8. UPTAKE OF m-CRESOL

This chapter describes the results of uptake measurements conducted with m-cresol. Although time limits did not allow a thorough investigation, the preliminary results obtained are presented. This chapter is structured similarly to those for phenol and 2-nitrophenol. In the first section the UV absorption spectrum of m-cresol is shown. The individual uptake regimes are estimated using typical experimental conditions and physical constants. In the final part the results are presented and discussed.

8.1 UV absorption spectrum of m-cresol

The UV absorption spectrum of m-cresol recorded with the Instrument SA spectrometer is shown in Figure 8.1. Using the absorption cross section of 10×10^{-18} cm^2 $molecule^{-1}$ at 278 nm given by *Trost et al.* [1997] for m-cresol, the initial concentration of m-cresol was calculated as about 10^{14} molecules cm^{-3}.

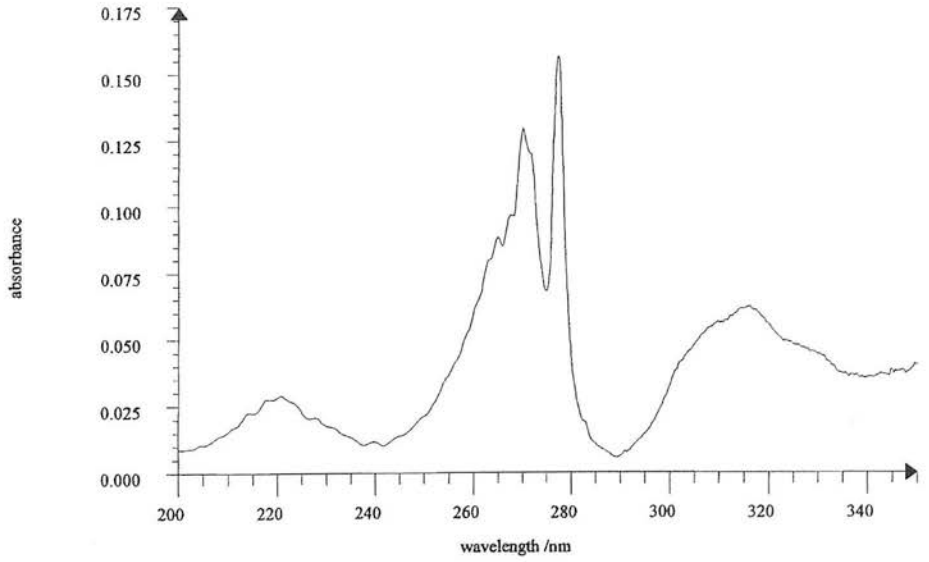

Figure 8.1 UV absorption spectrum of m-cresol.

8.2 Uptake measurements of m-cresol

8.2.1 Approach

As in the earlier chapters, the regime expected for the uptake of m-cresol was estimated using appropriate values. Table 8.1 lists the values of Henry's law coefficients of m-cresol previously reported in the literature and Table 8.2 shows typical parameters used for the estimation.

A possible pH change caused by the uptake of m-cresol does not have a significant effect on the Henry's law coefficient since the $pK_{A(m\text{-}cresol)}$ of 10.09 (at 298 K, *Howard and Meylan* [1997]) is larger than that of phenol. Therefore, the effective H^* is equal to H at near neutral pH (see Chapter 6 for details on calculation).

T /K	value of H /M atm^{-1}	reference
293	967	estimated from $\gamma^{\infty}_{C_6H_4(CH_3)OH}$, *Staudinger and Roberts* [1996]
	1382	*Yaws* [1999]
298	622	estimated from $\gamma^{\infty}_{C_6H_4(CH_3)OH}$, *Staudinger and Roberts* [1996]
	1156	estimated from vapour pressure and solubility; *Leuenberger et al.* [1985], *Howard and Meylan* [1997]
	1169	*Altschuh et al.* [1999]

Table 8.1 Literature values for Henry's law coefficients of m-cresol.

Parameter	Numerical value	Source/comments
ω	2.39 x 10^4 cm s^{-1}	calculated at T = 293 K, p = 70 Torr, F = 3000 cm^3 min^{-1} (STP), RH = 70 %
r	0.8 cm	radius of wetted-wall reactor
D_G	2.3 cm^2 s^{-1}	calculated at experimental conditions given for ω
t	2 s	typical liquid-gas contact time
H	967 M atm^{-1}	*Staudinger and Roberts* [1996]
T	293 K	
D_L	8.15 x 10^{-6} cm^2 s^{-1}	Wilke-Chang estimation

Table 8.2 Property values for typical experimental conditions for uptake of m-cresol at 293 K.

Table 8.3 lists the estimated values for individual uptake resistances. The uptake of m-cresol was measured on water and bromine water. No rate coefficient for the reaction of m-cresol with bromine could be found, but this is not relevant as long as the reaction is fast enough not to be the rate limiting step.

resistance	formula	value
GAS: $\frac{1}{\Gamma_G}$	$\frac{\omega\, r}{2\,(3.66\, D_G)}$	1136
LIQUID: $\frac{1}{\Gamma_{SOL}}$	$\frac{\pi^{1/2}\,\omega}{4\,H\,R\,T}\sqrt{\frac{t}{D_L}}$	226

Table 8.3 Estimation of resistances for the uptake of m-cresol based on values in Table 8.2.

Table 8.3 shows, that for uptake of m-cresol onto water, the resistance due to gas diffusion is, although greater, of about the same order of magnitude as the resistance due to liquid solubility. The uptake is gas diffusion limited on bromine water if it is assumed that the rate coefficient for the reaction of m-cresol with bromine is of a similar order of magnitude as that of the ortho (1.5×10^6 M^{-1} s^{-1}) and the para (6.6×10^3 M^{-1} s^{-1}) isomer [*Tee et al.*, 1989]. Mass accommodation becomes rate limiting in either case if $\alpha < 10^{-3}$.

Figure 8.2 shows Γ_{SOL} as function of liquid-gas contact time, using the formula in Table 8.3 and the values in Table 8.2. Measurements on water were performed with liquid-gas contact times between 2.4 and 8.4 s. The maximum change in contact time for a single experiment was 0.6 s. This corresponds to an expected change in Γ_{SOL} of about 10 % at the shortest total contact time, or less than this at longer total contact times. This variation in Γ_{SOL} was ignored within a single experiment in order to obtain a γ for the averaged contact time.

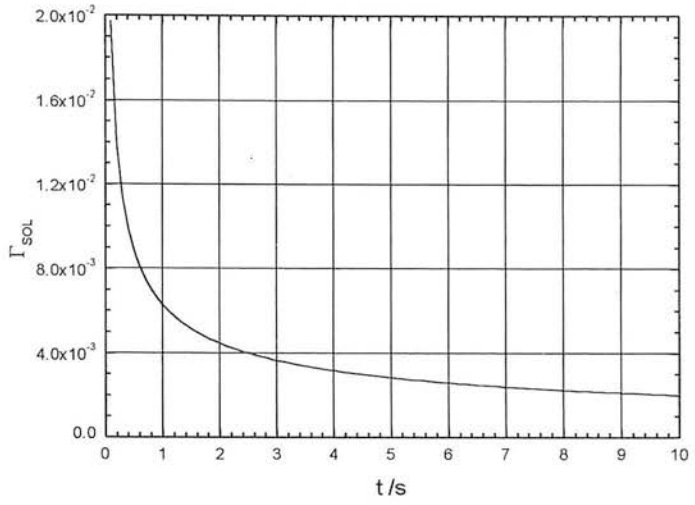

Figure 8.2 Γ_{SOL} as function of liquid-gas contact time for m-cresol at 293 K.

8.2.2 Uptake measured by changing contact area

The uptake of m-cresol on pure water was investigated at three temperatures. Changes in gas absorption were measured as a function of small changes in contact area and γ_{obs} derived from the gradient of plots of $\left(\ln\frac{A_1}{A_2}\right)$ *vs.* $\omega\,\Delta A_r/(4F)$. An example plot is shown in Figure 8.3.

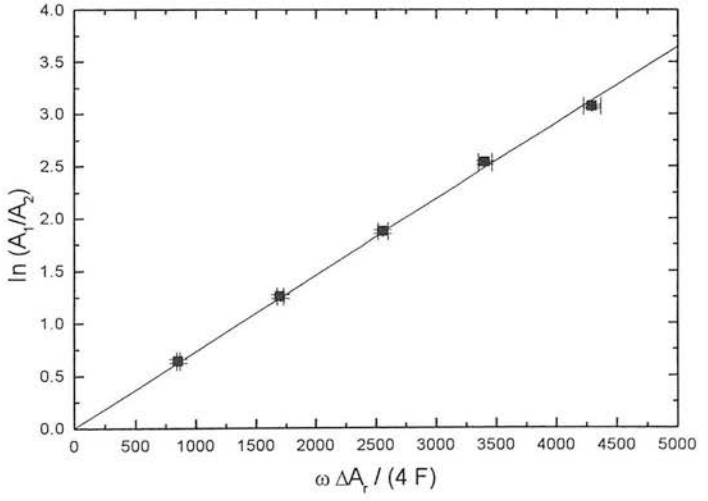

Figure 8.3 Typical plot of ln (A_1/A_2) as function of $\omega\ \Delta A_r/(4F)$ for m-cresol on pure water at 283 K. The solid line is a fit to the data and the gradient equals the uptake coefficient (γ_{obs} = 7.58 x 10^{-4}). The error bars represent a 10 % error in RH.

All results obtained are presented in Table 8.4 and plotted in Figure 8.4.

T /K	liquid-gas contact time /s	γ_{obs}
278	3.696	1.54×10^{-3}
	4.870	1.39×10^{-3}
	8.353	3.79×10^{-4}
283	2.415	1.08×10^{-3}
	3.561	6.63×10^{-4}
	3.562	6.44×10^{-4}
	4.680	7.58×10^{-4}
	5.797	6.44×10^{-4}
	5.818	6.01×10^{-4}
288	2.001	1.01×10^{-3}
	2.897	7.28×10^{-4}
	3.417	6.66×10^{-4}
	3.422	9.14×10^{-4}
	4.494	6.55×10^{-4}

Table 8.4 Observed uptake coefficients of m-cresol at three temperatures.

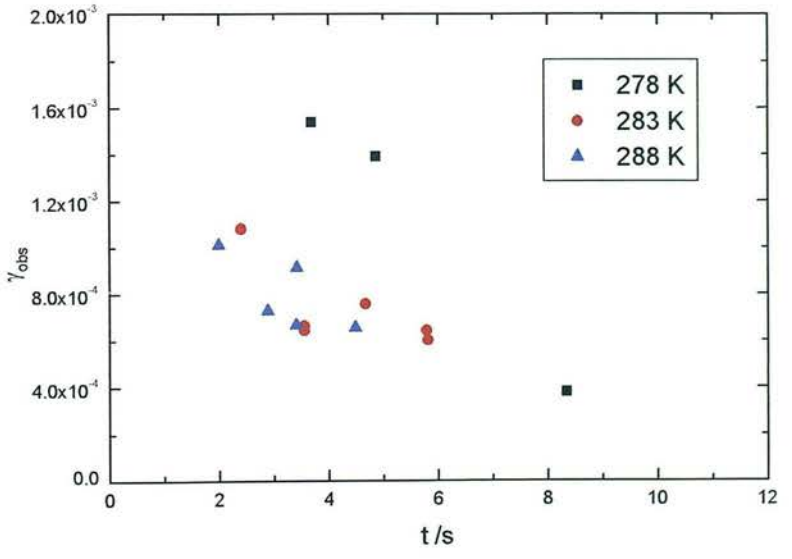

Figure 8.4 Observed uptake of m-cresol on water as function of liquid-gas contact time at three temperatures.

In Chapter 4 the total resistance contributing to the observed uptake was shown to equal the sum of the individual resistances, i.e.

$$\frac{1}{\gamma} = \frac{1}{\Gamma_G} + \frac{1}{\alpha} + \frac{\pi^{1/2}\,\omega}{4\,H\,R\,T}\sqrt{\frac{t}{D_L}} \qquad \textbf{(4.60)}$$

for the situation in which there is no reaction in the liquid phase. The standard procedure applied throughout this work to account for radial diffusion gradients was the method given by *Brown* [1978]. With this approach a plot of $1/\gamma$ (obtained after correction of γ_{obs}) *vs.* $\sqrt{t}$ yields a straight line with a gradient of $\frac{\sqrt{\pi}\,\omega}{4\,H\,R\,T\sqrt{D_L}}$ and an intercept of $1/\alpha$.

The uptake experiments of m-cresol had to be performed at higher pressures (~ 60 - 80 Torr) in order to detect changes in the absorption signal satisfactorily, because the absorption cross section of m-cresol is about 4 times smaller than that of phenol (at ~ 276 nm) [*Trost et al.*, 1997]. Consequently, corrections due to gas diffusion resistance are larger and were beyond the scope of the numerical correction procedure of *Brown* [1978]. However, a lower limit to α can be derived by plotting $1/\gamma_{obs}$ *vs.* $\sqrt{t}$ (see Figure 8.5), since the intercept is equal to the sum of $\frac{1}{\Gamma_G} + \frac{1}{\alpha}$, i.e. $\alpha > \frac{1}{\text{intercept}}$. The gradient corresponds to $\frac{\sqrt{\pi}\,\omega}{4\,H\,R\,T\sqrt{D_L}}$.

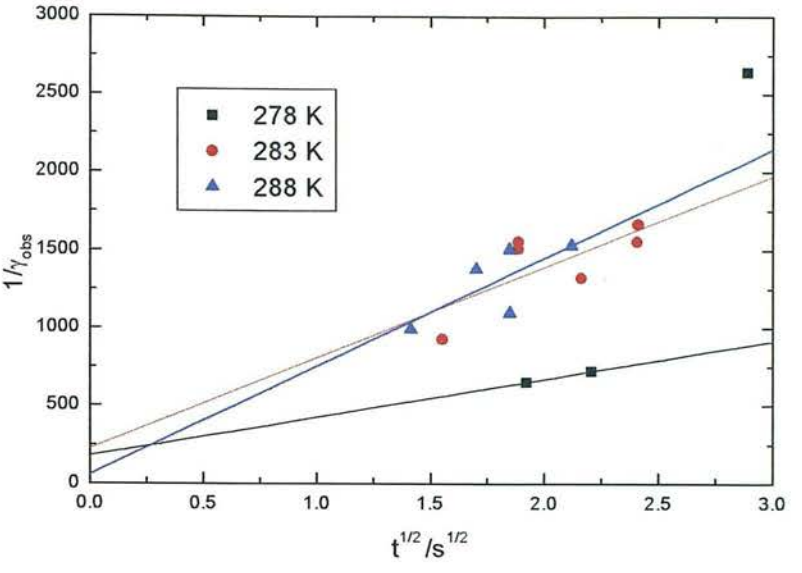

Figure 8.5 Plot of $\frac{1}{\gamma_{obs}}$ *vs.* $\sqrt{t}$ for m-cresol. The gradient is equal to $\frac{\sqrt{\pi}\,\omega}{4\,H\,R\,T\sqrt{D_L}}$. The intercept contains information about α (see text). The point at $t^{1/2} = 2.9\ s^{1/2}$ (278 K) was excluded from the fit.

Parameters derived from the gradients and the intercepts of Figure 8.5 are listed in Table 8.5 and Table 8.6, respectively.

T /K	gradient $[=\pi^{1/2}\omega/(4HRTD_L^{1/2})]$ $/s^{-1/2}$	ω /cm s^{-1}	$HD_L^{1/2}$ /M atm^{-1} $(cm^2\ s^{-1})^{1/2}$	D_L estimated /$cm^2\ s^{-1}$	H /M atm^{-1}
278	246	2.33×10^4	1.83	5.10×10^{-6}	812
283	584	2.35×10^4	0.77	6.03×10^{-6}	312
288	700	2.37×10^4	0.63	7.05×10^{-6}	239

Table 8.5 Values of $H\sqrt{D_L}$ and H for m-cresol derived from the gradient in Figure 8.5. The liquid diffusion coefficients were estimated after Wilke-Chang [*Reid et al.*, 1987].

T /K	intercept $(=1/\Gamma_G+1/\alpha)$	lower limit of α
278	176	5.7×10^{-3}
283	222	4.5×10^{-3}
288	46	2.1×10^{-2}

Table 8.6 Values of the lower limit of α of m-cresol derived from the intercept in Figure 8.5.

8.2.2.1 Gas diffusion coefficients

The pressure-independent binary diffusion coefficients (Torr cm^2 s^{-1}) of m-cresol in H_2O and helium, $D_G^P{}_{(C_6H_4(CH_3)OH\text{-}H_2O)}$ and $D_G^P{}_{(C_6H_4(CH_3)OH\text{-}He)}$, were calculated according to the Fuller-Schettler-Giddings [*Fuller et al.*, 1969] estimation method, as described in Chapter 4. Table 8.7 details the parameters used.

Parameter/ unit	Symbol	Value	Source/comments
molar mass of m-cresol /g mol^{-1}	$M_{C_6H_4(CH_3)OH}$	108.1	
molar mass of water /g mol^{-1}	M_{H_2O}	18.0	
molar mass of helium /g mol^{-1}	M_{He}	4.0	
atomic diffusion volume of m-cresol	$(\sum v)_{C_6H_4(CH_3)OH}$	117.6	calculated from values given in *Fuller et al.* [1969]
atomic diffusion volume of water	$(\sum v)_{H_2O}$	13.1	given in *Fuller et al.* [1969]
atomic diffusion volume of helium	$(\sum v)_{He}$	2.67	given in *Fuller et al.* [1969]

Table 8.7 Parameters used to calculate pressure-independent binary gas diffusion coefficients of m-cresol in H_2O and He following the method of *Fuller et al.* [1969].

The calculated gas diffusion coefficients at the different temperatures are listed in Table 8.8.

T /K	$D_G^P{}_{(C_6H_4(CH_3)OH\text{-}H_2O)}$ /Torr cm^2 s^{-1}	$D_G^P{}_{(C_6H_4(CH_3)OH\text{-}He)}$ /Torr cm^2 s^{-1}
278	69.4	184.9
283	71.6	190.8
288	73.8	196.7

Table 8.8 Pressure-independent gas diffusion coefficients for m-cresol in H_2O and in helium, respectively, at the experimental temperatures following the method of *Fuller et al.* [1969].

8.2.2.2 Liquid diffusion coefficients

The liquid diffusion coefficients for m-cresol in water at the experimental temperatures were calculated by the Wilke-Chang method, as described in Chapter 4, using a molar volume of m-cresol at boiling temperature $V_{C_6H_4(CH_3)OH} = 125.6\ cm^3\ mol^{-1}$. They are listed in Table 8.5.

8.2.3 Reactive uptake of m-cresol

When bromine water was used, uptake was time independent, because m-cresol reacts fast with bromine, so $\Gamma_{RXN} >> \Gamma_{SOL}$. The liquid uptake resistance $\left(\text{equal to } \frac{1}{\Gamma_{SOL} + \Gamma_{RXN}}\right)$ is therefore negligible. Since liquid uptake is then independent of liquid-gas contact time, the change in gas phase concentration over the whole reactor length can be used to derive the first-order wall loss coefficient. An example plot is shown in Figure 8.6. The observed uptakes were used to derive α according to

$$\frac{1}{\alpha} = \frac{\omega}{2\,r\,k_w} - \frac{\omega\,r}{7.32\,D_G} - \frac{1}{\gamma} \quad \textbf{(6.15)}$$

The result are listed in Table 8.9.

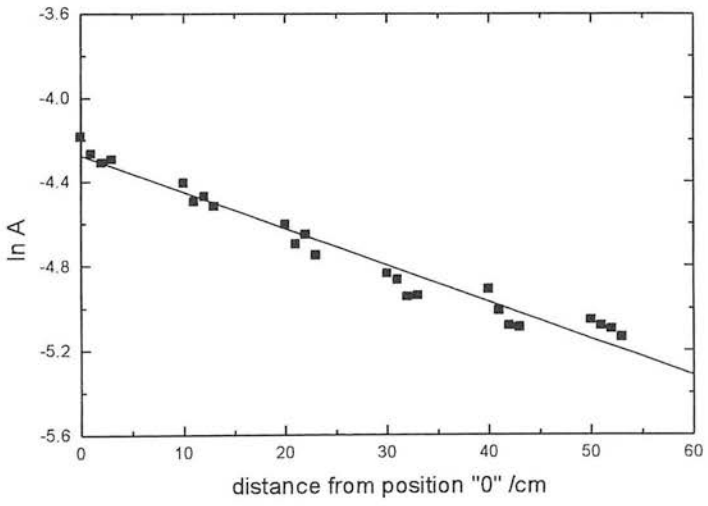

Figure 8.6 Typical plot of ln absorbance *vs.* distance from injector position "0" for uptake of m-cresol onto bromine water. Experiment at 278 K with a gas velocity of c = 330 cm s^{-1}.

T /K	ω /cm s^{-1}	D_G /cm^2 s^{-1}	k_w /s^{-1}	γ	α
278	2.33×10^4	2.755	5.74	6.63×10^{-4}	9.91×10^{-3}
283	2.35×10^4	2.727	10.63	4.43×10^{-3}	4.68×10^{-3}
288	2.37×10^4	2.536	5.82	7.26×10^{-4}	6.92×10^{-3}
293	2.39×10^4	2.313	4.63	5.17×10^{-4}	6.26×10^{-3}

Table 8.9 Experimental parameters and mass accommodation coefficients of m-cresol at different temperatures measured on bromine water.

8.3 Discussion

8.3.1 Solubility limited uptake

The uptake of m-cresol onto water was measured at three temperatures at various liquid-gas contact times (see Table 8.4). The uptake decreased with contact times verifying the time dependence caused by the approach to solubility equilibration. The uptake also decreases with temperature, although the data at 283 and 288 K do not show this very clearly (see Figure 8.4). The reasons for ambiguity in the temperature dependence lie in possible instabilities in the temperature control but more importantly in the general lack of data since the experiments on the m-cresol uptake could not be pursued thoroughly.

Due to high experimental pressures of up to 80 Torr required, it was not possible to obtain k_w^{corr} values. However, a plot of $1/\gamma_{obs}$ *vs.* $\sqrt{t}$ showed linearity at all temperatures (see Figure 8.5). The parameters $H\sqrt{D_L}$ and H were derived from the gradients in Figure 8.5 (see Table 8.5). These H values appear low compared with the previous literature values of H summarised in Table 8.1. Figure 8.7 shows a logarithmic plot of the dimensionless liquid-gas Henry's law coefficient as a function of the inverse temperature. The $\Delta H°$ and $\Delta S°$ values derived from the fitted line are listed in Table 8.10.

Although the difference between the data is quite substantial, the $\Delta H°$ and $\Delta S°$ values are within the stated error ranges. It should be noted that only *Altschuh et al.* [1999] have measured H, all other values are estimates.

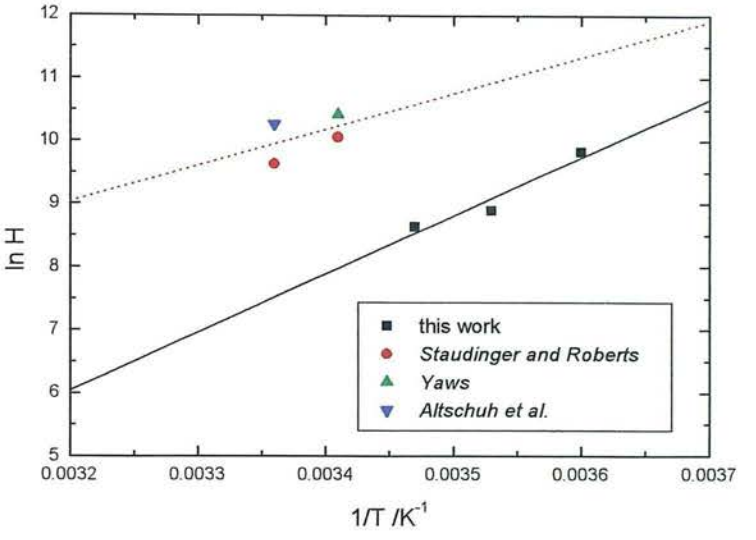

Figure 8.7 Plot of ln H (dimensionless liquid-gas coefficient) *vs.* 1/T for m-cresol. Straight lines were fitted to the data from this work (black solid) and to previous literature H (red dotted) [*Staudinger and Roberts*, 1996; *Yaws*, 1999; *Altschuh et al.*, 1999].

	$\Delta H°$ /kJ mol^{-1}	$\Delta S°$ /J mol^{-1} K^{-1}
this work	-77 ± 22	-196 ± 78
Staudinger and Roberts [1996], *Yaws* [1999], *Altschuh et al.* [1999]	-48 ± 60	-78 ± 204

Table 8.10 $\Delta H°$ and $\Delta S°$ derived from Figure 8.7. The errors given for $\Delta H°$ and $\Delta S°$ refer to errors in the fitted lines.

Another relation was used as a second approach for calculating $\Delta H°$ for gas-to-liquid transfer [*Schwarzenbach et al.*, 1993]. Over small temperature ranges (i.e. no change

in ΔH or volume of solution) the temperature dependence of the vapour pressure p^*_i and the solubility S can be expressed by

$$\ln p^*_i = -\frac{\Delta H_{vap}}{R}\frac{1}{T} + \text{constant} \qquad \text{and} \qquad \ln S = -\frac{\Delta H^E_S}{R}\frac{1}{T} + \text{constant}$$

(8.1)

where ΔH_{vap} is the enthalpy of vaporisation and ΔH^E_S is the excess[1] enthalpy of solution. In Chapter 2 a method for estimating Henry's law constant was given as

$$H = \frac{S}{p^*_i}.$$

(2.28)

The temperature dependence of the Henry's law constant can be expressed in a more general form as

$$\ln H = -\frac{\Delta H^\circ}{RT} + \text{constant}.$$

(8.2)

Combining eqn (8.2), (2.28) and (8.1) results in

$$\ln H = -\frac{\Delta H^\circ}{RT} + \text{constant} = \ln\left(\frac{S}{p^*_i}\right) = \left(\frac{-\Delta H^E_S + \Delta H_{vap}}{RT}\right) + \text{constant}.$$

(8.3)

For solid compounds at room temperature the excess enthalpy of solution is $\Delta H^E_S = \Delta H_S - \Delta H_{fus}$ where ΔH_S is the enthalpy of solution and ΔH_{fus} is the enthalpy of fusion [*Schwarzenbach et al.*, 1993]. However, since m-cresol is a liquid at room temperature it follows that

$$\Delta H^\circ = \Delta H_S - \Delta H_{vap} = (-8.8 - 61.7)\ \text{kJ mol}^{-1} = \underline{\underline{-70.5\ \text{kJ mol}^{-1}}}$$

(8.4)

using literature data for m-cresol [*International Critical Tables of numerical data, physics, chemistry, and technology*, 1929; *CRC Handbook of chemistry and physics*,

---

[1] An excess function is defined as the difference between the observed thermodynamic function of mixing and the function for an ideal solution [*Atkins*, 1986].

1993]. There is, in fact, very good agreement between $\Delta H°$ calculated in this way from the enthalpies and the $\Delta H°$ measured in this work.

The positive intercepts of Figure 8.5 were used to derive a lower limit of α (see Table 8.6) of about 5×10^{-3} at 283 K. Only three temperatures were investigated which was not enough to identify a clear trend of the temperature dependence since the intercept of Figure 8.5 is very sensitive to the fit.

8.3.2 Reactive uptake and mass accommodation of m-cresol

The reactive uptake of m-cresol was measured at four temperatures which allowed the derivation of values of α ranging from 1×10^{-2} at 278 K to 6×10^{-3} at 293 K with the exception of 5×10^{-3} at 283 K. Figure 8.8 shows α (and the lower limits of α obtained by uptake on water) as a function of temperature. Generally, α decreases with temperature. The drop in α at 283 K is most likely attributable to an unintentional variation in experimental conditions.

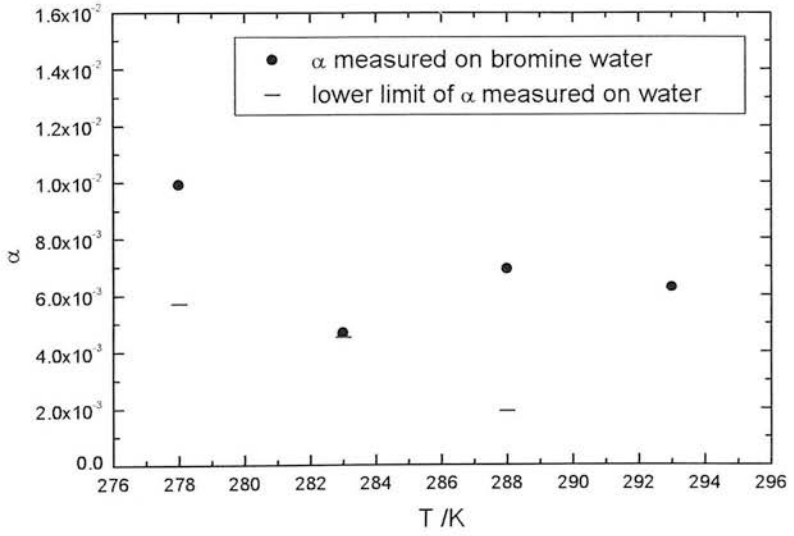

Figure 8.8 Mass accommodation of m-cresol measured on bromine water (reaction controlled uptake) and lower limits of α measured on water (solubility limited uptake) as a function of temperature.

The temperature dependence of α was used to derive ΔH_{obs} and ΔS_{obs} for the transition state between gas phase and aqueous phase solvation [*Davidovits et al.*, 1995]. Figure 8.9 shows a plot of ln (α/(1-α)) *vs.* 1/T for m-cresol. The ΔH_{obs} and ΔS_{obs} values derived from Figure 8.9 are -21.4 ± 2.4 kJ mol^{-1} and -115.3 ± 8.4 J mol^{-1} K^{-1}, respectively. This corresponds to a critical cluster value of N* of ~ 2 for m-cresol. This result, together with the data of phenol and 2-nitrophenol, is discussed in Chapter 9.

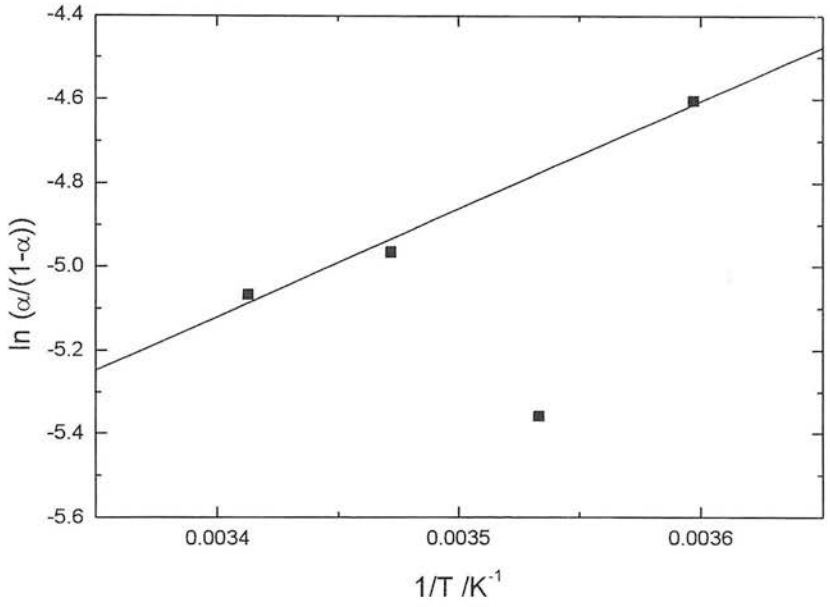

Figure 8.9 Plot of ln (α/(1-α)) *vs.* 1/T for m-cresol. Note that the data point at T^{-1} = (283 K)$^{-1}$ was excluded from the linear fit.

8.4 Conclusion

The uptake of m-cresol was investigated on water and bromine water as function of temperature. Although time limits did not allow a thorough study it was possible to derive mass accommodation as 10^{-2} at 278 K and 6×10^{-3} at 293 K. The number N* of ~ 2 fits well in the general trend of the aromatics investigated.

9. COMPARISON OF PHENOL, 2-NITROPHENOL AND m-CRESOL

Mass accommodation coefficients of phenol, 2-nitrophenol and m-cresol were measured as a function of temperature and used to derive values of ΔH_{obs} and ΔS_{obs}. In this chapter these results are compared and discussed in terms of the critical cluster model.

9.1 Comparison of mass accommodation coefficients

In Figure 9.1 the mass accommodation coefficients of phenol, 2-nitrophenol and m-cresol are plotted as a function of temperature. The α values for phenol are the highest and have the strongest dependence on temperature. The 2-nitrophenol and m-cresol α values are fairly similar, although temperature dependence for m-cresol is much smaller than for 2-nitrophenol. The α values of all substances show a negative temperature dependence.

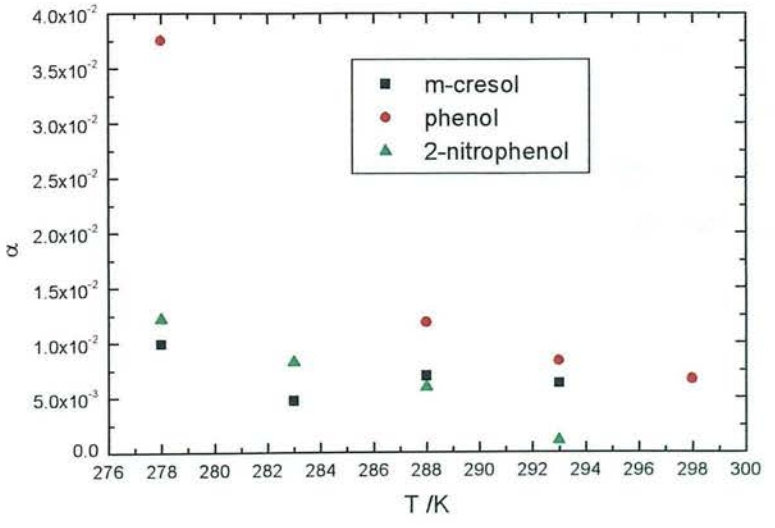

Figure 9.1 Plot of the mass accommodation of m-cresol, phenol and 2-nitrophenol as function of temperature, measured by reactive uptake.

9.2 Analysis in terms of the critical cluster model

The critical cluster nucleation model of gas uptake was formulated by *Davidovits et al.* [1991; 1995]. The uptake is controlled by aggregation of water molecules (solvent) around the incoming trace gas molecule within the interface. The interface itself is a dynamic region where these aggregates (clusters) continually form, fall apart and reform. The cluster is composed of N molecules which is the sum of the trace gas molecule and the surrounding water molecules. Clusters smaller than a critical size (N*) fall apart whereas clusters larger than N* serve as centres for further condensation and grow in size until they merge into the bulk liquid.

The equilibrium density of clusters at the surface is proportional to the molar free energy ($\Delta G_{obs} = \Delta H_{obs} - T\Delta S_{obs}$) for the formation of a cluster of N molecules. The relationship between the mass accommodation α and ΔG_{obs} is given as [*Davidovits et al.*, 1995; *Nathanson et al.*, 1996; *Shi et al.*, 1999b] (see also Chapter 2)

$$\ln\left(\frac{\alpha}{1-\alpha}\right) = -\frac{\Delta G_{obs}}{RT} = -\frac{\left(\Delta H_{obs} - T\Delta S_{obs}\right)}{RT} . \qquad (6.17)$$

Based on experimental data mainly for aliphatic alcohols, haloethanols and aliphatic acids *Davidovits et al.* [1995] and *Nathanson et al.* [1996] have provided expressions to calculate ΔH_{obs} and ΔS_{obs} for selected values of N*. Figure 9.2 plots these calculated values, where the numbers refer to N*, together with experimental data obtained for phenol, 2-nitrophenol and m-cresol from this work and for aniline and phenol from *Titcombe* [1997].

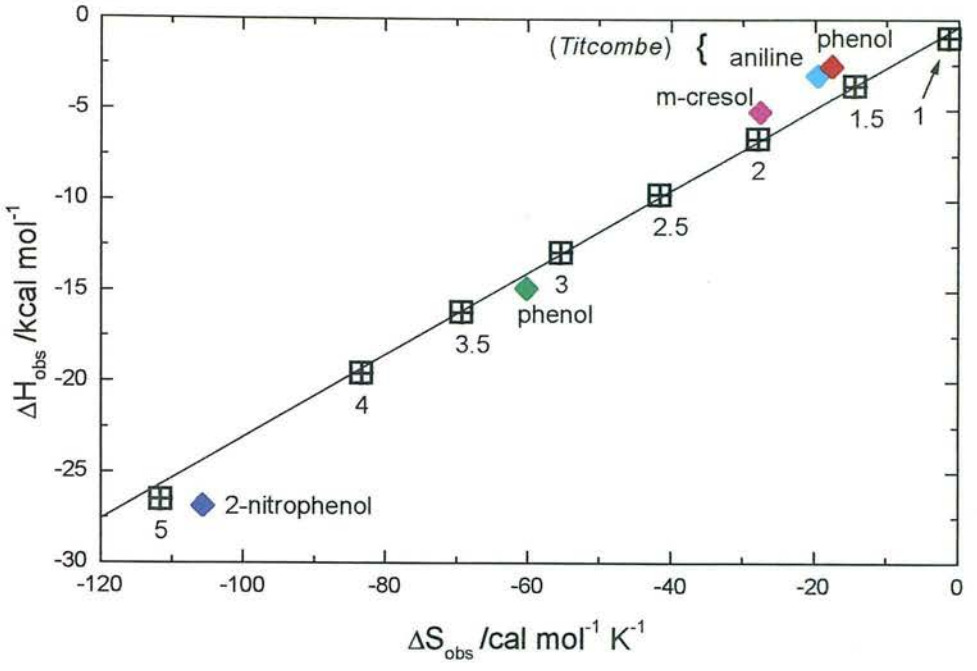

Figure 9.2 Plot of ΔH_{obs} *vs.* ΔS_{obs}. The black line connects calculated values of ΔH_{obs} and ΔS_{obs} according to the model by *Davidovits et al.* [1995; *Nathanson et al.*, 1996]. The numbers refer to the critical number N*. The coloured diamonds were derived in this work apart from aniline and phenol as labelled [*Titcombe*, 1997].

All of the investigated compounds show negative values of ΔH_{obs} and ΔS_{obs}, in accordance with the model by *Davidovits et al.* [1995]. The pairs of ΔH_{obs} and ΔS_{obs} values for all aromatics show a consistent relationship between them and all lie on the same line derived by *Davidovits et al.* [1995].

The critical number N* is a measure of how readily a molecule is incorporated into the bulk liquid. *Davidovits et al.* [1995] postulated that the number N* required to form a critical cluster depends on the structure of the specific molecule undergoing the uptake process. They further proposed that the ease with which the cluster is formed is determined primarily by the number of hydrophilic functional groups. Once the critical cluster is formed around the hydrophilic part, the cluster continues to grow independent of the size of the hydrophobic portion of the molecule.

This is not the case for the aromatics investigated. The molar volumes of m-cresol and 2-nitrophenol are very similar, yet ΔH_{obs} differs by a factor of about 5. The previous cavity model of gas uptake predicted a direct relation between the hydrogen-bonding ability of species of comparable size and ΔH_{obs} whereas *Davidovits et al.* [1995] have found the inverse correlation for aliphatic alcohols and acids.

The excess enthalpy of dissolution, ΔH_S^E, is a measure of the interaction between solute and solvent. A negative ΔH_S^E (exothermic) value indicates attraction between solute and solvent, associated with a high degree of solubility, whereas endothermic ΔH_S^E often reflect low solubilities. In Figure 9.3 values of ΔH_{obs} are plotted against known and estimated values of ΔH_S^E [*Schwarzenbach et al.*, 1993; *Maskill*, 1990].

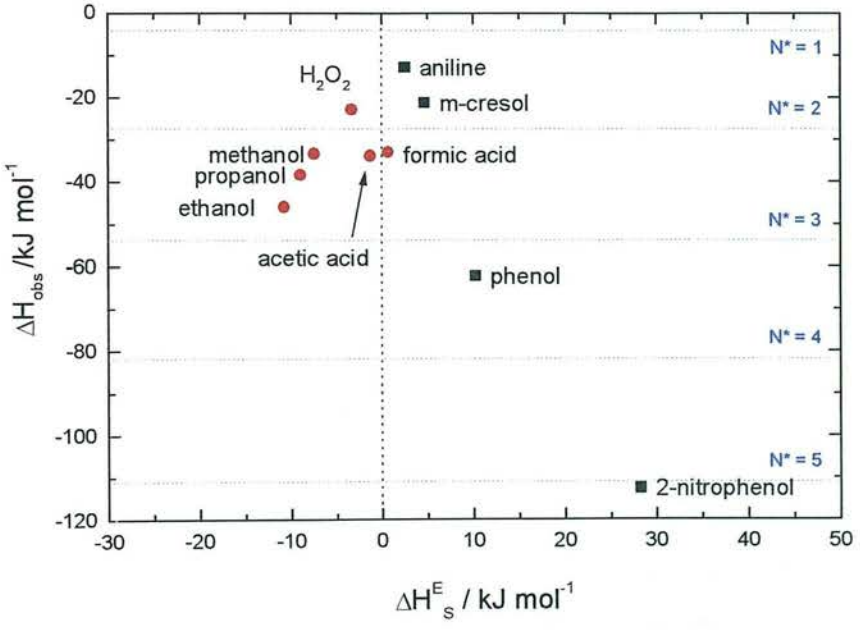

Figure 9.3 Plot of ΔH_{obs} *vs.* excess enthalpy of solution ΔH_S^E. Values of ΔH_{obs} for aromatic compounds were measured in this work except aniline [*Titcombe*, 1997]. Values of aromatic ΔH_S^E were estimated from a plot of ln solubility *vs.* 1/T [*Schwarzenbach et al.*, 1993; *Heron et al.*, 1998]; solubility values from *Landolt-Börnstein Physikalisch-Chemische Tabellen* [1931]. Values of ΔH_{obs} for aliphatic compounds were taken from *Davidovits et al.* [1995] and of ΔH_S^E from *Schwarzenbach et al.* [1993] and *Maskill* [1990]. All values at room temperature. N* lines based on ΔH_{obs}.

Only very limited data regarding ΔH_{obs} for the aliphatic alcohols are available which makes it difficult to conclude general trends. All values of ΔH_{obs} are negative, but there is a distinctive difference in the values of ΔH_S^E. The 3 short chain aliphatic alcohols for which α values are known have negative values of ΔH_S^E. However, there is a general trend that ΔH_S^E increases with increasing chain length of aliphatic alcohol, e.g. $\Delta H_S^E = +0.5$ kJ mol^{-1} for octanol and $\Delta H_S^E = +10.7$ kJ mol^{-1} for dodecanol [*Schwarzenbach et al.*, 1993], but no α values are available for these compounds, and therefore no ΔH_{obs}.

The aromatic compounds on the other hand show without exception positive ΔH_S^E. There appears to be a direct relation between ΔH_{obs} and ΔH_S^E. For example, 2-nitrophenol as the bulkiest molecule has the highest ΔH_S^E, i.e. relatively more energy is needed to dissolve it. It therefore seems reasonable that 2-nitrophenol should have the highest N*, i.e. more water molecules are necessary to form a cluster to accommodate 2-nitrophenol. In general, as ΔH_S^E of the aromatic species decreases, the number size of the critical cluster, N*, decreases, i.e. with stronger attractive forces between solute and solvent (i.e. more negative ΔH_S^E) less water molecules are necessary to form a critical cluster which seems entirely reasonable.

Therefore, for aromatics of comparable size both the hydrophilic and the hydrophobic part of the molecule appear to determine the ease with which the critical cluster in the mass accommodation is formed, unlike the aliphatic alcohols where that is not necessarily true. More data on the uptake of aromatic compounds are needed to draw more unambiguous conclusions about the applicability of the Davidovits model for aromatics compounds.

10. BUBBLE COLUMN EXPERIMENT

Reliable Henry's law coefficients are of interest for environmental fate and risk assessment of organic pollutants. Experimental data are often scarce so that only estimates of Henry's law coefficients are available. Frequently these estimates are very diverse. Since this work focused on uptake measurements of 2-nitrophenol (where the Henry's law coefficient is needed in the analysis) its Henry's law coefficient was directly measured using a bubble purge method. The results of these measurements are presented and discussed in this chapter.

10.1 Analysis methods

In trial experiments, the concentration changes with time of 2-nitrophenol in both gas and liquid phase were measured in order to find the more suitable analysis method. The humidified gas entered the diluted 2-nitrophenol solution through a sintered disk. Bubbles formed and ascended to the liquid surface. The concentration of purged 2-nitrophenol in the exit gas flow was determined by in-line UV absorption. At the same time samples of the solution were taken and the UV absorbance measured.

The absorbance of solutions of 2-nitrophenol in water of different concentrations was measured to verify a linear relation between absorbance and 2-nitrophenol concentration (see Figure 10.1). A molar absorption coefficient of $\varepsilon = 6230$ l mol^{-1} cm^{-1} at 278 nm was derived from the gradient in Figure 10.1. A value of $\varepsilon_{(278nm)} = 6400$ l mol^{-1} cm^{-1} was found in the literature [*Perkampus*, 1992]. However, *Schwarzenbach et al.* [1988] have given $\varepsilon_{(278nm)} = 6250$ l mol^{-1} cm^{-1} which is in excellent agreement with the measurements from this work.

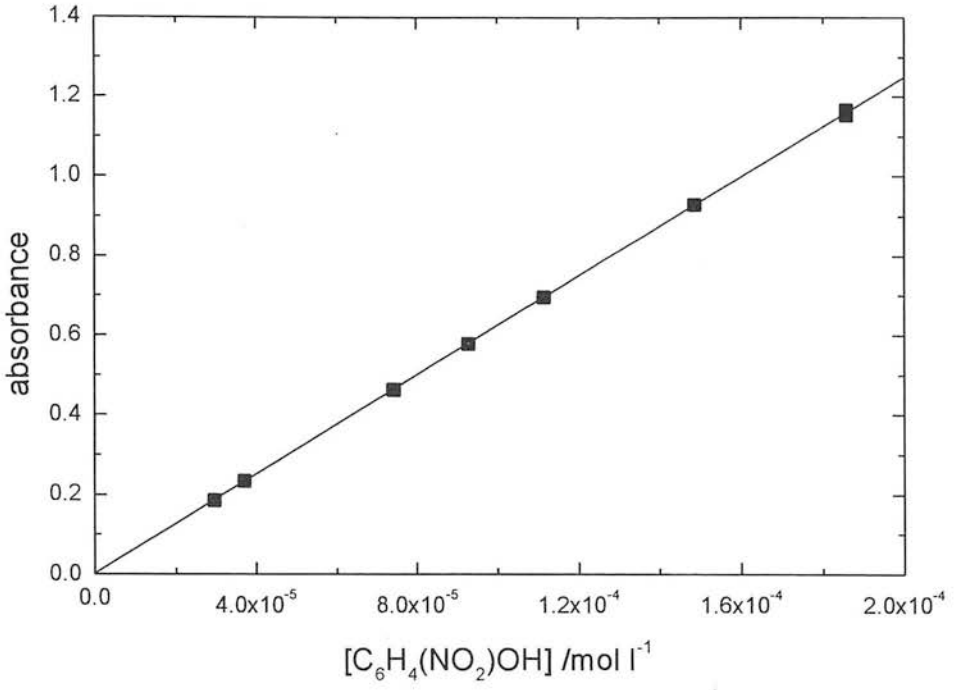

Figure 10.1 Plot of absorbance measured at 278 nm as a function of aqueous concentration of 2-nitrophenol.

The gas and liquid absorbance values decreased exponentially with purge time, as expected. However, gas absorption values were very low. An example calculation confirmed this. Equation (4.70) stated that

$$-\frac{dn^{aq}}{dt} = +\frac{dn^{gas}}{dt} \qquad \textbf{(4.70)}$$

therefore the change in gas phase concentration follows as

$$d[i]^{gas} = \frac{dn^{gas}}{V^{gas}} = \frac{dn^{gas}}{Fdt} = -\frac{dn^{aq}}{Fdt}. \qquad \textbf{(10.1)}$$

Using typical experimental conditions eqn (10.1) gives

$$d[i]^{gas} = -\frac{4 \times 10^{-7}\ \text{mol}}{300\ \text{cm}^3\ \text{min}^{-1} \times 30\,\text{min}} \approx 4 \times 10^{-11}\ \text{mol cm}^{-3} \approx 3 \times 10^{13}\ \text{molecules cm}^{-3}. \qquad \textbf{(10.2)}$$

This is about an order of magnitude smaller than the estimated concentration of gaseous 2-nitrophenol in the wetted-wall experiments. Since the analysis of the liquid phase was straightforward it was decided to continue the bubble experiments solely with concentration measurements in the aqueous solution.

10.2 Henry's law coefficient of 2-nitrophenol

10.2.1 Measured Henry's law coefficients

The Henry's law coefficient of 2-nitrophenol was measured at 6 temperatures between 278 and 303 K. As described in Chapter 4, plots of the change in absorbance in the liquid, ln (A_t/A_0), *vs.* time gave a gradient of $-F/(HRTV^{aq})$. The quantity $F/(HRTV^{aq})$ was then plotted against F/V^{aq} for different liquid volumes, but constant flow rate F. Values of H were derived from the gradient (= 1/(HRT)) of the second plot. This method of deriving Henry's law constant is based on the assumption that equilibrium (or very-nearly equilibrium) is reached between the bubble and the liquid. Table 10.1 shows the results for all temperatures and the associated plots of $F/(HRTV^{aq})$ *vs.* F/V^{aq} are shown in Figure 10.2.

T /K	liquid volume V^{aq} /cm^3	liquid height z /cm	F/V^{aq} /min^{-1}	$F/(HRTV^{aq})$ (= "-gradient [1]") /min^{-1}
278	23	4.0	13.2	1.59×10^{-3}
	46	8.9	6.7	7.41×10^{-4}
	69	14.0	4.5	5.36×10^{-4}
	91	18.8	3.4	4.28×10^{-4}
	116	24.1	2.6	3.04×10^{-4}
	138	28.9	2.2	2.64×10^{-4}
	160	33.9	1.9	2.10×10^{-4}
	184	39.0	1.7	1.69×10^{-4}
283	23	3.9	13.5	2.54×10^{-3}
	44	8.5	7.2	1.29×10^{-3}
	69	13.9	4.5	8.67×10^{-4}
	89	18.2	3.5	7.96×10^{-4}
	116	24.2	2.7	5.68×10^{-4}
	134	28.0	2.4	3.53×10^{-4}
	161	33.9	1.9	3.42×10^{-4}
	183	38.9	1.7	3.23×10^{-4}
288	24	4.1	13.3	3.26×10^{-3}
	46	8.9	6.9	1.77×10^{-3}
	70	14.2	4.5	1.17×10^{-3}
	91	18.8	3.5	8.50×10^{-4}
	115	24.0	2.7	7.07×10^{-4}
	138	29.0	2.3	6.56×10^{-4}
	161	34.0	2.0	5.58×10^{-4}
	183	38.9	1.7	4.34×10^{-4}
293	20	3.3	16.0	3.84×10^{-3}
	42	8.0	7.7	2.27×10^{-3}
	68	13.7	4.9	1.63×10^{-3}
	83	16.9	3.9	1.24×10^{-3}
	96	19.9	3.4	1.06×10^{-3}
	105	21.8	3.2	7.62×10^{-4}
	120	25.0	2.7	9.91×10^{-4}
	134	28.0	2.5	7.53×10^{-4}
	169	35.8	2.0	7.20×10^{-4}
298	24	4.0	14.2	7.03×10^{-3}
	46	8.8	7.4	4.02×10^{-3}
	68	13.8	4.9	2.58×10^{-3}
	91	18.7	3.7	1.95×10^{-3}
	115	24.0	2.9	1.60×10^{-3}
	137	28.7	2.4	1.31×10^{-3}
	161	33.9	2.1	1.15×10^{-3}
	183	38.9	1.8	1.16×10^{-3}
303	24	4.0	14.5	9.50×10^{-3}
	46	8.9	7.4	5.11×10^{-3}
	69	13.9	5.0	3.35×10^{-3}
	92	18.9	3.7	2.71×10^{-3}
	114	23.8	3.0	2.11×10^{-3}
	137	28.9	2.5	1.84×10^{-3}
	160	33.8	2.1	1.47×10^{-3}
	183	38.9	1.9	1.41×10^{-3}

Table 10.1 Results of Henry's law measurements of 2-nitrophenol.

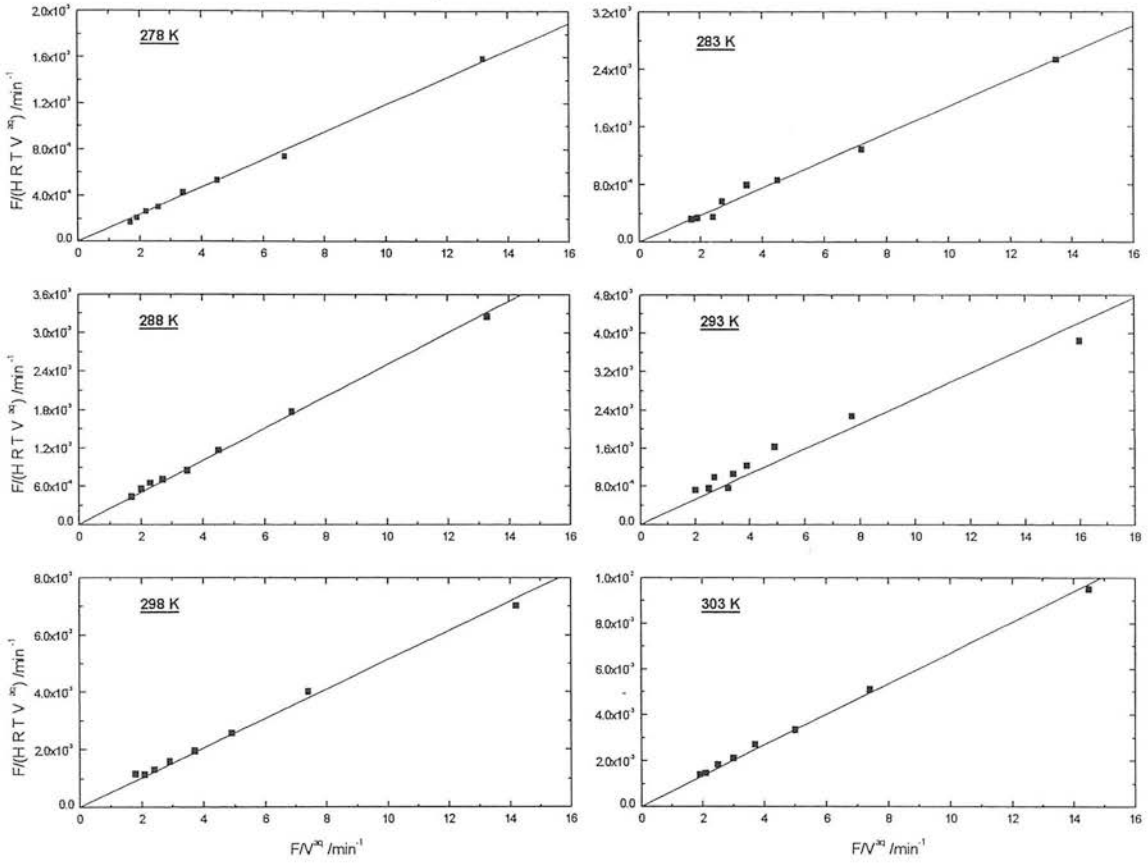

Figure 10.2 Plots of $F/(HRTV^{aq})$ *vs.* F/V^{aq} for 6 temperatures. The gradient equals 1/(HRT) ("gradient [2]").

The Henry's law coefficients derived from the gradients in Figure 10.2 are listed in Table 10.2.

T /K	gradient [2] = 1/(HRT)	H /M atm^{-1}
278	1.18×10^{-4}	370 ± 5
283	1.88×10^{-4}	230 ± 5
288	2.50×10^{-4}	170 ± 2
293	2.64×10^{-4}	160 ± 8
298	5.12×10^{-4}	80 ± 2
303	6.70×10^{-4}	60 ± 1

Table 10.2 Values for H of 2-nitrophenol derived from the gradients in Figure 10.2. Quoted errors represent only those of the statistical fits.

10.2.2 Derivation of equilibrium Henry's law coefficients

In Section 4.3.1 it was noted that the validity of the above method for deriving Henry's law coefficients depends on the extent to which equilibrium is reached between gas and liquid as the gas bubble exits the liquid. The linear plots in Figure 10.2 already indicate that the measured Henry's law coefficients are the equilibrium values, or very close to the equilibrium values. However, it is possible to derive more accurate values for the equilibrium Henry's law coefficient, H^{equi}, from the measured H (in the quantity $F/(HRTV^{aq})$) by using eqn (4.91) (see also Chapter 4)

$$(-\text{gradient } [1]) = \frac{B}{H^{equi}} \times \frac{\left(1 - \exp\left(-A H^{equi} z\right)\right)}{z} \qquad (4.91)$$

where (-gradient [1]) = $F/(HRTV^{aq})$, $B = F/(RTS_r)$ and $A = K_{OL}k_zRT/F$. Figure 10.3 shows plots of $F/(HRTV^{aq})$ from Table 10.1 as a function of liquid height for the 6 experimental temperatures. The quantities A and H^{equi} were treated as adjustable parameters in the fitting program whereas the value of B contains entirely known parameters.

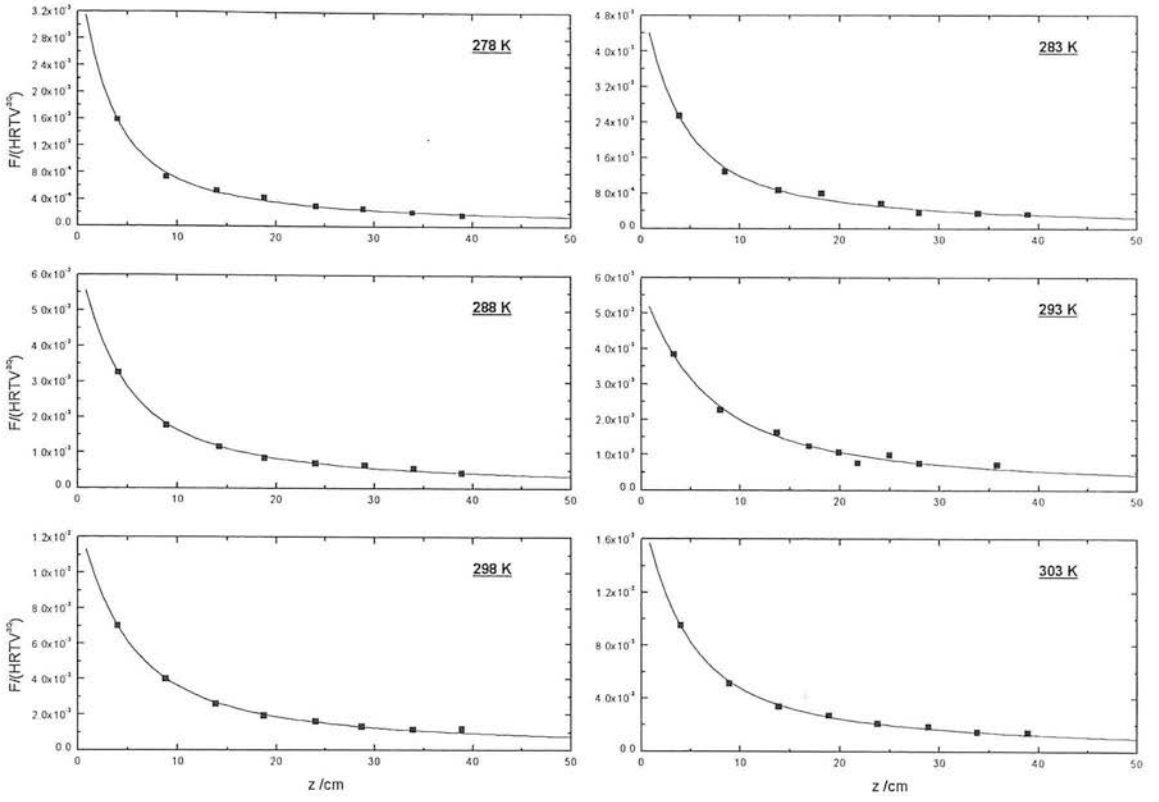

Figure 10.3 Plots of $F/(HRTV^{aq})$ *vs.* liquid height z for 6 temperatures. The lines are fits of eqn (4.91) to the data with A and H^{equi} as adjustable parameters. The parameter B is known and was fixed in the fitting. NB. H in the quantity $F/(HRTV^{aq})$ is the measured H (see Figure 10.2 and Table 10.2).

The results of the fittings in Figure 10.3 are listed in Table 10.3.

T /K	B (= F/(R T S_r)) /mol cm l^{-1} atm^{-1} min^{-1} (fixed)	H^{equi} /M atm^{-1}	A (= K_{OL} k_z R T/F) /l atm mol^{-1} cm^{-1}
278	2.99	420 ± 13	(1.3 ± 0.16) x 10^{-3}
283	2.98	250 ± 12	(1.8 ± 0.21) x 10^{-3}
288	2.96	180 ± 4	(2.2 ± 0.12) x 10^{-3}
293	3.02	140 ± 6	(1.9 ± 0.12) x 10^{-3}
298	3.03	80 ± 2	(4.3 ± 0.18) x 10^{-3}
303	3.04	60 ± 1	(6.1 ± 0.29) x 10^{-3}

Table 10.3 Results of the fittings from Figure 10.3. Errors in H^{equi} and A are the errors in the fitting.

10.3 Discussion

The Henry's law coefficient of 2-nitrophenol was measured at 6 temperatures. The change of absorbance in the liquid was used to derive $F/(HRTV^{aq})$. The values obtained were then plotted as function of F/V^{aq} to obtain Henry's law coefficients (see Figure 10.2 and Table 10.2). The straight lines in Figure 10.2 fit the data very well for all temperatures.

The observed Henry's law coefficients depend on the attainment of equilibrium between gas and liquid in the bubble column. A second plot of $F/(HRTV^{aq})$ *vs.* liquid height z was used to derive the equilibrium Henry's law coefficient, H^{equi} (see Figure 10.3). Again, the function described by eqn (4.91) fitted the data very well for all temperatures. The results are listed in Table 10.3.

Comparison between both derivation methods reveals very good agreement, as Table 10.4 shows. This indicates that equilibrium is attained in the bubble column at the liquid heights used.

T /K	$H^{non\text{-}equi}$ /M atm^{-1}	H^{equi} /M atm^{-1}
278	370	420
283	230	250
288	170	180
293	160	140
298	80	80
303	60	60

Table 10.4 Comparison between results obtained from Figure 10.2 and Figure 10.3.

The degree of equilibrium at a certain liquid height can be calculated (see Section 4.3.1.2). For example, eqn (4.94) gives an expression for 99 % attainment of equilibrium

$$z_{(99\%)} = -\frac{F \ln(0.01)}{k_z R T K_{OL} H^{equi}} \quad \textbf{(4.94)}$$

Table 10.5 lists the liquid heights of 99 % equilibrium at different temperatures using parameters of Table 10.3 and eqn (4.94).

T /K	$z_{(99\%)}$ /cm
278	8.3
283	10.4
288	11.7
293	16.9
298	13.1
303	12.2

Table 10.5 Liquid heights for 99 % equilibrium between gas and liquid in the bubble column at different temperatures. $z_{(99\%)}$ was calculated with values from Table 10.3.

Generally only 2 liquid heights used in the experimental measurements were shorter than these calculated values of $z_{(99\%)}$, namely ~ 4 and 9 cm (see Table 10.1). Therefore, for the vast majority of experiments the assumption that the bubbles exiting the liquid were in equilibrium with the liquid was correct. The trend in $z_{(99\%)}$ as function of temperature reflects two opposing influences (see eqn (4.94)): $z_{(99\%)}$ increases as the temperature decreases, but H^{equi} increases as the temperature decreases. H^{equi} increases at a faster rate with decreasing T which causes $z_{(99\%)}$ first to increase and then to decrease with increasing T.

10.3.1 Comparison with literature values

Figure 10.4 compares the measured Henry's law coefficient for 2-nitrophenol from the bubble column with results from the wetted-wall experiment and a selection of literature values from Table 7.1.

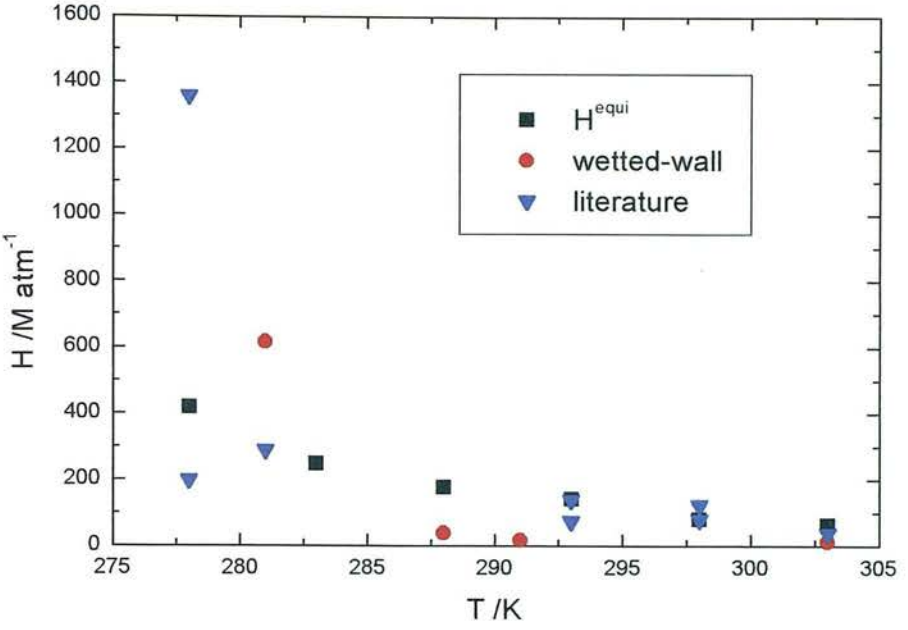

Figure 10.4 Henry's law coefficients of 2-nitrophenol measured with the bubble column (H^{equi}) and the wetted-wall experiment. The literature values were taken from Table 7.1 [*Lüttke and Levsen*, 1997; *Schwarzenbach et al.*, 1988; *Rippen et al.*, 1987; *Benes and Dohnal*, 1999; *Tremp et al.*, 1993].

The agreement between the bubble column and literature data is very good and the data complement each other. The only exception is at T = 278 K. There is a large difference between the experimental literature value (H = 1359 M atm^{-1}) [*Lüttke and Levsen*, 1997] and the calculated literature value (H = 197 M atm^{-1}) [*Lüttke and Levsen*, 1997]. The authors could not provide a satisfactory explanation for their observed enrichment of 2-nitrophenol in the liquid phase. On the other hand, the experimental values of this work continue the trend shown between 281 and 303 K.

The wetted-wall results are generally lower except at T = 281 K, as already pointed out (see Chapter 7). The wetted-wall experiment only allows the derivation of the quantity $H\sqrt{D_L}$. The liquid diffusion coefficients are directly required to determine the Henry's law coefficient, however, the value of D_L is always estimated. Therefore, the Henry's law coefficients observed from the wetted-wall reactor are possibly associated with a systematic error.

10.3.2 Temperature dependence of H

The enthalpy and entropy for the gas-liquid solubility were obtained from a plot of ln H (where H is the dimensionless Henry's constant) *vs.* 1/T. Figure 10.5 shows such a plot. The gradient corresponds to $-\frac{\Delta H^\circ}{R}$ and the intercept to $\frac{\Delta S^\circ}{R}$.

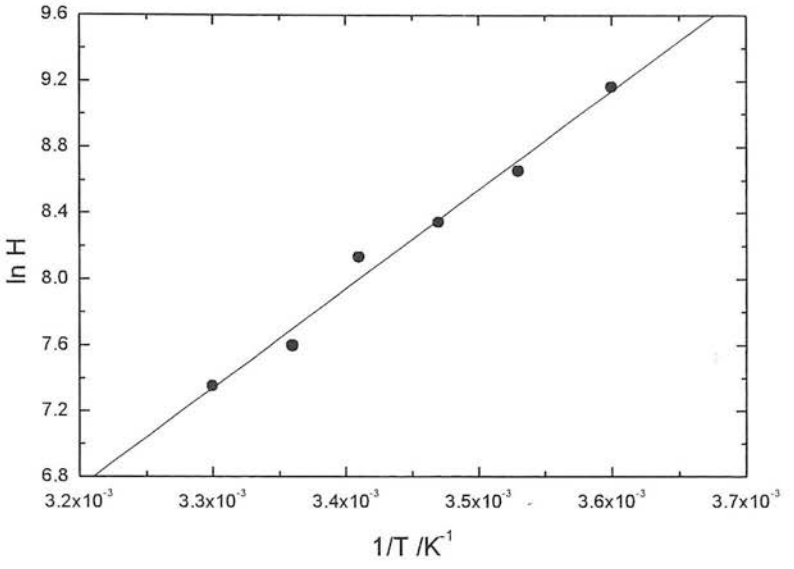

Figure 10.5 Plot of ln H (dimensionless liquid-gas Henry's law coefficient) *vs.* 1/T for 2-nitrophenol.

The fitted straight line allows derivation of ΔH° and ΔS° as (-50.0 ± 3.1) kJ mol^{-1} and (-104.0 ± 10.6) J mol^{-1} K^{-1}, respectively. These values agree very well with the estimate from the wetted-wall experiment of ΔH° = -42.7 kJ mol^{-1} and ΔS° = -93.9 J mol^{-1} K^{-1}, obtained by ignoring the value of H = 615 M atm^{-1} at 281 K (see Table 7.10, Section 7.3.1). This very good agreement gives confidence in the previously derived values from the wetted-wall uptake experiments.

On the basis of the obtained data the following expression is recommended to determine Henry's law coefficient of 2-nitrophenol between 278 and 303 K

$$\ln H\,(M\ atm^{-1}) = \frac{6300}{T} - 16.7\ .$$

(10.3)

10.4 Conclusion

The bubble column experiment is a reliable and straightforward technique for the measurement of Henry's law coefficients. Values of H were measured for 2-nitrophenol in the temperature range of 278 to 303 K. The results agree well with literature data and were used to derive $\Delta H°$ and $\Delta S°$. Equilibration between gas and liquid as function of liquid height was checked and a high degree of equilibrium verified.

11. IMPLICATIONS FOR THE ATMOSPHERE

The impact of a chemical in the atmosphere can be assessed by modelling its reaction paths. The fate depends on the atmospheric conditions and the physico-chemical properties of the species. This chapter gives an overview over the atmospheric significance of the measured mass accommodation coefficients with respect to competing removal processes.

11.1 Introduction

Chemical compounds emitted into the troposphere can be removed by either physical processes or by chemical transformation. Whereas dry deposition does not involve precipitation, wet deposition refers to uptake of material by cloud or rain droplets followed by precipitation. Chemical removal in the atmosphere occurs mainly by photolysis or reaction with OH and/or NO_3 radicals or with ozone.

Atmospheric lifetimes, τ^L, are used as a measure of the average length of time a species survives under given particular conditions. For a second order reaction A + B $\rightarrow$ products, in which the concentration of B is assumed constant, τ^L is given by

$$\tau^L = \frac{1}{k\,[B]} \qquad \textbf{(11.1)}$$

In the case of the gas phase reaction of trace gas with the OH or NO_3 radical, [B] is the radical concentration. If several processes are simultaneously responsible for the removal of a species, then the overall lifetime is given by

$$(\tau^L)^{-1} = \left(\tau_1{}^L\right)^{-1} + \left(\tau_2{}^L\right)^{-1} + \ldots. \qquad \textbf{(11.2)}$$

Heterogeneous loss in the atmosphere is only significant if the lifetime due to heterogeneous loss is of comparable magnitude to the lifetime due to homogeneous gas phase processing. This will be assessed for the investigated phenols.

11.2 Atmospheric lifetimes of the investigated phenols

In the following sections gas and heterogeneous loss processes are estimated and compared for the investigated phenols.

11.2.1 Gas phase reactions

The main removal processes in the gas phase are *via* reaction with the OH radical at daytime and NO_3 radical during night time. Further loss could be reaction with ozone or photolysis. Table 11.1 lists the kinetic data for these removal processes for phenol, 2-nitrophenol and m-cresol. No value of the rate coefficient for the reaction of 2-nitrophenol with ozone was found but this can be expected to be similar to that of phenol and m-cresol.

	rate coefficients /cm^3 molecule^{-1} s^{-1}		
	OH radical	**NO_3 radical**	**O_3**
phenol	2.6×10^{-11} [*Atkinson et al.*, 1992]	3.9×10^{-12} [*Atkinson et al.*, 1992]	$\leq 5 \times 10^{-19}$ (estimated) [*Finlayson-Pitts and Pitts, Jr.*, 1986]
2-nitrophenol	9.0×10^{-13} [*Atkinson et al.*, 1992]	$< 0.02 \times 10^{-12}$ [*Atkinson et al.*, 1992]	
m-cresol	6.4×10^{-11} [*Atkinson et al.*, 1992]	9.7×10^{-12} [*Atkinson et al.*, 1992]	1.9×10^{-19} [*Grosjean*, 1991]

Table 11.1 Rate coefficients for the gas phase reactions of phenol, 2-nitrophenol and m-cresol with the OH radical, NO_3 radical and ozone at 296 ± 2 K.

Concentrations of the oxidising species representative of remote and heavily polluted atmospheres were used to estimate the lifetime of the phenols due to gas phase reaction (Table 11.2). The lifetime of phenol due to photolysis is estimated as 66 to 250 hours (2.8 to 10.4 days) [*Howard et al.*, 1991]. Therefore photolysis is not significant compared with the reaction with OH. The same was assumed for m-cresol and 2-nitrophenol where no photolysis data were available.

	individual τ_{gas}					
	OH radical		NO_3 radical		O_3	
concentration /molecules cm^{-3}	remote 5×10^5	heavily polluted 1×10^7	remote 5×10^7	heavily polluted 5×10^9	remote 5×10^{11}	heavily polluted 5×10^{12}
phenol	21 h	1 h	1.4 h	51 s	> 46 days	> 4.6 days
2-nitrophenol	26 days	1.3 days	> 12 days	> 2.8 h		
m-cresol	8.7 h	26 min	34 min	21 s	4 months	12 days

Table 11.2 Estimated individual lifetimes of phenol, 2-nitrophenol and m-cresol due to gas phase reaction with OH, NO_3 and O_3. Typical concentrations of OH, NO_3 and O_3 for remote and heavily polluted atmosphere were taken from *Finlayson-Pitts and Pitts* [1986]. Rate constants from Table 11.1.

Table 11.2 shows that the reactions with OH and NO_3 radicals dominate the gas phase removal, i.e. reaction with ozone can be neglected for overall gas lifetime. Phenols react with NO_3 very fast so that lifetimes range from only minutes to hours, whereas OH oxidation takes places within hours. The exception is 2-nitrophenol which generally reacts more slowly (hours to days). However, it is important to remember that these reactions are not competing since the OH radical is produced only in daylight whereas NO_3 is a nighttime oxidant.

11.2.2 Heterogeneous loss

11.2.2.1 Interfacial mass transfer

The major influence on the rate of heterogeneous mass transfer is the droplet size and the liquid water content of a cloud. For a tropospheric cloud the condensed phase mixing ratio L_c, i.e. volume water to volume air ratio, varies from 5×10^{-8} to 3×10^{-6} with a typical value of 3×10^{-7}. The droplet sizes can range from a few μm to 50 μm diameter but is usually 10 - 20 μm [*Kolb et al.*, 1995; *Seinfeld and Pandis*, 1998]. The condensed surface to air volume ratio A_c can then be calculated as

$$A_c = \frac{6\,L_c}{d} = \frac{6\,(3 \times 10^{-7}\ cm^3\ cm^{-3})}{2 \times 10^{-3}\ cm} \approx 10^{-3}\ cm^2\ cm^{-3} \quad . \qquad (11.3)$$

The minimum lifetime due to heterogeneous loss is the inverse of the collision frequency with the total condensed surface area [*Kolb et al.*, 1995], i.e.

$$\tau^{L}_{\text{interface(min)}} = \frac{4}{\omega\, A_c\, \Gamma_G} \qquad (11.4)$$

where Γ_G is the transfer coefficient in the gas phase to the droplet surface. Equation (11.4) assumes the probability that a molecules striking the surface is accommodated as unity, i.e. $\alpha = 1$. Since the mass accommodation coefficients were measured in this work, α can be incorporated into eqn (11.4) to give the lifetime characterising the interfacial loss

$$\tau^{L}_{\text{interface}} = \frac{4}{\omega\, A_c}\left(\frac{1}{\Gamma_G} + \frac{1}{\alpha}\right). \qquad (11.5)$$

Substituting Γ_G for a droplet (see Chapter 2) gives

$$\tau^{L}_{\text{interface}} = \frac{4}{\omega\, A_c}\left(\frac{\omega\, d}{8\, D_G} - \frac{1}{2} + \frac{1}{\alpha}\right). \qquad (11.6)$$

Using $d = 20$ μm, $A_c = 10^{-3}$ cm^2 cm^{-3} and the measured mass accommodation coefficients the lifetimes given in Table 11.3 were obtained. The gas diffusion coefficient D_G was estimated for 1 atm and 293 K after Fuller-Schettler-Giddings [*Fuller et al.*, 1969]. For comparison, $\tau^{L}_{\text{interface(min)}}$ is also listed in Table 11.3.

	ω /cm s^{-1}	D_G /cm^2 s^{-1}	$\tau^{L}_{\text{interface(min)}}$ (i.e. $\alpha = 1$)	α (from this work)	$\tau^{L}_{\text{interface}}$
phenol	2.6×10^4	0.082	12 s	8.3×10^{-3}	31 s
2-nitrophenol	2.1×10^4	0.075	13 s	9.4×10^{-4}	3.6 min
m-cresol	2.4×10^4	0.075	13 s	6.3×10^{-3}	40 s

Table 11.3 Lifetimes for interfacial loss calculated using eqn (11.6) at 293 K.

These lifetimes are short compared to gas phase reactions (Table 11.2) where the only competing reaction is the nighttime oxidation by NO_3 in heavily polluted atmosphere. Therefore heterogeneous transfer has the potential to compete significantly with gas

phase oxidation. However, the above calculation only considers the interfacial mass transfer. To simulate actual situations, the overall uptake must include liquid phase processing.

11.2.2.2 Liquid phase processing

Liquid phase processing is determined by the rate of the liquid phase reaction within the droplet. Additionally, it is necessary to consider the time required for diffusive mixing within the liquid phase (τ_{liqmix}). Both kinetic regimes can be combined to derive an expression for the lifetime due to heterogeneous reactive loss at steady-state [*Kolb et al.*, 1995]

$$\tau^{L}_{liq} = \frac{1}{L_c\, H\, R\, T \sqrt{k_{RXN}}} \left(k_{RXN}^{-1/2} + \sqrt{\tau_{liqmix}} \right) \qquad \textbf{(11.7)}$$

with

$$\sqrt{\tau_{liqmix}} = \frac{d}{6\sqrt{D_L}} . \qquad \textbf{(11.8)}$$

The time for diffusion within the droplet is very short, $\tau_{liqmix} \approx 0.01$ s. It is therefore entirely reasonable to assume that the droplet is always uniformly saturated, so that the term including $\sqrt{\tau_{liqmix}}$ in eqn (11.7) can be neglected.

The pseudo-first-order reaction rate of the dissolved gas in the condensed phase, k_{RXN}, is expressed as

$$k_{RXN} = k'' \, [i] \qquad \textbf{(2.47)}$$

for a bimolecular reaction in solution where k" is the second-order rate coefficient and [i] is the concentration of reactant in solution. Aqueous phase chemistry is also driven by free radicals, such as OH, NO_3, SO_4^- and Cl_2^- [*Herrmann et al.*, 1995]. The two main sources of free radicals in atmospheric water drops are aqueous phase

photochemistry and gas-to-liquid partitioning [*Faust*, 1994]. For multiple liquid reaction pathways an overall k_{RXN} is calculated by

$$k_{RXN} = k_{RXN_1} + k_{RXN_2} + \ldots = \sum_i k_i'' [i]. \qquad (11.9)$$

Only very limited kinetic data are available for aqueous phase reactions of aromatic compounds. Although the aqueous phase rate coefficients of aliphatic compounds could be correlated to the corresponding gas phase rate coefficients, this was not possible for aromatic compounds [*Herrmann et al.*, 1995]. The available data were used to estimate the overall liquid reaction rate of phenol.

A rate coefficient for the aqueous reaction of phenol with OH has been recommended as 1.8×10^{10} l mol^{-1} s^{-1} [*Buxton et al.*, 1988] . The rate coefficients for the reaction of phenol with the SO_4^- and the HPO_4^- radicals have been given as 2.2×10^9 l mol^{-1} s^{-1} and 5.3×10^8 l mol^{-1} s^{-1}, respectively, at 298 K [*Gonzalez and Mártire*, 1999; *Cencione et al.*, 1998]. Finally, *Herrmann et al.* [1995] have measured the rate coefficients for the reaction of p-cresol with NO_3 as 8.4×10^8 l mol^{-1} s^{-1} at 298 K. Using estimates of tropospheric aqueous concentrations of free radicals the pseudo-first-order reaction rates in Table 11.4 were calculated.

The overall liquid reaction rate for all reactions during the day is estimated as k_{RXN} (day) = 0.015 s^{-1} whereas at night k_{RXN} (night) = 0.006 s^{-1}. Using eqn (11.7) and typical tropospheric parameters and the Henry's law constant at 293 K measured in this work with the wetted-wall flow reactor (i.e. $L_c = 3 \times 10^{-7}$, $H_{Phenol}^{293K} = 106$ M atm^{-1}), the lifetimes due to heterogeneous liquid reaction at steady state are τ^L_{liq}(day) = 87200 s = 1 day and τ^L_{liq}(night) = 2.2×10^5 s = 2.5 days. These lifetimes refer to the lifetimes within a cloud. *Kolb et al.* [1995] include a factor of 1/0.15 into τ^L_{liq} to account for the fact that clouds occupy ~ 15 % of the volume within the troposphere. This gives an estimate for the fate in the troposphere, rather than within the cloud itself.

radical	radical concentration /mol l^{-1}	k" /l mol^{-1} s^{-1}	individual k_{RXN} /s^{-1}
OH	6×10^{-13} [*Lelieveld and Crutzen*, 1990]	1.8×10^{10} [*Buxton et al.*, 1988]	0.01
SO_4^-	10^{-12} [*Zellner and Herrmann*, 1995]	2.2×10^{9} [*Gonzalez and Mártire*, 1999]	0.002
NO_3	10^{-12} nighttime continental cloud [*Seinfeld and Pandis*, 1998]	8.4×10^{8} (for reaction with p-cresol) [*Herrmann et al.*, 1995]	0.001
Cl_2^-	8×10^{-12} [*Zellner and Herrmann*, 1995]	2.5×10^{8} [*Hasegawa and Neta*, 1978]	0.002
CO_3^-	1.4×10^{-10} [*Zellner and Herrmann*, 1995]	4.9×10^{6} [*Chen et al.*, 1975]	7×10^{-4}
HPO_4^-	10^{-13} estimated	5.3×10^{8} [*Cencione et al.*, 1998]	5×10^{-5}

Table 11.4 Estimated pseudo-first order reactions rates of phenol in the troposphere at 293 K. Temperature differences between k" within 5 K were ignored.

11.2.2.3 Overall heterogeneous loss

The overall heterogeneous lifetime of phenol can now be derived from the lifetimes due to mass accommodation and liquid phase processing as

$$\left(\tau^{L}_{het}\right) \approx \left(\tau^{L}_{interface}\right) + \left(\tau^{L}_{liq}\right) \qquad \textbf{(11.10)}$$

which yields a net lifetime of τ^{L}_{het} (day) = 1 day and τ^{L}_{het} (night) = 2.5 days. Clearly, as expected, the lifetime due to heterogeneous processing is controlled by the rate of liquid phase reaction.

11.2.3 Gas *vs.* heterogeneous removal

In the previous sections, representative pathways in gas and liquid phase were chosen to calculate the respective lifetimes in gas and liquid phase. These are compared in

Figure 11.1. The two different τ^{L}_{het} displayed in Figure 11.1 are based on two different values of Henry's law coefficient of phenol at 293 K: 106 M atm^{-1} derived in the wetted-wall experiment in this work and 1500 M atm^{-1} given by *Tremp et al.* [1993].

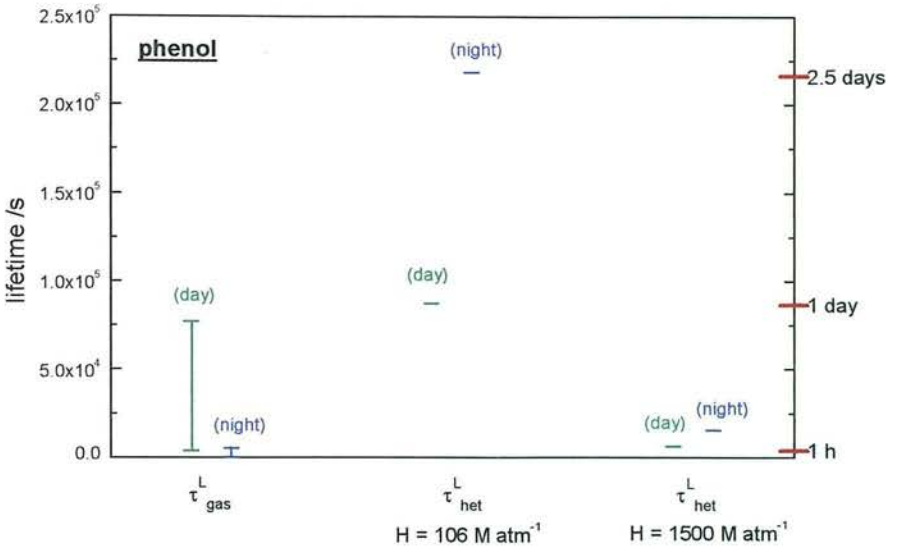

Figure 11.1 Comparison between estimated lifetimes due to heterogeneous and gas phase removal of phenol during day and night time. The limits of τ^{L}_{gas} refer to estimated concentrations in remote and heavily polluted atmosphere. τ^{L}_{het} was calculated using H = 106 M atm^{-1} from this work and H = 1500 M atm^{-1} [*Tremp et al.*, 1993].

Figure 11.1 shows that τ^{L}_{gas} and τ^{L}_{het} are of a comparable order of magnitude, particularly during the day. However, Figure 11.1 also indicates the impact of the parameters chosen in this estimation on the resulting lifetimes. The two different values of Henry's law coefficient change the heterogeneous lifetime from days to hours, as shown in Table 11.5. Since the Henry's law coefficients from the wetted-wall experiment seem generally low, the heterogeneous lifetimes calculated with H = 106 M atm^{-1} can possibly be considered their maximum. The temperature dependence of H causes τ^{L}_{het} to decrease with decreasing temperature. For comparison, Table 11.5 also shows the gas lifetimes (see Table 11.2).

	τ^L_{het}		τ^L_{gas}
	H = 106 M atm^{-1}	H = 1500 M atm^{-1}	
daytime	1 day	1.7 h	1 h to 21 h
nighttime	2.5 days	4.3 h	51 s to 1.4 h

Table 11.5 Calculated τ^L_{het} of phenol at 293 K using different Henry's law coefficients. τ^L_{gas} from Table 11.2 are also listed for comparison.

Similarly, the value of liquid reaction rate, k_{RXN}, significantly influences the lifetimes due to heterogeneous loss, because of the wide uncertainties and variations in the concentrations of the free radicals in the aqueous phase. For example, *Mill et al.* [1980; 1989] estimated OH radical concentrations in natural waters as 5×10^{-19} to 2×10^{-17} mol l^{-1} which are several orders of magnitude lower than that given by *Lelieveld and Crutzen* [1990]. This would reduce k_{RXN} (day) to about 0.005 s^{-1} (using [OH] of 10^{-17} mol l^{-1}), a similar value to k_{RXN} (night), and make the aqueous reaction with the OH radical insignificant compared with other aqueous phase radical reactions (see Table 11.4). However, more recently *Herrmann et al.* [1999] applied a box model to determine the concentration of several aqueous phase radicals. The maximum concentration given for OH at noon was ~ 2×10^{-12} mol l^{-1} whereas nighttime NO_3 concentrations reached 2×10^{-13} mol l^{-1} (for comparison see Table 11.4). Consequently, all the given lifetimes have to be considered as estimates under particular conditions.

Gas diffusion resistance increases with droplet size which could influence the interfacial lifetime (see eqn. (11.6)). However, the overall lifetime τ^L_{het} is not significantly affected by this variation since the lifetimes due to liquid phase reaction are larger by several orders of magnitude (e.g. $\tau^L_{interface} \approx 50$ s at d = 50 μm).

A similar procedure to that of phenol was applied to estimate the lifetimes of 2-nitrophenol and m-cresol using the same pseudo-first order reaction liquid rates and the appropriate values of H and α, as measured in this work.

	2-nitrophenol		m-cresol	
	τ^{L}_{het}	τ^{L}_{gas}	τ^{L}_{het}	τ^{L}_{gas}
daytime	18 h	1.3 days to 26 days	1.8 h	26 min to 8.7 h
nighttime	1.9 days	> 2.8 h to > 12 days	4.6 h	21 s to 34 min

Table 11.6 Estimated heterogeneous and gas phase lifetimes of 2-nitrophenol and m-cresol during daytime and nighttime at 293 K. Gas phase lifetimes from Table 11.2. τ^{L}_{het} was calculated using $H_{2\text{-nitrophenol}}$ = 140 M atm^{-1} (this work, bubble column) and $H_{m\text{-cresol}}$ = 1400 M atm^{-1} [*Yaws*, 1999] and the same k_{RXN} (i.e. day: 0.015 s^{-1}, night: 0.006 s^{-1}) and L_c (=3 x 10^{-7}) as for phenol.

Table 11.6 shows that heterogeneous loss is sufficiently fast to compete with reactions in the gas phase. Therefore, heterogeneous processes must be taken into account when assessing the atmospheric fates of these species.

11.3 Summary

Measured mass accommodation coefficients and Henry's law coefficients of phenol, 2-nitrophenol and m-cresol were used to estimate their lifetimes due to heterogeneous processing. Although mass accommodation limits the gas-interfacial transfer, it is the reaction in the liquid phase that is the limiting process overall for the total heterogeneous loss process.

Lifetimes of the phenols under investigation were estimated under a range of possible anticipated scenarios. This work shows that overall heterogeneous processing can be sufficiently fast to compete with reactions in the gas phase, particularly during the day. Estimated tropospheric lifetimes are short, about one hour for phenol and m-cresol and about one day for 2-nitrophenol during daytime, whereas nighttime loss is generally faster. As a consequence, these species are unlikely to be transported over long distances within tropospheric air masses.

Reactions of the investigated phenols in the aqueous phase are very fast, especially with the OH radical. This not only leads to degradation products in the liquid but alters the concentrations of aqueous phase free radicals in the troposphere.

It should be remembered that the calculated lifetimes are only estimates. Concentrations ranges in the gas phase for polluted environments might be exaggerations for average urban locations. Data on concentrations and mechanisms in the aqueous phase are scarce. The lifetimes were calculated at 293 K, however, the temperature in the troposphere decreases with distance from the earth surface by about 10 K km^{-1}. Also, no temperature effects between day and night were included in the calculations. Henry's law coefficient is a strong function of temperature in a direction such as to increase the impact of the heterogeneous phase at lower temperatures.

As mentioned above, the tropospheric lifetimes here refer to lifetimes within the gas phase and within the cloud. To obtain an average tropospheric lifetime, the tropospheric volume occupied by the clouds has to be taken into account. However, a mean value of cloud coverage is difficult to designate since clouds form and evaporate repeatedly and their occurrence shows dramatic geographical variation. The short lifetimes of the investigated phenols imply that these species experience only local conditions and an average tropospheric condition is fairly meaningless.

Kinetic information on the transfer from gas to liquid as well as on the subsequent reactions in the liquid phase are needed to elucidate the role of heterogeneous chemistry in the troposphere. Data such as these presented in this thesis can be used in atmospheric models to provide a more complete picture of the complex chemical processes of the atmosphere.

12. REFERENCES

International Critical Tables of numerical data, physics, chemistry, and technology, Washburn, E. W. (Ed.), National Research Council (USA), McGraw Hill, New York, 1929.

Landolt-Börnstein Physikalisch-Chemische Tabellen, 5th Ed., Roth, W. A. and Scheel, K. (Ed.), Springer, Berlin, 1931.

Academic press dictionary of science and technology, Morris, C. (Ed.), Academic Press, San Diego, 1992.

CRC Handbook of chemistry and physics, 74th Ed., Lide, D. R. and Frederikse, H. P. R. (Ed.), CRC Press, Boca Raton, 1993.

A guide to the measurement of humidity, Institute of measurement and control, National Physical Laboratory, London, 1996.

Akita, K., Diffusivities of gases in aqueous electrolyte solutions, *Ind.Eng.Chem.Fundamentals*, **20**, 89-94, 1981.

Altschuh, J., Bruggemann, R., Santl, H., Eichinger, G. and Piringer, O. G., Henry's law constants for a diverse set of organic chemicals: Experimental determination and comparison of estimation methods, *Chemosphere*, **39**, 1871-1887, 1999.

Anderson, P. N. and Hites, R. A., System to measure relative rate constants of semivolatile organic compounds with hydroxyl radicals, *Environ.Sci.Technol.*, **30**, 301-306, 1996.

Andino, J. M., Smith, J. N., Flagan, R. C., Goddard, W. A. and Seinfeld, J. H., Mechanism of atmospheric photooxidation of aromatics: A theoretical study, *J.Phys.Chem.*, **100**, 10967-10980, 1996.

Ashworth, R. A., Howe, G. B., Mullins, M. E. and Rogers, T. N., Air-water partitioning coefficients of organics in dilute aqueous solutions, *J.Hazard.Mater.*, **18**, 25-36, 1988.

Atkins, P. W., *Physical chemistry*, 3rd Ed., Oxford University Press, Oxford, 1986.

Atkinson, R., Carter, W. P. L., Plum, C. N., Winer, A. M. and Pitts, J. N., Kinetics of the gas-phase reactions of NO_3 radicals with a series of aromatics at 296 K +/- 2 K, *Int.J.Chem.Kinet.*, **16**, 887-898, 1984.

Atkinson, R., Aschmann, S. M. and Arey, J., Reactions of OH and NO_3 radicals with phenol, cresols, and 2- nitrophenol at 296 K +/- 2 K, *Environ.Sci.Technol.*, **26**, 1397-1403, 1992.

Atkinson, R., Gas-phase degradation of organic compounds in the troposphere, *Pure Appl.Chem.*, **70**, 1327-1334, 1998.

Baker, J., Ashbourn, S. F. M. and Cox, R. A., Heterogeneous reactivity of nitrous acid on submicron sulfuric acid aerosol, *Phys.Chem.Chem.Phys.*, **1**, 683-690, 1999.

Baldwin, A. C. and Golden, D. M., Heterogeneous atmospheric reactions: sulfuric acid aerosols as tropospheric sinks, *Science* , **206**, 562-563, 1979.

Baldwin, A. C. and Golden, D. M., Heterogeneous atmospheric reactions 2. Atom and radical reactions with sulfuric acid, *J.Geophys.Res.*, **85**, 2888-2889, 1980.

Behnke, W., George, C., Scheer, V. and Zetzsch, C., Production and decay of $ClNO_2$ from the reaction of gaseous N_2O_5 with NaCl solution: Bulk and aerosol experiments, *J.Geophys.Res.*, **102**, 3795-3804, 1997.

Bell, R. P. and Rawlinson, D. J., Kinetics of the bromination of some anisoles and phenols, *J.Chem.Soc.*, 63-68, 1961.

Benes, M. and Dohnal, V., Limiting activity coefficients of some aromatic and aliphatic nitro compounds in water, *J.Chem.Eng.Data*, **44**, 1097-1102, 1999.

Betterton, E. A. and Hoffmann, M. R., Henry's law constants of some environmentally important aldehydes, *Environ.Sci.Technol.*, **22**, 1415-1418, 1988.

Beyer, H., Walter, W. and Lloyd, D., *Organic chemistry*, 22nd Ed., Albion Publishing, Chichester, 1997.

Brown, R. L., Tubular flow reactors with first-order kinetics, *J.Res.Nat.Bur.Stand.*, **83**, 1-8, 1978.

Buxton, G. V., Greenstock, C. L., Helman, W. P. and Ross, A. B., Critical review of rate constants for reactions of hydrated electrons, hydrogen atoms and hydroxyl radicals (OH/O^-) in aqueous solution, *J.Phys.Chem.Ref.Data*, **17**, 513-886, 1988.

Cencione, S. S., Gonzalez, M. C. and Mártire, D. O., Reactions of phosphate radicals with substituted benzenes. A structure-reactivity correlation study, *J.Chem.Soc.Faraday Trans.*, **94**, 2933-2937, 1998.

Chameides, W. L., The photochemistry of a remote marine stratiform cloud, *J.Geophys.Res.*, **89**, 4739-4755, 1984.

Chen, S., Hoffmann, M. Z. and Parsons, G. H., Reactivity of the carbonate radical toward aromatic compounds in aqueous solution, *J.Phys.Chem.*, **79**, 1911-1912, 1975.

Coulson, J. M., Richardson, J. F., Backhurst, J. R. and Harker, J. H., *Coulson & Richardson's chemical engineering*, Vol. 1: Fluid flow, heat transfer and mass transfer, 4th Ed., Pergamon Press, Oxford, 1990.

Danckwerts, P. V., Absorption by simultaneous diffusion and chemical reaction into particles of various shapes and into falling drops, *Trans.Faraday Soc.*, **47**, 1014-1023, 1951.

Danckwerts, P. V., *Gas-liquid reactions*, McGraw Hill, New York, 1970.

Davidovits, P., Jayne, J. T., Duan, S. X., Worsnop, D. R., Zahniser, M. S. and Kolb, C. E., Uptake of gas molecules by liquids: A model, *J.Phys.Chem.*, **95**, 6337-6340, 1991.

Davidovits, P., Hu, J. H., Worsnop, D. R., Zahniser, M. S. and Kolb, C. E., Entry of gas molecules into liquids, *Faraday Discuss.*, **100**, 65-81, 1995.

De Bruyn, W. J., Swartz, E., Hu, J. H., Shorter, J. A., Davidovits, P., Worsnop, D. R., Zahniser, M. S. and Kolb, C. E., Henry's law solubilities and Setchenow coefficients for biogenic reduced sulfur species obtained from gas-liquid uptake measurements, *J.Geophys.Res.*, **100**, 7245-7251, 1995.

Dong, S. and Dasgupta, P. K., Solubility of gaseous formaldehyde in liquid water and generation of trace standard gaseous formaldehyde, *Environ.Sci.Technol.*, **20**, 637-640, 1986.

Dunnivant, F. M., Coates, J. T. and Elzerman, A. W., Experimentally determined Henry's law constants for 17 polychlorobiphenyl congeners, *Environ.Sci.Technol.*, **22**, 448-453, 1988.

ECETOC, QSARs in the assessment of the environmental fate and effects of chemicals, in *ECETOC technical report*, No. 74, Carpanini, F. (Ed.), European centre for ecotoxicology and toxicology of chemicals, Brussels, 1998.

EUROTRAC, Heterogeneous and liquid phase processes: laboratory studies related to aerosols and clouds, in *Transport and chemical transformation of pollutants in the troposphere*, Warneck, P. (Ed.), Vol. 2, Springer, Berlin, 1996.

Faust, B. C., Photochemistry of clouds, fogs, and aerosols, *Environ.Sci.Technol.*, **28**, A217-A222, 1994.

Fendinger, N. J. and Glotfelty, D. E., A laboratory method for the experimental determination of air-water Henry's law constants for several pesticides, *Environ.Sci.Technol.*, **22**, 1289-1293, 1988.

Fendinger, N. J., Glotfelty, D. E. and Freeman, H. P., Comparison of 2 experimental techniques for determining air-water Henry's law constants, *Environ.Sci.Technol.*, **23**, 1528-1531, 1989.

Fickert, S., Helleis, F., Adams, J. W., Moortgat, G. K. and Crowley, J. N., Reactive uptake of $ClNO_2$ on aqueous bromide solutions, *J.Phys.Chem.A*, **102**, 10689-10696, 1998.

Fickert, S., Adams, J. W. and Crowley, J. N., Activation of Br_2 and BrCl *via* uptake of HOBr onto aqueous salt solutions, *J.Geophys.Res.*, **104**, 23719-23727, 1999.

Finlayson-Pitts, B. J. and Pitts, J. N., Jr., *Atmospheric chemistry: Fundamentals and experimental techniques*, John Wiley & Sons, New York, 1986.

Frenzel, A., Scheer, V., Sikorski, R., George, C., Behnke, W. and Zetzsch, C., Heterogeneous interconversion reactions of $BrNO_2$, $ClNO_2$, Br_2, and Cl_2, *J.Phys.Chem.A*, **102**, 1329-1337, 1998.

Fuller, E. D., Ensley, K. and Giddings, J. C., Diffusion of halogenated hydrocarbons in helium. The effect of structure on collision cross sections, *J.Phys.Chem.*, **73**, 3679-3685, 1969.

Gardner, J. A., Watson, L. R., Adewuyi, Y. G., Davidovits, P., Zahniser, M. S., Worsnop, D. R. and Kolb, C. E., Measurement of the mass accommodation coefficient of SO_2 (g) on water droplets, *J.Geophys.Res.*, **92**, 10887-10895, 1987.

George, C., Ponche, J. L., Mirabel, P., Behnke, W., Scheer, V. and Zetzsch, C., Study of the uptake of N_2O_5 by water and NaCl solutions, *J.Phys.Chem.*, **98**, 8780-8784, 1994.

George, C., Behnke, W., Scheer, V., Zetzsch, C., Magi, L., Ponche, J. L. and Mirabel, P., Fate of $ClNO_2$ over aqueous solutions containing iodide, *Geophys.Res.Lett.*, **22**, 1505-1508, 1995.

Ghosh, S., On the diffusivity of trace gases under stratospheric conditions, *J.Atmos.Chem.*, **17**, 391-397, 1993.

Golden, D. M., Spokes, G. N. and Benson, S. W., Very-low pressure pyrolysis (VLPP): a versatile kinetic tool, *Angew.Chem.Int.Ed.*, **12**, 534-546, 1973.

Gonzalez, M. C. and Mártire, D. O., The reactions of sulphate radicals with substituted benzenes studied by time-resolved spectroscopy. A structure-reactivity correlation analysis, *Asian J.Spectros.*, **3**, 125-128, 1999.

Graedel, T. E. and Crutzen, P. J., *Atmospheric change: an earth system perspective*, W. H. Freeman, New York, 1993.

Grosjean, D., Atmospheric fate of toxic aromatic compounds, *Sci.Total Environ.*, **100**, 367-414, 1991.

Hamelink, J. L., Simon, P. B. and Silberhorn, E. M., Henry's law constant, volatilization rate, and aquatic half-life of octamethylcyclotetrasiloxane, *Environ.Sci.Technol.*, **30**, 1946-1952, 1996.

Hanson, D. R. and Ravishankara, A. R., The reaction probabilities of $ClONO_2$ and N_2O_5 on 40 to 75 % sulfuric acid solutions, *J.Geophys.Res.*, **96**, 17307-17314, 1991.

Hanson, D. R., Burkholder, J. B., Howard, C. J. and Ravishankara, A. R., Measurement of OH and HO_2 radical uptake coefficients on water and sulfuric acid surfaces, *J.Phys.Chem.*, **96**, 4979-4985, 1992.

Hanson, D. R., The uptake of HNO_3 onto ice, NAT, and frozen sulfuric acid, *Geophys.Res.Lett.*, **19**, 2063-2066, 1992.

Hanson, D. R. and Ravishankara, A. R., Uptake of HCl and HOCl onto sulfuric-acid: solubilities, diffusivities, and reaction, *J.Phys.Chem.*, **97**, 12309-12319, 1993.

Hanson, D. R. and Ravishankara, A. R., Reactive uptake of $ClONO_2$ onto sulfuric acid due to reaction with HCl and H_2O, *J.Phys.Chem.*, **98**, 5728-5735, 1994.

Hanson, D. R., Ravishankara, A. R. and Solomon, S., Heterogeneous reactions in sulfuric acid aerosols: A framework for model calculations, *J.Geophys.Res.*, **99**, 3615-3629, 1994.

Hanson, D. R. and Lovejoy, E. R., Heterogeneous reactions in liquid sulfuric acid: HOCl+HCl as a model system, *J.Phys.Chem.*, **100**, 6397-6405, 1996.

Hanson, D. R., Reaction of N_2O_5 with H_2O on bulk liquids and on particles and the effect of dissolved HNO_3, *Geophys.Res.Lett.*, **24** , 1087-1090, 1997.

Hasegawa, K. and Neta, P., Rate constants and mechanisms of reaction of Cl_2^- radicals, *J.Phys.Chem.*, **82**, 854-857, 1978.

Heal, M. R., Pilling, M. J., Titcombe, P. E. and Whitaker, B. J., Mass accommodation of aniline, phenol and toluene on aqueous droplets, *Geophys.Res.Lett.*, **22**, 3043-3046, 1995.

Hemond, H. F. and Fechner, E. J., *Chemical fate and transport in the environment*, Academic Press, London, 1994.

Heron, G., Christensen, T. H. and Enfield, C. G., Henry's law constant for trichloroethylene between 10 and 95 °C, *Environ.Sci.Technol.*, **32**, 1433-1437, 1998.

Herrmann, H., Exner, M., Jacobi, H. W., Raabe, G., Reese, A. and Zellner, R., Laboratory studies of atmospheric aqueous-phase free-radical chemistry: Kinetic and spectroscopic studies of reactions of NO_3 and SO_4^- radicals with aromatic compounds, *Faraday Discuss.*, **100**, 129-153, 1995.

Herrmann, H., Jacobi, H. W., Raabe, G., Reese, A. and Zellner, R., Laser-spectroscopic laboratory studies of atmospheric aqueous phase free radical chemistry, *Fresenius J.Anal.Chem.*, **355**, 343-344, 1996.

Herrmann, H., Ervens, B., Nowacki, P., Wolke, R. and Zellner, R., A chemical aqueous phase radical mechanism for tropospheric chemistry, *Chemosphere*, **38**, 1223-1232, 1999.

Herterich, R. and Herrmann, R., Comparing the distribution of nitrated phenols in the atmosphere of 2 german hill sites, *Environ.Technol.*, **11**, 961-972, 1990.

Hickinbottom, W. J., *Reactions of organic compounds*, 3rd Ed., Longmans, London, 1962.

Howard, C. J., Kinetic measurements using flow tubes, *J.Phys.Chem.*, **83**, 3-9, 1979.

Howard, P. H., Boethling, R. S., Jarvis, W. F., Meylan, W. M. and Michalenko, E. M., *Handbook of environmental degradation rates*, Lewis Publishers, Chelsea, 1991.

Howard, P. H. and Meylan, W. M., *Handbook of physical properties of organic chemicals*, Lewis Publishers (CRC Press), Boca Raton, 1997.

Hu, J. H., Shi, Q., Davidovits, P., Worsnop, D. R., Zahniser, M. S. and Kolb, C. E., Reactive uptake of Cl_2(g) and Br_2(g) by aqueous surfaces as a function of Br^- and I^- ion concentration: The effect of chemical reaction at the interface, *J.Phys.Chem.*, **99**, 8768-8776, 1995.

Hu, J. H. and Abbatt, J. P. D., Reaction probabilities for N_2O_5 hydrolysis on sulfuric acid and ammonium sulfate aerosols at room temperature, *J.Phys.Chem.A*, **101**, 871-878, 1997.

Imamura, T., Rudich, Y., Talukdar, R. K., Fox, R. W. and Ravishankara, A. R., Uptake of NO_3 on water solutions: Rate coefficients for reactions of NO_3 with cloud water constituents, *J.Phys.Chem.A*, **101**, 2316-2322, 1997.

Jayasinghe, D. S., Brownawell, B. J., Hua, C. and Westall, J. C., Determination of Henry's constants of organic compounds of low volatility: Methylanilines in methanol-water, *Environ.Sci.Technol.*, **26**, 2275-2281, 1992.

Jayne, J. T., Duan, S. X., Davidovits, P., Worsnop, D. R., Zahniser, M. S. and Kolb, C. E., Uptake of gas-phase alcohol and organic acid molecules by water surfaces, *J.Phys.Chem.*, **95**, 6329-6336, 1991.

Jayne, J. T., Duan, S. X., Davidovits, P., Worsnop, D. R., Zahniser, M. S. and Kolb, C. E., Uptake of gas-phase aldehydes by water surfaces, *J.Phys.Chem.*, **96**, 5452-5460, 1992.

Kames, J. and Schurath, U., Alkyl nitrates and bifunctional nitrates of atmospheric interest: Henry's law constants and their temperature dependencies, *J.Atmos.Chem.*, **15**, 79-95, 1992.

Kames, J. and Schurath, U., Henry's law and hydrolysis rate constants for peroxyacyl nitrates (PANs) using a homogeneous gas-phase source, *J.Atmos.Chem.*, **21**, 151-164, 1995.

Kaye, G. W. C. and Laby, T. H., *Tables of physical and chemical constants*, 16th Ed., Longman, London, 1995.

Keyser, L. F., High-pressure flow kinetics. A study of the OH + HCl reaction from 2 to 100 Torr, *J.Phys.Chem.*, **88**, 4750-4758, 1984.

Kirchner, W., Welter, F., Bongartz, A., Kames, J., Schweighoefer, S. and Schurath, U., Trace gas exchange at the air/water interface: Measurements of mass accommodation coefficients, *J.Atmos.Chem.*, **10**, 427-449, 1990.

Kley, D., Tropospheric chemistry and transport, *Science*, **276**, 1043-1045, 1997.

Klotz, B., Barnes, I. and Becker, K. H., New results on the atmospheric photooxidation of simple alkylbenzenes, *Chem.Phys.*, **231**, 289-301, 1998.

Knispel, R., Koch, R., Siese, M. and Zetzsch, C., Adduct formation of OH radicals with benzene, toluene, and phenol and consecutive reactions of the adducts with NO_x and O_2, *Ber.Bunsenges.Phys.Chem.*, **94**, 1375-1379, 1990.

Kolb, C. E., Worsnop, D. R., Zahniser, M. S., Davidovits, P., Keyser, L. F., Leu, M. T., Molina, M. J., Hanson, D. R., Ravishankara, A. R., Williams, L. R. and Tolbert, M. A., Laboratory Studies of Atmospheric Heterogeneous Chemistry, in *Progress and Problems in Atmospheric Chemistry*, Vol. 3, Barker, J. R. (Ed.), pp. 771-875, World Scientific, Singapore, 1995.

Kosak-Channing, L. F. and Helz, G. R., Solubility of ozone in aqueous solutions of 0 - 0.6 M ionic strength at 5 - 30 °C, *Environ.Sci.Technol.*, **17**, 145-149, 1983.

Kwok, E. S. C., Atkinson, R. and Arey, J., Kinetics and mechanisms of the gas-phase reactions of the NO_3 radical with aromatic compounds, *Int.J.Chem.Kinet.*, **26**, 511-525, 1994.

Lee, J. H. and Tang, I. N., Accommodation coefficient of gaseous NO_2 on water surfaces, *Atmos.Environ.*, **22**, 1147-1151, 1988.

Lelieveld, J. and Crutzen, P. J., Influences of cloud photochemical processes on tropospheric ozone, *Nature*, **343**, 227-233, 1990.

Leu, M. T., Timonen, R. S., Keyser, L. F. and Yung, Y. L., Heterogeneous reactions of $HNO_3(g)$ + $NaCl(s)$ -> $HCl(g)$ + $NaNO_3(s)$ and $N_2O_5(g)$ + $NaCl(s)$ -> $ClNO_2(g)$ + $NaNO_3(s)$, *J.Phys.Chem.*, **99**, 13203-13212, 1995.

Leuenberger, C., Ligocki, M. P. and Pankow, J. F., Trace organic compounds in rain. 4. Identities, concentrations, and scavenging mechanisms for phenols in urban air and rain, *Environ.Sci.Technol.*, **19**, 1053-1058, 1985.

Levsen, K., Behnert, S., Prieß, B., Svoboda, M., Winkeler, H. D. and Zietlow, J., Organic compounds in precipitation, *Chemosphere*, **21**, 1037-1061, 1990.

Lincoff, A. H. and Gossett, J. M., The determination of Henry's constant for volatile organics by equilibrium partitioning in closed systems, in *Gas transfer at water surfaces*, Brutsaert, W. and Jirka, G. H. (Ed.), pp. 17-25, D. Reidel Publishing Company, Dordrecht, 1984.

Liss, P. S. and Slater, P. G., Flux of gases across the air-sea interface, *Nature*, **247**, 181-184, 1974.

Logan, B. E., *Environmental transport processes*, John Wiley & Sons, New York, 1999.

Lovejoy, E. R., Huey, L. G. and Hanson, D. R., Atmospheric fate of CF_3OH. 2. Heterogeneous reaction, *J.Geophys.Res.*, **100**, 18775-18780, 1995.

Lovejoy, E. R. and Hanson, D. R., Measurement of the kinetics of reactive uptake by submicron sulfuric acid particles, *J.Phys.Chem.*, **99**, 2080-2087, 1995.

Lüttke, J., Scheer, V., Levsen, K., Wünsch, G., Cape, J. N., Hargreaves, K. J., Storeton-West, R. L., Acker, K., Wieprecht, W. and Jones, B., Occurrence and formation of nitrated phenols in and out of cloud, *Atmos.Environ.*, **31**, 2637-2648, 1997.

Lüttke, J. and Levsen, K., Phase partitioning of phenol and nitrophenols in clouds, *Atmos.Environ.*, **31**, 2649-2655, 1997.

Lüttke, J., Levsen, K., Acker, K., Wieprecht, W. and Möller, D., Phenols and nitrated phenols in clouds at Mount Brocken, *Int.J.Environ.Anal.Chem.*, **74**, 69-89, 1999.

Lyman, W. J., Reehl, W. F. and Rosenblatt, D. H., *Handbook of chemical property estimation methods*, American Chemical Society, Washington, 1990.

Mabey, W. R., Smith, J. H., Podoll, R. T., Johnson, H. L., Mill, T., Chou, T. W., Gates, J., Waight Partiridge, I., Jaber, H. and Vandenberg, D., Aquatic fate process data for organic priority pollutants, EPA-440/4-81-014, SRI International, Washington, 1982.

Mackay, D., Shiu, W. Y. and Sutherland, R. P., Determination of air-water Henry's law constants for hydrophobic pollutants, *Environ.Sci.Technol.*, **13**, 333-337, 1979.

Mackay, D. and Shiu, W. Y., Physical-chemical phenomena and molecular properties, in *Gas transfer at water surfaces*, Brutsaert, W. and Jirka, G. H. (Ed.), pp. 3-16, D. Reidel Publishing Company, Dordrecht, 1984.

Mackay, D., Shiu, W. Y. and Ma, K. C., *Illustrated handbook of physical-chemical properties and environmental fate for organic chemicals*, Vol. 1: Monoaromatic hydrocarbons, chlorobenzenes, and PCBs, Lewis Publishers, Boca Raton, 1992.

Magi, L., Schweitzer, F., Pallares, C., Cherif, S., Mirabel, P. and George, C., Investigation of the uptake rate of ozone and methyl hydroperoxide by water surfaces, *J.Phys.Chem.A*, **101**, 4943-4949, 1997.

Maskill, H., *The physical basis of organic chemistry*, Oxford University Press, Oxford, 1990.

Mertes, S. and Wahner, A., Uptake of nitrogen dioxide and nitrous acid on aqueous surfaces, *J.Phys.Chem.*, **99**, 14000-14006, 1995.

Mill, T., Hendry, D. G. and Richardson, H., Free-radical oxidants in natural waters, *Science*, **207**, 886-887, 1980.

Mill, T., Structure-activity relationships for photooxidation processes in the environment, *Environ.Toxicol.Chem.*, **8**, 31-43, 1989.

Molina, M. J., Molina, L. T. and Kolb, C. E., Gas-phase and heterogeneous chemical kinetics of the troposphere and stratosphere, *Ann.Rev.Phys.Chem.*, **47**, 327-367, 1996a.

Molina, M. J., Molina, L. T. and Golden, D. M., Environmental chemistry (gas and gas-solid interactions): The role of physical chemistry, *J.Phys.Chem.*, **100**, 12888-12896, 1996b.

Motz, H. and Wise, H., Diffusion and heterogeneous reaction. III. Atom recombination at a catalytic boundary, *J.Chem.Phys.*, **32**, 1893-1894, 1960.

Munz, C. and Roberts, P. V., Effects of solute concentration and cosolvents on the aqueous activity-coefficient of halogenated hydrocarbons, *Environ.Sci.Technol.*, **20**, 830-836, 1986.

Natangelo, M., Mangiapan, S., Bagnati, R., Benfenati, E. and Fanelli, R., Increased concentrations of nitrophenols in leaves from a damaged forestal site, *Chemosphere*, **38**, 1495-1503, 1999.

Nathanson, G. M., Davidovits, P., Worsnop, D. R. and Kolb, C. E., Dynamics and kinetics at the gas-liquid interface, *J.Phys.Chem.*, **100**, 13007-13020, 1996.

Nojima, K., Fukaya, K., Fukui, S. and Kanno, S., The formation of nitrophenols and nitrobenzene by the photochemical reaction of benzene in the presence of nitrogen monoxide, *Chemosphere*, **2**, 77-82, 1975.

Palm, W. U., Elend, M., Krüger, H. U. and Zetzsch, C., OH radical reactivity of airborne terbuthylazine adsorbed on inert aerosol, *Environ.Sci.Technol.*, **31**, 3389-3396, 1997.

Pawlikowski, E. M. and Prausnitz, J. M., Estimation of setchenow constants for non-polar gases in common salts at moderate temperatures, *Ind.Eng.Chem.Fundamentals*, **22**, 86-90, 1983.

Pawlikowski, E. M., Correction, *Ind.Eng.Chem.Fundamentals*, **23**, 270, 1984.

Perkampus, H. H., *UV-VIS Atlas of organic compounds*, 2nd Ed., VCH, Weinheim, 1992.

Perry, R. H. and Green, D. W., *Perry's chemical engineers handbook*, 7th Ed., McGraw Hill, New York, 1997.

Platz, J., Nielsen, O. J., Wallington, T. J., Ball, J. C., Hurley, M. D., Straccia, A. M., Schneider, W. F. and Sehested, J., Atmospheric chemistry of the phenoxy radical, $C_6H_5O(\bullet)$: UV spectrum and kinetics of its reaction with NO, NO_2, and O_2, *J.Phys.Chem.A*, **102**, 7964-7974, 1998.

Pollack, G. L., Why gases dissolve in liquids, *Science*, **251**, 1323-1330, 1991.

Ponche, J. L., George, C. and Mirabel, P., Mass transfer at the air/water interface: Mass accommodation coefficients of SO_2, HNO_3, NO_2 and NH_3, *J.Atmos.Chem.*, **16**, 1-21, 1993.

Pöschl, U., Canagaratna, M., Jayne, J. T., Molina, L. T., Worsnop, D. R., Kolb, C. E. and Molina, M. J., Mass accommodation coefficient of H_2SO_4 vapor on aqueous sulfuric acid surfaces and gaseous diffusion coefficient of H_2SO_4 in N_2/H_2O, *J.Phys.Chem.A*, **102**, 10082-10089, 1998.

Prausnitz, J. M., Lichtenthaler, R. N. and Azevedo, E. G. de, *Molecular thermodynamics of fluid-phase equilibria*, 2nd Ed., Englewood Cliffs, PTR Prentice-Hall, New Jersey, 1986.

Pun, B. K., Seigneur, C., Grosjean, D. and Saxena, P., Gas-phase formation of water-soluble organic compounds in the atmosphere: A retrosynthetic analysis, *J.Atmos.Chem.*, **35**, 199-223, 1999.

Ravishankara, A. R., Heterogeneous and multiphase chemistry in the troposphere, *Science*, **276**, 1058-1065, 1997.

Reible, D. D., *Fundamentals of environmental engineering*, Springer: Lewis Publishers, Heidelberg, 1999.

Reid, R. C., Prausnitz, J. M. and Poling, B. E., *The properties of gases and liquids*, 4th Ed., McGraw Hill, New York, 1987.

Richartz, H., Reischl, A., Trautner, F. and Hutzinger, O., Nitrated phenols in fog, *Atmos.Environ.*, **24**, 3067-3071, 1990.

Rippen, G., Zietz, E., Frank, R., Knacker, T. and Klöpffer, W., Do airborne nitrophenols contribute to forest decline?, *Environ.Technol.Lett.*, **8**, 475-482, 1987.

Robinson, R. A. and Stokes, R. H., *Electrolyte solutions: the measurement and interpretation of conductance, chemical potential and diffusion in solutions of simple electrolytes*, 2nd Ed., Butterworths, London, 1959.

Rossi, M. J., Atmospheric pollution: The role of heterogeneous chemical reactions, *Chimia*, **50**, 199-208, 1996.

Rubel, G. O. and Gentry, J. W., Measurement of the kinetics of solution droplets in the presence of adsorbed monolayers: Determination of water accommodation coefficients, *J.Phys.Chem.*, **88**, 3142-3148, 1984.

Rudich, Y., Talukdar, R. K. and Ravishankara, A. R., Reactive uptake of NO_3 on pure water and ionic solutions, *J.Geophys.Res.*, **101**, 21023-21031, 1996a.

Rudich, Y., Talukdar, R. K., Imamura, T., Fox, R. W. and Ravishankara, A. R., Uptake of NO_3 on KI solutions: Rate coefficient for the $NO_3 + I^-$ reaction and gas-phase diffusion coefficients for NO_3, *Chem.Phys.Lett.*, **261**, 467-473, 1996b.

Sawyer, C. N., McCarty, P. L. and Parkin, G. F., *Chemistry for environmental engineering*, 4th Ed., McGraw Hill, New York, 1994.

Scheer, V., Frenzel, A., Behnke, W., Zetzsch, C., Magi, L., George, C. and Mirabel, P., Uptake of nitrosyl chloride (NOCl) by aqueous solutions, *J.Phys.Chem.A*, **101**, 9359-9366, 1997.

Schmidt-Bäumler, K., Heberer, T. and Stan, H. J., Occurrence and distribution of organic contaminants in the aquatic system in Berlin. Part II: Substituted phenols in Berlin surface water, *Acta Hydrochim.hydrobiol.*, **27**, 143-149, 1999.

Schwartz, S. E., Mass-transport considerations pertinent to aqueous phase reactions of gases in liquid-water clouds, in *Chemistry of multiphase atmospheric systems*, Vol. G6, Jaeschke, W. (Ed.), pp. 415-471, Springer Verlag, Berlin Heidelberg, 1986.

Schwarzenbach, R. P., Stierli, R., Folsom, B. R. and Zeyer, J., Compound properties relevant for assessing the environmental partitioning of nitrophenols, *Environ.Sci.Technol.*, **22**, 83-92, 1988.

Schwarzenbach, R. P., Gschwend, P. M. and Imboden, D. M., *Environmental organic chemistry*, John Wiley & Sons, New York, 1993.

Schweitzer, F., Mirabel, P. and George, C., Multiphase chemistry of N_2O_5, $ClNO_2$, and $BrNO_2$, *J.Phys.Chem.A*, **102**, 3942-3952, 1998.

Seinfeld, J. H. and Pandis, S. N., *Atmospheric chemistry and physics*, John Wiley & Sons, New York, 1998.

Seuwen, R. and Warneck, P., Oxidation of toluene in NO_x free air: Product distribution and mechanism, *Int.J.Chem.Kinet.*, **28**, 315-332, 1996.

Shepson, P. B., Mackay, E. and Muthuramu, K., Henry's law constants and removal processes for several atmospheric β-Hydroxy alkyl nitrates, *Environ.Sci.Technol.*, **30**, 3618-3623, 1996.

Shi, Q., Li, Y. Q., Davidovits, P., Jayne, J. T., Worsnop, D. R., Mozurkewich, M. and Kolb, C. E., Isotope exchange for gas-phase acetic acid and ethanol at aqueous interfaces: A study of surface reactions, *J.Phys.Chem.B*, **103**, 2417-2430, 1999a.

Shi, Q., Davidovits, P., Jayne, J. T., Worsnop, D. R. and Kolb, C. E., Uptake of gas-phase ammonia. 1. Uptake by aqueous surfaces as a function of pH, *J.Phys.Chem.A*, **103**, 8812-8823, 1999b.

Shiu, W. Y. and Mackay, D., Henry's law constants of selected aromatic hydrocarbons, alcohols, and ketones, *J.Chem.Eng.Data*, **42**, 27-30, 1997.

Shorter, J. A., De Bruyn, W. J., Hu, J. H., Swartz, E., Davidovits, P., Worsnop, D. R., Zahniser, M. S. and Kolb, C. E., Bubble column apparatus for gas-liquid heterogeneous chemistry studies, *Environ.Sci.Technol.*, **29**, 1171-1178, 1995.

Sinnott, R. K., *Coulson & Richardson's chemical engineering*, Vol. 6: Chemical engineering design, 2nd Ed., Pergamon Press, Oxford, 1996.

Staudinger, J. and Roberts, P. V., A critical review of Henry's law constants for environmental applications, *Crit.Rev.Environ.Sci.Technol.*, **26**, 205-297, 1996.

Suntio, L. R., Shiu, W. Y., Mackay, D., Seiber, J. N. and Glotfelty, D. E., Critical review of Henry's law constants for pesticides, in *Reviews of environmental contamination and toxicology*, Ware, G. W. (Ed.), Vol. 103, pp. 1-59, Springer Verlag, New York, 1988.

Swartz, E., Boniface, J., Tchertkov, I., Rattigan, O. V., Robinson, D. V., Davidovits, P., Worsnop, D. R., Jayne, J. T. and Kolb, C. E., Horizontal bubble train apparatus for heterogeneous chemistry studies: Uptake of gas-phase formaldehyde, *Environ.Sci.Technol.*, **31**, 2634-2641, 1997.

Takami, A., Kato, S., Shimono, A. and Koda, S., Uptake coefficient of OH radical on aqueous surface, *Chem.Phys.*, **231**, 215-227, 1998.

Tang, I. N. and Lee, J. H., Accommodation coefficients of ozone and SO_2: Implications on SO_2 oxidation in cloud water, *ACS Symp.S.*, **349**, 109-117, 1987.

Tee, O. S., Paventi, M. and Bennett, J. M., Kinetics and mechanism of the bromination of phenols and phenoxide ions in aqueous solution. Diffusion-controlled rates, *J.Am.Chem.Soc.*, **111**, 2233-2240, 1989.

Thibodeaux, L. J., *Environmental chemodynamics*, 2nd Ed., John Wiley & Sons, New York, 1996.

Titcombe, P. E., Gas-liquid interactions in tropospheric chemistry, *PhD*, School of Chemistry, University of Leeds, 1997.

Tremp, J., Mattrel, P., Fingler, S. and Giger, W., Phenols and nitrophenols as tropospheric pollutants - emissions from automobile exhausts and phase-transfer in the atmosphere, *Water Air Soil Pollut.*, **68**, 113-123, 1993.

Trost, B., Stutz, J. and Platt, U., UV-absorption cross sections of a series of monocyclic aromatic compounds, *Atmos.Environ.*, **31**, 3999-4008, 1997.

Utter, R. G., Burkholder, J. B., Howard, C. J. and Ravishankara, A. R., Measurement of the mass accommodation coefficient of ozone on aqueous surfaces, *J.Phys.Chem.*, **96**, 4973-4979, 1992.

Van Doren, J. M., Watson, L. R., Davidovits, P., Worsnop, D. R., Zahniser, M. S. and Kolb, C. E., Temperature dependence of the uptake coefficients of HNO_3, HCl, and N_2O_5 by water droplets, *J.Phys.Chem.*, **94**, 3265-3269, 1990.

Verschueren, K., *Handbook of environmental data on organic chemicals*, 3rd Ed., John Wiley & Sons, New York, 1996.

vonSonntag, C., Degradation of aromatics by Advanced Oxidation Processes in water remediation: Some basic considerations, *J.Water Suppl.Res.Technol.-Aqua*, **45**, 84-91, 1996.

Wahner, A., Mentel, T. F., Sohn, M. and Stier, J., Heterogeneous reaction of N_2O_5 on sodium nitrate aerosol, *J.Geophys.Res.*, **103**, 31103-31112, 1998.

Worsnop, D. R., Zahniser, M. S., Kolb, C. E., Gardner, J. A., Watson, L. R., Van Doren, J. M., Jayne, J. T. and Davidovits, P., Temperature-dependence of mass accommodation of SO_2 and H_2O_2 on aqueous surfaces, *J.Phys.Chem.*, **93**, 1159-1172, 1989.

Yaws, C. L., Yang, H. C. and Pan, X., Henry's law constants for 362 organic compounds in water, *Chem.Eng.*, **98**, 179-185, 1991.

Yaws, C. L., *Handbook of transport property data: viscosity, thermal conductivity, and diffusion coefficients of liquids and gases*, Gulf Publishing Company, Houston, 1995.

Yaws, C. L., *Chemical properties handbook: physical, thermodynamic, environmental, transport, safety, and health related properties for organic and inorganic chemicals*, McGraw Hill, New York, 1999.

Zellner, R. and Herrmann, H., Free radical chemistry of the aqueous atmospheric phase, in *Spectroscopy in Environmental Science*, Clark, R. J. H. and Hester, R. E. (Ed.), pp. 381-451, John Wiley & Sons, Chichester, 1995.

Zhang, R. Y. and Leu, M. T., Heterogeneous interaction of peroxyacetyl nitrate with liquid sulfuric acid, *J.Geophys.Res.*, **102**, 8837-8843, 1997.

13. APPENDIX

Computer program for derivation of k_w^{corr}

```
PROGRAM KWALL
!  Z,ZW,ZS are dimensionless parameters for true first-order gas-phase loss,
!  true first-order wall loss, and observed overall first-order loss coeffs.
!  D is dimensionless parameter for diffusion coefficient.
     DIMENSION B(30)
!  Read in experimental parameters
     WRITE (6,FMT=*) "Input experimental first-order loss / s-1"
     READ (5,*) ZS
     WRITE (6,FMT=*) "Input experimental diffusion coefficient / cm2 s-1"
     READ (5,*) D
     WRITE (6,FMT=*) "Input experimental gas flow velocity / cm s-1"
     READ (5,*) GASVEL
     PRINT *
     RADIUS = 0.90
!  Convert to dimensionless parameters for equation ROOT to solve
     Z = 0.0
     ZW = 0.0
     ZS = ZS*RADIUS/GASVEL
     D = D/(2*RADIUS*GASVEL)
     IOPT = 4
     CALL ROOTS(ZS,Z,ZW,D,IOPT,F,B,NB,IFLAG)
!  First print out dimensionless paramters to compare with valid ranges
     WRITE (6,FMT=*) "Values for the dimensionless parameters D, K* and KW"
     PRINT *, D, ZS, ZW
     PRINT *
!  Reconvert back to experimental data units
     ZS = ZS*GASVEL/RADIUS
     ZW = ZW*GASVEL*2/RADIUS
     WRITE (6,FMT=*) "Observed and corrected first-order losses / s-1"
     PRINT *, ZS, ZW
     END

     SUBROUTINE ROOTS(ZS,Z,ZW,D,IOPT,F,B,NB,IFLAG)
     DIMENSION B(30), DB(30)
     DATA PREC1,PREC2,NMAX,IMAX/0.0001,0.0001,30,10/
     IFLAG=0
     R2D=1.0/(2.0*D)
     ZWD=ZW*R2D
     RD=1.0/D
     ITAB=0
70    ZSD=ZS*RD
     A=ZS*ZS+ZSD-Z*R2D
     IF(IOPT.EQ.2) DA=2.0*ZS+RD
     IF(IOPT.EQ.3) DA=-0.5*RD
     B(1)=-0.25*A
     DB(1)=-0.25*DA
     B(2)=0.0625*(ZSD-A*B(1))
     IF (IOPT.EQ.2) DB(2)=0.0625*(RD-DA*B(1)-A*DB(1))
     IF (IOPT.EQ.3) DB(2)=0.0625*(-DA*B(1)-A*DB(1))
     F=ZWD
     DF=0.0
```

```
      GN=0.0
      GD=1.0
      DO 15 N=1,2
       Q1=2*N
       Q2=Q1+ZWD
       IF (IOPT.EQ.4) GO TO 16
       F=F+B(N)*Q2
       IF ((IOPT.EQ.2).OR.(IOPT.EQ.3)) DF=DF+DB(N)*Q2
       GO TO 15
   16   GD=GD+B(N)
       GN=GN+B(N)*Q1
   15  CONTINUE
      DO 10 N=3,NMAX
       NB=N
       Q1=2*N
       Q2=Q1*Q1
       RQ2=1.0/Q2
       B(N)=RQ2*(ZSD*B(N-2)-A*B(N-1))
       GO TO (11,12,13,20), IOPT
   12    DB(N)=RQ2*(RD*B(N-2)+ZSD*DB(N-2)-DA*B(N-1)-A*DB(N-1))
        GO TO 11
   13    DB(N)=RQ2*(ZSD*DB(N-2)-DA*B(N-1)-A*DB(N-1))
   11    Q3=Q1+ZWD
        FOLD=F
        F=F+B(N)*Q3
        IF ((IOPT.EQ.2).OR.(IOPT.EQ.3)) DF=DF+DB(N)*Q3
        IF (ABS(F-FOLD).LT.PREC1) GO TO 21
        GO TO 10
   20    GD=GD+B(N)
        GNOLD=GN
        GN=GN+B(N)*Q1
        IF (ABS(GN-GNOLD).LT.PREC1) GO TO 21
   10  CONTINUE
   21  GO TO (99,30,32,50), IOPT
   30   ZSOLD=ZS
       ZS=ZS-F/DF
       IF (ABS(ZS-ZSOLD).LT.PREC2) GO TO 99
       GO TO 31
   32   ZOLD=Z
       Z=Z-F/DF
       IF (ABS(Z-ZOLD).LT.PREC2) GO TO 99
   31   ITAB=ITAB+1
       IF (ITAB.GT.IMAX) GO TO 41
       GO TO 70
   50  ZW=-2.0*D*GN/GD
      GO TO 99
   41  IFLAG=1
   99  RETURN
      END
```